



University of Leicester

Investigating the Potential of Novel Bivalent Pharmacophores and Tetra-Branched Opioids to Produce Analgesics with Diminished Tolerance and Dependence Profiles

Thesis submitted in partial fulfilment of the requirements for the
degree of **Doctor of Philosophy**

Written by:

MARK BIRD

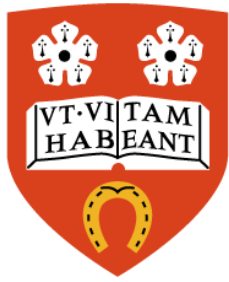
Department of Cardiovascular Sciences

Supervisors:

D.G. Lambert

D.J. Rowbotham

December 2014



University of Leicester

Investigating the Potential of Novel Bivalent Pharmacophores and Tetra-Branched Opioids to Produce Analgesics with Diminished Tolerance and Dependence Profiles

Thesis submitted in partial fulfilment of the requirements for the
degree of **Doctor of Philosophy**

Written by:

MARK BIRD

Department of Cardiovascular Sciences

Supervisors:

D.G. Lambert

D.J. Rowbotham

October 2014

Funded by the **British Journal of Anaesthesia**

BJA

Investigating the Potential of Novel Bivalent Pharmacophores and Tetra-Branched Opioids to Produce Analgesics with Diminished Tolerance and Dependence Profiles.

Mark Bird

All clinical opioid analgesics target the MOP (Mu Opioid Peptide) receptor. While these drugs provide analgesia, long-term treatment leads to tolerance and dependence. By targeting MOP and another member of the opioid receptor family, such as DOP (Delta Opioid Peptide receptor) or NOP (Nociceptin Orphanin F/Q Opioid Peptide receptor), these adverse effects are attenuated. Furthermore, solely targeting DOP or NOP may produce analgesia without the adverse effects associated with MOP. Three groups of variably mixed ligands have been developed; i) Fentanyl-based DOP and NOP bivalents, ii) peptide based MOP and NOP bivalents iii) tetrabranching NOP and DOP monovalent ligands. The pharmacology of these ligands has been investigated in a range of intracellular signalling assays.

All compounds were tested in Chinese hamster ovary (CHO) cells expressing human MOP, NOP, DOP or KOP (Kappa Opioid Peptide receptor) receptors. Initial work with Fentanyl-based DOP bivalents resulted in a loss of functional activity at the MOP receptor. Further Fentanyl-derivatives conjugated with Ro65-6570 displayed partial agonist activity at MOP and full agonist activity at MOP. A second MOP/NOP bivalent pharmacophore, (DeNO), based on the peptides **D**ermorphin (MOP) and **N/O**FQ demonstrated full agonist activity at both receptors. A tetrabranching ligand formed from N/O/FQ, displayed increased potency at the NOP receptor compared to N/O/FQ. DeNO was investigated in human embryo kidney (HEK) cells which co-expressed MOP and NOP. The results of functional assays demonstrated a loss of MOP activity caused by the presence of NOP. Further studies with the opioids, Dermorphin and N/O/FQ, and antagonists naloxone (MOP) and UFP-101(NOP), have demonstrated a structural interaction between MOP and NOP in this cell line.

The work in this thesis demonstrates how modification of peptide structures was more successful in the development of multitarget ligands. The findings from this thesis provide a significant contribution to theory of receptor heterodimerisation between MOP and NOP, as demonstrated by the loss of potency of MOP agonists in the co-expression system.

Acknowledgements

Firstly I would like to thank the **British Journal of Anaesthesia** for funding this PhD and making this thesis possible. I would also like to extend my thanks to **Dr Ruben Vardanyan** for making the Fentanyl-derivatives which enabled this PhD project to happen.

I would like to thank **Professor Rowbotham** for his many encouraging words and the interesting chats about cricket. Many thanks to **Dr Thompson** and the anaesthetic research team for being so welcoming and open to my many dubious lunch choices. I'd also like to extend my thanks to the members of Cardiovascular Sciences in the RKCSB for providing a warm environment in which to work.

A huge thank you goes to Drs **Girolamo Calò, Remo Guerrini** and **Claudio Trapella**, for providing the compounds for this thesis. I would also like to extend my immense gratitude to them for making my stay in Ferrara so incredible. Their hospitality will never be forgotten, nor will I forget eating steak in a book store! I would also like to thank **Davide, Cammi, Fede** and **Anna** for sharing their office with me, helping with the experiments and providing me with incredible food and drink.

I would also like to thank all the other students (**Nik, Roisin, Rob, Mark, Mike, Jon** and **Will**) I've had the pleasure of working with over the past three years. You've all made the lab a more exciting place to work. I would also like to extend my thanks to **Dr Catherine Vial** for allowing me to gain huge amounts of experience in her lab.

I would like to thank my family for putting up with my moods when experiments went wrong and for having to listen to me practice for presentations repeatedly. I would like to thank them for encouraging me to go back to university. Thank you mom, dad and bro!

I cannot thank **John McDonald** enough for huge impact he has had during my PhD. From teaching me new assays to having to listen to "I'd like to present new data from our laboratory" constantly, he has been incredibly supportive throughout the PhD. John's friendship and humour has made this PhD incredibly fun. I'd also like to apologise for constantly using counter-transference incorrectly.

Finally, my biggest thanks goes to **Professor David Lambert** for providing constant support throughout my PhD. His door is always open for any problem and the help he has provided, both scientifically and personally, cannot be thanked enough. I'd also like to thank Dave for his encouragement and help in turning me into someone who can speak in front of a crowd, and not do an 8 minute talk in 3 minutes and 32 seconds! I will get you to eat a Rustlers™ burger one day!

“The most exciting phrase to hear in science, the one that heralds new discoveries, is not 'Eureka!' but 'That's funny...’”

Isaac Asimov

Contents

Chapter 1	General Introduction.....	1
1.1	Pain pathways	1
1.1.1	Regulation of painful stimuli in the CNS	2
1.1.2	The descending inhibitory tract	3
1.2	Opioid receptors.....	4
1.2.1	Opioid history and nomenclature	4
1.2.2	General G-protein coupled receptor signalling	5
1.2.3	Opioid receptor signalling	8
1.2.4	Opioid activation of the Mitogen-activated protein kinase pathway.....	10
1.2.5	Opioid receptor desensitisation and internalisation.....	11
1.2.6	Functional selectivity.....	12
1.2.7	MOP (μ)	13
1.2.8	DOP (δ).....	15
1.2.9	KOP (κ)	15
1.2.10	NOP	16
1.2.11	Endogenous ligands.....	17
1.2.12	Exogenous ligands.....	18
1.3	Bivalent Pharmacophores	20
1.4	Tolerance	21
1.4.1	Definition and implications of opioid tolerance.....	21
1.4.2	The role of opioid receptor phosphorylation and trafficking in tolerance.....	21
1.4.3	Opioid Dependence and Addiction	24
1.4.4	Cellular adaptations and opioid dependence	24
1.4.5	Opioid reinforcement and addiction.....	29

1.4.6	Role of other members of the opioid family in tolerance, dependence and addiction.....	31
1.4.7	MOP/DOP heterodimers in tolerance.....	32
1.4.8	NOP and addiction	39
1.4.9	MOP and NOP interactions in tolerance	40
1.5	Fentanyl Derivatives	43
1.6	The F-compound series of ligands (synthesised by Dr R. Vardanyan and Dr R Guerrini).....	44
1.7	PWT derivatives	46
1.8	Dermorphin-N/OFQ and Dermorphin-UFP-101	47
1.9	Aims.....	49
Chapter 2	Materials and Methods	51
2.1	Materials	51
2.2	Buffer compositions.....	52
2.2.1	Tissue culture buffers	52
2.2.2	Saturation/Displacement Buffers.....	52
2.2.3	GTP γ ³⁵ S buffers.....	53
2.2.4	Cyclic Adenosine Monophosphate Buffers.....	53
2.2.5	Calcium mobilisation buffers	53
2.2.6	Western blot buffers	53
2.3	Methods- Overview	55
2.4	Cell culture.....	56
2.5	Radioligand Binding assays-Cell preparation.....	56
2.5.1	Membrane preparation.....	56
2.5.2	Lowry Protein Assay	57
2.6	Basic principles of ligand binding	58
2.6.1	Theory.....	58

2.6.2	Radioligands	58
2.7	Saturation Binding Assay	59
2.7.1	Theory.....	59
2.7.2	Methods	61
2.8	Displacement Assay.....	62
2.8.1	Theory.....	62
2.8.2	Methods	63
2.9	GTP γ S functional assay	64
2.9.1	Theory.....	64
2.9.2	Methods-GTP γ [³⁵ S] agonist assay.....	65
2.9.3	Antagonist determination (pK _b) in a GTP γ [³⁵ S] functional assay.....	66
2.10	Cyclic adenosine monophosphate assay	68
2.10.1	Theory.....	68
2.10.2	Methods	69
2.11	PathHunter β -Arrestin recruitment Assays	70
2.11.1	Theory.....	70
2.11.2	Methods	71
2.12	Calcium mobilisation assays.....	72
2.12.1	Theory.....	72
2.12.2	Methods	73
2.13	Mouse <i>Vas deferens</i> Bio-assays.....	74
2.13.1	Theory.....	74
2.13.2	Methods	74
2.14	Western Blotting for MAPK activity.....	75
2.14.1	Theory.....	75
2.14.2	Methods	77
2.15	Development of a MOP/NOP co-expression system.....	79

2.15.1	Theory.....	79
2.15.2	Concentration-death plot	79
2.15.3	Stable transfection	80
2.15.4	Sub-cloning.....	80
2.16	Reverse Transcription-PCR.....	81
2.16.1	Theory.....	81
2.16.2	TaqMan™ probes	83
2.16.3	Total RNA extraction and reverse transcription.....	84
2.16.4	Reverse transcription	85
2.16.5	Polymerase chain reaction.....	86
2.17	Data analysis	87
Chapter 3	Characterisation of Novel Fentanyl-Based Bivalent Pharmacophores	88
3.1	Introduction.....	88
3.2	Hypothesis	89
3.3	Aims.....	89
3.4	Results.....	93
3.4.1	Displacement binding assays-unconjugated F-compounds (#1, #2, #3)..	93
3.4.2	Displacement Binding assays- F-compounds (#4, #5 and #6)	95
3.4.3	GTPγ[³⁵ S] functional assays-Compounds #4, #5 and #6	97
3.4.4	Displacement Binding Assays- The Gly-extended (#7-extended by 2 carbon atoms and #8- extended by 4 carbon atoms) linker compounds	101
3.4.5	GTPγ[³⁵ S] functional assays- The gly-extended linker compounds activity 103	
3.4.6	Beta-Arrestin Assays	107
3.4.7	Characterisation and selection of potential Fentanyl pharmacophores for conjugation with Ro65-6570.....	110
3.4.8	GTPγ[³⁵ S] functional assays- The MN compounds	115
3.5	Discussion.....	118

Chapter 4	Characterisation of Novel Tetra-Branched Peptides	122
4.1	Introduction.....	122
4.2	Hypothesis	123
4.3	Aims.....	123
4.4	Results.....	124
4.4.1	PWT-N/OFQ derivatives.....	124
4.4.2	PWT-Leu-Enk-Displacement binding studies.....	126
4.4.3	GTP γ [³⁵ S] functional assays.....	128
4.4.4	Calcium mobilisation assays	129
4.4.5	Bioassays	132
4.5	Discussion.....	132
Chapter 5	The Characterisation of Novel Peptidic Bivalent Pharmacophores Targeting MOP and NOP	136
5.1	Introduction.....	136
5.2	Hypothesis	136
5.3	Aims.....	136
5.4	Results.....	138
5.4.1	Displacement Binding assays	138
5.4.2	GTP γ [³⁵ S] functional Assays.....	141
5.4.3	Cyclic AMP functional assays.....	147
5.4.4	Detection of MAPK activity through Western blot Densitometry	149
5.5	Discussion.....	151
Chapter 6	Development of a MOP/NOP Co-Expression System	155
6.1	Introduction.....	155
6.2	Hypothesis	155
6.3	Aims.....	155
6.4	Results-CHO cell lines.....	156

6.4.1	Selection of an appropriate monoclonal CHO _{hMOP/NOP} cell batch.....	156
6.5	Results- Development of HEK cell lines.....	161
6.5.1	Cell death curve.....	162
6.5.2	Selection of appropriate HEK _{hMOP} and HEK _{hNOP} monoclonal cell lines	164
6.5.3	Optimising GTP γ [³⁵ S] assay in HEK cells.....	169
6.5.4	Development and selection of an appropriate monoclonal HEK _{hMOP/NOP} co-expression system	176
6.5.5	Determination of HEK _{hMOP/hNOP} functional ability-GTP γ [³⁵ S].....	178
6.6	Discussion.....	180
Chapter 7	Study of Receptor Interactions in a Dual Expression System.....	184
7.1	Introduction.....	184
7.2	Hypothesis	184
7.3	Aims.....	184
7.4	Results.....	185
7.4.1	Displacement Binding studies of the Dermorphin derivatives.....	185
7.4.2	GTP γ [³⁵ S] functional studies.....	191
7.4.3	Determination of MAPK activity	196
7.5	Discussion.....	198
Chapter 8	General Discussion.....	202
8.1	Summary of the main findings.....	204
8.2	Comparing results to existing literature.....	213
8.2.1	The MOP/DOP bivalent pharmacophores.....	213
8.2.2	The MOP/NOP bivalent pharmacophores.....	214
8.2.3	Peptides with prolonged duration of action.....	215
8.2.4	Activity of agonists in a dual-expression system	215
8.3	Mechanisms of action	216
8.3.1	Evidence of MOP/NOP heterodimerisation	216

8.4	Unexpected and contentious issues arising from this thesis	222
8.4.1	Alteration of the chemical structure of known ligands	222
8.4.2	Clinical outcomes with MOP/DOP multiparmacophoric research	225
8.4.3	UFP-101: Cell line specific functional activity?	225
8.4.4	Interactions with p38	226
8.4.5	Discrepancies between RT-qPCR and radioligand binding	227
8.5	Limitations	227
8.5.1	Comparisons between assays	227
8.5.2	Evidence of physical interaction between MOP and NOP.....	228
8.6	Importance of the findings	228
8.7	Future Work.....	231
8.8	Publications arising from this thesis	232
	References	234

Abbreviations

AC	adenyl cyclase
AMPA	α -amino-3-hydroxy-5-methyl-4-isoxazolepropionic acid
AMY	amygdala
BP	binding protein
BRET	bioluminescence resonance energy transfer
BSA	bovine serum albumin
cAMP	3'-5'-Cyclic adenosine monophosphate
cDNA	copy DNA
CGRP	calcitonin gene-related peptide
CHO	Chinese hamster ovary
CNS	central nervous system
CPP	conditioned place preference
CREB	cAMP response element-binding
C _t	cycle threshold
DAG	diacyl glycerol
DAMGO	([D-Ala ² , N-MePhe ⁴ , Gly-ol]-enkephalin)
DeNO	Dermorphin-N/OFQ
DeUFP	Dermorphin-UFP-101
DOP	Delta opioid receptor
DPDPE	[D-Pen(2),D-Pen(5)]-enkephalin
EC	endogenous control
ERK1/2	extracellular signal-regulated kinases 1/2
FAM	6-carboxyfluoscein
FRET	fluorescence resonance energy transfer
GABA	γ -amino butyric acid
gDNA	genomic DNA
GDP	guanosine 5'-disphosphate
GFP	green fluorescent protein
GIRK	G-protein inwardly rectifying potassium
GOI	gene of interest
GPCR	G-protein coupled receptors
GRK	G-protein receptor kinase
GTP	guanosine triphosphate

GTP γ S	guanosine 5'-[γ -thio]triphosphate
HEK	human embryo kidney
HIPP	hippocampus
IP ₃	inositol trisphosphate
IUPHAR	International Union of Basic and Clinical Pharmacology
JNK/SAPK	c-Jun N-terminal kinase/Stress-activated protein kinases
KO	knock out
KOP	Kappa opioid receptor
LC	locus coeruleus
LDCV	Large dense-core vesicles
LTP	long term potentiation
MAPK	mitogen-activated protein kinases
MDAN	MOP DOP agonist antagonist
MGB	minor groove binder
MOP	Mu opioid receptor
MVD	mouse <i>vas deferens</i>
N/OFG	Nociceptin/Orphanin FQ
NAc	nucleus accumbens
NMDA	N-methyl-D-aspartic acid
NOP	Nociceptin/Orphanin FQ receptor
NRM	nucleus raphe magnus
NRPG	reticularis paragigantocellularis
NSB	non-specific binding
ORL-1	opioid receptor-like
PAG	periaqueductal grey area
PCR	Polymerase chain reaction
PDYN	pre-prodynorphin
PFC	prefrontal cortex
PGi	nucleus paragigantocellularis
PKA	protein kinase A
PKC	protein kinase C
PLC	phospholipase C
POMC	pre-proopiomelanocortin
ppENK	pre-proenkephalin

ppN/OFQ	pre-pronociceptin/orphanin FQ
PWT	peptide wielding technology
RAVE	receptor activation versus endocytosis
RTP	receptor transporter protein
RVM	rostral ventral medulla
SG	substantia gelatinosa
TM	transmembrane domain
VP	ventral pallidum
VSCC	voltage sensitive calcium channels
VTA	ventral tegmental area
W/T	Wild type

Chapter 1 **General Introduction**

For centuries, opioids have been widely used to treat various forms of pain. Long-term use of opioids, such as Morphine, which is often the reality of chronic pain management, has unfortunately been shown to lead to the development of drug tolerance or dependence. Recent studies have provided a greater insight into both the cause, and possible prevention, of Morphine tolerance, which includes interacting with various opioid receptors, while maintaining agonist activity at the MOP (μ) receptor. Bivalent pharmacophores, which act simultaneously on various opioid receptors to inhibit tolerance or dependence, provide the basis of this thesis.

1.1 Pain pathways

The sensation of pain is usually initiated when a noxious stimulus acts upon nerve endings located throughout the periphery. These endings are attached to small diameter primary afferent peripheral neurones, which are either myelinated A(δ) fibres or unmyelinated C fibres. A(δ) fibres are mainly attached to high threshold mechanoreceptors and respond primarily to mechanical stimuli. They have a diameter of approximately 2-5 μm and transmit impulses at a rate of between 4 and 30 m.s^{-1} . A(δ) fibres are usually responsible for producing sharp, well-defined sensations of pain. The unmyelinated C fibres are polymodal nociceptors that have a diameter of approximately 0.4-1.2 μm . These fibres have a conduction velocity of 0.5-2.5 m.s^{-1} and respond to chemical, mechanical and thermal stimuli. C fibres are responsible for producing a dull poorly localised pain sensation (Rang et al., 2007). Chemical stimulation occurs through the release of chemical mediators (potassium ions, kinins, prostaglandins, and 5-HT), often released during an inflammatory response, and activates local signalling mechanisms, which activate transmission through the primary afferent neurons (Rang et al., 2007).

1.1.1 Regulation of painful stimuli in the CNS

Nociceptive afferent cell bodies lie within an area situated just outside the spinal cord, the dorsal root ganglia. The axons of the C and A (δ) fibres synapse with the cell bodies of interneurons (spinothalamic neurons) located in the I, II and V laminae of the dorsal horn (Figure 1.1). The substantia gelatinosa (SG), neurons located in lamina II, has short axons which run to either lamina I or V. They represent interneurons between primary afferent neurons that terminate in lamina II and second order neurons of lamina I and V (Calvino and Grilo, 2006). These neurons represent the 'gate' in the theory of spinal nociceptive transmission, in the original theory put forward by Wall and Melzack (Melzack, 1965). They are considered to be inhibitory interneurons, which can be stimulated by various non-nociceptive inputs to inhibit nociceptive afferent signalling (Figure 1.2). The projections from lamina I and V travel via the lateral spinothalamic tract to the thalamus. Painful sensations are relayed by the axons of cells in the thalamus to the somatosensory cortex-precentral gyrus (Rang et al., 2007).

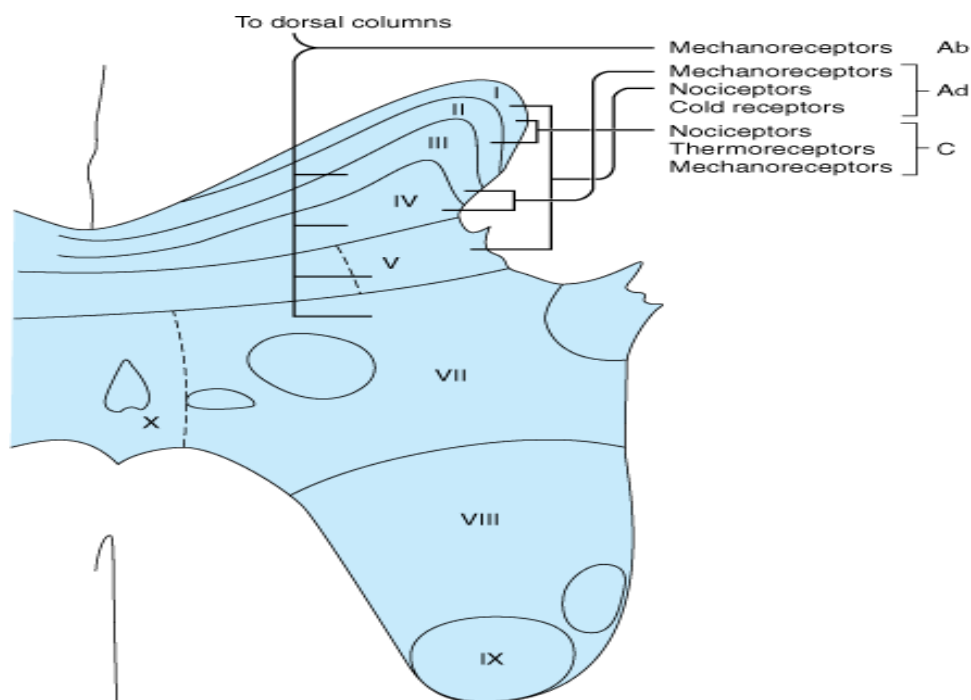


Figure 1.1: A representative picture of the termination of the various afferent fibres in the laminae of the dorsal horn. Taken from Clinical anaesthesiology, 4th Edition (G. E. Morgan *et al.*, 2006).

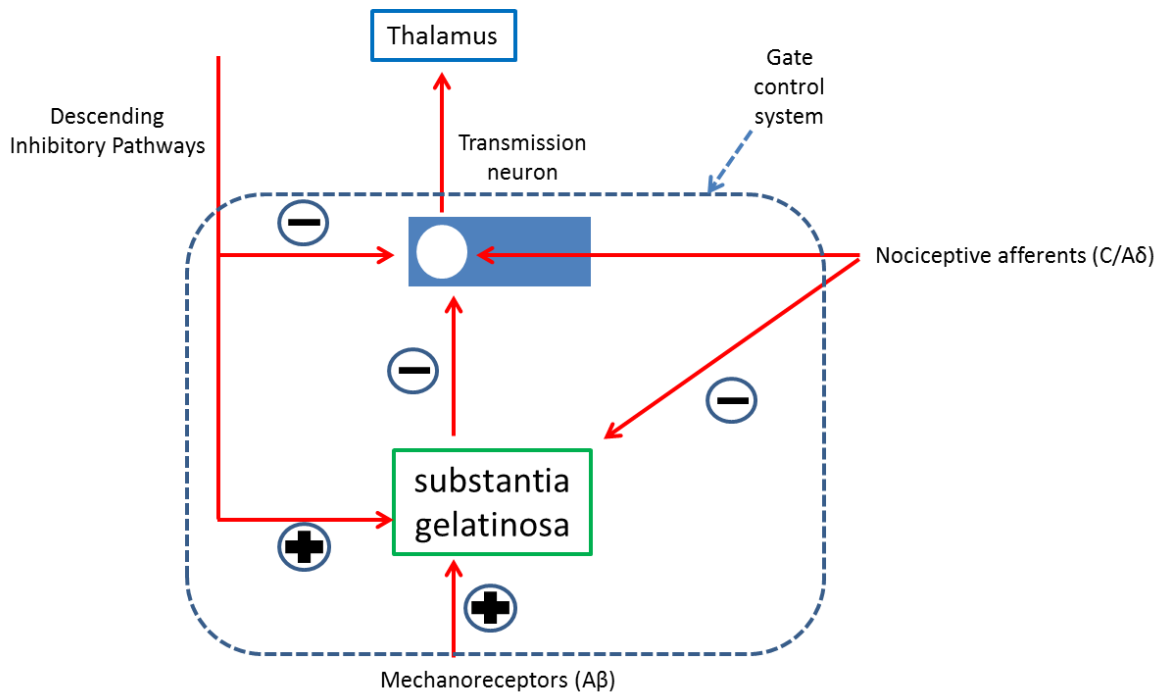


Figure 1.2: The gate control system regulates flow of nociceptive signals from peripheral afferent fibres to the thalamus. This is mediated by transmission neurones in the dorsal horn. Inhibition of this transmission pathway occurs through inhibitory neurones within the substantia gelatinosa, which are activated by descending inhibitory neurones or by non-nociceptive afferent input. The inhibitory neurones are inhibited by C fibre input. (Rang et al., 2007).

1.1.2 The descending inhibitory tract

Part of the gating mechanisms responsible for controlling nociceptive impulse transmission in the dorsal horn is the descending inhibitory pathway system. The periaqueductal grey area (PAG), located in the midbrain, is a key part of the inhibitory descending system. Various regions of the brain, such as the thalamus, cortex, and hypothalamus, extend inputs to the PAG and it acts as the main pathway through which descending nociceptive gating in the dorsal horn is controlled. Upon excitation, the neuronal transmissions from the PAG descend to the rostral ventral medulla (RVM) of the midbrain, into an area known as the nucleus raphe magnus (NRM). This in turn leads down the dorsolateral funiculus of the spinal cord to the dorsal horn. The descending fibres of the dorsolateral funiculus synapse with the interneurons of the SG, leading to their activation and the subsequent inhibition of nociceptive transmissions. Furthermore, indirect input is received from the amygdala and prefrontal cortex (Bee and Dickenson, 2009). Further control of the inhibitory descending pathways is

provided by spinothalamic neuronal pathways, which synapse in the NRM via the nucleus reticularis paragigantocellularis (NRPG) (Rang et al., 2007).

Through various electrophysiological experiments, it has been shown that the RVM contains a number of distinct neurones, which are able to produce inhibitory or positive effects on spinal nociception (Fields, 2004). These altering effects depend upon the intensity of the signal the RVM receives, with high intensity signals leading to an inhibition of the nociceptive signal, while low intensity signals produce a facilitation of this signal (Kerchner and Zhuo, 2002). The ability of the RVM to produce these altering signals is due to the presence of two types of cells, the **ON** and **OFF** cells (Figure 1.3). ON cells act to increase dorsal horn activity with regards to nociception, while OFF cells decrease this activity (Botney and Fields, 1983). The RVM is known to have a high density of a number of opioid receptor subtypes (Marinelli et al., 2002).

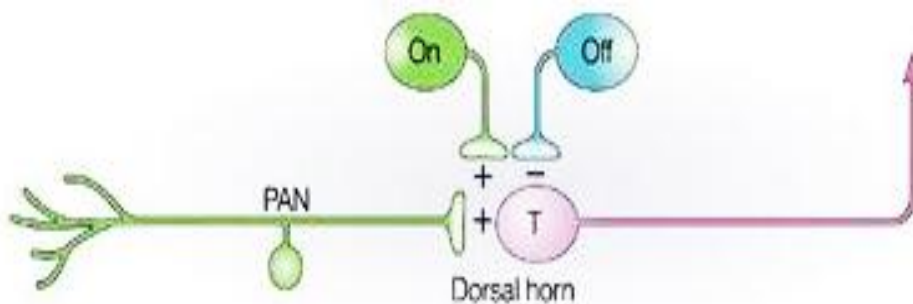


Figure 1.3: Nociceptive transmissions from the PAG is facilitated by ON cells and inhibited by OFF cells. (PAN-primary afferent neuron) (Fields, 2004).

1.2 Opioid receptors

1.2.1 *Opioid history and nomenclature*

While compounds, such as Morphine, had been used as analgesics since the 18th century, the existence of opioid receptors was not proposed till midway through the 20th century, following the structure-activity relationship studies of synthetic opioids analgesic activity (Beckett and Casy, 1954). Different pharmacological profiles, as well as tissue distribution, indicated multiple opioid receptor subtypes. Initially, these receptors were named by the prototypic drugs used to identify them, μ (Mu) for Morphine or κ for ketocyclazocine, or from their anatomical distribution (δ for vas

deferens) (Kieffer et al., 1992, Evans et al., 1992, Sharman et al., 2013). Homology cloning led to the identification of a fourth receptor which shared significant sequence homology with the opioid receptors. This receptor was initially termed opioid receptor-like 1 (ORL-1) or LC132. Currently, the International Union of Basic and Clinical Pharmacology (IUPHAR), the governing body on receptor nomenclature, has amended the current phrasing for the opioid receptors. The four opioid receptors are now referred to as MOP (μ), DOP (δ), KOP (κ) and NOP (ORL-1). Unlike MOP, DOP and KOP, termed the “classical opioid receptors” due to their affinity for the opioid antagonist Naloxone, the NOP receptor displays no affinity for this compound. With the exception of Dynorphin A, which displays weak affinity for NOP, the NOP receptor displays no affinity for endogenous opioids other than Nociceptin/Orphanin FQ (N/OFQ). Therefore, NOP is often referred to as a “non-classical” opioid receptor. The opioid receptors form a sub-part of a larger family of receptors, known as G-protein coupled receptors (GPCR). These receptors form the largest family of cell surface receptors. Due to the size of this family of receptors, they have been separated into sub-families, termed classes, based on common characteristics or sequence homology (Table 1.1). Opioid receptors are members of the largest sub-family, Class A, the rhodopsin-like receptor family.

1.2.2 *General G-protein coupled receptor signalling*

The GPCR has a seven-transmembrane spanning structure, with the N-terminus exposed to the extracellular domain, and the C-terminus existing in the intracellular domain. The structure of the GPCR binding pocket varies from receptor to receptor, but is always found on the extracellular domain. G-protein coupled receptors do not directly act with effector proteins; instead they interact with a heterotrimeric complex called a G-protein. The G-protein consists of three sub-units termed α , β and γ . The α -subunit has a guanonucleotide binding pocket which, in its inactivated state, houses a guanosine 5'-disphosphate (GDP) molecule. Once a GPCR is activated by a ligand, it leads to a conformation change in the receptor, activating the G-protein. The G-protein α -subunit exchanges GDP for guanosine triphosphate (GTP). At this point, α and $\beta\gamma$ subunits separate, both from the receptor and each other. Both separated subunits can influence effector proteins, such as adenylyl cyclase (AC) or ion channels within the cell (Figure 1.4).

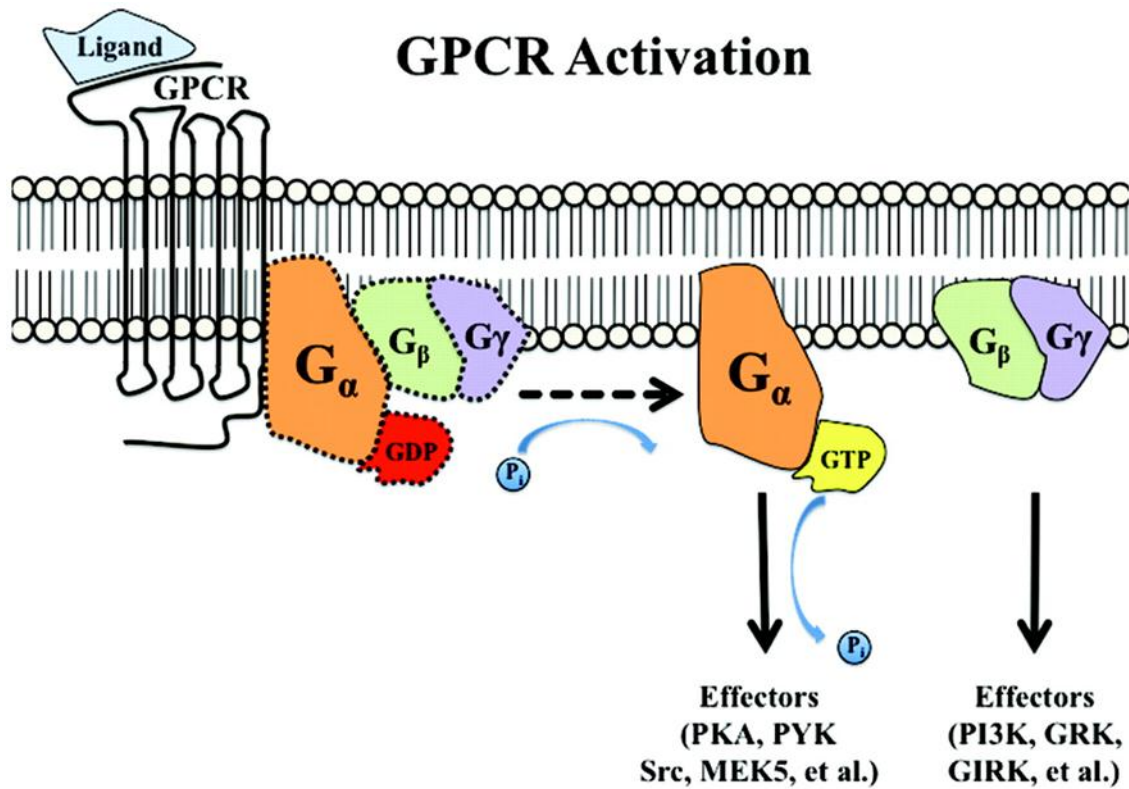


Figure 1.4: A single α -subunit can lead to an increase or decrease in the signalling of multiple second messenger systems, leading to signal amplification. G-protein signalling is terminated by the intrinsic GTPase activity of the α -subunit, breaking down GTP to GDP. At this point, all three subunits reform as one complex, terminating the signal transduction mechanism (Lohse et al., 2014).

G-PROTEIN COUPLED RECEPTORS					
CLASS A (Rhodopsin-like)	CLASS B (Secretin)	Class C (Metabotropic glutamate)	Class D (Fungal mating pheromone receptors)	Class E (cyclic AMP receptors)	Class F (Frizzled/smoothened)
Amine	Calcitonin	Calcium-sensing like	Fungal pheromone A	cAMP	frizzled
Peptide	Corticotropin-RF	Putative pheromone receptors	Fungal pheromone B		Smoothened
Hormone protein	Gastric inhibitory peptide	GABA-B	Fungal pheromone M- and P-Factor		
(Rhod)opsin	Glucagon	Orphan GPRC5	Fungal pheromone other		
Olfactory	Growth HRH	Orphan GPCR6			
Prostanoid	Parathyroid hormone	Bride of sevenless proteins (BOSS)			
Nucleotide-like	Secretin	Taste receptors (T1R)			
Cannabinoid	Vasoactive intestinal polypeptide				
Platelet activating factor	Diuretic hormone				
Gonadotropin-RH	EMR1				
Thyrotropin-RH	Latrophilin				
Melatonin	Brain-specific angiogenesis inhibitor (BAI)				
Viral	Methuselah-like proteins (MTH)				
Lysosphingolipid & LPA (EDG)	Cadherin EGF LAG (CELSR)				
Leukotriene B4 receptor					

Table 1.1: G-protein coupled receptors are separated into six classes. Classes are separated based on shared sequence homology, ligand interaction or tissue distribution. Sequence homology between classes is not common. Within the classes themselves, sub-families (main sub-families shown in table) do share sequence homology (Foord et al., 2005).

Heterotrimeric G protein G protein α ($G\alpha$) subunits	Function
$G_{\alpha s}$	Stimulate adenylyl cyclase
$G_{\alpha olf}$	Stimulate adenylyl cyclase
$G_{\alpha i1}$	Inhibit adenylyl cyclase
$G_{\alpha i2}$	Inhibit adenylyl cyclase
$G_{\alpha i3}$	Inhibit adenylyl cyclase
$G_{\alpha o1}$	Inhibit adenylyl cyclase
$G_{\alpha o2}$	Inhibit adenylyl cyclase
G_z	inhibits adenylyl cyclase Close K^+ channels. Inhibits exocytosis. Pertussis toxin-insensitive
$G_{\alpha t1}$	Stimulate cyclic GMP phosphodiesterase in rod photoreceptors
$G_{\alpha t2}$	Stimulate cyclic GMP phosphodiesterase in rod photoreceptors
$G_{\alpha gust}$	Stimulate phospholipase $C\beta$ (PLC β)
$G_{\alpha q}$	Stimulate phospholipase $C\beta$ (PLC β)
$G_{\alpha 11}$	Stimulate phospholipase $C\beta$ (PLC β)
$G_{\alpha 14}$	Stimulate phospholipase $C\beta$ (PLC β)
$G_{\alpha 15}$	Stimulate phospholipase $C\beta$ (PLC β)
$G_{\alpha 16}$	Stimulate phospholipase $C\beta$ (PLC β)
$G_{\alpha 12}$	Stimulate RhoGEFs to activate Rho
$G_{\alpha 13}$	Stimulate RhoGEFs to activate Rho

Table 1.2. G_{α} subunits and their downstream activity (Wettschureck and Offermanns, 2005).

There are a number of subtypes of G protein alpha subunits, all of which interact with various effector molecules (Table 1.2). These include, but are not limited to, $G_{\alpha s}$ (increases adenylyl cyclase activity-increasing production of cyclic AMP), $G_{\alpha i/o}$ (inhibits adenylyl cyclase-decreasing cyclic AMP) and $G_{\alpha q}$ (activates phospholipase C- leads to the hydrolysis of Phosphatidylinositol 4,5-bisphosphate to diacyl glycerol and inositol trisphosphate) proteins (Ellis, 2004). The $\beta\gamma$ subunits have been implicated in the regulation of ion channels, as well as playing a role in the recruitment of the MAPK pathway (Ito et al., 1992, Faure et al., 1994, Koch et al., 1994, Kofuji et al., 1995).

1.2.3 Opioid receptor signalling

As mentioned previously, the opioid receptors are GPCR's, which are coupled to the G alpha-inhibitory ($G_{\alpha i/o}$) subtype of G-proteins. When a ligand binds to an opioid

receptor it causes a conformational change in the receptor, leading to the activation of $G_{\alpha_{i/o}}$. Once the $G_{\alpha_{i/o}}$ protein is activated, it leads to a number of signalling events including inhibition of the enzyme, adenylyl cyclase, which in turn leads to a reduction in the synthesis of cyclic adenosine monophosphate (cAMP), leading to a reduction in membrane K^+ current (I_h) (Ingram and Williams, 1994). Furthermore, opioid receptor activation leads to the closing of N/P type voltage sensitive calcium channels (VSCC) and hyperpolarisation of the cell, through the stimulation of potassium efflux (Law et al., 2000). The net result of this activation is an inhibition of neurotransmitter release, resulting in the dampening of pain signalling. While the $G_{\alpha_{i/o}}$ protein is responsible for the interactions with adenylyl cyclase and cAMP, the $\beta\gamma$ subunit of the G-protein is believed to be responsible for the interactions with the VSCC and G-protein inwardly rectifying potassium (GIRK) channels, as depicted in Figure 1.5 (Herlitze et al., 1996, Dascal, 2001, Wolfe et al., 2003).

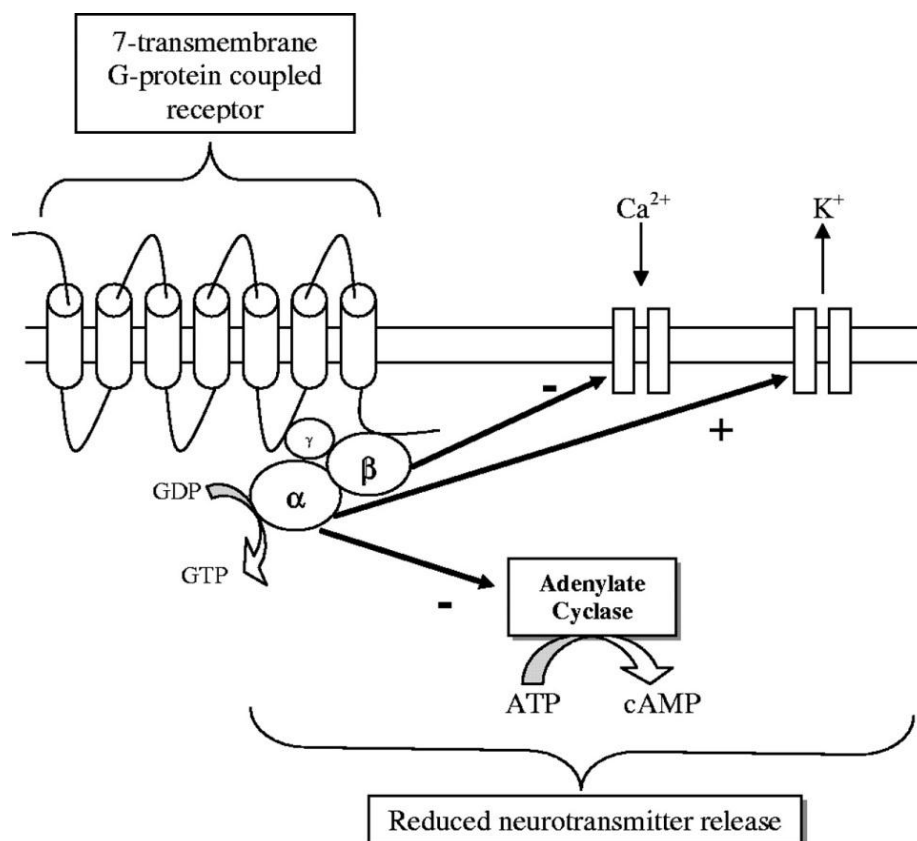


Figure 1.5: Initial signalling cascades of opioid receptors promoted by ligand binding. (McDonald and Lambert, 2005)

1.2.4 Opioid activation of the Mitogen-activated protein kinase pathway

While the initial actions of opioids are to disrupt nociceptive signalling through interactions via ion channels and neurotransmitter release, further downstream signalling events are also known to occur. Opioid receptors have been shown to interact with a family of serine/threonine kinases, the mitogen-activated protein kinases (MAPK). The MAPK pathway regulates DNA synthesis, cell growth, apoptosis and regulation of nuclear transcription factors (Seger and Krebs, 1995, Fukuda et al., 1996, Moulédous et al., 2007). The MAPK pathways are divided into three classes, extracellular signal-regulated kinases (ERK1/2), the p38 MAPKs and the c-Jun N-terminal kinase/Stress-activated protein kinases (JNK/SAPK). The pathway functions in a series of three kinase cascades, whereby phosphorylation of the first member leads to activation of the second and, subsequently, third kinase (Figure 1.6) (Strungs and Luttrell, 2014). This signalling pathway is known to be influential in opioid receptor desensitisation and neuronal survival or apoptosis (Polakiewicz et al., 1998a, Polakiewicz et al., 1998b). Opioid receptors have been shown to activate the MAPK pathways through multiple routes. The $\beta\gamma$ subunit can effect ERK1/2 activity through interactions with a member of the small GTPase family, *Ras* (Belcheva et al., 1998). Furthermore, opioid inhibition of both protein kinase A (PKA) and stimulation protein kinase C (PKC) affects ERK 1/2 and p38 signalling (Zhang et al., 1999). More recently, the scaffold proteins, β -arrestin 1 and 2 involvement in opioid activation of MAPK signalling has been demonstrated (Song et al., 2009, Clayton et al., 2009, Miyatake et al., 2009, Strungs and Luttrell, 2014). Morphine appears to interact with ERK1/2 through GRK 5 activation, while Fentanyl was shown to activate ERK1/2 through GRK 3 phosphorylation of the receptor and recruitment of β -arrestins in striatal neurons (Macey et al., 2006, Kohout and Lefkowitz, 2003). Multiple methods of activation, both homologous and heterologous that produce distinct temporospatial features, allow opioid receptors to modulate members of the MAPK family (Strungs and Luttrell, 2014). By changing the duration or intensity of stimulation on the MAPK pathway, the kinase activity can be targeted to perform specific functions.

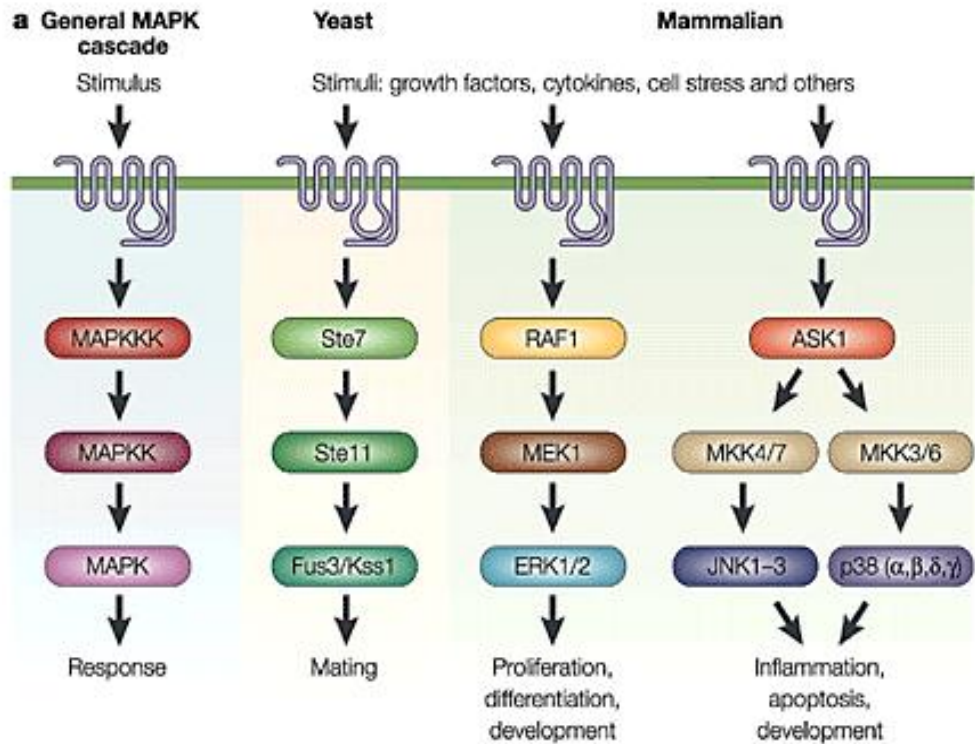


Figure 1.6: MAPK signalling cascades. Activation of the MAPK pathway by GPCRs occurs via sequential activation (MAPK kinase kinase \rightarrow MAPK kinase \rightarrow MAPK). In yeast, activation occurs through $G_{\beta\gamma}$ protein-dependent means, while in mammalian cells activation of ERK 1/2, p38 and JNK pathways has been shown to occur via $G_{\alpha i}$, $G_{\beta\gamma}$ and β -arrestin-dependent mechanisms (Pierce and Lefkowitz, 2001).

1.2.5 Opioid receptor desensitisation and internalisation

Following receptor activation, a number of cellular mechanisms occur to regulate GPCR signalling (Figure 1.7). Initially, receptors stop registering an ongoing stimulus, a phase termed desensitisation. This occurs through receptor phosphorylation, either through heterologous protein kinases such as PKA or PKC, or, mainly, through a family of kinases called the G-protein receptor kinases (GRKs), termed homologous phosphorylation (Pitcher et al., 1998). Phosphorylation via the GRK's leads to recruitment of β -arrestins (either β -arrestin 1 or β -arrestin 2), sorting and either recycling to the surface or degradation (Shenoy and Lefkowitz, 2011). The ability of β -arrestins to mediate numerous signalling pathways, as well as affecting receptor recycling or degradation, has led to the hypothesis of differential phosphorylation of receptors. In this case, varying phosphorylation sites would allow various patterns, and/or numbers, of β -arrestin recruitment allowing for multiple signalling pathways.

This hypothesis, termed bar code theory, was first demonstrated in β_2 -adrenergic receptors (Nobles et al., 2011). Interestingly, it has been demonstrated that various opioids produce varying responses with regards to desensitisation (Tsao and von Zastrow, 2000), internalisation and recycling/degradation (Keith et al., 1996, Keith et al., 1998). This will be further expanded in section 1.4.2.

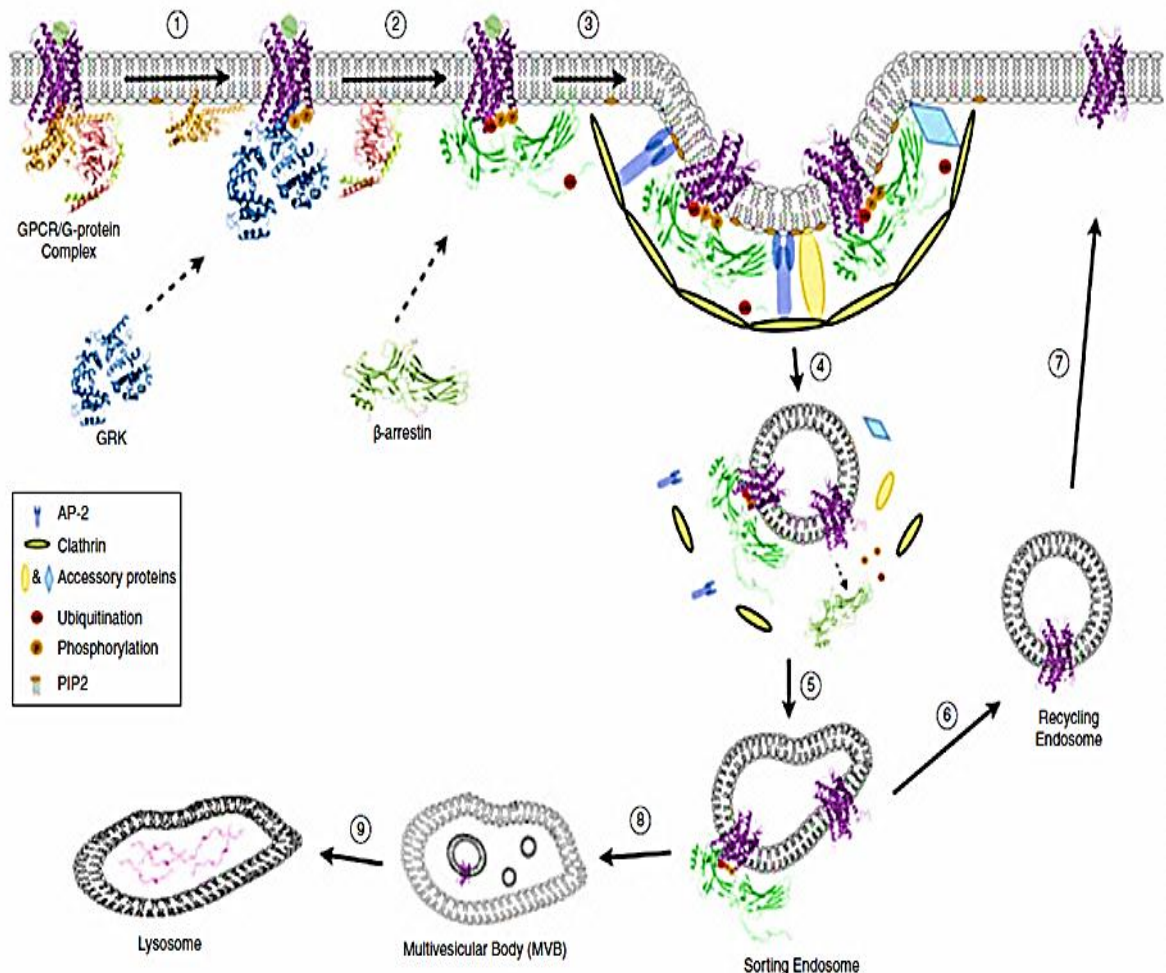


Figure 1.7: Following agonist induced activation (1) the receptor is phosphorylated due to GRK association (2). This leads to the translocation of β -arrestin to the receptor, leading to conformation changes in the β -arrestin (3), promoting recruitment of endocytosis (4). The GPCR- β -arrestin complex is transported to endosomes (5) where they are either recycled to the surface (6-7) or sorted to lysosomes and degraded (8-9). (Strungs and Luttrell, 2014)

1.2.6 Functional selectivity

The discovery of the β -arrestin signalling pathway has led to the implication that opioid ligands may have a biased signalling route (Figure 1.8) (Raehal et al., 2011). The

ability of a ligand to produce this biased agonism is believed to be due the process of different agonists forming different active conformations when bound to the opioid receptor (Kenakin, 2011, Kahsai et al., 2011). For instance, the endogenous opioid, Endomorphin-2, causes significant receptor phosphorylation and early recruitment of β -arrestins (Rivero et al., 2012). Conversely a novel MOP-selective opioid, Herkinorin, does not recruit β -arrestins and is biased towards G-protein signalling (Groer et al., 2007). Since β -arrestin recruitment is mediated by phosphorylation of the receptor, recruitment of subtypes of GRKs (in the case of the opioid receptors it is believed to be due to regulation by any of GRK2, GRK3, GRK5 or GRK 6), as well as other kinases such as PKA, PKC or ERK 1/2 may also be subject to biased recruitment after ligand binding (Raehal et al., 2011, Premont and Gainetdinov, 2007). Further understanding of the active states that lead to specific signalling pathways may help produce more effective opioids in the future (Rominger et al., 2014).

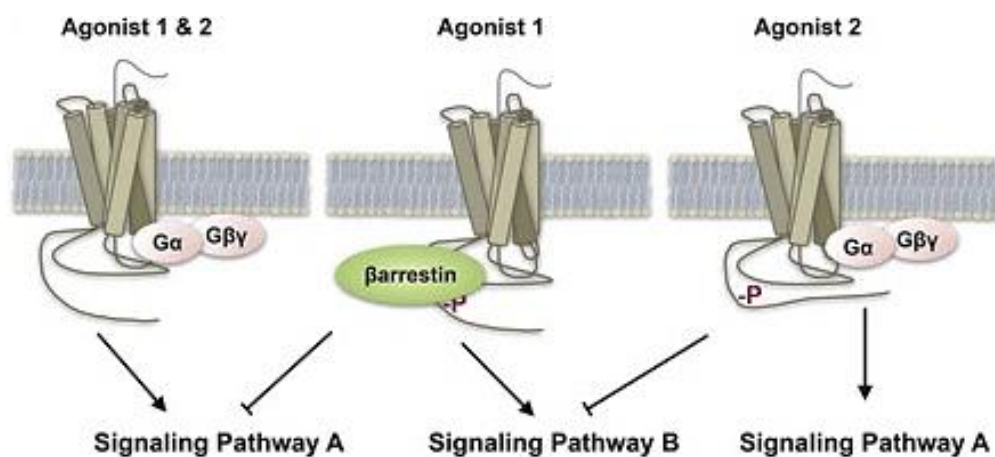


Figure 1.8: Functional selectivity of a ligand can lead to equal or preferential signalling through either G protein signalling or β -arrestin recruitment. In the figure above, both agonists 1 and 2 activate G-protein signalling (signalling pathway A). However, agonist 1 leads to β -arrestin recruitment, whereas agonist 2 does not. Recruitment of β -arrestin disrupts G-protein mediated signalling, but may influence signalling in alternate pathways (signalling pathway B). Agonist 2 would, therefore, only engage signalling pathway A. Agonist 2 would therefore be considered a biased agonist towards signalling pathway A (Raehal et al., 2011).

1.2.7 MOP (μ)

The MOP receptor is the major target for analgesic therapeutic treatment. MOP is expressed from the gene OPRM1. The MOP receptor was shown to be responsible for the majority of the effects produced by opioids, analgesic or deleterious, through work

with MOP $-/-$ knockout mice (Matthes et al., 1996, Kieffer, 1999, Le Merrer et al., 2009). The receptor is located throughout the central nervous system, with high densities of MOP receptors located in the caudate putamen, presynaptically on primary afferent neurons within the dorsal horn of the spinal cord and in the PAG. The location of the MOP receptors in the dorsal horn is significant, as their activation in this area leads to the inhibition of glutamate release and, subsequently, the transmission of nociceptive signals from both $A\delta$ and C fibres (Bee and Dickenson, 2009). As mentioned previously, the PAG is involved in the descending inhibitory control pathway (Bee and Dickenson, 2009). The PAG has been shown to have high densities of MOP receptors, which, after receptor activation, are believed to cause analgesia through inhibition of the neurotransmitter γ -amino butyric acid (GABA), one of the main inhibitory neurotransmitters in the brain. The presence of GABA leads to inhibition of antinociceptive transmissions through the PAG and, reciprocally, its absence aids nociception (McNally and Akil, 2003). The MOP receptor can be found on ON cells, previously mentioned in section 1.1.2, and when an agonist, such as Morphine or Fentanyl, activates the MOP receptor, it results in direct inhibition of these cells. This leads to an increase in the nociceptive signal to the dorsal horn from the descending inhibitory tract (Bee and Dickenson, 2009). Activation of the MOP receptor, while causing analgesia, can also cause moderate to severe side effects after a period of time. These include tolerance to the drug, constipation and, in severe cases, respiratory depression.

Recently, the crystal structure of MOP has been solved. The seven transmembrane domains of the receptor form three extracellular loops and three intracellular loops. Interestingly, unlike previously crystallised GPCRs, the MOP receptor's binding pocket is exposed to the extracellular surface (Manglik et al., 2012). While a large number of residues in the binding pockets of MOP, DOP and KOP are conserved, ligand-selectivity is demonstrated through variances in a number of key residues within the binding pocket (Wu et al., 2012, Manglik et al., 2012, Granier et al., 2012, Thompson et al., 2012).

1.2.8 DOP (δ)

The DOP receptor was the first receptor to be cloned and is found in areas such as the nucleus accumbens, caudate putamen, olfactory bulb and cerebral cortex (Waldhoer *et al*, 2004). Activation of the DOP receptor can lead to analgesic actions due to their location within spinal and supraspinal sites (Waldhoer *et al*, 2004). DOP receptors are located on primary afferents and act to inhibit the release of neurotransmitters from presynaptic terminals. Structurally, DOP shares a number of highly conserved features with the other opioid receptors. It has a typical seven transmembrane domain, with high similarity in structure to that of the other opioid receptors (Thompson *et al*, 2012, Wu *et al*, 2012, Manglik *et al*, 2012, Granier *et al*, 2012). Its binding pocket, like the other member of the opioid receptor family, can be split into two sections. The lower section is highly conserved amongst all of the opioid receptors, while the upper section confers ligand selectivity (Granier *et al*, 2012). Currently, there are no clinically available DOP-specific drugs available. However, the DOP receptor has been implicated in the treatment of emotional disorders, neurological disorders and negatively influencing reward and addiction (Pradhan *et al*, 2011). Work in DOP receptor KO mice has demonstrated an increased anxiety, indicating the potential for DOP agonists in affective disorders (Gavériaux-Ruff and Kieffer, 2002). With regards to potential unwanted effects, DOP agonists have been shown to be proconvulsive (Jutkiewicz *et al*, 2006).

1.2.9 KOP (κ)

The KOP receptor (named for *ketocyclazocine*), is located throughout the CNS, with large numbers being located in the diencephalic and limbic areas, brain stem and spinal cord. Activation of the KOP receptor, while causing analgesia, does not lead to respiratory depression over time. However, it does cause sedation, dysphoria and dependence (Trescott *et al*, 2008). The crystal structure of the KOP receptor has demonstrated a large binding pocket with a number of potential anchoring points for ligands. These unique features explain diversity of drugs able to interact with KOP. The receptor shares structural homology with the other members of the opioid receptor family (Wu *et al*, 2012). Furthermore, work in KO mice has demonstrated the role KOP activation plays in non-opioid mediated dysphoria. Tetrahydrocannabinol (THC)

mediated dysphoria was attenuated in KOP KO mice, indicating KOP-Dynorphin A interactions play an important role in the development of dysphoria (Gavériaux-Ruff and Kieffer, 2002).

1.2.10 *NOP*

The Nociceptin/Orphanin FQ receptor (NOP), so named for its endogenous peptide nociception/orphanin FQ (N/OFQ), has been classified as a non-opioid member of the opioid receptor family and, although it shares a number of structural and localisation features with other opioid receptors, is insensitive to naloxone (Lambert, 2008, Schröder et al., 2014). NOP shares approximately 60% homology with the classical opioid receptors. Structural studies have shown that the NOP receptor has substantial variance in its binding pocket compared to that of the classical opioid receptors (Thompson et al., 2012). The actions of the N/OFQ-NOP system in pain are complicated. Upon its original discovery, it was thought N/OFQ and NOP produced antiopioid effects, due to the onset of hyperalgesia when injected into the intracerebroventricular region of mice (Meunier et al., 1995). Supraspinally, N/OFQ produces an anti-opioid effect, reversing both external opioid influences and the release of classical endogenous opioid peptides (Tian et al., 1998, Zeilhofer and Calò, 2003). However, spinal administration produces analgesia (King et al., 1997, Ko et al., 2006). The contradictory actions of NOP and N/OFQ may be explained by its expression supraspinally. The NOP receptor is expressed within the RVM, more specifically on both ON and OFF cells (section 1.1.2) (Pan et al., 2000, Lambert, 2008). Activation of NOP leads to a reduction in signalling, with the net effect of blocking both ON and OFF cells being an increase in nociceptive signalling (Figure 1.9) (Lambert, 2008, Schröder et al., 2014). Interestingly, much work has identified the NOP receptor in attenuating reinforcing behaviour such as drug taking and alcohol abuse (Ciccocioppo et al., 2003). Work in animal models and non-human primates identified analgesic responses from both N/OFQ and a synthetic compound, Ro 64-6198, which were not accompanied by reinforcing effects (Ko et al., 2009). Therefore, the NOP receptor may be a suitable target for drugs with reduced abuse liability.

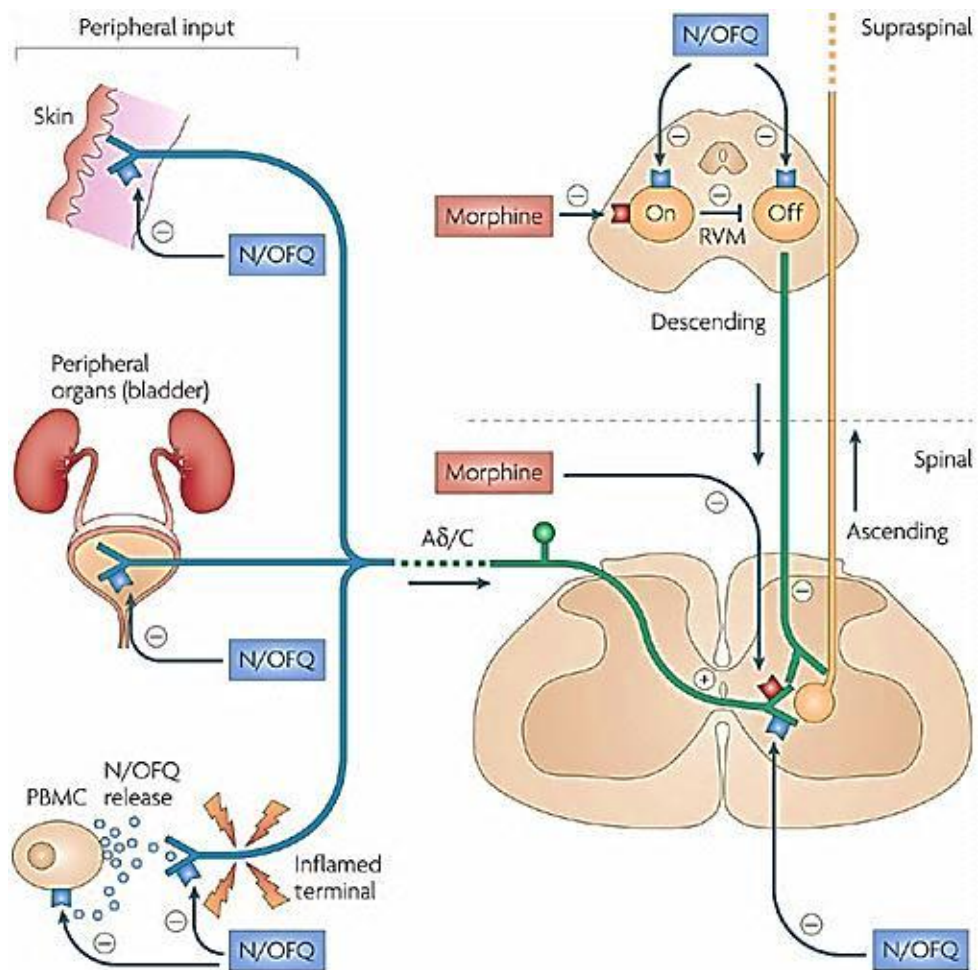


Figure 1.9: The hyperalgesic/anti-opioid effects of N/OFQ are produced through inhibition of both ON and OFF cells in the RVM (section 1.1.2). Administration of N/OFQ supraspinally leads to inhibition of both ON and OFF cells, leading to a net increase in nociceptive signalling and producing the anti-opioid effect. Conversely, N/OFQ produces analgesia spinally, through inhibition of nociceptive signalling. N/OFQ can act in the periphery to inhibit nociceptive afferents, potentially in collaboration with the neuroimmune axis (PBMC= peripheral blood mononuclear cells) (Lambert, 2008).

1.2.11 Endogenous ligands

The opioid receptors are activated by both endogenous and synthetic ligands. The endogenous opioid peptides are initially synthesised as peptide precursors from four genes: pre-proenkephalin (ppENK), pre-proopiomelanocortin (POMC), pre-prodynorphin (PDYN) and pre-pronociceptin/orphanin FQ (ppN/OFQ) (Waldhoer et al., 2004). The first three genes code precursor peptides that act on the classical opioids, while the latter codes an agonist for the NOP receptor. Many complex post-translational modifications on these precursor peptides result in the synthesis of multiple active

peptides and, with regards to the peptides associated with the classical opioid receptors, they share a common N-terminal sequence of Tyr-Gly-Gly-Phe. This motif is accompanied by various extensions and can yield a peptide that ranges in length from 5-31 residues (Davis, 2002, Waldhoer et al., 2004, Evans, 2004). Pre-proopiomelanocortin encodes the opioid peptide β -endorphin, as well as other non-opioid related peptides. Pre-proenkephalin produces Leu-Enkephalin and multiple copies of Met-Enkephalin. Dynorphin A, Dynorphin B and Neoendorphin are all opioid peptides produced from pre-prodynorphin. Beta-endorphin shows affinity for all three of the classical opioid receptors, Leu-Enkephalin shows high affinity for the DOP receptor, Met-Enkephalin has a high affinity for the DOP receptor and some affinity for the MOP receptor, while the Dynorphins primarily show affinity for the KOP receptor (Davis, 2002, Waldhoer et al., 2004). Pre-pronociceptin/orphanin FQ produces the peptide Nociceptin/Orphanin FQ that acts on the NOP receptor with high affinity, but does not interact with the classical opioid receptors. Endogenous opioid ligands are shown in Table 1.3, with accompanying receptor selectivity.

1.2.12 *Exogenous ligands*

Exogenous ligands available for opioids can range from natural compounds to synthetically synthesised compounds to peptides found in animals. The most well-known group of opioids are the natural alkaloids, such as those derived from the poppy plant, from which Morphine and codeine are derived. Chemical alterations to alkaloids have led to the development of semi-synthetic alkaloids such as Hydromorphone and Hydrocodone. The piperidine series of opioids, a synthetic series of opioids, consist of potent analgesics such as Fentanyl. Most clinically available opioids act solely at the MOP receptor. However, buprenorphine acts as a partial agonist at MOP and NOP, while acting as an antagonist at KOP (Table 1.3).

While the analgesic properties of the opioids are undoubted, they are marred by adverse effects and limited ability to function in certain disease states, such as neuropathic pain. The long-term use of opioids can lead to tolerance or dependence as well as addiction.

Opioid	Receptor Subtypes			
	MOP	DOP	KOP	NOP
Peptides				
β-Endorphin	***	***	***	/
Leu-enkephalin	*	***	***	
Met-enkephalin	**	***	/	/
Dynorphin A&B	**	***	*	*
Dermorphin	***	*	/	/
N/OFQ	/	/	/	***
Opioid Clinical Drugs				
Morphine	***	*	*	/
Pethidine	***	*	*	/
Diamorphine	***	*	*	/
Fentanyl	***	*	*	/
Meperidine	***	/	/	/
Partial Agonists				
Buprenorphine	**	/	*	*
Pentazocine	/	**	/	/
Antagonists				
Naloxone	***	**	**	/
Naltrexone	***	**	**	/

*** =High Affinity ** =moderate affinity * =low affinity /=no affinity

Table 1.3: The table above displays various endogenous opioids as well as synthetic compounds (Rang et al., 2007).

1.3 Bivalent Pharmacophores

Previous work in the opioid field has concentrated on highly selective agonists/antagonists for a single opioid receptor. However, due to numerous studies, which will be described in further sections, drug development has moved on to the targeting of two or more receptors. Potential strategies to target multiple receptors include polypharmacy, bifunctional drugs (two drug moieties in one chemical structure) or bivalent pharmacophores (two pharmacophores joined by a linker molecule to act as one drug) (Figure 1.10). The evidence provided by knockout animals (section 1.4.6) provides a strong case for the development of bivalent ligands. These ligands generally contain differing pharmacophores, whose distance from each other can be manipulated by a chemical spacer. The importance of the chemical spacer is thought to be dependent on the distance between the targeted active sites. There are a number of advantages to developing a bivalent ligand for use in clinical settings, rather than simply administering two separate drugs. The single drug administration reduces patient self-dosing errors and would reduce the risk of possible interactions between multiple drugs. The pharmacokinetic and pharmacodynamic properties of bivalent ligands are more predictable than a cocktail of separate drugs (Edwards and Aronson, 2000; Schiller, 2010). Recent work in this field has shown some bifunctional ligands to have an improved pharmacological profile; an example of a mixed bifunctional pharmacophore would be the drug Tapentadol, which contains a MOP agonist that also acts as a noradrenaline reuptake inhibitor (Dietis *et al*, 2009). When developing a mixed ligand, a need for similarity in affinity for both receptors is of high importance, in order to reduce any potential biased selectivity. The potential benefits of these mixed molecules will be further discussed with regards to their functions in tolerance and dependence, as well as providing novel therapies for drug abuse.

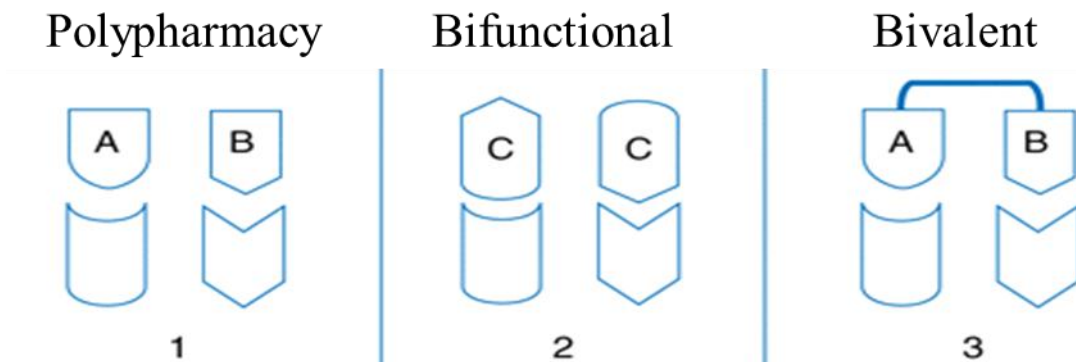


Figure 1.10: When targeting multiple (and different) receptors it is possible to use a variety of methods. In the diagram above, such methods are depicted. **1)** Two separate drugs (A and B) can be used simultaneously to illicit the desired biological response. **2)** A non-selective ligand (C) can be developed which has a structure which binds to both of the receptors. **3)** The two separate drugs (A and B) can be joined by a linker to form a bivalent pharmacophore which can bind to both receptors (Dietis et al., 2009).

1.4 Tolerance

1.4.1 *Definition and implications of opioid tolerance*

While opioids are the most potent clinically available analgesics, their long term use is blighted by adverse effects. One such implication of long-term use is the development of tolerance. Tolerance can be seen as a drug's loss of efficacy over time despite escalating the dosage. This onset of tolerance provides issues for the treatment of long term pain. For instance, up to 88% of cancer patients, within the last year of their life, suffered with a distressing amount of pain (Nersesyan and Slavin, 2007).

1.4.2 *The role of opioid receptor phosphorylation and trafficking in tolerance*

The cellular mechanisms that lead to tolerance have proven to be complicated, with a large number of intracellular signalling pathways implicated in its onset. To further complicate the understanding of tolerance, evidence suggests that different opioids engage variable mechanisms of desensitization and phosphorylation, as well as differential recruitment of β -arrestins and endocytotic pathways, all upon activation of the MOP receptor (Enquist et al., 2011, Rivero et al., 2012, Williams et al., 2013). For instance, Morphine -induced endocytosis of MOP is cell-type specific, proving to be

poor in the spinal cord (*in vivo*) and locus coeruleus (*in vitro*), however, in medium spiny, striatal neuron dendrites it effectively induces endocytosis (Arttamangkul et al., 2008, Haberstock-Debic et al., 2005, Trafton and Basbaum, 2004).

Beta-arrestin recruitment is likewise ligand dependent, with Morphine displaying selectivity for β -arrestin 1, while [D-Ala²,N-Me-Phe⁴,Gly⁵-ol]-Enkephalin (DAMGO) can recruit either β -arrestin (Groer et al., 2011). DAMGO's interactions with MOP lead to substantial phosphorylation of the receptor and β -arrestin recruitment, resulting in a net increase in receptor trafficking (Groer et al., 2011, Raehal et al., 2011, Keith et al., 1996, Zuo, 2005). A theory was put forward, whereby β -arrestin recruitment and, subsequently, internalisation of the opioid receptor were thought to be paramount in attenuating tolerance. **R**eceptor **a**ctivation **v**ersus **e**ndocytosis (RAVE) relates to the ability of a ligand to induce internalisation of the receptor (Figure 1.11). Those ligands that promote receptor signalling leading to endocytosis, which would have higher RAVE values, when compared with those that demonstrated bias for either signalling or endocytosis would have low RAVE scores. The RAVE hypothesis implies that for tolerance to be attenuated, a compound that induces recruitment of β -arrestin and leads to receptor internalisation would have a low tolerance profile (Whistler and von Zastrow, 1998, Finn and Whistler, 2001). However, work with β -arrestin2 knock-out mice provided evidence that recruitment of this β -arrestin to the MOP receptor produces (rather than attenuates) opioid tolerance as well as a number of opioid side effects, including constipation and respiratory depression (Bohn et al., 1999, Raehal et al., 2005). As mentioned previously, recruitment of β -arrestins can be cell-specific which in turn does not provide a consistent method of measuring RAVE (Williams et al., 2013). Multiple downstream signalling cascades can be activated by differential recruitment of β -arrestin through various interactions of multiple opioids with the MOP receptor. DAMGO, but not Morphine, engages the p38 MAPK pathway to produce endocytosis in dorsal root ganglion (Tan et al., 2009a). The functional activity and outcomes of the ERK 1/2 cascade are also dependent on the type of ligand and its recruitment of β -arrestins. Morphine interacts with a PKC-dependent pathway to activate the ERK signalling cascade resulting in the activation of the cAMP response element-binding (CREB) protein, whereas, Fentanyl produces β -arrestin dependent ERK 1/2 signalling, resulting in translocation to the nucleus, and an increase in the

activity of Elk-1. The net result of this latter pathway is an increase in β -arrestin2 and GRK2 transcription (Zheng et al., 2008).

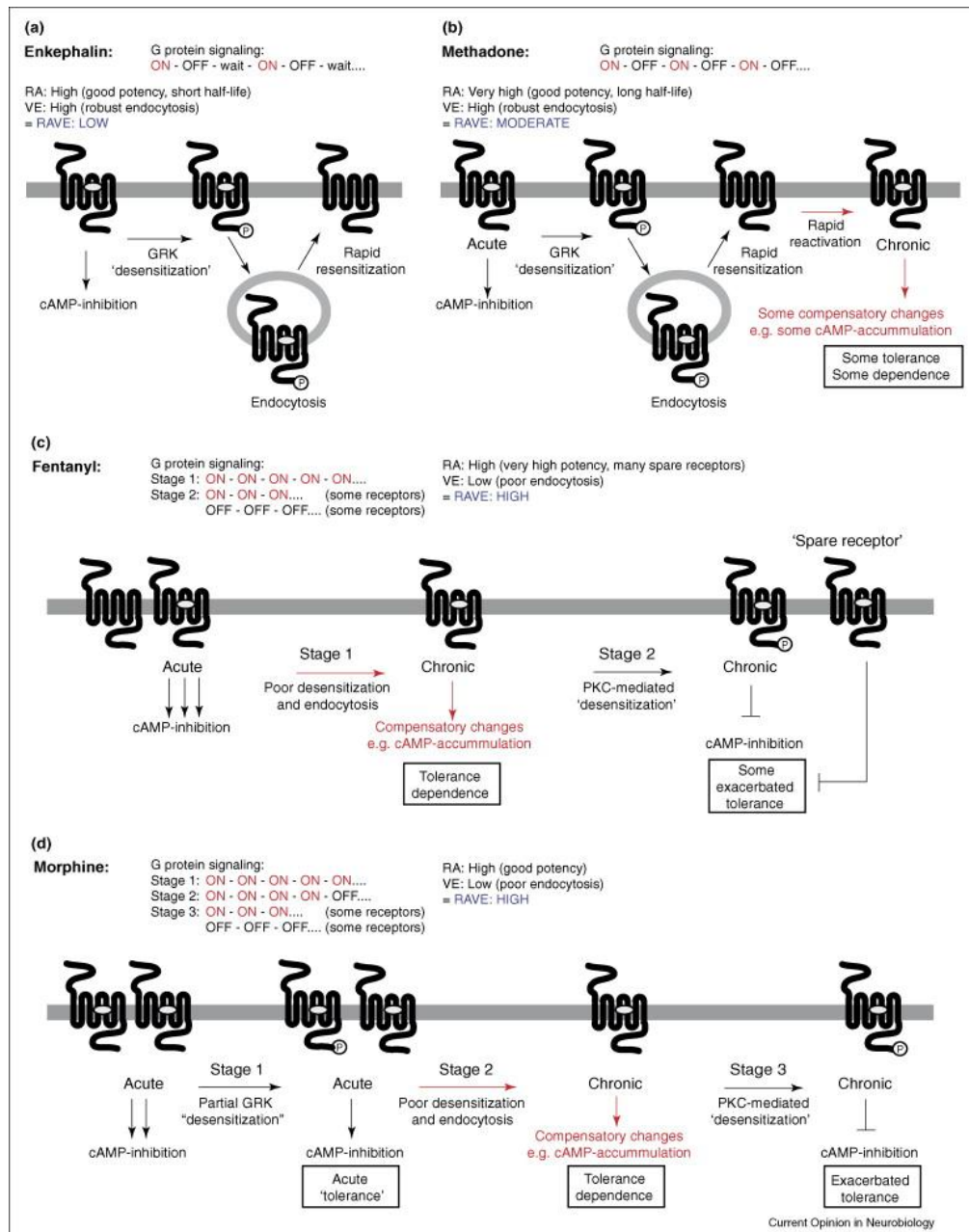


Figure 1.11: The RAVE hypothesis. Differential signalling at MOP occurs, dependent on the agonist used and the length of time the opioid is administered. In the RAVE hypothesis (A) Enkephalin would have a receptor activation (RA) due to its potency, and also has a high (VE) because it promotes endocytosis. In this theory, Enkephalin would have a low risk of tolerance and dependence developing. (B) Methadone would have a higher risk of tolerance and dependence formation, due to its increased RAVE values, leading to compensatory changes in signal transduction. (C) Fentanyl has high potency and therefore a high RA score, but due to low drug dose requirement and, consequently, low receptor occupancy it has a low VE score. This equates to a high risk of tolerance and dependence. Finally, Morphine (D) has a high RA due to its potency but, due to its failure to induce MOP internalisation, it has a low VE rating and therefore a high risk of tolerance and dependence (Martini and Whistler, 2007).

The endpoint of these various actions is the sorting of MOP receptors into “tolerance-inducing” pathways, or pathways whereby tolerance is negated. Understanding which elements lead to the attenuation of tolerance to opioids would potentially improve the development of drugs lacking in adverse effects. Recently, the role of other members of the opioid family has been highlighted with regards to their roles in opioid receptor phosphorylation, internalisation and recycling or ubiquitination, as well as their roles in tolerance and dependence.

1.4.3 *Opioid Dependence and Addiction*

Use of opioids can lead to states of dependence and addiction. The definitions of addiction and dependence are often grouped together. However, in this section opioid dependence will be defined as the cellular and tissue adaptations incurred by opioid use, whereupon removal of the opioid leads to physical harm. Addiction refers to the neurobiological changes that occur that lead to a “craving” for the drug and addiction can also encompass the detrimental effects of tolerance and dependence associated with long term opioid use (Ballantyne et al., 2012, Ingram et al., 1998). Opioid abuse and dependence have far-reaching implications, with approximately 11 million people dependent on Heroin or other opioids. The risk of morbidity is increased 15-fold through risk of overdose and exposure to diseases such as HIV and hepatitis C (WHO, 2009)

1.4.4 *Cellular adaptations and opioid dependence*

Once dependence occurs, removal of an opioid leads to withdrawal symptoms such as hyperalgesia, gastro-intestinal cramp and joint and muscle aches (Tso and Wong, 2003). These symptoms lessen if opioids are reintroduced to the system. The development of opioid dependence is a complex mix of changes in receptor expression, signal transduction and cellular adaptations and synaptic plasticity. On a cellular level, chronic opioid use leads to a compensatory increase in adenylyl cyclase activity or adenylyl cyclase superactivation, which may be adenylyl cyclase isoform dependent (Jolas et al., 1999, Sharma et al., 1975). There are numerous hypotheses for this compensatory change (Watts and Neve, 2005, Sadée et al., 2005, Schallmach et al., 2006, Christie,

2008) (Figure 1.12). Adaptations to chronic opioid use in the noradrenergic neurones of the locus coeruleus (LC) as well as a number of neuronal bodies in the PAG, are believed to mediate the symptoms associated with opioid withdrawal (Punch et al., 1997, Han et al., 2006, Mazei-Robison and Nestler, 2012).

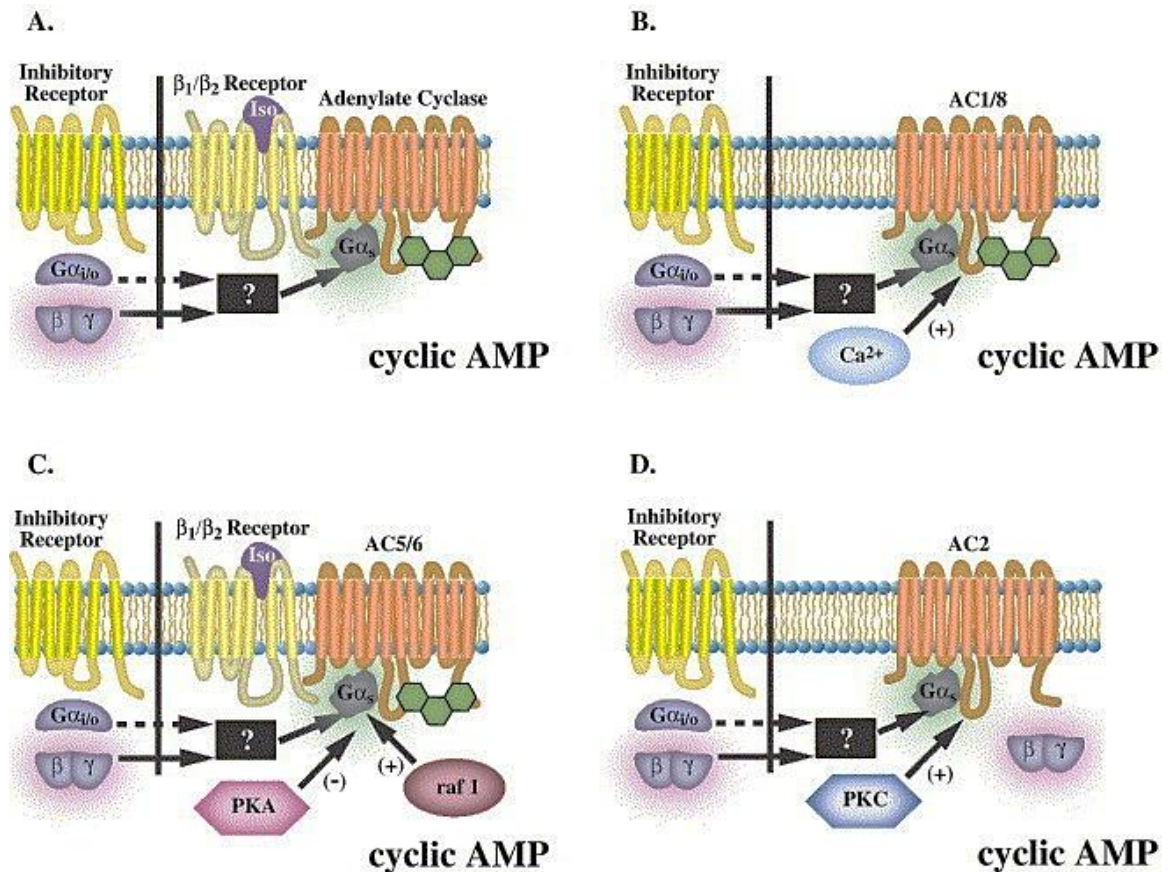


Figure 1.12: Adenyl cyclase heterologous sensitisation is isoform dependent. (A) Constant activation of a $G_{\alpha i/o}$ coupled receptor leads to activation and dissociation of the α and $\beta\gamma$ subunits. This in turn leads to sensitisation via $G_{\alpha s}$ independent mechanisms. The signalling processes that follow remain unclear, but it is thought that $G_{\alpha s}$ interaction with Adenyl cyclase is enhanced. (B) Persistent activation by MOP leads to the adenyl cyclase isoforms AC1 and AC8, which are Ca^{2+} sensitive, developing selective sensitisation for Ca^{2+} in the absence of $G_{\alpha s}$. (C) AC5 and AC6 are negatively regulated by PKA and $G_{\alpha i/o}$. However, persistent activation leads to sensitisation of these isoforms in a $\beta\gamma$ subunit dependent manner, which may involve Raf1-dependent phosphorylation. (D) AC2, in the presence of $G_{\alpha s}$ and or activators of PKC, shows conditional activation by $G_{\beta\gamma}$ (Watts and Neve, 2005).

Alterations in adenyl cyclase can affect numerous protein signalling systems, and the degree of mediation may be cell line or tissue specific (Christie, 2008). For instance, in noradrenergic neurones of the LC, increased production of cAMP leads to amplified phosphorylation of PKA and the transcription factor CREB (Figure 1.13). CREB

protein is known to affect the synthesis of a large number of neurotransmitter receptors, AC isoforms, as well as other signalling proteins, with the net result of CREB's up-regulation leading to an increase in neuronal excitability, *in vivo* (Carlezon et al., 2005, Han et al., 2006). Within the PAG, elevation of increased cAMP and protein kinase A signalling, during opioid withdrawal, leads to the opening of cation channels, usually inhibited by MOP in acute settings, and hyperexcitation (Bagley et al., 2005a). The links between this cation channel and GABA transporter type 1 and studies using c-fos suggest that opioid-sensitive GABAergic neurons are the focal point of opioid withdrawal in the PAG (Hacker et al., 2006, Bagley et al., 2005b). Increase in GABAergic neurotransmission is also noted in the ventral tegmental area (VTA), nucleus accumbens (NA) and RVM, indicating PKA-mediated phosphorylation of GABAergic vesicles (Ma and Pan, 2006, Chieng and Christie, 1996, Bonci and Williams, 1997, Ford et al., 2006).

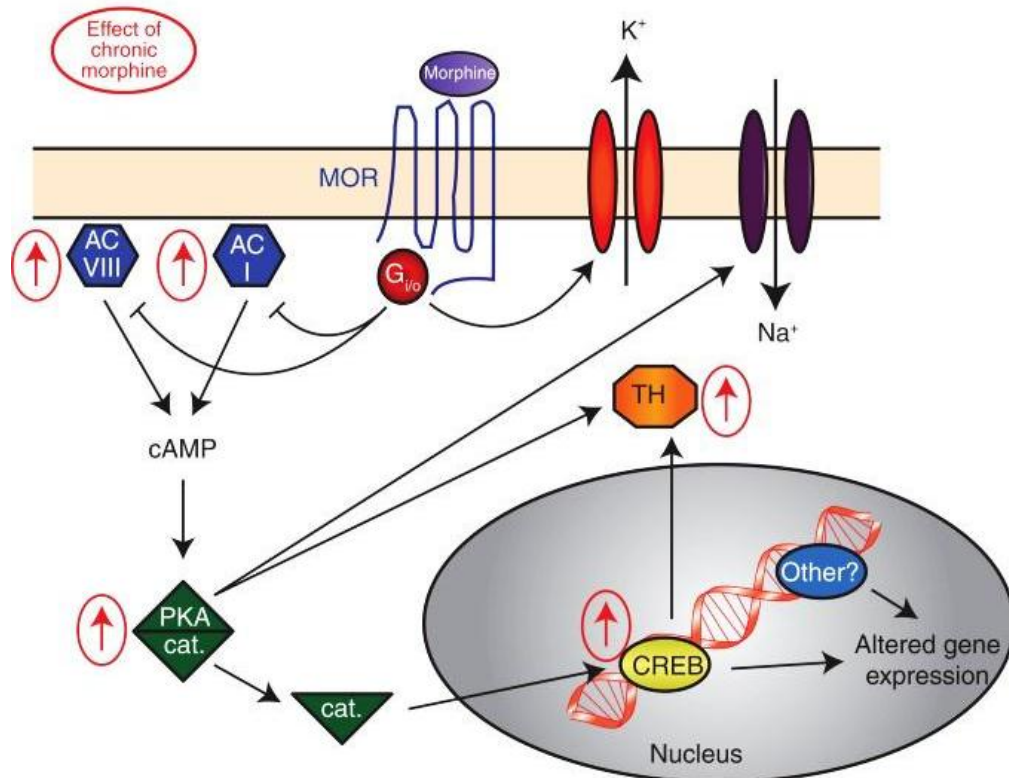


Figure 1.13: The acute actions of opioid in locus coeruleus (LC) neurons lead to inhibition of the cAMP pathway, which in turn affects numerous other neuronal processes, such as a reduction in CREB phosphorylation and activity. This in turn leads to the initiation of some of the long-term changes in LC function. Chronic Morphine use leads to increased levels of adenylyl cyclase I and VIII, as well as PKA catalytic (cat) and regulatory subunits. This in turn leads to increased activation of numerous phosphoproteins including CREB and tyrosine hydroxylase. These changes in activity lead to a change in LC which facilitates drug dependence. Abbreviations; MOR (Mu Opioid Receptor); TH (Tyrosine Hydroxylase) (Mazei-Robison and Nestler, 2012).

The MAPK pathway has also shown adaptive changes to prolonged opioid use (Figure 1.14). In SH-SY5Y cells, prolonged exposure to Morphine led to a decrease in activity of phosphorylated-ERK 1/2 (p-ERK), which rebounded strongly after Morphine withdrawal (Bilecki et al., 2005). These findings were matched *in vivo*, with chronic Morphine treatment reducing p-ERK levels in the nucleus accumbens of mice and rats, the mouse central amygdala and human hypothalamic nuclei, cerebral cortex and median eminence (Schulz and Holtt, 1998, Ferrer-Alcon et al., 2004, Muller and Unterwald, 2004, Li et al., 2008). Morphine withdrawal leads to upregulation of p-ERK in rat nucleus accumbens and lateral septum, mirroring *in vitro* findings (Ciccarelli et al., 2013). However, levels of p-ERK have also been found to increase during chronic Morphine use and withdrawal, with increased levels shown in the rat LC as well as the

mouse frontal cortex, hippocampus and striatum, indicating site-specific activation of the ERK pathway in chronic opioid use and withdrawal (Chen and Sommer, 2009, Li et al., 2008). At the level of the spinal cord, p-ERK activity is increased during chronic Morphine use in rat dorsal horn neurons, with levels rising further after naloxone-precipitated withdrawal (Cao et al., 2005, Cao et al., 2006). Contrasting results have been found, demonstrating increased p-ERK and p38 MAPK activity in astrocytes, via opioid induced synthesis of calcitonin gene-related peptide (CGRP) and subsequent activation of the CGRP receptor (Wang et al., 2009). These contrasting results may be explained by differential routes of administration and drug dosage, with the former study using intrathecal routes and a steady concentration of 15 µg/day for 5 days and the latter subcutaneous administration and escalating doses of 10-50 mg over 7 days (Chen and Sommer, 2009). Further work in this area has shown increased p-ERK activity during prolonged Morphine treatment in neurons *in vivo* and in cultured dorsal root ganglia (Ma et al., 2001, Almela et al., 2009).

With regards to p38 MAPK activation, phosphorylation of this kinase was shown to increase in rat spinal immunoreactive cells after 3 days of intrathecal (i.t) Morphine administration, which was not matched by acute Morphine administration (Cui et al., 2006). However, it has been shown that Morphine, failed to phosphorylate p38 in cultured dorsal root ganglion cells, whereas DAMGO caused significant up-regulation of this kinase pathway (Tan et al., 2009a). These contradictory findings would suggest that more than one opioid should be evaluated in order to assess any biased agonism with regards to p38 signalling, before its role in dependence can be fully understood.

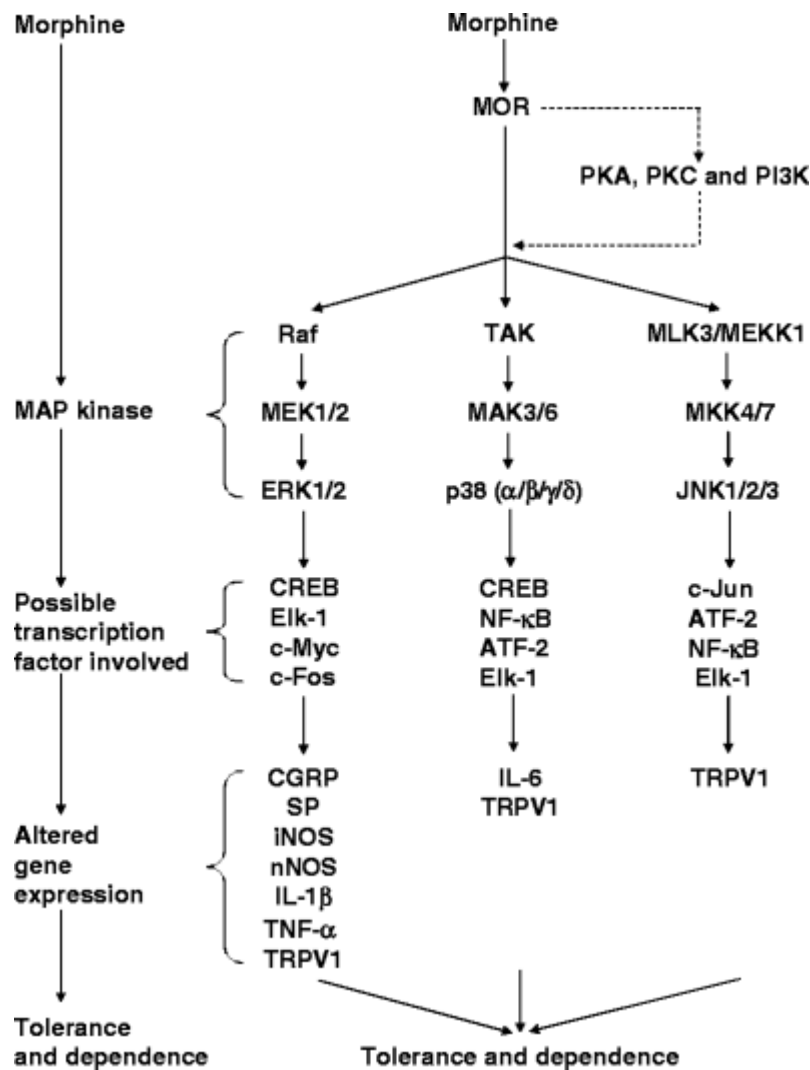


Figure 1.14: The MAPK pathway and its role in the development of dependence and tolerance. Prolonged use of opioids leads to the activation of the MAPK pathway, which includes ERK1/2, p38 and JNK. Activation can occur through a number of mediators. PKA, PKC and phosphatidylinositol 3-kinase (PI3K) are all thought to mediate MAPK function. Beta-arrestin recruitment to the receptor also leads to activation of this kinase cascade. Following activation and nuclear translocation, MAPKs interact with various transcription factors, which in turn leads to enhanced expression of downstream effectors (Chen and Sommer, 2009).

1.4.5 Opioid reinforcement and addiction

Addiction to opioids is likely a result of complex neurobiological changes, involving dopaminergic pathways of reward. The release of GABAergic tone through MOP receptor activation, leads to up-regulation of dopamine release in the mesolimbic pathway (beginning in the VTA and connecting with the limbic system via the nucleus accumbens, the amygdala, and the hippocampus as well as to the medial prefrontal cortex – demonstrated in Figure 1.15) (Koob and Volkow, 2010, Le Merrer et al.,

2009). Long-term use of opioids can lead to synaptic plasticity and cellular adaptations in both the VTA and locus coeruleus (Mazei-Robison and Nestler, 2012). Due to its role in reward, the VTA has become a focal point for the study of opioid addiction. The VTA is rich in dopaminergic neurons, whilst also containing a significant number of GABA neurons and a small number of glutamatergic neurons (Sesack and Grace, 2010, Mazei-Robison and Nestler, 2012). These changes in neural activity are reciprocated, in an acute setting, with regards to synaptic plasticity. A single dose of Morphine leads to an increase of α -amino-3-hydroxy-5-methyl-4-isoxazolepropionic acid (AMPA) postsynaptic excitatory currents when compared to N-methyl-D-aspartic acid (NMDA) receptors, 24 hours after administration. This change is consistent with long term potentiation (LTP) of glutamatergic synapses on to dopaminergic neurones (Saal et al., 2003). Acute administration of opioids also leads to disruption of LTP in GABAergic neurons, by interfering with the activation of protein kinase G, and the increase in dopaminergic neuron activity (Nestler, 2012).

These cellular adaptations have been confirmed by a large number of animal model studies whereby conditioned place preference or intra-cerebral self-administration have implicated the VTA in opioid reinforcement (Le Merrer et al., 2009, McBride et al., 1999). Activation of the MOP receptor appears to be the critical factor in the development of addiction, with regards to the VTA, as MOP knockout mice (but not wild-type or DOP KO mice) did not self-administer Morphine into the VTA (David et al., 2008). Within the nucleus accumbens, it would appear that interplay between dopamine receptors and MOP have a roll in reinforcing drug-seeking behaviour, as proved by the dose-dependent decrease in self-administration of speedball (heroin and cocaine) when CTOP (MOP antagonist), SCH23390 (D1 dopamine receptor antagonist) and raclopride (D2 dopamine receptor antagonist) were injected into the nucleus accumbens (Cornish et al., 2005). Understanding the complex cellular and structural adaptations leading to opioid addiction remains a challenging prospect.

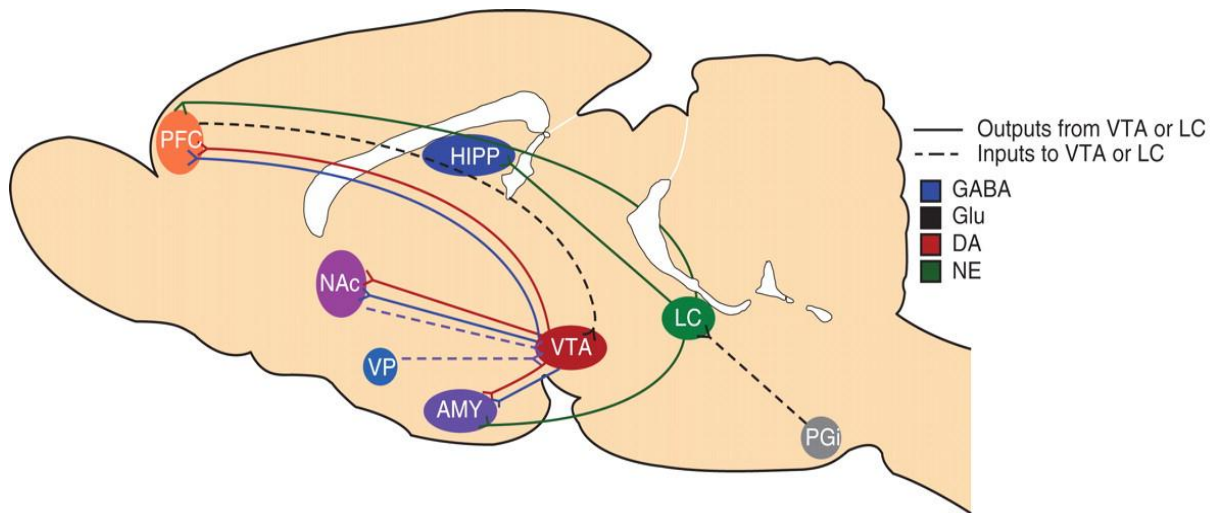


Figure 1.15: Sagittal section of a rodent brain, highlighting the locus coeruleus and ventral tegmental area, as well as their afferent and efferent projections. Dopaminergic (red) and GABAergic (blue) neurons in the VTA project to cortical and limbic area and are innervated by GABAergic (blue dash) neurones from the nucleus accumbens and prefrontal cortex as well as glutamatergic (black-dash)neurones from the prefrontal cortex. The locus coeruleus projects a number of noradrenergic neurons (green) to areas such as the hippocampus and prefrontal cortex. It receives glutamatergic input from the nucleus paragigantocellularis. Abbreviations: AMY, amygdala; HIPP, hippocampus; LC, locus coeruleus; NAc, nucleus accumbens; PFC, prefrontal cortex; PGi, nucleus paragigantocellularis; VP, ventral pallidum; VTA, ventral tegmental area (Mazei-Robison and Nestler, 2012)

1.4.6 *Role of other members of the opioid family in tolerance, dependence and addiction*

The role of the DOP receptor in the development of tolerance was first suggested by Abdelhamid and colleagues (1991), in experiments involving the co-administration of Morphine and the DOP antagonist, Naltrindole. In these experiments, mice were administered Naltrindole both before and during treatment with 100mg/kg Morphine sulphate. The results showed a marked decrease in the development of Morphine tolerance (Abdelhamid et al., 1991). The involvement of DOP was further validated by studies of DOR-1 knockout mice, missing exon 2, in which analgesic tolerance failed to occur (Zhu et al., 1999). In further studies involving these DOP receptor knockout mice or a DOP antisense oligodeoxynucleotide, an arrest in the development of dependence was seen (Kest et al., 1996, Sanchez-Blazquez et al., 1997, Zhu et al., 1999). Furthermore, studies in preproenkephalin knockout mice, which encodes the gene for the DOP-selective Leu-Enkephalin, also showed an attenuation of tolerance indicating activation of DOP is required for this process to occur (Nitsche et al., 2002). The

interactions between MOP and DOP are believed to be based on heterodimerisation, the physical association of two GPCR's to form a single functional unit, which will be further expanded upon in section 1.4.7 (Prinster et al., 2005).

The NOP receptor was implicated in tolerance, after studies in mice lacking the NOP receptor gene showed partial loss of tolerance to Morphine (Ueda et al., 1997). These findings were rebuked when Kest and colleagues demonstrated no difference in the onset of tolerance in NOP knockout mice when compared to wild type controls, or showed a limited ability to halt tolerance (Kest et al., 2001). Further experiments have showed mixed results with some studies displaying attenuation tolerance in both knockout mice and wild type mice and pre-treatment with the NOP antagonist, J-113397, however this tolerance may be site-directed as intrathecal injections delayed tolerance while intracerebroventricular injections failed to halt the development of tolerance (Ueda et al., 2000). This was corroborated by studies involving N/OFQ knockout mice, whereby loss of N/OFQ delayed the onset of tolerance in mice injected with 10mg/kg of Morphine for 3 weeks. In the same study, the NOP non-peptide antagonist J-113397, was co-administered with Morphine, leading to an attenuation of tolerance (Chung et al., 2006). While evidence would suggest there is a link between NOP and MOP in the development tolerance, the interplay between the receptors remains to be determined, with receptor heterodimerisation, or neuronal adaptations via the influence of NOP proving to be the most likely theories.

1.4.7 *MOP/DOP heterodimers in tolerance*

As previously mentioned, the role of DOP in tolerance has been studied extensively, with a large body of evidence leading to the belief that MOP and DOP are co-expressed as a heterodimers. Bioluminescence resonance energy transfer (BRET) studies provided evidence for MOP and DOP being expressed in close proximity to one another on the cell surface (Gomes et al., 2004, Gomes et al., 2000). From a structural standpoint, while the MOP/DOP heterodimer has not been crystallised, *in silico* studies have postulated that the physical interaction between MOP and DOP is likely to occur at TM1 (transmembrane domain 1) of MOP and TM4 of DOP (Filizola et al., 2002, Liu et al., 2009).

Furthermore, the possibility of MOP-DOP heterodimer occurring *in vivo* was greatly enhanced through the discovery that both receptors are co-localized on the dorsal root ganglia and, furthermore, on the same axonal terminals of the superficial dorsal horn neurons (Rau et al., 2005, Cheng et al., 1997). Studies using immunoelectron microscopy or epitope-tagged receptors have shown that DOP receptors are localised in large dense-core vesicles (LDCVs) in both dorsal root ganglion and PAG neurons, with low expression on the cell surface (Figure 1.16). The cell surface expression levels of DOP change with an increase in Morphine use, implying that DOP receptor trafficking to the receptor surface is increased, thus increasing the potential for the formation of MOP-DOP heterodimers (Zhang et al., 2006).

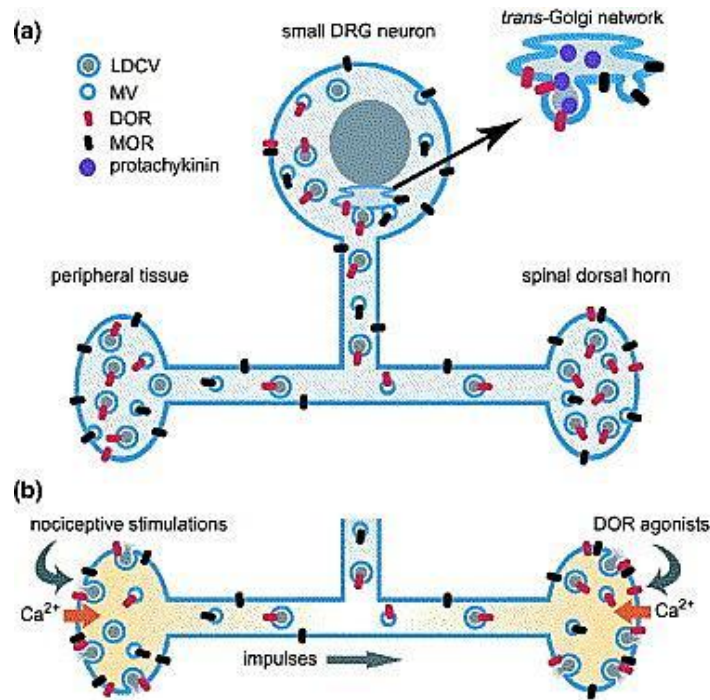


Figure 1.16: Potential models of stimulus-induced surface expression of DOP in small dorsal root ganglia neurons (DRG). (A) DOP receptors are sorted into low density core vesicles (LDCV) in the cell body of the small DRG neuron via direct interaction with protachykinin in the *trans*Golgi network. A limited number of MOP and DOP receptors are sorted into microvesicles in a constitutive secretory pathway. Both receptors in the microvesicles and LDCVs are transported to peripheral terminals in peripheral tissue, as well as to the central terminals in the superficial dorsal horn of the spinal cord. The DOP receptors transported via the LDCVs are stored in the cytoplasm, whilst those transported with MOP in the microvesicles are spontaneously inserted into the plasma membrane. (B) Nociceptive stimuli lead to an increase in levels of Ca^{2+} which, in turn, leads to LDCV secretion. This results in DOP receptor insertion in the membrane. Dorsal horn neuronal release of enkephalins, or intrathecal DOP receptor agonists, trigger Ca^{2+} -store-induced Ca^{2+} entry to induce the surface expression of DOP receptors in the central terminals (Zhang et al., 2006).

Contrary to previous findings, the ability of these heterodimers to form in the DRG was called into question after a study was presented in which knock-in mice expressing a DOP receptor, fused with green fluorescent protein (GFP) detected this receptor in approximately 5% of DRG neurones, instead locating them on different subsets of primary afferents to that of the MOP receptor (Scherrer et al., 2009). These knock-in mice experiments also showed that, contrary to previous studies, the DOP receptor is trafficked to the cell surface under resting conditions, rather than being stored in LDCV's (Scherrer et al., 2009). In response to these findings a number of studies were published using multiple methods demonstrating the co-expression of MOP and DOP in the neurones of the pain pathway. DOP receptors have been shown to be co-

expressed in both large and small DRG neurones as well as in the dendrites of the striatum using *in situ*, single cell polymerase chain reaction experiments (PCR) and immunostaining, as well as electrophysiological studies showing a reduction in depolarisation-induced calcium currents for both MOP and DOP agonists in small DRG neurones (Wang et al., 2010, Fujita et al., 2014). The contrasting results of the DOP-GFP-tagged mouse model are believed to be the result of overexpression of the GFP-tagged receptor, as demonstrated in PC12 cell lines where the native DOP receptors were mainly located in the LDCV, whereas tagged DOP receptors displayed varying degrees of cell surface expression (Wang et al., 2008). Furthermore, increased expression of DOP leads to a decrease in expression of MOP, leading to bias in the detection of DOP over MOP (Ong and Cahill, 2014). More recently, GFP-tagged MOP and DOP receptors have been shown to have high co-expression levels within the RVM, spinal cord and DRG's, providing more evidence for the formation of heterodimers (Figure 1.17) (Erbs et al., 2014).

The expression of a MOP/DOP heterodimer within neurones of the pain pathway led to speculations of its involvement in the development of tolerance. Initially, it was understood that DOP expression was increased in chronic opioid use (Chieng and Christie, 2009, Gendron et al., 2006, Cahill et al., 2001), however it is now thought that the increase in DOP receptors is more likely due to increased expression of the MOP/DOP heterodimer after chronic treatment with opioids (Gupta et al., 2010). Heterodimer expression is regulated by its own chaperone protein, receptor transporter protein 4 (RTP4) (Figure 1.18). RTP4 protects the heterodimer from ubiquitination, thereby increasing abundance at the cell surface (Décaillot et al., 2008).

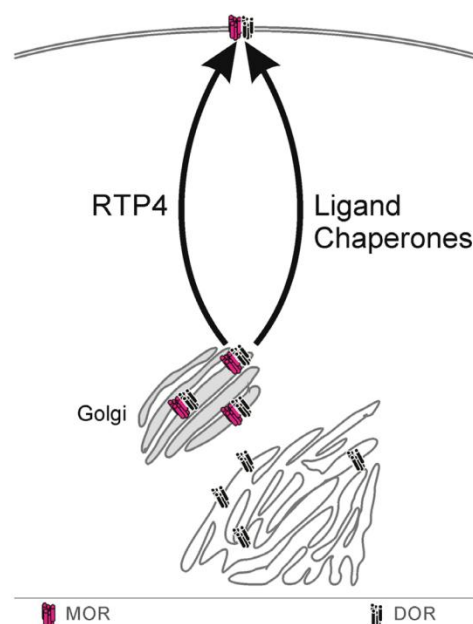


Figure 1.18: Selective transport of MOP/DOP heterodimers by the chaperone RTP4 (Ong and Cahill, 2014).

Formation of the heterodimer has direct effects on the development of tolerance. In studies in which disruption of the heterodimer occurs, it is demonstrated that the DOP receptor preferentially directs the heterodimer to the degradation pathway after internalisation. When the heterodimer was disrupted, via alteration of the MOP receptor to express duplicate TM3 (and deletion of TM1), the MOP receptor showed increased recycling to the cell surface (He et al., 2011). The ability of the heterodimer to internalise and enter the post-endocytotic pathway, however, has been questioned. The co-internalisation of MOP and DOP was demonstrated in response to agonist exposure in experiments, using immunolabelled MOP and DOP receptors expressed in HEK-293

(human embryo kidney) cells (He et al., 2002). Administration of either DAMGO ([D-Ala², N-MePhe⁴, Gly-ol]-enkephalin), or the DOP agonist's Deltorphin-I, Deltorphin-II and SNC80 led to internalisation of both receptors to a similar location within the cell. Moreover, immunoblotting demonstrated that deltorphin-I increased the co-localisation of MOP and DOP to lysosome-like organelles and caused an increase in ubiquitination, which was not demonstrated following administration of DAMGO (He et al., 2002). In a contrasting experiment, it was demonstrated that methadone produced MOP/DOP internalisation and degradation, demonstrating the ability of a MOP agonist to cause degradation. The opposing findings could be due to the types of drugs used, or that MOP/DOP heterodimers are not so easily pigeonholed with regards to which receptor selectively chooses a receptor trafficking pathway (Ong and Cahill, 2014).

From a signalling perspective, the heterodimer shows pharmacologically distinct ligand binding and activation when compared to either receptor alone (Fan et al., 2005). For instance, BRET studies demonstrated that the MOP/DOP heterodimer preferentially coupled to the pertussis toxin insensitive G-protein, G_{αz} (Hasbi et al., 2007). Interestingly, G_{αz} knock-out mice produce hyper-tolerance to Morphine (Leck et al., 2004, Hendry et al., 2000). G_{αz} signalling may positively influence the attenuation of tolerance; however evidence suggests that the MOP/DOP heterodimer is favourably biased towards β-arrestin signalling. Rozenfeld *et al* (2007) demonstrated that constitutive recruitment of β-arrestins is increased by the heterodimerisation of MOP and DOP. In response to the formation of this receptor-arrestin complex, the spatio-temporal regulation of ERK 1/2 is changed (Rozenfeld and Devi, 2007). There is a time-delay in the activation of ERK 1/2, indicating a shift from PKC-dependent activation to β-arrestin mediated activation (Rozenfeld and Devi, 2007). The delay in activity of ERK 1/2 and its effects on the development of tolerance remain unclear.

In regards to the development of tolerance, the increased expression of MOP/DOP heterodimers, as well as their effects on signalling and receptor recycling makes them suitable targets for dual drug therapy for the delay of opioid tolerance. Numerous mixed molecules have been developed to target this heterodimer. The MDAN series of compounds, which linked a **MOP** agonist (oxymorphone) to a **DOP antagonist**, provided a large body of evidence supporting both the existence of heterodimers and structural requirements for developing a bivalent pharmacophore (Daniels et al., 2005).

In mouse model experiments, it was shown that MDAN molecules with linkers of 19 atoms or greater produced an attenuation of tolerance and dependence. The most potent compound, MDAN-21 (linker distance 21 atoms) had 50-fold higher potency than Morphine, with a reduced side effect profile (Daniels et al., 2005). The effects of linker length would indicate that physical interaction between MOP and DOP is responsible for mediating MOP tolerance and dependence. However, inconsistent results in experiments involving rhesus monkeys, indicated that MDAN-21 may struggle to cross the blood brain barrier in higher primates or provide the tolerance seen in mice and rats (Aceto et al., 2012). These experiments highlighted the need for choice in the size of the compound as well as the properties of the molecules for ligation. Numerous MOP agonist/DOP antagonist bifunctional molecules have been developed. DIPP-NH(2)[Psi], a peptidic molecule, was shown to act as a potent analgesic in rat tail flick assays, while showing no development of dependence or tolerance in an acute setting. The compound also showed subnanomolar binding affinities for both MOP and DOP (Schiller et al., 1999). More recently, UFP-505 (a bifunctional molecule) was shown to act as a potent DOP antagonist, while demonstrating similar potency to Morphine (Dietis et al., 2012). The actions of MOP/DOP mixed ligands highlights the role DOP plays in tolerance and dependence.

1.4.8 *NOP and addiction*

Numerous studies have detailed the ability of NOP to block the rewarding properties of opioids, such as Morphine and Heroin, curtailing the addictive tendencies of these drugs (Ciccocioppo et al., 2000, Di Giannuario and Pieretti, 2000, Murphy and Maidment, 1999). This is represented by NOP expression within multiple regions of the brain associated with the reward pathways. This includes expression in the mesolimbic pathway regions including the VTA and nucleus accumbens (Zaveri, 2011, Neal et al., 1999b, Neal et al., 1999a). Within these regions, NOP activity leads to a decrease in basal and drug induced dopamine release. Furthermore, presynaptic NOP receptor activation in the nucleus accumbens or striatum inhibits tyrosine hydroxylase and, therefore, dopamine synthesis or it can act post-synaptically to down-regulate dopamine D₁ receptors (Olianas et al., 2008). The net results of NOP activity in these neurones is an inhibitory effect on dopamine release. A number of opioids with addictive properties, such as heroin and Morphine, were co-administered with the NOP-selective

synthetic agonist Ro65-6570 in rats undertaking conditioned place preference (CPP) tasks. These studies are used to determine the reinforcing properties of drugs. The resulting study demonstrated that higher concentrations of Morphine and heroin were required to produce CPP in the presence of Ro65-6570 (Rutten et al., 2010). Furthermore, NOP knockout rats were more sensitive to the rewarding properties of Morphine than W/T rats (Rutten et al., 2011). NOP receptor stimulation has also been shown to be beneficial in non-opioid addictive states such as alcohol or cocaine addiction (Ciccocioppo et al., 2003, Sakoori and Murphy, 2008). The location of the NOP receptor within dopaminergic neurones of the reward pathway, and its inhibitory effects on these rewarding pathways, makes it an ideal target to study with regards to anti-addictive drug therapy.

1.4.9 *MOP and NOP interactions in tolerance*

The NOP receptor has demonstrated an ability to delay the onset of tolerance. While substantial evidence points to the direct interactions of MOP and DOP mediating opioid tolerance, the interactions of NOP in regards to the development of tolerance are still unclear. Both the formation of MOP-NOP heterodimers, or NOP mediated changes in pain pathway plasticity are potential candidates for the attenuation of tolerance and dependence via NOP. In regards to the potential formation of a MOP-NOP heterodimer, both MOP and NOP receptors have been shown to co-localise *in vitro* (Figure 1.19), a core requirement of the formation of a heterodimer. The surface expression of NOP was also affected by MOP internalisation, suggesting a physical interaction between the two receptors (Pan et al., 2002, Evans et al., 2010, Wang et al., 2005).

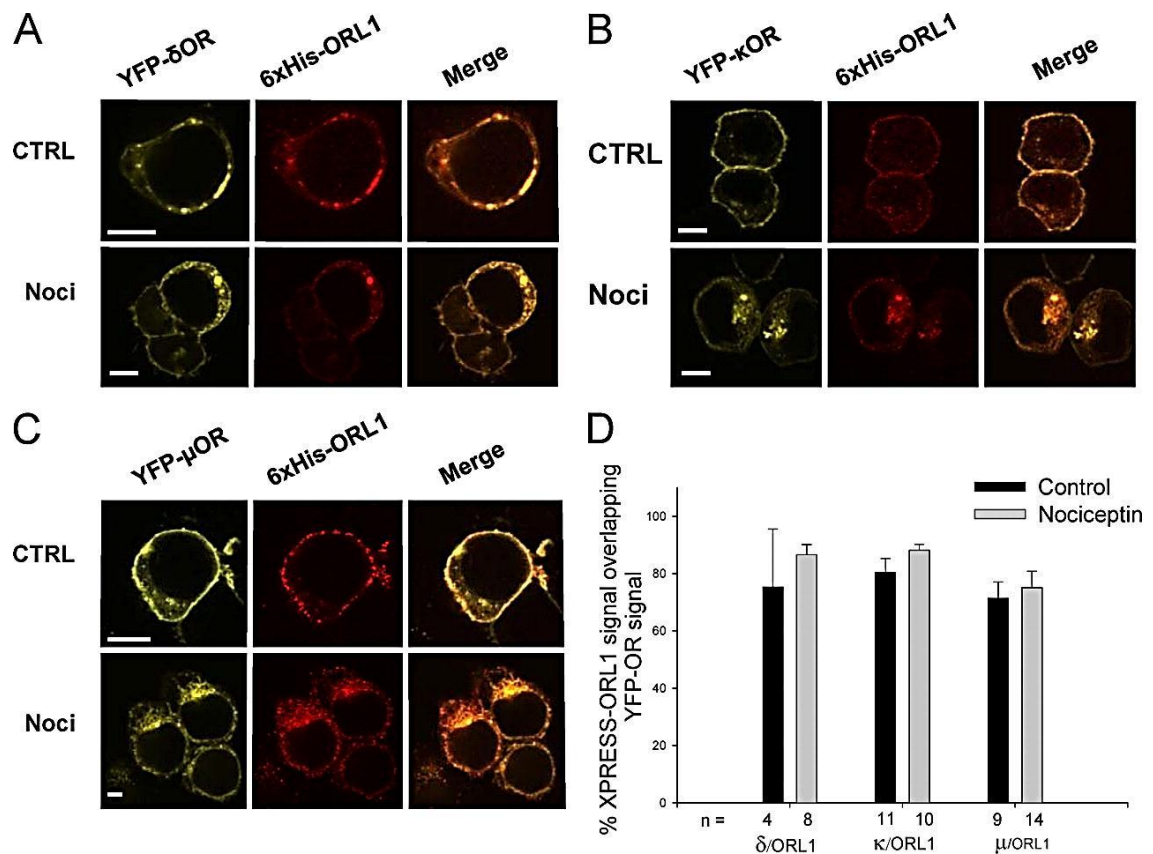


Figure 1.19: Confocal images of tsA-201 cells coexpressing His₆/XPRESS-tagged NOP receptors (shown in red above) and YFP-tagged DOP (A), KOP (B) or MOP (C) receptors, under control conditions or 30 minute N/OFQ treatment. The graph (D) depicts the percentage overlap of His₆/XPRESS-tagged NOP and the YFP-tagged opioids (Evans et al., 2010).

Evans and colleagues also demonstrated that NOP is co-localised with both DOP and KOP (Figure 1.19), indicating its potential ability to form dimers with all members of the classical opioid family (Evans et al., 2010). The dimerization of MOP and NOP is believed to occur via the interactions of both receptors C-termini (Wang et al., 2005). On a cellular level, it would appear that NOP receptor activity can lead to cross-desensitisation of MOP, with the MOP/NOP heterodimer having decreased efficacy after activation via the potent MOP agonist DAMGO (Khroyan et al., 2009b, Wang et al., 2005). Furthermore, the ability of MOP to stimulate ERK 1/2 was diminished in the presence of NOP (Wang et al., 2005).

While cellular studies have provided strong evidence for co-expression and heterodimerisation, *in vivo* studies demonstrated conflicting results. Initial studies, using immunohistochemistry in rodents, demonstrated that while MOP and NOP had over-lapping distributions, they did not co-localise in the pain processing pathways

(Monteillet-Agius et al., 1998, Schulz et al., 1996). However, due to doubts about the specificity of the NOP antibody, further studies were undertaken, which demonstrated co-localisation of MOP and NOP in rat DRG neurons as well as co-expression and heterodimerisation in human neuroblastoma cells (Mandyam et al., 2003, Abdulla and Smith, 1998). Interestingly, studies of the rat RVM demonstrated that MOP and NOP are co-expressed on ON cells, while only NOP receptors are expressed on OFF cells (Vaughan et al., 2001, Pan et al., 2000). Work in non-human primates (NHPs) has demonstrated, that antinociception induced by spinally administered Morphine is potentiated by co-administration of N/OFQ (Ko and Naughton, 2009). The administration of either N/OFQ or a NOP antagonist has led to varying success in the attenuation of tolerance. Due to its complex involvement in opposing cells of the pain pathway, the mechanisms by which NOP affects the development of tolerance at MOP requires further study.

The evidence provided by animal studies has led to an increased interest in mixed MOP/NOP ligands, with the focus falling on dual agonism of these receptors. A number of studies have illustrated improved analgesia, reduced tolerance and dependence as well as increased ability to halt neuropathic pain, which MOP selective agonists fail to treat (Spagnolo et al., 2008, Khroyan et al., 2009a, Sukhtankar et al., 2013). The most comprehensive study of mixed MOP/NOP agonist activity, involves the novel bifunctional non-peptide Cebranopadol. The drug displays subnanomolar affinity at MOP and NOP, while providing full agonist activity at MOP and high partial agonist activity at NOP. Cebranopadol displayed a long duration of action, with potent analgesia in both acute and chronic pain states in rats. Side-effects of the drug, when compared to standard opioids, were significantly reduced. Motor co-ordination and respiratory processes were unaffected by high doses of cebranopadol. Tolerance to the drug was delayed in comparison to Morphine, taking 26 days of constant dosing to appear, whereas Morphine tolerance appeared within 11 days (Linz et al., 2014). These results demonstrate a unique target for prolonged, potent analgesics with a reduced side effect profile. The development of MOP/NOP agonists and MOP agonists/NOP antagonists, would allow for the cellular processes and interactions of these two receptors to be studied in greater detail.

1.5 Fentanyl Derivatives

As mentioned in section 1.2.12, Fentanyl (a member of the phenylpiperidine series of synthetic opioids) is a potent MOP agonist, which provides strong analgesia when used therapeutically (Stanley, 1992). As Fentanyl is a synthetic opioid (Figure 1.20), it has a molecular structure which is different to that of opioids derived from Morphine. When administered to combat acute pain, Fentanyl can be delivered through multiple methods including: intravenous; buccal; epidural; intrathecal or inhalation. In cases involving chronic pain, Fentanyl is often administered as a transdermal patch (Nelson and Schwaner, 2009). While Fentanyl does have a higher potency than Morphine (approximately, 75-100 times greater), the introduction of tolerance, as well as most other negative effects associated with prolonged opioid use, occurs at an increased rate (Martini and Whistler, 2007). The ability of Fentanyl to provide potent analgesia through a variety of therapeutic routes (following many years of clinical development) makes it an ideal opioid to be used in a bivalent pharmacophore, as reducing its ability to induce tolerance will provide a potent and effective analgesic.

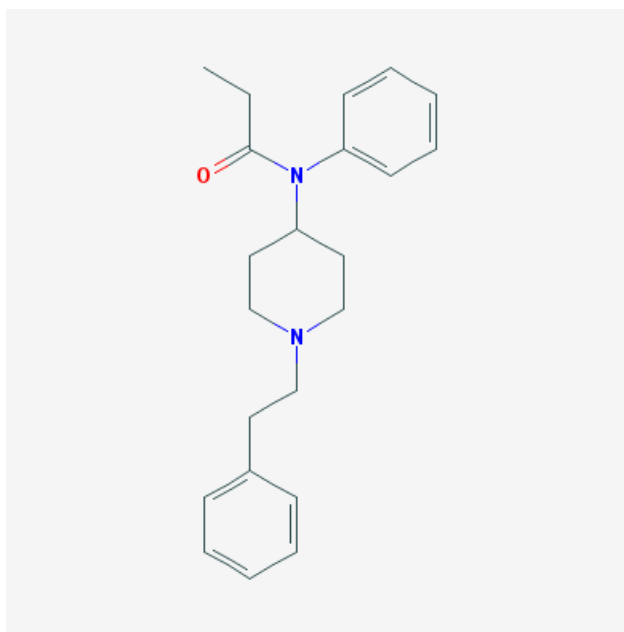


Figure 1.20: The chemical structure of Fentanyl (Stanley, 1992).

1.6 The F-compound series of ligands (synthesised by Dr R. Vardanyan and Dr R Guerrini)

Fentanyl is an ideal drug to use as the opioid agonist in a bivalent pharmacophore. A series of conjugates, labelled the F-compound series, have been formed linking Fentanyl with Dmt-Tic (2' 6'-dimethyl-*L*-tyrosyl-1,2,3,4-tetrahydroisoquinoline-3-carboxylic acid). The Dmt-Tic pharmacophore is a high-affinity DOP receptor antagonist, which also has a high selectivity for the DOP receptor (Salvadori et al., 1997). These two pharmacophores have been 'glued' together using three unique linker molecules. The first pharmacophore contains a linker which has two carbon atoms as a spacer, and will be referred to as the #4 compound from here on. The second compound contains three carbon atoms, which increases the distance between the pharmacophores, and will be further known as the #5 compound. The associated three carbon atom Fentanyl pharmacophore (#2) has demonstrated functional activity *in vivo*, when conjugated with Leu-Enkephalin (Podolsky et al., 2013). The third compound (#6) contains an oxygen atom in the linker molecule which can lead to further interactions through hydrogen bonding. When a molecule contains large groups, these groups may prevent chemical reactions when compared to related molecules that contain smaller groups, with this phenomenon being referred to as steric hindrance. Steric hindrance can be used to stop unwanted side-reactions, thereby changing the reactivity pattern of a molecule(s) (Weinhold, 2001). The final sets of MOP-DOP compounds are adaptations of #6, whereby either one (#7) or two glycine molecules (#8) have been added in order to test the effects of linker length on the pharmacophores (Table 1.4). Further Fentanyl derivatives (named RR4-RR9), with extended linker molecules in the northern hemisphere of the Fentanyl structure, were developed, with compounds of interest in this group conjugated with the NOP agonist, Ro65-6570. Three compounds were synthesised and called MN1, MN2 and MN3 (Figure 1.21). *These ligands were synthesised and provided to us by Dr Ruben Vardanyan (University of Arizona), Dr Remo Guerrini and Dr Claudio Trapella (University of Ferrara).*

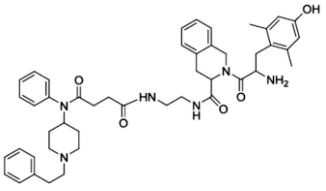
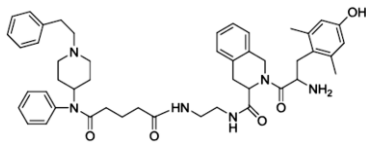
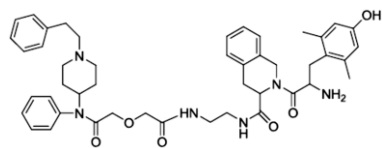
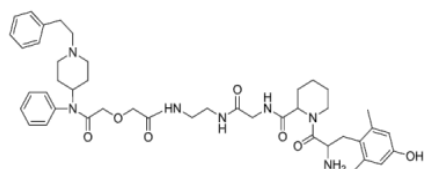
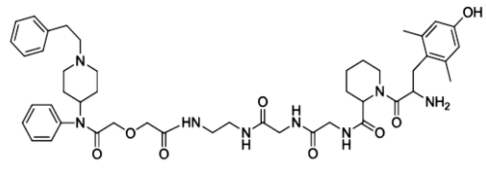
Structure	Compound #
	#4
	#5
	#6
	#7
	#8

Table 1.4. The chemical structure of the [Fentanyl]-[Dmt-Tic] analogues. The nomenclature used in the thesis for the compounds is shown in the right hand column.

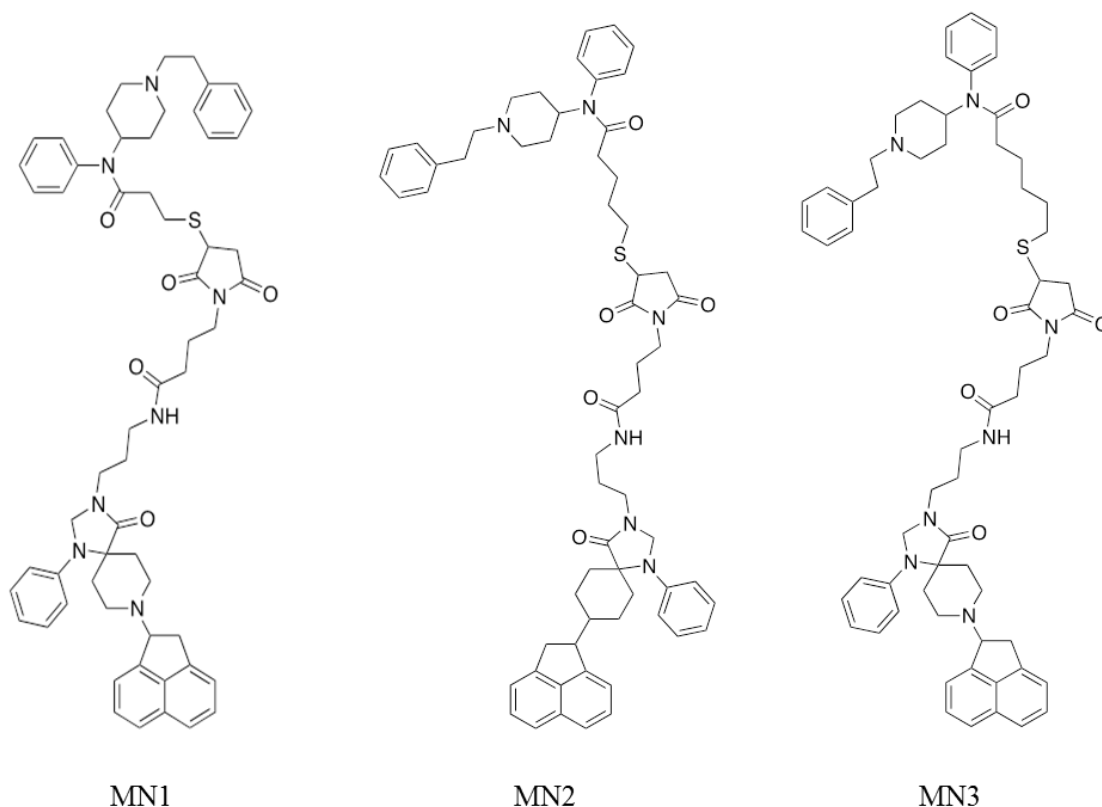


Figure 1.21: The MOP-NOP (MN) bivalent compounds based on the conjugation of Fentanyl and Ro-65-6570.

1.7 PWT derivatives

Opioid peptides have proven to have lower side-effect profiles than synthetic analogues, however limitations such as degradation by peptidases limits their use in the clinical setting (Janecka et al., 2010). A novel chemical technique, termed protein welding technology (PWT), allows four peptides to be joined together around a scaffold structure (Figure 1.22) (Guerrini et al., 2014). We will determine how this process affects the binding and functional activity of N/OFQ and Leu-Enkephalin. *These compounds were synthesised by Dr Guerrini (University of Ferrara).*

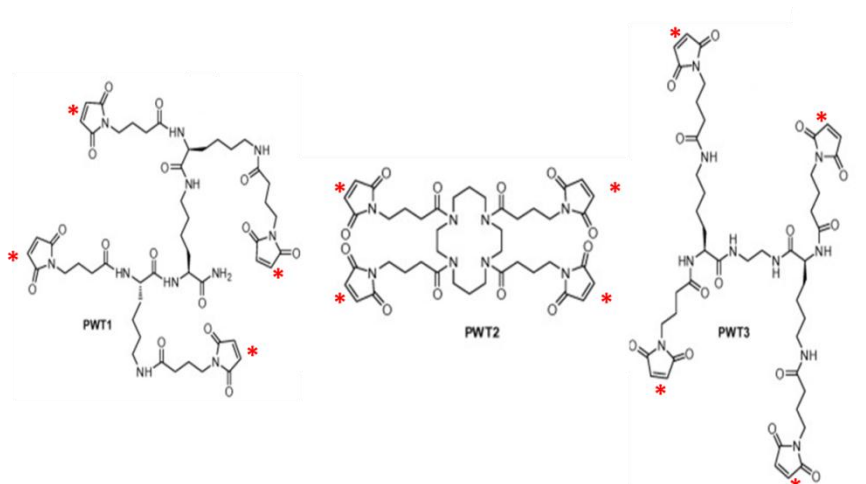


Figure 1.22: The PWT1, PWT2 and PWT3 core molecules. The sections indicated with (*), are the conjugation points for the protein of interest (Guerrini et al., 2014).

1.8 Dermorphin-N/OFQ and Dermorphin-UFP-101

In order to study the interactions between MOP and NOP, two novel Dermorphin peptidic pharmacophores have been synthesised. Dermorphin is a peptide originally isolated from the skin of South America frogs, from the genus *Phyllomedusa* (Melchiorri and Negri, 1996). It is a potent MOP agonist. Either N/OFQ (Figure 1.23) or the antagonist, UFP-101 (Figure 1.24), have been conjugated with Dermorphin. *These compounds were synthesised by Dr Guerrini (University of Ferrara).*

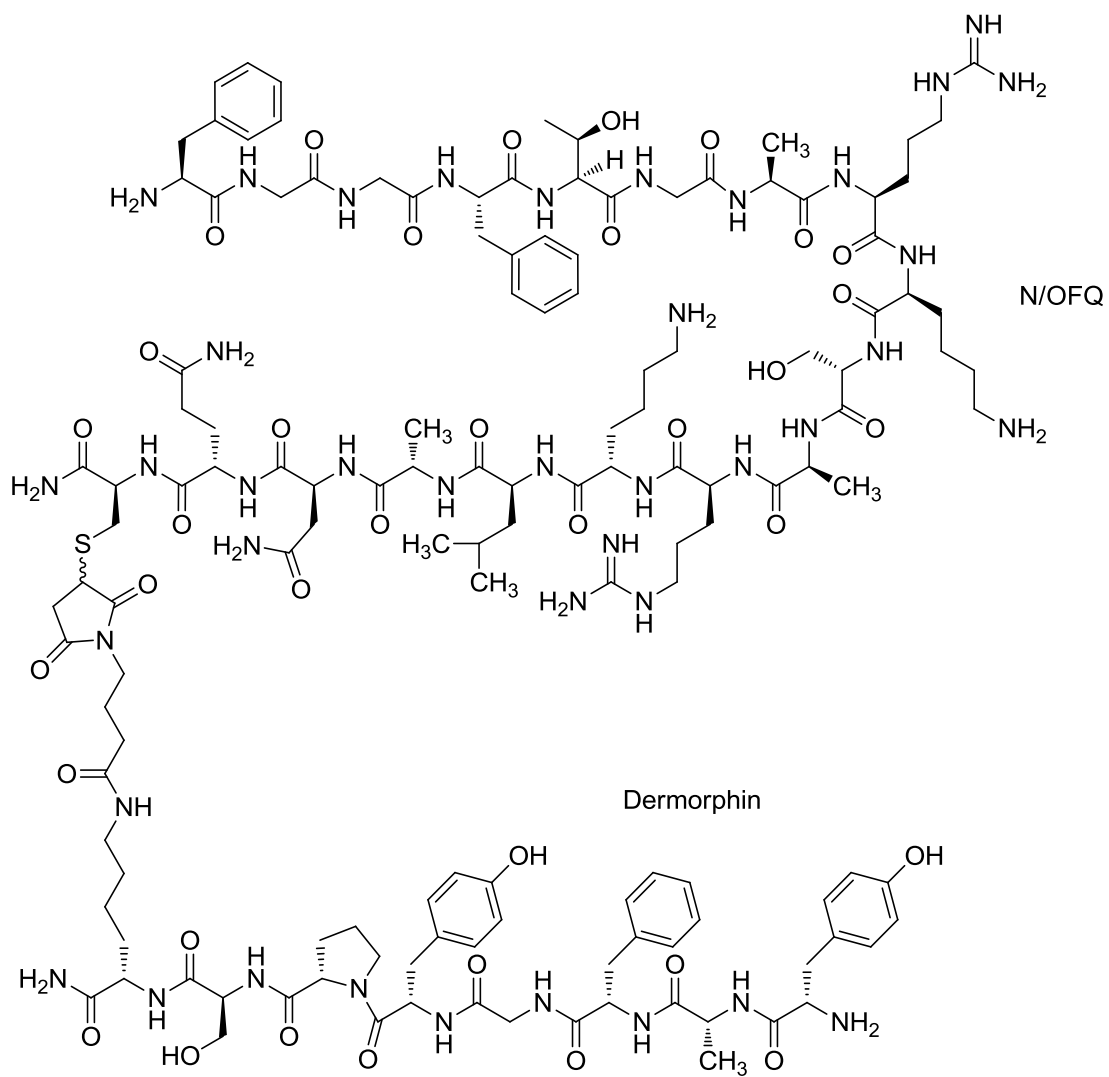


Figure 1.23: The chemical structure of the bivalent pharmacophore, DeNO.

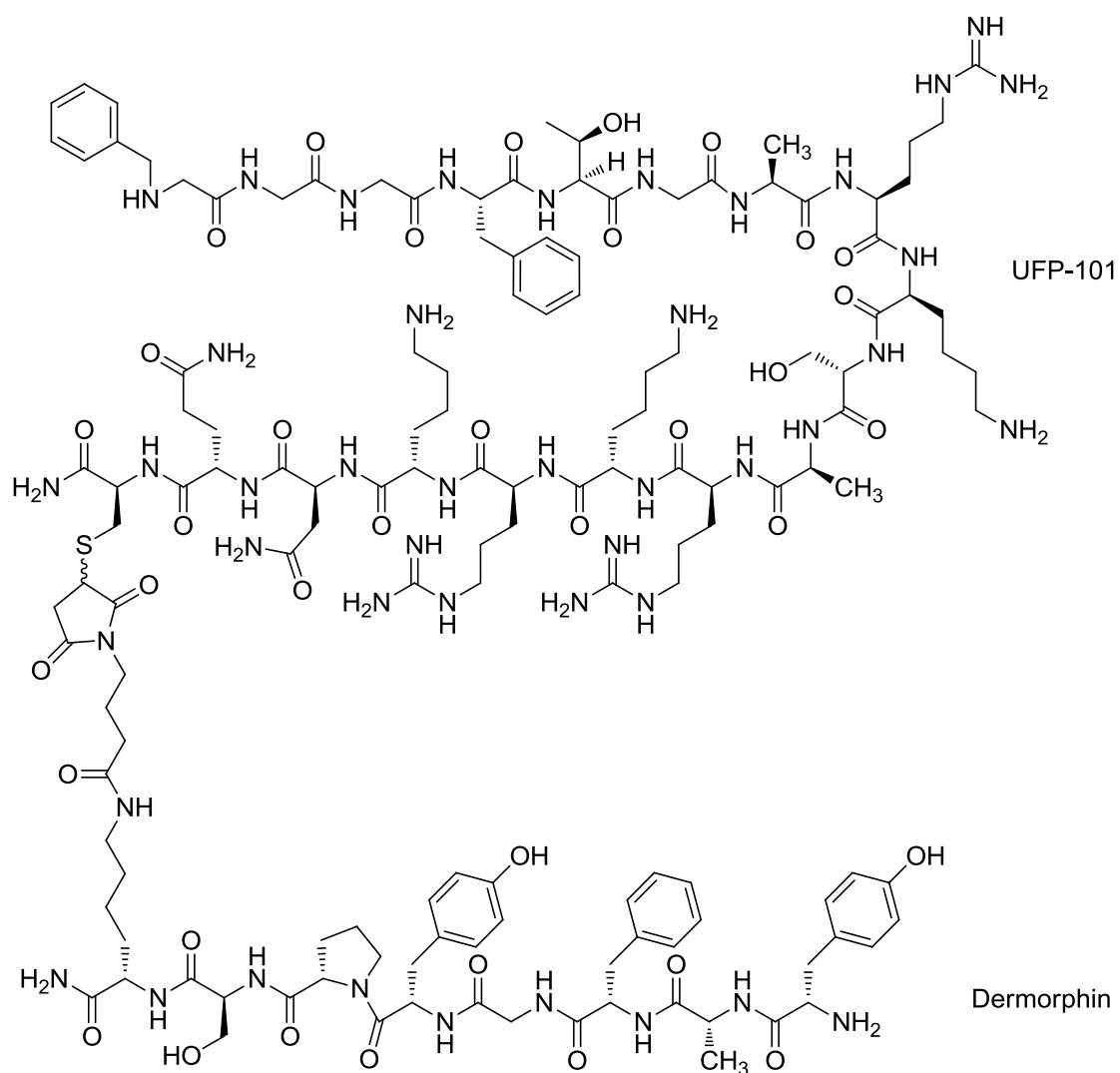


Figure 1.24: The chemical structure of the bivalent pharmacophore, DeUFP.

1.9 Aims

With regards to the treatment of chronic pain, the MOP receptor provides the best target for the production of analgesia. The large number of studies implicating DOP or NOP opioid receptors in the development of tolerance and dependence provides a target to exploit through the use of bivalent pharmacophores. Furthermore, direct targeting of the DOP and/or NOP receptors may provide potent analgesics without the adverse affects seen in MOP-based drugs. The basis of this thesis is the investigation of these multi-pharmacophoric ligands, through monitoring of their cellular activities.

During this PhD, the aims will be initially to determine how conjugation of two or more pharmacophores affects binding affinity for the opioid receptors of interest. Once

binding affinity has been determined, the functional activity of these novel, multi-branched opioids will be assessed at various stages in the signal transduction pathway ($G_{\alpha i}$ -pathway, β -arrestin activity, MAPK pathway) to determine any potential changes caused by chemical conjugation of the pharmacophores.

Chapter 2 Materials and Methods

2.1 Materials

The materials used in this thesis for buffer preparation were of the highest quality. The materials used, the company they were purchased from and the buffer recipes are described below.

BDH Limited (Poole, UK): Potassium dihydrogen phosphate

Biorad: Tris-gly-SDS (10x).

Biological Research Center of Hungarian Academy of Sciences (Szeged, Hungary):

[³H]UFP-101

Cell Signalling: phosphorylated p38 primary antibody, phosphorylated ERK 1/2 primary antibody, total p38 primary antibody, total ERK 1/2 primary antibody, prestained ladder, biotinylated ladder, anti-biotin secondary antibody.

Fisher Chemicals (Leicestershire, UK): Absolute ethanol, tris(hydroxymethyl)aminomethane hydrogen chloride (Tris-HCl) & tris(hydroxymethyl)aminomethane Base (Tris-Base), magnesium sulphate (MgSO₄), potassium hydroxide (KOH), sodium hydroxide (NaOH), Protein A, Protein B, penicillin/streptomycin, Scintisafe gel, HiSafe3, Glucose, Glycerol, sodium hydrogen carbonate (NaHCO₃), disodium hydrogen phosphate (Na₂HPO₄).

Fisons (Loughborough): Calcium chloride (CaCl₂), potassium dihydrogen sulphate (KH₂PO₄).

GE Healthcare: ECL developing reagent, photographic film.

Gibco (Scotland): Foetal bovine serum, fungizone, geneticin (G418), Hams nutrient mixture F-12 Media, Dulbecco's modified Eagle medium: nutrient Mixture F-12 media.

Gilson Scientific (Luton, UK): Nitrocellulose membrane.

Invitrogen (Scotland): Hygromycin B, RNAlater[®] stabilisation solution, TURBO DNA-free[™] kit, cDNA reverse transcription kit, TaqMan[®] universal PCR master mix, TaqMan[®] probes

Lonza (Slough, UK): Trypsin-EDTA

Perkin-Elmer (Massachusetts, US): [³H]-Diprenorphine ([³H]-DPN), guanosine 5'-[γ-thio-triphosphate [³⁵S] (GTPγ[³⁵S]), [³H]-3'-5'-cyclic adenosine monophosphate ([³H]-cAMP).

Roche Applied Sciences: Water (PCR-grade).

Sigma Aldrich (Poole, Dorset, UK): Bovine serum albumin (BSA), naloxone, Polyethylenimine (PEI), Ethylene glycol tetraacetic acid (EGTA), sodium chloride (NaCl₂), magnesium chloride hexahydrate (MgCl₂-6H₂O), guanosine 5'-diphosphate (GDP), guanosine 5'-[γ-thio]triphosphate (GTPγS), activated charcoal, sodium dodecyl sulphate (SDS), bromophenol blue, Tween-20, Glycine, anti-rabbit IgG secondary antibody, 4-(2-hydroxyethyl)-1-piperazineethanesulfonic acid (HEPES), forskolin, 3-isobutyl-1-methylxanthine (IBMX), ethylenediaminetetraacetic acid (EDTA), 3'-5'-cyclic adenosine monophosphate (cAMP), pepstatin, leupeptin, benzamide, phenylmethylsulfonyl fluoride (PMSF), Tri-reagent[®], Chloroform, Propan-2-ol, β-glycerolphosphate, Sodium orthovanadate.

Thermo Scientific: Restore Plus[™] stripping buffer, DL-dithiothreitol (DTT).

Tocris: [D-Pen(2),D-Pen(5)]-enkephalin (DPDPE), Norbinaltorphimine (Nor-BNI), Naltrindole.

University of Arizona: Fentanyl derivatives.

University of Ferrara Peptide Research (Ferrara, Italy): Dermorphin, N/OFQ, UFP-101, DeNO, DeUFP, PWT1-N/OFQ, PWT2-N/OFQ, PWT3-N/OFQ, PWT2-Leu-Enk, Leu-Enkephalin, Dynorphin-A.

2.2 Buffer compositions

2.2.1 *Tissue culture buffers*

Harvest Buffer: HEPES (10mM), EDTA (1.1mM), NaCl (154mM), pH7.4 NaOH.

2.2.2 *Saturation/Displacement Buffers*

Saturation/Displacement Wash Buffer: Tris-HCl (50mM), pH7.4 KOH

Sat/Disp Binding Buffer: Tris-HCl (50mM), 0.5% BSA, pH7.4 KOH

MgSO₄ (For CHO_hNOP cells only)

2.2.3 *GTP γ ³⁵S buffers*

GTP γ [³⁵S] Reconstitution: Tris-HCl (50mM), DTT (10mM), pH7.4 NaOH.

GTP γ [³⁵S] Homogenising: Tris-HCl (50mM), EGTA (0.2mM), pH7.4 NaOH.

GTP γ [³⁵S] Assay (CHO): Tris-HCl (50mM), EGTA(0.2mM), NaCl(100mM), MgCl₂ (1mM), pH7.4 NaOH.

GTP γ [³⁵S] Assay (HEK) : HEPES (50mM), MgCl₂ (5mM), NaCl (100mM), EDTA (1mM), DTT (1mM), pH 7.4 NaOH.

2.2.4 *Cyclic Adenosine Monophosphate Buffers*

cAMP experimental Buffer (Krebs/HEPES): NaCl (143mM), HEPES (10mM), glucose (12mM), KH₂PO₄, KCl (1.2mM), CaCl₂ (2.6mM), MgSO₄ (1.2mM), pH to 7.4 with NaOH.

cAMP Assay Buffer: Tris-HCl (50mM), EDTA (4mM), pH 7.4 with NaOH.

Charcoal Suspension: Activated charcoal (250mg), BSA (100mg) in 25ml cAMP assay buffer.

2.2.5 *Calcium mobilisation buffers*

Hank's balanced salt solution (HBBS) buffer: NaCl (137mM), KCl (5.4mM), Na₂HPO₄ (0.25mM), CaCl₂ (1.3mM), KH₂PO₄ (0.44mM), MgSO₄ (1mM), NaHCO₃ (4.2mM), glucose (5mM), HEPES (20mM) and 0.005% BSA fraction V.

Loading Buffer; HBBS buffer: probenecid (2.5mM), Fluo-4-AM (3 μ M) pluronic acid (0.01%).

Experimental buffer; HBBS, HEPES (20mM), probenecid (2.5mM), Brilliant Black (500 μ M).

2.2.6 *Western blot buffers*

Krebs-HEPES buffer: NaCl (118mM), KCl (4.7mM), KH₂PO₄ (1.2mM), MgSO₄ (1.2mM), NaHCO₃ (1.3mM), Glucose (11.9mM), HEPES (10mM), CaCl₂ (1.3mM), pH 7.4 NaOH.

Lysis Buffer: Tris-HCl (20mM), NaCl (137mM), EDTA (2mM), Glycerol (10% w/v), Triton X-100 (10% w/v), β -glycerolphosphate (54mg/10ml), Sodium orthovanadate (18mg/10ml), benzamide (200 μ g/ml), Pepstatin (2mM), leupeptin (10mg/ml), PMSF (560mM).

2x SDS Sample/loading buffer: Tris-HCl (100mM), SDS (2% w/v), glycerol (10% w/v), bromophenol blue (0.1% w/v), dH₂O.

Running buffer: 10x Tris/Glycine/SDS buffer, H₂O.

Semi-dry blotting buffer: Tris-base (48mM), glycine (39mM), SDS (0.037% w/v), Methanol (20% w/v).

Tris-buffered saline/tween (TBS-T): NaCl (5M), Tris-HCl (1M), Tween-20
Stacking gel; ddH₂O, Acrylamide, Tris-HCl (1M, pH6.8 with NaOH), SDS (10% w/v).

2.3 Methods- Overview

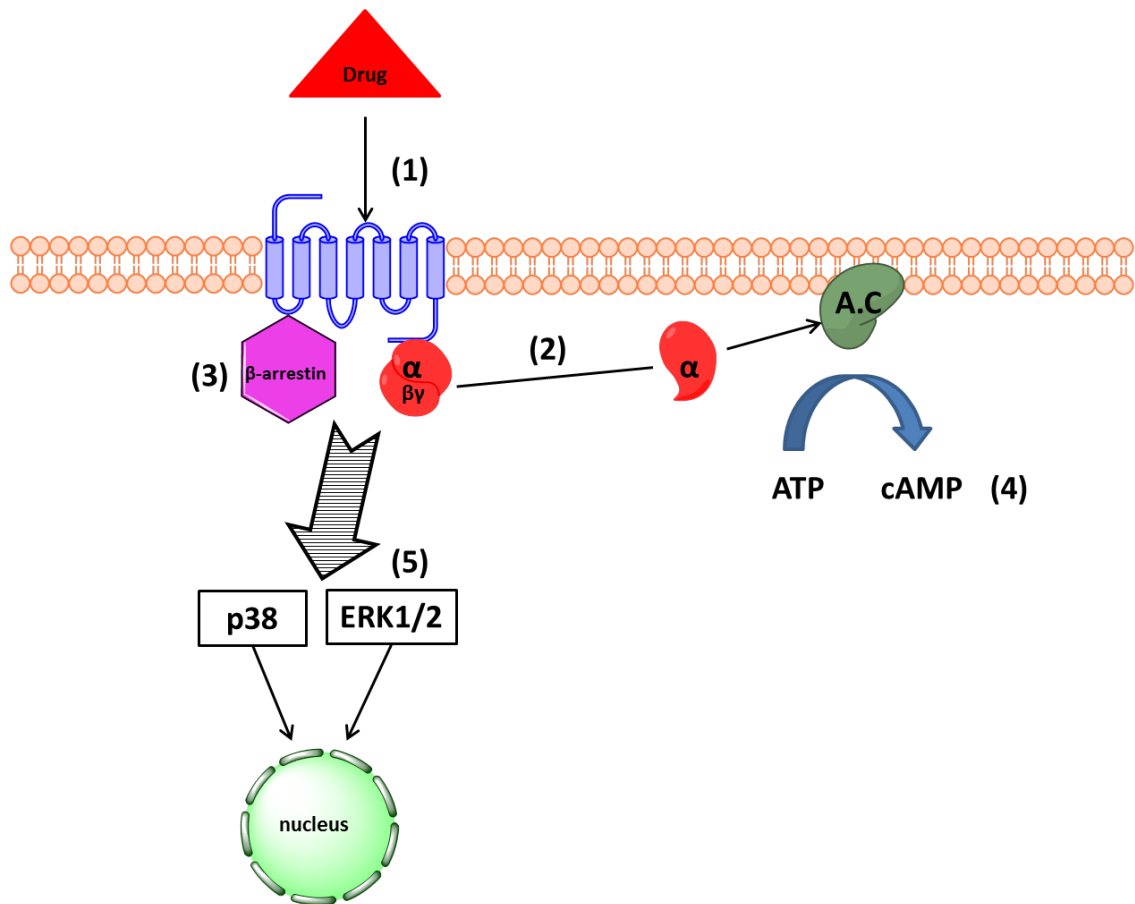


Figure 2.1: Drug interactions lead to numerous measurable events within the cell. Techniques described in the materials and methods to measure these events include: (1) The affinity of the drug to interact with the receptor can be measured in a **displacement binding assay** (section 2.8). (2) The activation of an opioid receptor leads to an increase in G_{α} subunit activity, which was measured in a **GTP γ [35 S] functional assay** (section 2.9). (3) The recruitment of β -arrestins to the opioid receptor was monitored using a **PathHunterTM β -arrestin recruitment assay** (section 2.11) (4) The activation of opioid receptors leads to inhibition of adenylyl cyclase (A.C), which was measured using a **cyclic AMP (cAMP) assay** (section 2.10). (5) Opioid receptor activation leads to the up-regulation of the MAPK pathway, specifically p38 and ERK1/2. The effects of opioids on this pathway was through **Western blotting densitometry** (section 2.14).

2.4 Cell culture

Chinese hamster ovary (CHO) cells and human embryo kidney (HEK) cells were used as *in vitro* models. Cell-lines were cultured in 5% carbon dioxide humidified air, at 37°C, and sub-cultured using trypsin EDTA as required. Cells were used experimentally when confluent. CHO_{hMOP/DOP/KOP} cells were cultured in Dulbeccos HAMS F12, which was supplemented with 10% foetal bovine serum (100 IU/ml), streptomycin (100µg/ml) and fungizone (2.5µg/ml). CHO_{hNOP} cells were cultured in Dulbecco's MEM / HAMS F12 (50/50) supplemented with 5% FCS, penicillin (100 IU/ml), streptomycin (100µg/ml) and fungizone (2.5µg/ml). HEK_{hMOP}, HEK_{hNOP} and the co-expressed HEK_{hMOP/NOP} cells were cultured in minimum essential medium (MEM) supplemented with 10% foetal bovine serum (100 IU/ml), streptomycin (100µg/ml) and fungizone (2.5µg/ml). The CHO_{hMOP/DOP/KOP} and HEK_{hMOP} stocks were supplemented with geneticin (G418) (400µg/ml), while CHO_{hNOP} cells and HEK_{hMOP/NOP} cells were supplemented with Geneticin (G418) (400µg/ml) and hygromycin B (200µg/ml). HEK_{hNOP} were supplemented with hygromycin B (200µg/ml). Treatment with the novel compounds, as well as control ligands, did not lead to cell death in the experimental models.

2.5 Radioligand Binding assays-Cell preparation

2.5.1 Membrane preparation

In order to harvest cells, harvest buffer and gentle agitation of the flasks was required. Cells were collected and centrifuged at 1500rpm for 3 minutes before being resuspended in the appropriate buffer. Dependent on the experiment, cells were suspended in either wash buffer (displacement, saturation assays) or homogenizing buffer (GTP γ ³⁵S assay). An Ultra-Turrax was used, to homogenise the cells, for a minimum of 10 seconds. The homogenate was then centrifuged at 13,500rpm for 10 minutes, at 4°C. This step is repeated three times.

2.5.2 Lowry Protein Assay

In order to obtain the protein concentrations from the membrane fractions obtained from the previous steps, methods set out by Lowry (Lowry et al., 1951) were used:

BSA protein standards were made in 0.1M NaOH, at set concentrations of 0, 50, 100, 150, 200, 250 μg protein/ml. The membrane fractions were diluted in 0.1M NaOH. 0.5ml volumes of the samples and standards were incubated in 2.5 ml of a solution, which consisted of: A (NaHCO_3 in 0.1M NaOH) B (1% CuSO_4) and C (2% $\text{Na}^+ \text{K}^+$ tartrate) mixed to the ratio 100:1:1, for 10 minutes. Folin's reagent, which is diluted at a 1:4 ratio in H_2O , is then added to the standards and sample and incubated at room temperature for 30 minutes. A spectrophotometer is used to determine the absorbance, at 750nm, of the standards and samples. A standard curve is produced from the linear regression of the known BSA standards, which then allows the sample protein concentration to be determined from this curve. A typical BSA standard curve can be seen in Figure 2.2, below.

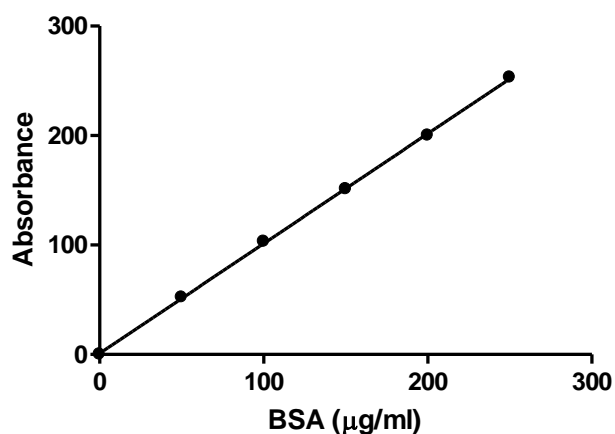


Figure 2.2: The standard curve generated by a Lowry protein assay. An unknown amount of protein can be determined from this line using its absorbance values. $R^2 = 0.99$

2.6 Basic principles of ligand binding

2.6.1 *Theory*

The law of mass action is the basis for the model of receptor-ligand binding and is interpreted in such a way as to show that, at any given time, for a proportion of receptors that are bound to a ligand, there are also proportions that remain unbound. This law can be represented by the equation:



In the above equation, L represents the ligand, R the receptor and LR would be the ligand-receptor complex formed after binding. The rate of association of the ligand and receptor to form the ligand-receptor complex, is termed K_{+1} , while the dissociation rate from bound to unbound state is termed K_{-1} . Both these values are expressed as constants, and are contingent on various factors, such as the affinity of the receptor for the ligand and which of these states best exhibits a state of minimal free energy. When equilibrium is reached in the above equation, it can be defined in terms of concentration by the following equation:

$$\mathbf{[L] \times [R] \times K_{+1} = [LR] \times K_{-1} \text{ therefore}}$$

$$\mathbf{[L] \times [R] / [LR] = K_{-1} / K_{+1} = K_d}$$

When the equation is rearranged in this way, the dissociation constant K_d can be determined. The dissociation constant is considered to represent the concentration of ligand required to bind to half the total number of receptors at equilibrium. It is expressed in units of M . The K_d is usually expressed on a logarithmic value. This is represented by the equation:

$$\mathbf{pK_d = -\log(pK_d)}$$

2.6.2 *Radioligands*

In order to measure ligand binding, radioactive isotopes are incorporated into the structure of the ligand. Isotopes such as tritium [^3H] and radioactive sulphur [^{35}S] are popular choices, as they can be incorporated into the structure of ligands without compromising biological activity or native structure of the ligand of choice. Both of these isotopes emit beta (β) radiation, which has a low intrusion profile due to their low energy capacity. This procedure proves to be a reliable method of measuring the interaction between the receptor and ligand bound. The radioactive isotopes attached to these ligands are subject to decay over time, which is represented by the isotopes half-life (represented as $t_{1/2}$). Different isotopes have unique half-lives, with tritium being 12.43 years and [^{35}S] being 87 days. The activity per unit mass of a sample of radioactive material is referred to as its specific activity and is measured in curies per mmol ($\text{Ci}\cdot\text{mmol}^{-1}$).

In order to detect the amount of radioactivity being emitted from a sample, it is first mixed with scintillation cocktail. As the radioligand disintegrates, it emits β -particles that collide with fluor molecules present in the scintillation cocktail. This collision produces photons, which in turn produce a measurable luminescence. A scintillation β -counter is used to detect and measure radioactivity through detection of this luminescence. The counter measures this luminescence and expresses it as counts per minute (cpm). When this figure is corrected for quenching, it is represented as disintegrations per minute (dpm). The reading is therefore a quantified expression of the radioactivity present in the sample, since 2.22×10^6 disintegrations per minute are detected in $1\mu\text{Ci}$ of radioactive material.

2.7 Saturation Binding Assay

2.7.1 Theory

This assay allows for the experimental determination of the K_d of the radioligand and the B_{max} (the maximum number of receptor binding sites). In order to determine these values, an increasing concentration of the radioligand is incubated in both the presence and absence of a saturating concentration of a non-specific binding ligand (NSB). An NSB is usually a ligand with a high affinity for the receptor, and will out-compete the radioligand in regards to binding to the target receptor. This allows us to determine

whether radioligand binding occurs at any other sites beside that of the target receptor. The results of this experiment produce a hyperbolic curve, which is dependent on the varying concentrations of the radioligand and the amount of radioligand bound to the target receptor. The results of the NSB are subtracted from the total binding to provide specific binding. Typical results can be seen in Figure 2.3 below. The K_d is defined as the concentration of the radioligand which occupies 50% of the receptor sites. The B_{max} (receptor density) is determined at the point where specific binding will no longer increase (saturated) with increasing concentrations of radioligand.

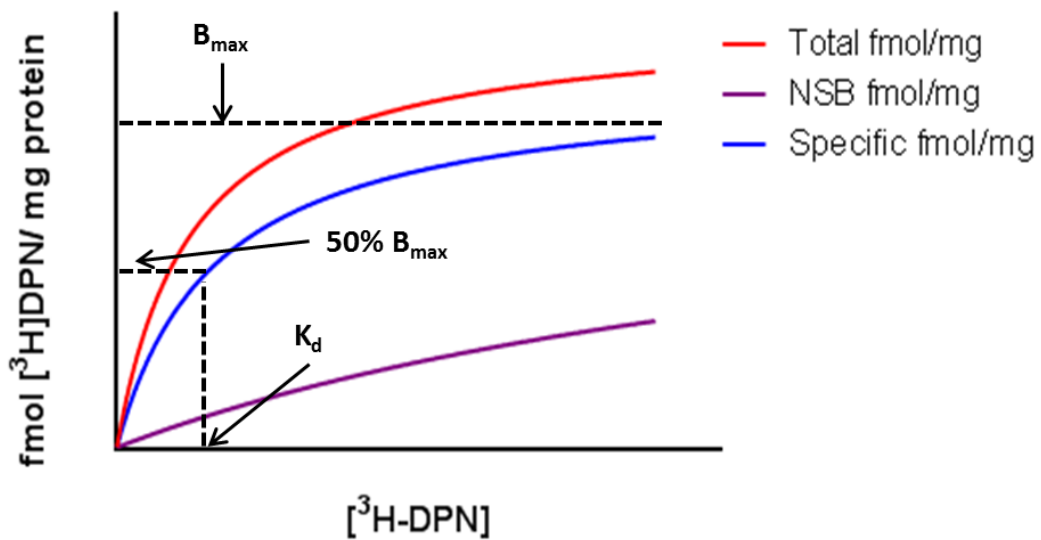


Figure 2.3: Saturation binding assay hyperbolic curve graph, which determines both the K_d and B_{max} .

The data acquired from these experiments is usually transformed into a semi-logarithmic plot, as shown in Figure 2.4, which measures the amount of radioligand bound against the Log [radioligand concentration].

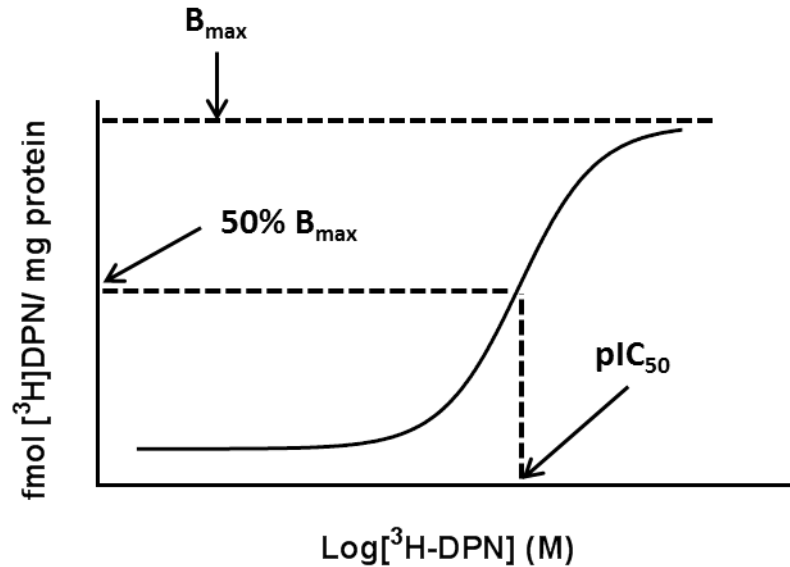


Figure 2.4: Semi-logarithmic sigmoidal curve of receptor binding versus the log [radioligand concentration obtained from the saturation assay].

2.7.2 Methods

In order to prepare such an assay, confluent cells were harvested using a harvest buffer (section 2.2) at 37⁰C. After harvesting, cells were centrifuged at 1500rpm for 3 minutes, before being resuspended in wash buffer (section 2.2). This suspension was homogenized and centrifuged at 13500rpm for 10 minutes at 4⁰C. The cell homogenate was then resuspended and centrifuged twice more in wash buffer. Forty micrograms of membrane protein was incubated in 0.5ml volumes of Binding buffer (section 2.2). The CHO_{hMOP/DOP/KOP}/HEK_{hMOP}/HEK_{hMOP/NOP} protein was incubated with varying concentrations of [³H]-DPN for 1 hour, while CHO_{hNOP}/HEK_{hNOP}/HEK_{hMOP/NOP} was incubated with [³H]UFP-101 for 1 hour. The NSB was determined by the presence of 10 μM naloxone for CHO_{hMOP/DOP/KOP}/HEK_{hMOP}/HEK_{hMOP/NOP} cell lines, where [³H]-DPN was used, while 1 μM N/OFQ was used to define the NSB in CHO_{hNOP}/HEK_{hNOP}/HEK_{hMOP/NOP} cell lines, where [³H]UFP-101 was used. Following the incubation period, the free and bound radioligand was separated using vacuum filtration onto polyethylemine (PEI 0.5%)-soaked Whatman glass fibre filters in a Brandel harvester. The collected filters were placed in scintillation fluid for an incubation period of 8hrs before being counted in a liquid scintillation spectrometer. The typical components of a saturation binding assay are shown in Table 2.1.

Solution Type	Binding Buffer	Solution Elements		
		Radioligand	Membrane	NSB
Total Binding	300µl	100µl	100µl	-
Non-Specific Binding	200µl	100µl	100µl	100µl

Table 2.1: Solution components and volumes (total volume used was 500µl) used in a standard saturation binding assay. Total and non-specific binding tubes were prepared for each radioligand concentration.

2.8 Displacement Assay

2.8.1 *Theory*

This experiment is used to determine the binding affinity of non-radiolabelled ligands for target receptors. The experiment requires the use of a set concentration of a radioligand incubated alongside increasing concentrations of the non-labeled ligand. The amount of radioligand that is displaced by the ligand of interest depends upon this ligands affinity for the receptor. The IC_{50} of the radioligand is determined using a semi-logarithmic plot, depicted in Figure 2.5. The graph describes the bound ligand, as a percentage displacement of the radioligand, against the log of the free ligand.

The concentration of the radioligand has an effect on the position of the curve, with higher concentrations of a radioligand causing the curve to shift further to the right. Since the amount of radioligand used may vary slightly in each experiment, the Cheng-Prusoff equation is used to normalize the resulting curve shifts and produce the K_i (Cheng and Prusoff, 1973). The equation reads as follows:

$$K_i = IC_{50}/1+ ([L]/K_d)$$

In the above equation, K_i represents the binding affinity; $[L]$ the concentration of radioligand and K_d the dissociation constant of the radioligand. The K_i is usually expressed as a logarithmic value and is then referred to as the pK_i . This changes the equation as follows:

$$pK_i = -\log_{10}[IC_{50}/1+([L]/K_d)]$$

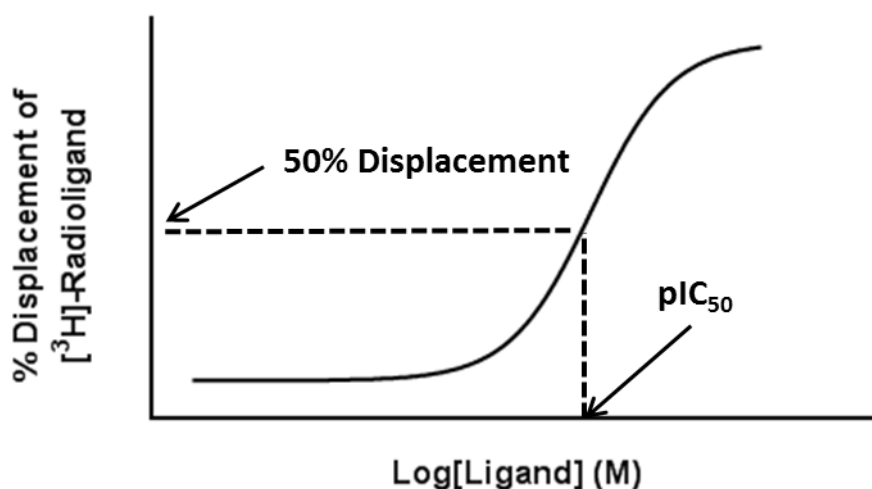


Figure 2.5: Semi-logarithmic sigmoidal plot of percentage displacement of radioligand versus the log of the concentration of the ligand used as a competitive displacer in the experiment.

2.8.2 Methods

This experiment requires the use of a single concentration of the radioligand in all experimental tubes. The ligands of interest, however, were used in varying concentrations (1 pM- 10 μ M). Dependent on the cell line and its receptor expression between 20-200 μ g of membrane protein was used in each experiment. CHO_{hMOP/DOP/KOP}/HEK_{hMOP}/HEK_{hMOP/NOP} cells were incubated with ~0.8nM of [³H]-Diprenorphine, while CHO_{hNOP}/ HEK_{hNOP}/HEK_{hMOP/NOP} cells were incubated with ~1 nM of [³H]UFP-101. In order to define non-specific binding, 10 μ M of naloxone was used in CHO_{hMOP/DOP/KOP}/HEK_{hMOP}/HEK_{hMOP/NOP} cells, where [³H]-DPN was used, while 1 μ M of N/OFQ was used for the CHO_{hNOP}/ HEK_{hNOP}/HEK_{hMOP/NOP} cells, where [³H]UFP-101 was used. The cells were incubated for one hour at room temperature, followed by separation of the free and bound radioligand using vacuum filtration onto polyethylemine (PEI 0.5%)-soaked Whatman glass fibre filters in a Brandel harvester. The collected filters were placed in scintillation fluid for an incubation period of 8hrs before being counted in a liquid scintillation spectrometer. The typical components of displacement binding assay are shown in Table 2.2.

Solution Type	Binding Buffer	Solution Elements			
		Radioligand	Membrane	NSB	Drugs
Total Binding	300µl	100µl	100µl	-	-
Non-Specific Binding	200µl	100µl	100µl	100µl	-
Displacer	200µl	100µl	100µl	-	100µl

Table 2.2: The typical solution components and volumes for a 500 µl total volume displacement binding assay. In a displacement binding assay, there are typical 8 displacer tubes.

2.9 GTPγS functional assay

2.9.1 *Theory*

The activation and response of receptors to drug interactions is measured by functional assays. The GTPγ[³⁵S] assay measures the coupling of the receptor to a G-protein. When a ligand binds to a GPCR, it alters the conformation of the receptor and its ability to interact with G-proteins. This change in interaction leads to the G-protein exchanging GDP for GTP. The exchange of GDP for GTP can be measured using a stable, radiolabelled analogue of GTP, namely GTPγ[³⁵S], which replaces GTP in these interactions. Rather than the GTPase activity of the Gα subunit hydrolyzing the γ-phosphate bond of the bound GTP (releasing a phosphate group and transforming the purine group back to GDP), the presence of the γ-thiophosphate bond in GTPγ[³⁵S] prohibits this action from occurring. This process requires the presence of GDP in order to reduce the basal binding of GTPγ[³⁵S]. The conformational state of the receptor is in a constant state of flux, and there will therefore be some tonic activation of G-proteins through non-ligand bound receptors. This allows for the basal level activation of G-proteins to be measured, in the absence of any ligands, and the results expressed as the increase above basal, which can be seen in Figure 2.6.

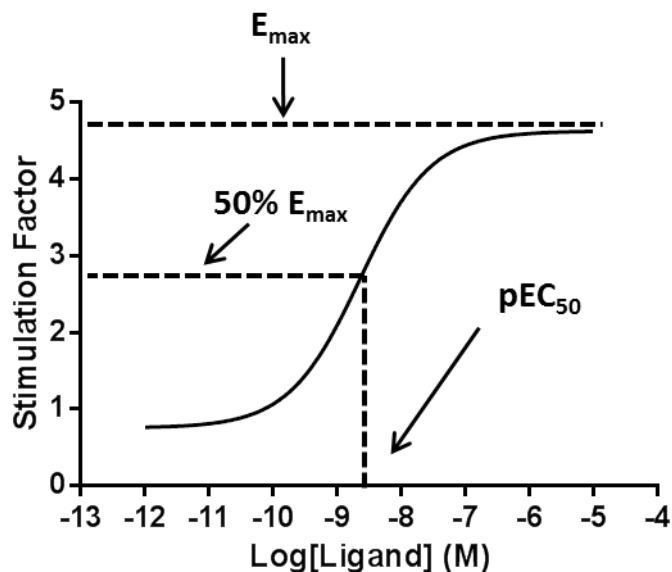


Figure 2.6: The above diagram represents the stimulation factor of various concentrations of a ligand (the amount of stimulation of the ligand when compared to the cells own basal levels.)

2.9.2 Methods-GTP γ [35 S] agonist assay

The cell membranes for this assay are prepared using the methods described in section 2.7.2, except with the homogenization buffer, mention in section 2.2.2, replacing the wash buffer. Forty micrograms of the CHO membrane protein is resuspended in 0.5ml volumes of the CHO assay buffer (section 2.2.3). This volume includes bacitracin (0.15mM), BSA (0.15mM), GDP (classical opioids-33 μ M; NOP-100 μ M) and \sim 150pM of GTP γ [35 S] (Table 2.3). For HEK cell membranes, 20 μ g is resuspended in HEK assay buffer with the volume including bacitracin (0.15mM), BSA (0.15mM), GDP (HEK_{hMOP}-3 μ M; HEK_{hNOP}/HEK_{hMOP/NOP}-33 μ M) and \sim 150pM of GTP γ [35 S]. In order to define non-specific binding, 10 μ M of non-radiolabelled GTP γ S was used in all cell membranes. The assay was incubated for 1hr in a 30 $^{\circ}$ C degree water bath, before being harvested, in the absence of PEI, using the protocols mentioned in section 2.7.2.

Solution Type	Solution Elements							
	AB	RL	M	NSB	Drugs	BAC	GDP	BSA
Total Binding	240µl	100µl	100µl	-	-	20µl	20µl	20µl
Non-Specific Binding	220µl	100µl	100µl	20µl	-	20µl	20µl	20µl
Drug	220µl	100µl	100µl	-	20µl	20µl	20µl	20µl

Table 2.3: The typical volumes and components used in a $GTP\gamma[^{35}S]$ assay (total volume: 500µl). There are typically 8 tubes prepared per agonist. AB; assay buffer, BSA; bovine serum albumin, BAC; bacitracin, GDP; guanosine diphosphate, RL; radioligand, M; membrane, NSB; non-specific binding.

2.9.3 Antagonist determination (pK_b) in a $GTP\gamma[^{35}S]$ functional assay

In order to determine whether compounds of interest have any antagonist properties, a $GTP\gamma[^{35}S]$ assay was undertaken, whereby a control agonists activity is monitored with or without ligand of interest. In this assay, various concentrations of a known agonist (e.g. Fentanyl) are co-incubated with, and without, a single concentration of the ligand of interest (Table 2.4). Should the ligand of interest have antagonist activity, it may be seen to shift the functional curve to the right when compared to the control assay, altering the pEC_{50} (Figure 2.7). The shift in pEC_{50} can be used to determine the antagonist affinity of the compound of interest by using the Gaddum-Schild equation:

$$pK_b = \log[(EC_{50}(\text{test})/EC_{50}(\text{control}) - 1) - \log[\text{concentration of antagonist}(M)]$$

Solution Type	Solution Elements								
	AB	RL	M	NSB	Drugs	BAC	GDP	BSA	A
Total Binding	240μl	100μl	100μl	-	-	20μl	20μl	20μl	-
Non-Specific Binding	220μl	100μl	100μl	20μl	-	20μl	20μl	20μl	-
Antagonist	200μl	100μl	100μl	-	20μl	20μl	20μl	20μl	20μl
Drug	220μl	100μl	100μl	-	20μl	20μl	20μl	20μl	-

Table 2.4: The typical volumes and components used in a $\text{GTP}\gamma[^{35}\text{S}]$ assay (total volume: 500μl). There are typically 8 tubes prepared per agonist. A; Antagonist.

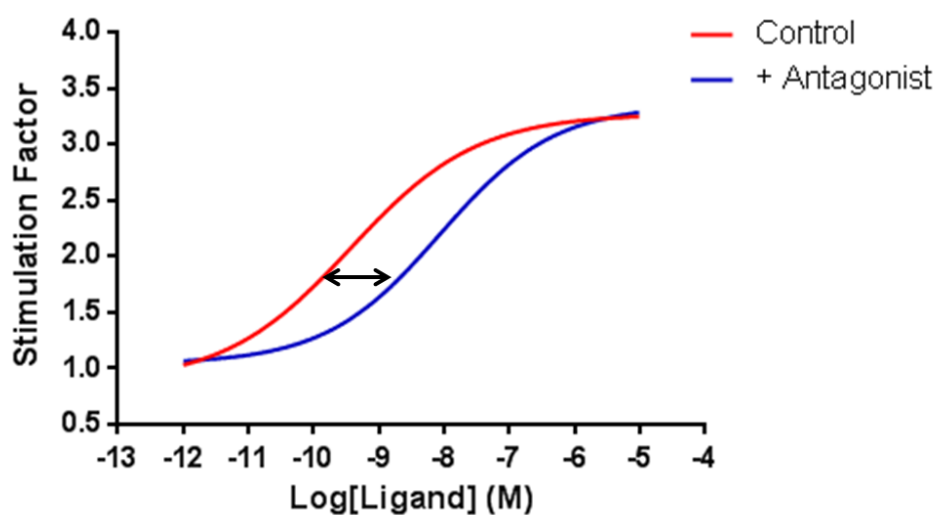


Figure 2.7: The above diagram represents the stimulation factor of various concentrations of a ligand in the absence, and presence of an antagonist. The antagonist leads to a rightward shift of the concentration response curve (indicated by the arrow). This resulting change in the pEC_{50} can be used to determine the antagonists pK_b value, through the Gaddum-Schild equation.

2.10 Cyclic adenosine monophosphate assay

2.10.1 *Theory*

Opioid receptors are $G_{\alpha i/o}$ coupled receptors and, upon activation, leads to the inhibition of adenylyl cyclase (which converts ATP to adenosine 3',5' cyclic monophosphate or cAMP), resulting in a measurable reduction in cAMP levels. The cAMP assay allows for the quantification of downstream opioid signalling through the measurement of cAMP.

In order to determine the concentration of cAMP in a sample, tritiated-cAMP ($[^3\text{H}]$ -cAMP) and bovine binding protein (BB), extracted from bovine adrenal glands, are used in a protein binding assay. In this assay, unlabelled cAMP and $[^3\text{H}]$ -cAMP bind competitively to the BB binding sites (protein kinase A), producing an inverse relationship between the two. The larger the concentration of unlabelled cAMP, the more $[^3\text{H}]$ -cAMP is displaced from the binding protein, which in turn leads to a measurable decrease in radioactivity. A concentration-related displacement curve is developed using increasing amounts of unlabelled cAMP (0, 0.25, 0.5, 1, 2, 4, 6, 8 and 10 pmol/50 μl^{-1}). Using this standard curve (Figure 2.8), the displacement of $[^3\text{H}]$ -cAMP by unknown quantities of cAMP in the samples of interest can be calculated using the RIASMART software associated with the β -counter (Packard Bell, Berkshire, UK).

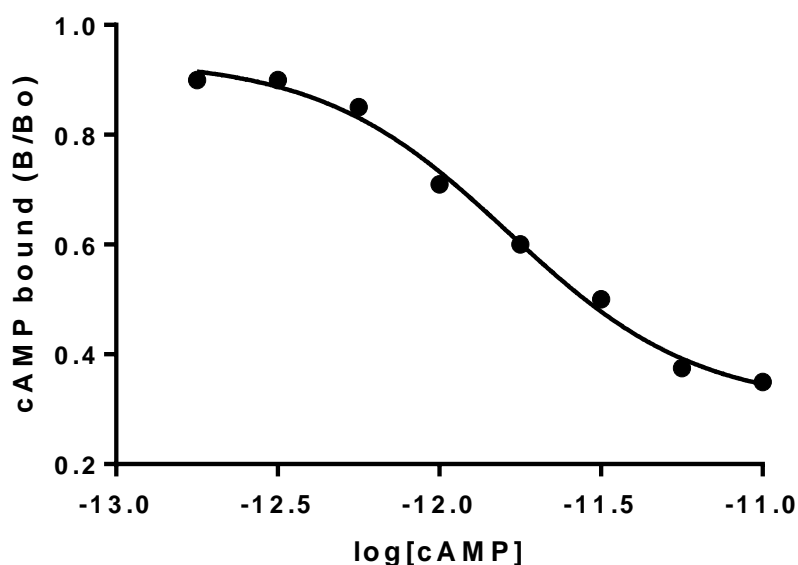


Figure 2.8. A cAMP standard curve produced by the RIASMART software.

2.10.2 Methods

Cells were harvested, when confluent, using harvest buffer and centrifuged at 1500rpm for 3 minutes. The supernatant was discarded and the cell pellet was resuspended in Krebs/HEPES buffer. The cells were washed twice more, following which they were resuspended in the desired amount of Krebs/BSA buffer (0.5% BSA).

Whole cell suspensions were incubated in 300 μ l of Krebs/BSA for 15 minutes at 37⁰C, in the presence of 1mM isobutylmethylxanthine (IBMX). Barring cells in which the basal activity was to be measured, cells were also incubated with 1 μ M forskolin, an adenylyl cyclase activator, and an opioid ligand (10 μ M) (Table 2.5).

Solution Type	Solution Elements				Cells
	Buffer	Forskolin 1 μ M	Drug	IBMX 1mM	
Basal	60 μ l			40 μ l	200 μ l
Forskolin	40 μ l	20 μ l		40 μ l	200 μ l
Drug	20 μ l	20 μ l	20 μ l	40 μ l	200 μ l

Table 2.5: The components of a cAMP assay. IBMX; isobutylmethylxanthine

Reactions were terminated by the addition of 20µl of HCl (10M) and the pH was equilibrated with the addition of 20µl NaOH (10M) and 200µl Tris-HCl buffer (pH 7.4). Following vortexing, the solutions were centrifuged at 16100g for 2 minutes. Subsequently, the concentration of cAMP in the supernatant is measured using binding protein (BP), with this assay being undertaken at 4⁰C. A low concentration of [³H]-cAMP (100µl, ~0.5nM) and diluted BP (150µl, ~1/20 from pre-prepared stock) was added to each standard and sample, with a minimum of 4 hours incubation period (preferred overnight incubation), at 4⁰C, undertaken to allow for equilibration of the samples. In order to determine non-specific binding, 5µM of cAMP was used (Table 2.6).

Solution Elements						
Solution	Buffer	NSB	Standards	SS	Radioligand	Binding Protein
Total	50µl	-	-	-	100µl	150µl
NSB	-	50µl	-	-	100µl	150µl
Standards	-	-	50µl	-	100µl	150µl
Sample	-	-	-	50µl	100µl	150µl

Table 2.6: Components of a cAMP assay. A known amount of cAMP is included in the standards solutions, allowing for the construction of a standard curve. The total volume for this assay is 300µl. SS; supernatant sample.

Two hundred and fifty microliters of charcoal suspension was added to the solution to separate free and bound radiolabel. After one minute, tubes were centrifuged at 16100g at room temperature, following which the supernatant was collected and mixed with 1ml of Optiphase Hi-Safe scintillation fluid. Radioactivity was measured using liquid scintillation spectroscopy.

2.11 PathHunter β-Arrestin recruitment Assays

2.11.1 Theory

In the PathHunter[®] β-arrestin recruitment assay, translocation of β-arrestin to the active receptor leads to complementary β-galactosidase fragments, fused to both the arrestin and receptor, interacting to form a functional enzyme (Figure 2.9). Formation of the

enzyme leads to increased production of a substrate which can be detected by chemiluminescent PathHunter® detection reagents (DiscoverX, 2013).

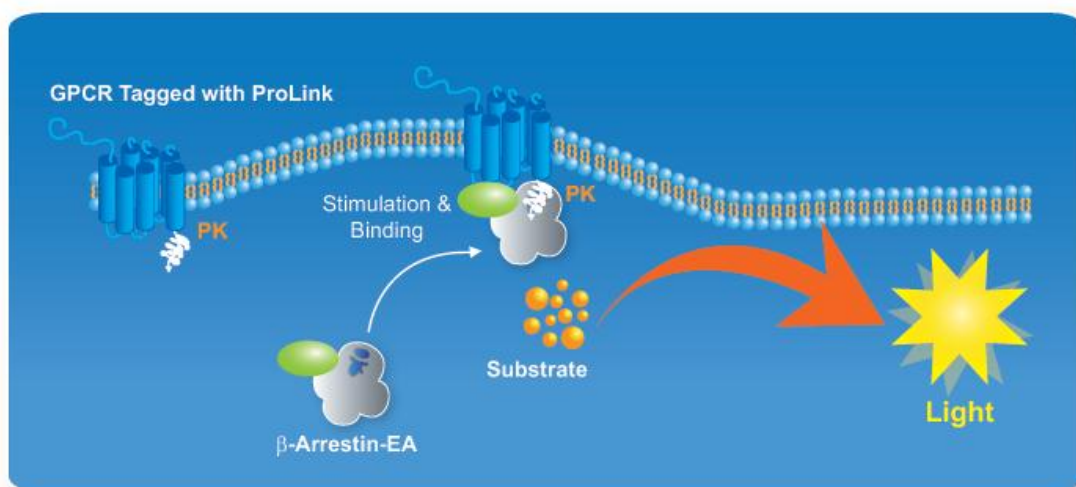


Figure 2.9: In a PathHunter® β -Arrestin recruitment assay, the MOP or DOP receptor is fused with the small enzyme fragment (ProLink™). This receptor is co-expressed in a system which stably expresses a fusion protein of β -Arrestin and the N-terminal deletion mutant of β -gal (in the above diagram referred to as β -Arrestin-EA). Activation of the GPCR leads to binding of β -Arrestin-EA, which forces complementation of the two enzyme fragments, resulting in the formation of an active β -gal enzyme. This newly formed enzyme activity can be measured through chemiluminescence (DiscoverX, 2013).

2.11.2 Methods

Assays were undertaken as described by DiscoverX (DiscoverX, 2013). The necessary reagents for experiments are provided with the PathHunter® express β -arrestin assay kit. Frozen cells, expressing either human MOP or human DOP receptor, are thawed and resuspended in 12 ml cell plating reagent (warmed to 37°C) provided with the kit. Cells are plated onto transparent bottom 96 wells plates (100 μ l/well) and are incubated for 24 hours, following which the desired concentration of the compound of interest is added. For MOP cells, a range of concentrations of Fentanyl (1pM-10 μ M) or Morphine (1pM-10 μ M) was added. A single concentration (10 μ M) of the compounds of interest incubated with MOP cells. For DOP cells, a range of concentrations of DPDPE (1pM-10 μ M) is added in the absence and presence of 1 μ M Dmt-Tic-OH. A top concentration of DPDPE (10 μ M) was incubated with 10 μ M of the compounds of interest to determine antagonist ability. The cells are incubated for 90 minutes at 37°C, following which 55 μ l

of the working detection reagent solution is added. The cells are incubated at room temperature for 1 hour, following which the plates are read using a Dynex MLX luminometer, set at 1 second/well to measure relative light units (RLU). Compound Activity is measured relative to basal activity.

2.12 Calcium mobilisation assays

2.12.1 Theory

Calcium mobilisation assays, in which increases in intracellular calcium levels can be monitored, allow for high throughput screening of the pharmacological profile of $G\alpha_q$ coupled GPCR's. This method can be adapted to $G\alpha_i$ coupled receptors. This adaptation is possible through the alteration of the C-terminal amino acids which confer selectivity to the desired G-protein. By changing between three and nine amino acids to match those of a $G\alpha_q$ coupled receptor, $G\alpha_i$ coupled receptors can stimulate the $G\alpha_q$ -phospholipase C (PLC) - inositol trisphosphate (IP_3)/ diacyl glycerol (DAG) pathway (Conklin et al., 1993). Activation of this pathway leads to an increase in intracellular calcium levels.

Measurement of calcium release is facilitated by the green-fluorescent calcium indicator, Fluo-4. Fluo-4 is usually provided as a non-fluorescent acetoxymethyl (AM) ester, called Fluo-4 AM, which is cleaved inside the cell to produce the fluorescent molecule, Fluo-4. Fluo-4 binds to calcium, and this complex is excited by light at 488nm wavelengths, emitting light at 516nm, providing high fluorescence levels (Figure 2.10) (Simpson, 2006).

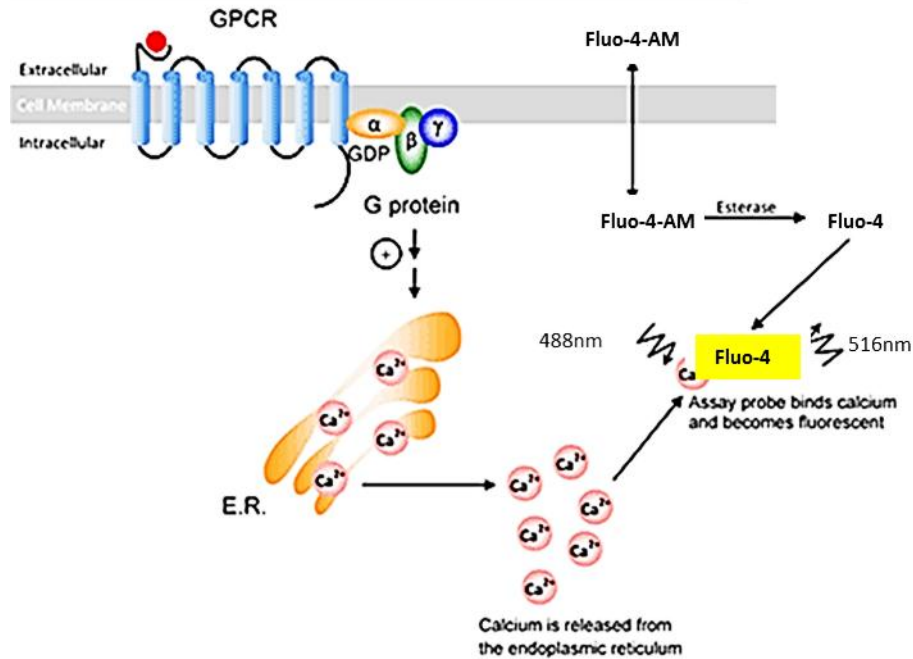


Figure 2.10: Following activation of a G_q α -subunit, cellular calcium levels increase. Fluo-4 binds to intracellular calcium, and this complex can be excited by light at 488nm wavelengths. Excitation of this complex leads to light being emitted at 516nm, which provides a detectable and measurable fluorescence level.

2.12.2 Methods

Stocks of cells are seeded in 96-well black clear bottomed plates at a density of 50 000 cells/well and incubated at 37⁰C overnight. Following this incubation period, cell media is aspirated and replaced with loading buffer (section 2.2.5) and incubated for a further 30 minutes at 37⁰C. Ligands of interest are used at a range of between 0.1pM-10 μ M. The loading buffer is aspirated and replaced with 100 μ l experimental buffer, placed in a FlexStation II and left at room temperature for 10 minutes, allowing for equilibration of basal fluorescence. Next, the basal fluorescence is measured (excitation 488nm, emission wavelength 516nm). The drugs are added and the Softmax software calculates the difference between the maximum and minimum fluorescence intensity units (FIU) in each well, expressing these results as a percentage.

2.13 Mouse *Vas deferens* Bio-assays

2.13.1 *Theory*

The mouse *vas deferens* (MVD) is an ideal model for testing opioid ligands as it expresses all opioid receptor subtypes (Lord et al., 1977). Isolated MVD can be electrically stimulated to produce a measurable contraction. Opioid receptors in nerves inhibit the release of neurotransmitters, and therefore are able to inhibit the contractile response produced by electrical stimulation. It is therefore possible to measure the inhibition of contraction caused by opioid agonists in the MVD (Guerrini et al., 2005).

2.13.2 *Methods*

Tissues were taken from male CD-1 mice (30-35 g). The animals were treated in accordance with European guidelines (86/609/ECC) and national regulations (DL 116/92). On the day of the experiment, the animals were culled with isoflurane. The prostatic portion of the *vas deferens* was removed from mice, using the technique described by Hughes (Hughes et al., 1975). The tissues were mounted in a glass bath for isolated organs, consisting of two chambers: an outer chamber, containing water heated at 33° C and an internal chamber, where the tissue was placed, which contained 5 ml of Krebs. In order to buffer the solution to pH 7.4, gaseous mixture composed of 95 % O₂ and 5% CO₂ was bubbled through the solution.

The tissues were positioned inside the bath and fixed using cotton wire. The upper support is connected to a rack, which is in turn connected to an isotonic force transducer (Basile 7006; srl Ugo Basile, Varese, Italy), while the lower support serves as an anchor at the base of the bath. The operating conditions were the following: preload of 0.3 g (maintained throughout the duration of the experiment); electrical stimulation was maintained by means of two platinum electrodes placed in the bath and these in turn were connected to an electrical stimulator in order to produce rectangular waves (duration of 1 ms), supramaximal voltage amplitude and 0.05 Hz frequency. Electrical stimulation induces contractions (twitch) in tissues which are converted by an isotonic transducer into an electrical signal, amplified and recorded by the digital acquisition system Power Lab 4/25 (model ML845, AD Instrument, USA). Under these

conditions, whilst changing the Krebs solution every 20 minutes, a stable twitch is obtained after 60 minutes at which point the experiment proceeds. The substances functional activity is studied with cumulative concentration response curves. These tests involve injecting volumes of increasing concentrations of the test compound into the bath, without changing the Krebs solution between injections. The curve can be regarded as completed when the concentration injected is no longer producing any effect on the twitch, at which point the maximum response is obtained.

2.14 Western Blotting for MAPK activity

2.14.1 Theory

Sample preparation begins with 24 hour foetal calf serum (FCS) starvation. The MAPK pathway is involved in a number of cell cycle and cell proliferation pathways. Removal of FCS allows for a quiescent state, lowering basal levels of phosphorylated MAPK's and making changes in this pathway more detectable. In western blotting, cell lysates are the most common samples used, and protein extraction, through cell lysis, attempts to collect all the protein released from the cell cytosol. The cell lysis buffer contains detergents which disrupt the plasma membrane, releasing the aforementioned protein. Ice-cold lysis buffer is administered and contains protease inhibitors to stop protein degradation. Following collection of the intracellular protein supernatant through sedimentation, it is diluted into a loading buffer containing bromophenol blue, which allows for the progression of the gel to be monitored, and sodium dodecyl sulphate (SDS) which acts as a denaturing detergent. The mixture is heated to ensure denaturing of the protein higher order structure. Denaturing the protein in this manner facilitates the movement of the protein in an electric field, as the negative charge of the amino acids is not neutralised (Mahmood and Yang, 2012).

Following denaturing of the protein, the sample is run in a gel (Figure 2.11). The gel is separated into two sections, the stacking gel and the resolving gel. The stacking gel is moderately acidic (pH 6.8). It also has lower concentrations of acrylamide which makes the gel more porous. This leads to poorer separation of the protein, but does allow them to form thin, sharply defined bands. Conversely, the resolving gel has a higher acrylamide concentration and is basic (pH 8.8). This in turn, makes the gels

pores narrower, allowing protein to be separated by size, with smaller proteins travelling further than larger proteins. This movement is facilitated by the negative charge of the protein, which is attracted to the positive electrode in a gel tank (Mahmood and Yang, 2012).

Following the running and separating of the proteins in the gel, they are transferred to a nitrocellulose membrane. In this case the electric field moves the protein from its position on the gel to the nitrocellulose membrane, which is placed between the gel and a positive electrode. During this process the gel should be in close contact with the membrane to allow for a clear image. The blotting of the protein from the gel to the membrane can be done in wet (submersed in a transfer buffer) or semi dry (soaked filter pads in a semi-dry blotter) conditions.

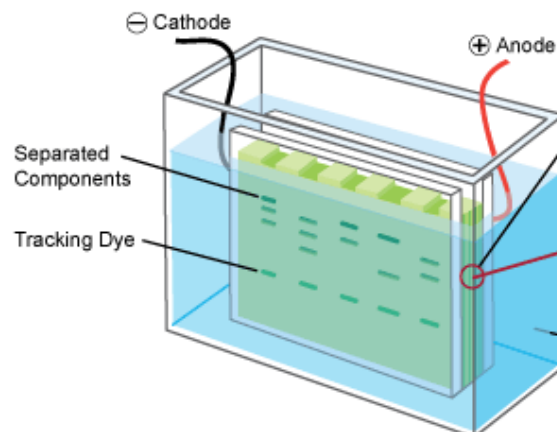


Figure 2.11: Schematic representation a of a SDS-PAGE gel separating proteins by size, through electrophoresis (Leinco Technologies, 2014).

In order to ensure that the antibodies used in this process do no bind to non-specific binding sites, the membrane is washed in blocking buffer made from TBST and 5% milk solution. This will reduce background noise.

The antibody used to detect the protein of interest (phospho-p38, phospho-ERK1/2, total p38 and total ERK1/2) is diluted in the desired ratio with TBST-5% BSA solution and incubated overnight. Following this incubation period, the membrane is washed several times to ensure removal of any excess antibody, decreasing background noise.

The membrane is then incubated in a secondary antibody targeted to the primary antibody. The secondary antibody is labelled with horseradish peroxidase (HRP), which is detected by the signal it produces relevant to the target proteins position (Figure 2.12).

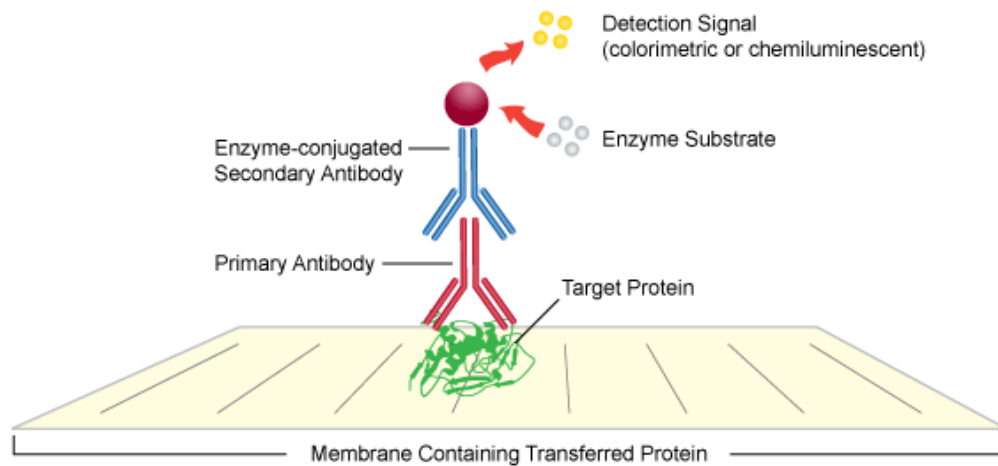


Figure 2.12: A primary antibody binds to the protein of interest on the nitrocellulose membrane. The primary antibody can be targeted by secondary antibodies which are attached to an enzyme. Addition of an enzyme substrate leads to a product which can be detected through chemiluminescence (Leinco Technologies, 2014).

2.14.2 Methods

Cells are plated on 6 well plates and allowed to grow to 90% confluency. Cells are serum-starved for 24 hours, following which the media is replaced by Krebs buffer (pre-warmed to 37⁰C) and incubated for a further 15 minutes. The desired concentrations of agonist are added to the wells and are again incubated at 37⁰C for 15 minutes. A ligand free well is also maintained to measure basal levels of the MAPK pathway of interest. The assay is terminated by aspirating the buffer and replacing it with ice cold lysis buffer (200µl), placing the plate on ice. Cells are removed by gentle scraping and trituration of the lysis buffer across the cell monolayer, and transferred into Eppendorf tubes. The lysate is spun at 14000rpm for 10 minutes at 4⁰C, whereupon 150µl of the supernatant is removed and added to 150µl 2x loading buffer. The protein is then denatured at 95⁰C, at which point it can be immediately used for experimentation or stored at -20⁰C.

In order to separate and identify the protein of interest, 50µl of denatured protein is run through 10% SDS-PAGE gels, alongside a protein ladder. Gels are loaded into a tank with 1x running buffer in a current of 150V for approximately 1.5 hours. Following running of the gel, it is placed onto a nitrocellulose membrane, placed into a semi-dry transfer buffer and transferred using a Trans-Blot® Turbo™ Transfer system (Bio-Rad, Hemel Hempstead) at 21V for 25 minutes. Immediately after completion of the transfer, the nitrocellulose membrane is blocked in a 5% milk/TBS-T solution for 1 hour. The blocking process is followed by incubation with the antibody of interest, either phosphorylated-p38 antibody (p-p38) (1µl in 3ml TBS-T) or phosphorylated-ERK1/2 (p-ERK1/2) (1µl in 6ml TBS-T), overnight with gentle agitation, at 4⁰C. The nitrocellulose is washed in TBS-T for 15 minutes, with this process being repeated three times. The nitrocellulose is then incubated in the secondary antibody, anti-rabbit IgG conjugated with horseradish peroxidase. The secondary antibody is diluted in a 5% milk/TBS-T solution (10µl on 10ml) for one hour, and then washed a further three times at 15 minute intervals.

The nitrocellulose membrane is coated with ECL (enhanced chemiluminescence) reagent, and left for 5 minutes. Excess reagent is removed, and the membrane is read in a ChemiDoc™ MP System (Bio-Rad, Hemel Hempstead).

Following analysis of the phosphorylated protein, the nitrocellulose membrane is washed in TBS-T, to remove excess ECL reagent, and the antibody is removed using Restore Plus™ stripping buffer. Following several washes to remove the stripping buffer, the membrane is again blocked in 5% milk-TBS-T solution and incubated with antibodies specific to the total (phosphorylated and unphosphorylated) protein present. The process is repeated as previously mentioned and the levels of total protein are measured, and used to normalise the phosphorylated protein measurements. This process is undertaken so that any variances in protein quantity in the loading process are accounted for.

2.15 Development of a MOP/NOP co-expression system

2.15.1 *Theory*

In order to determine how the presence of both receptors affects both the binding affinity of our drugs and the effects on the signal transduction pathways, a cell line was produced that stably expressed both MOP and NOP receptors. Expression of receptors in continuous cell lines is often higher than in *ex vivo* tissue. Furthermore, *ex vivo* tissue also expressed other members of the opioid family, which are also known to form heterodimers with our receptors of interest. The continuous cell line will allow for the interactions of MOP and NOP only to be studied. In the case of the CHO cell lines, a NOP plasmid vector, with hygromycin B⁺ resistance (pcDNA 3.1/Hygro (+)), was transfected into CHO cells which express the MOP receptor, and had resistance to G418 (geneticin). In the case of the HEK cells, both MOP and NOP vectors were individually expressed into HEK wild type cells and cells with stable expression chosen to be transfected with either the MOP or NOP cell lines, creating the dual expression system. Confirmation of transcription levels of MOP and NOP were measured by reverse transcription-quantitative polymerase chain reactions (RT-qPCR), using extracted RNA from monoclonal cell lines, following which cells demonstrating the desired transcription levels were screened in radioligand saturation binding assays.

2.15.2 *Concentration-death plot*

In order to ensure successful transfection, as well as avoiding reversion in monoclonal co-expressing cell lines, selected concentrations of the desired antibiotic are used. Concentration-death plots for hygromycin B and geneticin were constructed for HEK_{w/t} cells, using previously defined methods (Liu et al., 2004). A range of concentrations of hygromycin B (50-1000 $\mu\text{g}\cdot\text{ml}^{-1}$) and geneticin (50-1000 $\mu\text{g}\cdot\text{ml}^{-1}$) were separately added, in random order, to two 12-well plates containing HEK_{w/t} cells and observed by two blinded observers under the light microscope for 14 days. Observers estimated the percentage of live cells in each well when compared to an antibiotic free well and mean values were recorded. The concentration of geneticin or hygromycin B that causes 100% cell death at 4 days was used as the **selection pressure**, while the concentration that caused 100% cell death at 14 days was used as the **stock pressure**.

2.15.3 *Stable transfection*

An OPRM1-pcDNA 3.1/geneticin (+) plasmid vector (human MOP gene) was purchased from S&T (Missouri University of Science and Technology, cDNA Resource Centre, USA). For NOP receptor transfections, a pcDNA 3.1/hygromycin B plasmid vector was purchased from Invitrogen which S&T used to produce an OPRL1-pcDNA/Hygro (+) plasmid vector. Vector concentrations were estimated to be 500ng/ μ l using a NanoDrop[®].

Two 6-well plates of CHO_{hMOP}, or two 6-well plates of HEK_{w/t} cells, were cultured to ~60% confluency, following which medium was substituted with serum-free antibiotic free (SF-AF) medium, in order to promote optimal transfection. The desired plasmid vector was transfected using a FuGene[®] HD transfection reagent kit. The FuGene[®] HD transfection reagent kit uses a multi-component reagent that forms a complex with the cDNA which promotes access into the cells. Based on previous work, a transfection complex of 3:1 was prepared using 1861 μ l of SF-AF medium and 119 μ l of FuGene[®] HD reagent. The complex was incubated at room temperature for 15 minutes, following which 150 μ l of the complex was added to each well. The cells were incubated at 37⁰C for 24 hours to allow for incorporation of the complex.

2.15.4 *Sub-cloning*

Following the 24 hour incubation period, medium in the 6-well plates was substituted by the desired selection pressure medium (supplemented by the antibiotic required). Cells were incubated at 37⁰C, with the medium changed frequently to remove dead non-transfected cells, until 100% confluency was reached. Following this, cells were trypsinised and resuspended in 10ml of stock medium. The concentration of cells (cells. μ l⁻¹) was estimated using a haemocytometer and then adjusted to a desired concentration of 0.1cells. μ l⁻¹. The cell suspension was distributed into 96-well plates (200 μ l/well). Plates were incubated in a humidification box, at 37⁰C, for two weeks, during which time the medium was replaced every three days. Wells were observed under a microscope every four days. Wells which included one clear and spherical colony were identified as having grown from a single cell, and were marked and

allowed to grow to confluency. Wells that appeared to grow from more than one cell were excluded. Confluent cells were moved to 6-well plates and grown to confluency in stock medium, following which they were moved to T75 flask and measured in a primary PCR screen, to determine the relevant RNA expression levels, before saturation binding assays were undertaken. For CHO_{hMOP/NOP} cells, 42 monoclonal cell lines were grown. HEK_{hMOP} produced 10 monoclonal cell lines, HEK_{hNOP} 11 monoclonal cell lines and HEK_{hMOP/NOP} produced 8 monoclonal cell lines.

2.16 Reverse Transcription-PCR

2.16.1 Theory

In polymerase chain reaction (PCR) experiments, DNA can be amplified exponentially and allows for the starting quantity of DNA to be measured. PCR enables the identification of the presence or absence of a gene in an organism's genome. In the experiments detailed in this thesis, reverse transcription PCR, a variant of the PCR technique, was used to determine relative gene expression.

Total RNA is extracted from the sample of interest (section 2.16.3); following which genomic DNA (gDNA) is degraded, using DNase treatment, from the sample. This process is undertaken to ensure that gDNA is not amplified in the ensuing PCR reaction. The cleaned RNA is reverse transcribed, creating copy DNA (cDNA) from messenger RNA (mRNA). In order to ensure that DNase treatment was successful, two sets of samples are incubated, called RT⁺ and RT⁻. The RT⁺ sample contains the reverse transcriptase enzyme, which allows gene expression to be quantified during PCR. The RT⁻ reaction does not contain the reverse transcriptase enzyme and acts as a negative control. Any positive signal generated from the RT⁻ sample may indicate contamination by gDNA.

The reverse transcription PCR technique uses repeated thermal cycles to amplify sample cDNA. The thermal cycle can be broken down into three stages. The first of these stages separates the double-stranded DNA into single strands, and is known as the denaturation stage. The hybridisation stage follows and involves the binding of specific oligonucleotide primers, which are specifically designed for both strands of the

sequence. In the final stage, called the extension stage, the thermo-stable DNA polymerase enzyme is directed by the bound primers to produce complimentary strands to the single stranded DNA (from 5' to 3' end). Due to both the sense and antisense strands being duplicated during each cycle the amplicon (a piece of DNA or RNA that is the source and/or product of a replication event) is theoretically doubled per cycle.

In RT-qPCR, a fluorometric probe is used to measure the relative quantity of DNA at the end of each cycle. From these measures, an amplification curve is produced which demonstrates the amplification of DNA. Specialist software (in this thesis the StepOne™ programme) determines at which point the threshold quantity of fluorescence is reached (termed cycle threshold; C_t) (Figure 2.13). The C_t is inversely proportional to the starting quantity of cDNA. Therefore, a low C_t value is indicative of a high starting quantity of cDNA and *vice versa*. The C_t value is normalised to that of an endogenous control (EC) gene producing the ΔC_t , allowing the gene of interest (GOI) to be quantified. This is shown by the formula:

$$\Delta C_t = C_{tGOI} - C_{tEC}$$

The EC is selected on the basis that its expression remains unchanged regardless of the experimental conditions and effectively normalizes for variation and starting quantity in the reaction.

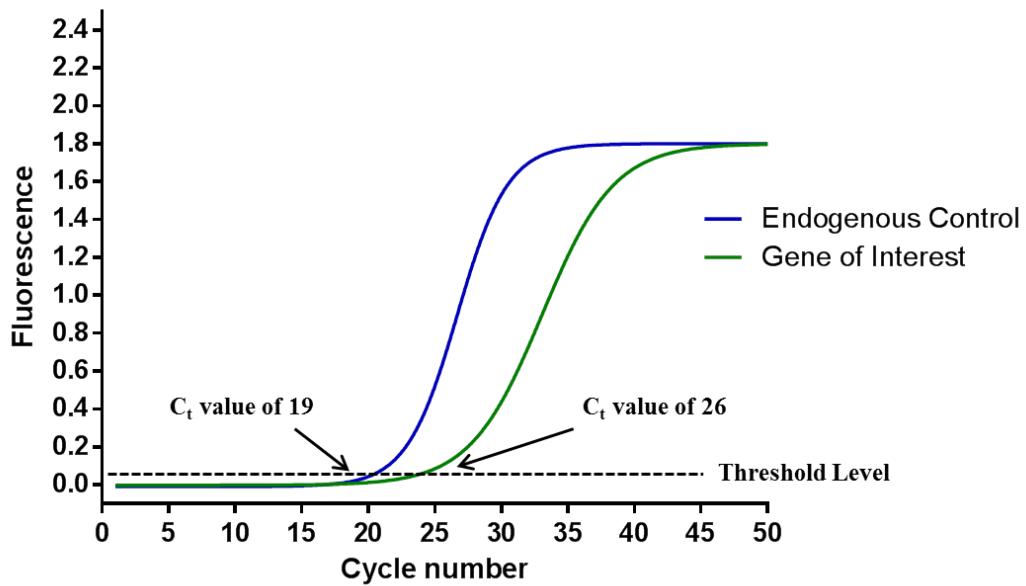


Figure 2.13: A representative PCR curve. The point at which the endogenous control (EC) and the gene of interest (GOI) cross the threshold level and produce their respective C_t values is shown above. The ΔC_t is the difference between these two values, in this case $26-19=7$.

2.16.2 *TaqMan*TM probes

*TaqMan*TM probes are hydrolysis probes that are designed to increase specificity in RT-qPCR experiments. These probes are specific to the target sequence which is to be amplified. The *TaqMan*TM probe possesses a fluorophore (6-carboxyfluorescein; FAM, VIC) covalently bonded to the 5'-end of the oligonucleotide probe and a quencher (minor groove binder; MGB) at the 3'-end (Kutyavin et al., 2000). These are bound in close proximity so that the fluorophore's fluorescence is suppressed by the quencher. The quencher molecule quenches the fluorescence emitted by the fluorophore when excited by the cyclor's light source via FRET (Fluorescence Resonance Energy Transfer). During the complementary strand extension, *Taq* polymerases nuclease activity hydrolyses the probe which, in turn, leads to separation of the fluorophore and quencher, releasing detectable fluorescence (Figure 2.14). *TaqMan*TM probes are specifically designed for a target sequence and, therefore, fluorescence is only generated by extension of this target sequence.

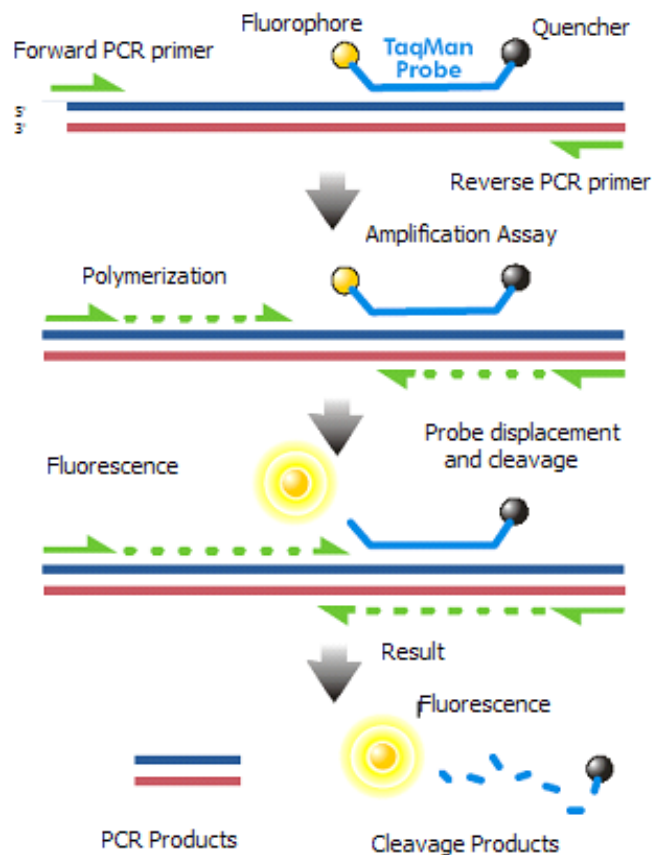


Figure 2.14: TaqMan probe activity in the PCR assay. The primers and probe bind to the template DNA and fluorescence is suppressed due to the close proximity of the probe and quencher. As the *Taq* polymerase extends the complementary strand in a 5' to 3' direction, the fluorophore is irreversibly cleaved due to polymerase nuclease activity. The cleaved fluorophore produces a signal (yellow) which can be measured (Wikipedia, 2014).

2.16.3 Total RNA extraction and reverse transcription

Total RNA from T75 flasks containing CHO_{hMOP/NOP}, HEK_{hMOP}, HEK_{hNOP} or HEK_{hMOP/NOP} cells were extracted using TriReagent[®]. Addition of 1ml TriReagent[®], which combines phenol and guanidine thiocyanate in a monophasic solution, leads to the immediate inhibition of RNase activity. The TriReagent[®] lyses the cells. Chloroform is added and the mixture was vortexed until an emulsion has formed. The emulsion was centrifuged (13000rpm/15 min/ 4⁰C), resulting in the separation of homogenate into aqueous and organic phases. RNA is separated into the aqueous phase, separating from DNA in the interphase, while proteins are located in the organic phase. The aqueous phase is collected, and RNA is precipitated from this phase by the addition

of isopropanol and incubation on ice for 10 minutes. The RNA was centrifuged at 13000rpm for 10 min at 4⁰C. The supernatant was removed and the pellet was resuspended in 50-100µl of PCR-grade water (dependent on size). Samples were stored at -80⁰C until DNase treatment.

The samples mentioned previously, were treated with TURBO™ DNase to enzymatically degrade any gDNA present. The total RNA present was determined by NanoDrop™. The concentration of RNA was adjusted so that a maximum of 10µg was included in each reaction. The reaction was incubated for 30 minutes at 37⁰C (Table 2.7).

Component	Volume (µl)
10x buffer	5
Dnase I	1
≤10µg RNA in PCR-grade water	44

Table 2.7: Reaction volumes for TURBO™ DNase total RNA treatment.

Following this incubation period, 5µl of inactivation reagent was added to the mixture. Following a further 3 minutes incubation period, the mixture was centrifuged(13000rpm/2 min/RT) and the supernatant (RNA solution) was removed and stored at -20⁰C.

2.16.4 *Reverse transcription*

The RNA solution was reverse transcribed using a cDNA reverse transcription kit. The master mix was prepared as per the manufacturers instructions (Table 2.8).

Component	Volume (µl)
10x RT buffer	2
25x dNTP mix	0.8
10x RT random primers	2
Multiscribe™ reverse transcriptase	1
Rnase inhibitor	1
PCR-grade water	3.2

Table 2.8: Reaction mixture for a cDNA reverse transcription master mix.

10µl of the DNase-treated RNA was mixed with an equal amount of the RT master mix and then incubated according to a predefined thermal cycler program (Table 2.9). Following this process, the samples were stored at -20⁰C until PCR was performed.

	Stage	Temperature (°C)	Time (min)
Pre-incubation	1	25	10
Reverse transcription	2	37	120
Enzyme inactivation	3	85	5
Hold	4	4	indefinite

Table 2.9: The thermal cycler program for the reverse transcription process.

2.16.5 *Polymerase chain reaction*

The TaqMan™ PCR kit was used in order to prepare the samples for the polymerase chain reaction using the StepOne® software, with components prepared as shown in Table 2.10. The master mix consists of the necessary components for a reaction (DNA polymerase, dNTPs, dUTP and uracil-DNA glycosylase). The assay mix for the EC or GOI contained the forward and reverse primers (final concentration of 900nM) and the dye-labelled (FAM or VIC) Taqman™ probe at a final concentration of 250nM. All samples were incubated according to the thermal cycler programme of the StepOne® instrument (Table 2.11). The assay mix for the EC or GOI contained the forward and

reverse primers (final concentration of 900nM) and the dye-labelled (FAM or VIC) Taqman™ probe at a final concentration of 250nM.

Component	Volume (µl)
2x Master Mix	10
20x Assay Mix for EC or GOI	1
Template cDNA	2
PCR-grade water	7

Table 2.10: Reaction mixture preparation for TaqMan™ PCR.

Stage	Steps per cycle	Description	Temperature (°C)	Time
1	1	Uracil-DNA glycosylase incubation	50	2 min
1	2	Polymerase activation	95	10 min
1	3	denaturation	95	15 sec
2	-	Annealing/extension*	60	1 min

Table 2.11: Thermal cycler programme for polymerase chain reaction. *Fluorescence measured at the end of this stage.

2.17 Data analysis

Data representation (i.e mean (\pm SEM)) and n values are shown in the figure legends of each graph, as are the details of the statistical analysis undertaken. GraphPad PRISM v6.01 (GraphPad Software Inc., San Diego, USA) was used to undertake all statistical analysis, curve fitting and linear or non-linear regression analysis. Saturation and displacement curves were analysed using non-linear regression (fit) one-site binding (hyperbolae) or dose-response with variable slope (sigmoidal). pK_i values were determined from displacement curves and values were determined using non-linear regression (corrected using the Cheng and Prusoff equation) (Cheng and Prusoff, 1973). pEC_{50} and E_{max} values in functional experiments were obtained from the sigmoidal curve with variable slope.

Chapter 3 **Characterisation of Novel Fentanyl-Based Bivalent Pharmacophores**

3.1 Introduction

Chemical alteration and conjugation of two ligands, for adaptation to form bivalent pharmacophores, can lead to the possibility of potential changes to each pharmacophore's selectivity and/or functional activity. Many attempts at synthesising bivalent pharmacophores have led to changes in functional ability, while some have shown a loss of selectivity, or gain in affinity, for receptor sub-types. This can be due to chemical alterations to the pharmacophores themselves, or involve the distance between the pharmacophores associated with linker length or chemical structure (Daniels et al., 2005, Del Giudice et al., 2011).

With this in mind, the newly synthesised Fentanyl bivalents (Table 3.1, Figure 3.2 and Figure 3.4) will be tested in traditional radioligand binding assays to determine affinity (pK_i) and functional assays, used to determine potency (pEC_{50}) and efficacy (E_{max}) at various stages through the signal transduction pathway (Figure 3.1), to determine how the chemical alterations and numerous linkers could potentially affect our synthetic MOP agonist(Fentanyl)-DOP antagonists (Dmt-Tic-OH). In this case, signal transduction will be monitored through activation of G-proteins and recruitment of β -arrestins. Furthermore, newly conjugated [Fentanyl]-[Ro65-6570] (MOP agonist/NOP agonist) bivalent pharmacophores will be screened to assess G-protein activation.

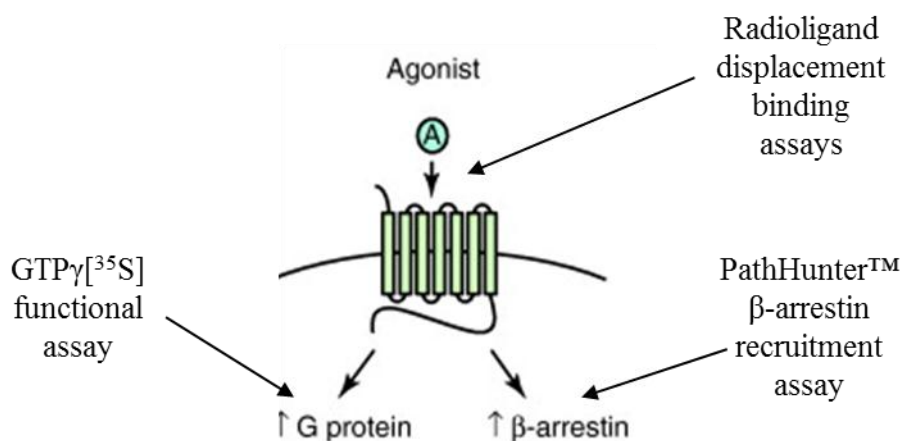


Figure 3.1: Ligand interactions will be studied through radioligand displacement bindings assays (Affinity of the drug), GTPγ[³⁵S] functional assays (to determine potency and efficacy) and the PathHunter™ β-arrestin recruitment assay (to determine ability to recruit β-arrestins). (Whalen et al., 2011).

3.2 Hypothesis

In this chapter we will investigate the hypothesis that chemical alteration of Fentanyl and linking of this novel structure to the DOP antagonist Dmt-Tic-OH, or the NOP agonist Ro65-6570, will lead to the formation of a compound that retains the full agonist ability of Fentanyl, while obtaining DOP antagonist activity or NOP agonist activity.

3.3 Aims

In this chapter, we will study the effects of conjugating synthetic pharmacophores by using CHO cells expressing recombinant opioid receptors (CHO_{hMOP}, CHO_{hDOP}, CHO_{hKOP} and CHO_{hNOP}) to define their pharmacological properties (binding affinity and functional activity). Binding affinity will be determined using previously determined radioligand affinities (Ibba et al., 2008). Functional activity will be determined using GTPγ[³⁵S] and a β-arrestin recruitment assay. This work will allow us to determine whether the formation of [Fentanyl]-[Dmt-tic] bivalents, or the [Fentanyl]-[Ro65-6570] bivalents, has successfully retained the desired activity (MOP agonist and DOP antagonist/NOP agonist) and whether linker length has an effect on the actions of these novel compounds.

For reference, the unconjugated functionalised Fentanyl molecules (no linker molecule or second pharmacophore attached) will be referred to as an RR compounds. Compounds with a second pharmacophore and/or linker molecule (Figure 3.3) attached will be referred to by number (Table 3.1) or, when discussed as a group, the F-compound series. For the [Fentanyl]-[Ro65-6570] bivalents, these compounds will be referred to as Mop/NOP1-3 (MN1-MN3) (Figure 3.4).

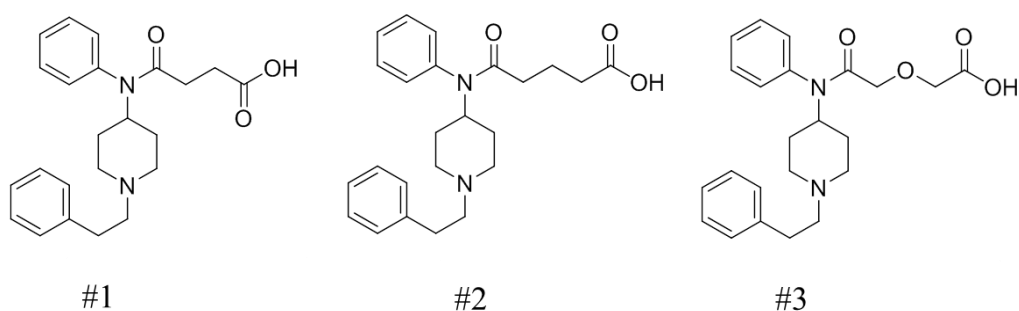


Figure 3.2: Chemical structures of the unconjugated Fentanyl derivatives. The compounds have linker molecules attached in the northern hemisphere of the Fentanyl structure. Compound #1 has a linker of 2 carbon atoms, #2 has a linker of 3 carbons atoms and #3 has a linker consisting of two carbon atoms and an oxygen atom. These derivatives were developed by *Dr Ruben Vardanyan (University of Arizona)*.

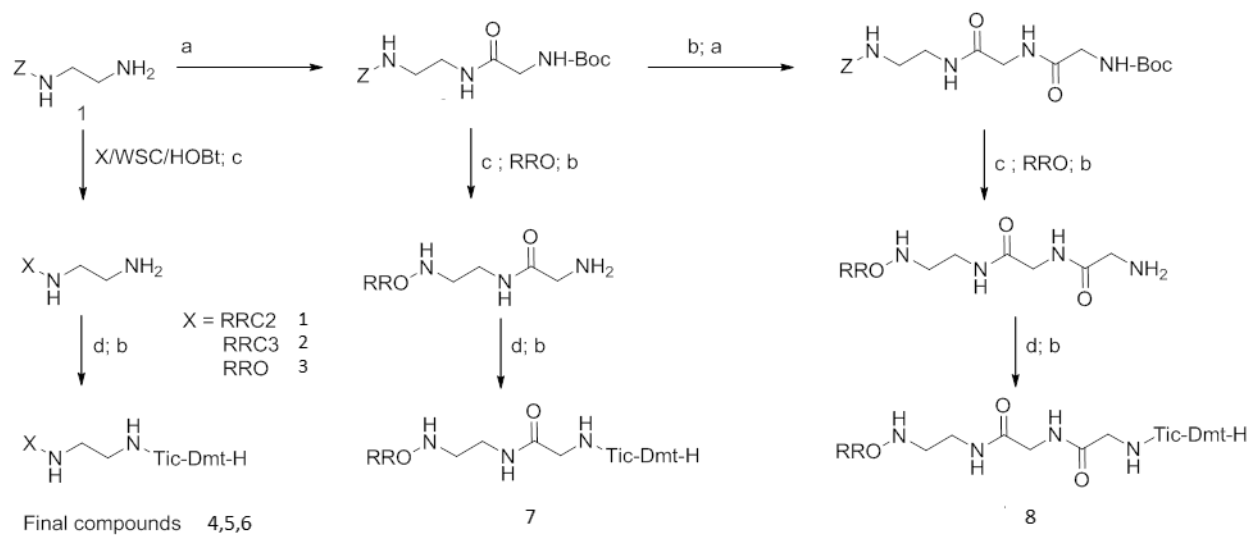


Figure 3.3: Synthesis of Fentanyl/Dmt-Tic based bivalent ligands. The intermediate compounds (F-compound attached to a linker molecule), are called #1, #2 and #3, while final compounds (Fentanyl-linker-Dmt-Tic-OH) are called #4 - #8 respectively.

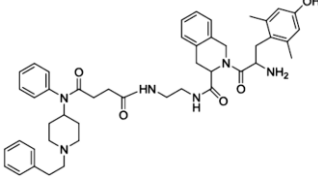
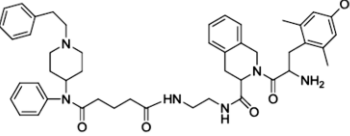
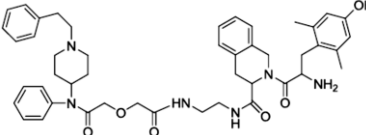
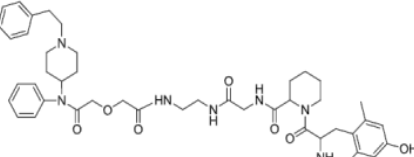
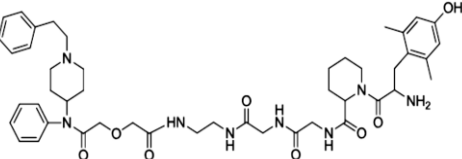
Structure	Compound #
	#4
	#5
	#6
	#7
	#8

Table 3.1: The chemical structure of the [Fentanyl]-[Dmt-Tic] analogues. The nomenclature used in the thesis for the compounds is shown in the right hand column.

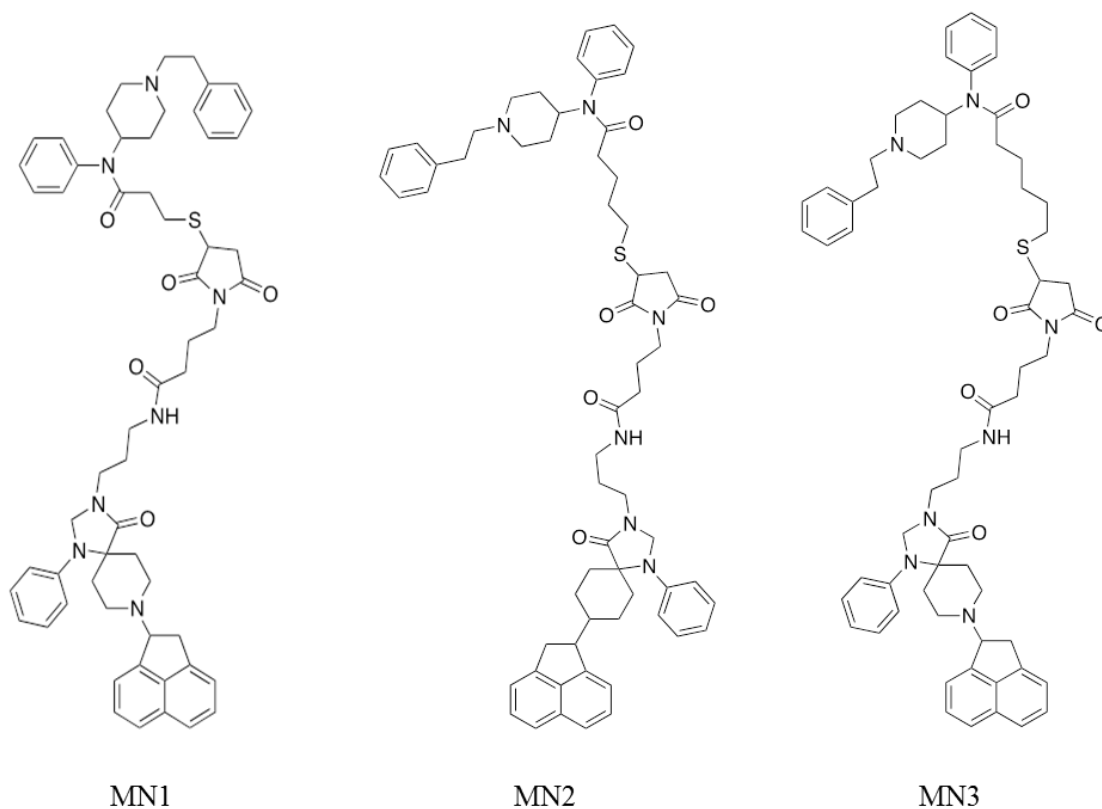


Figure 3.4: The MOP-NOP (MN) bivalent compounds based on the conjugation of Fentanyl and Ro65-6570.

3.4 Results

3.4.1 *Displacement binding assays-unconjugated F-compounds (#1, #2, #3).*

F-compounds attached to a linker, but without the second pharmacophore, (#1; #2; #3) failed to displace [³H]-DPN in CHO cell membranes expressing the MOP, DOP and KOP receptors. These compounds also failed to displace [³H]UFP-101 in CHO cell membranes expressing NOP receptors (Figure 3.5).

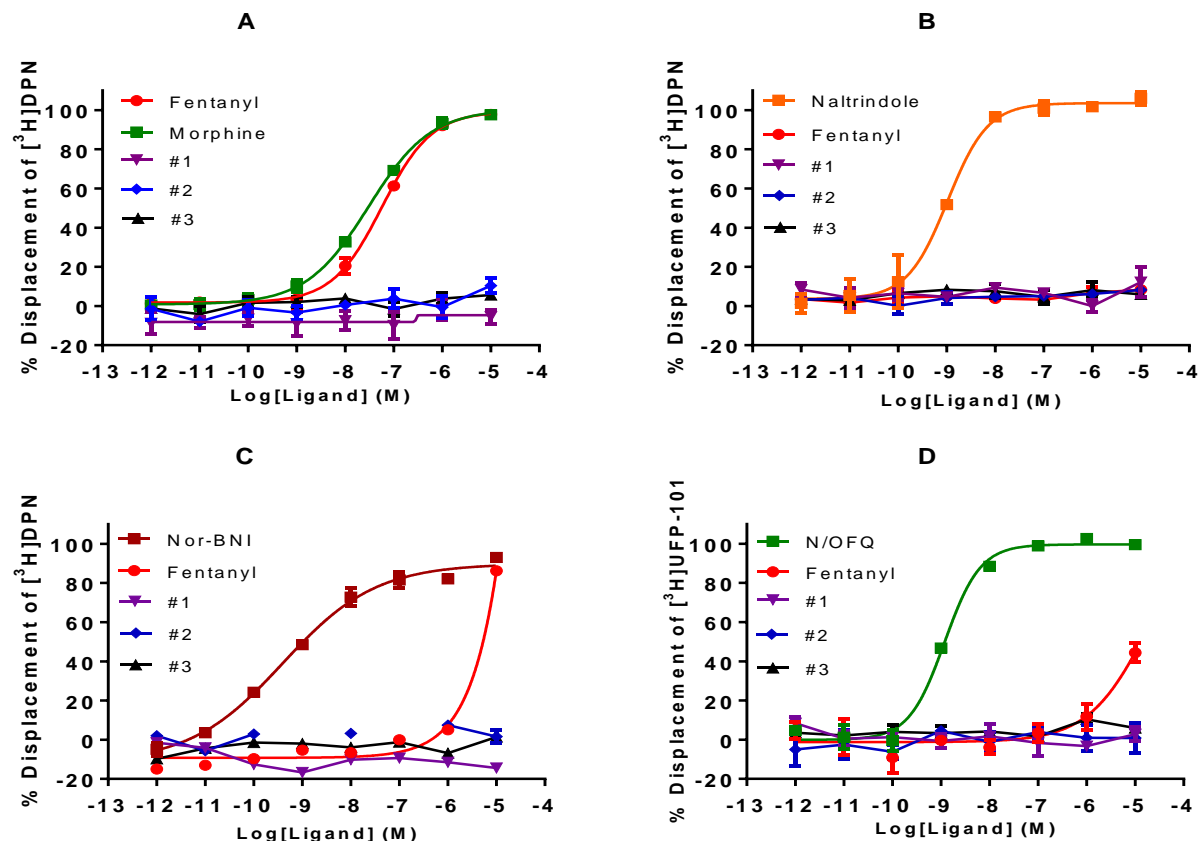


Figure 3.5: Displacement of tritiated Diprenorphine (³H-DPN) by Fentanyl, the unconjugated F-compounds (#1, #2, #3) and reference ligands at (A) CHO_{hMOP}, (B) CHO_{hDOP}, (C) CHO_{hKOP} and the displacement of tritiated UFP-101 (³H]UFP-101) by the unconjugated F-compounds, Fentanyl and Nociception/Orphanin FQ at (D) CHO_{hNOP} cell membranes. Data are means (±SEM) of five experiments for all cell lines. Reference ligands: Fentanyl; Naltrindole; Nor-BNI (Norbinaltorphimine); N/OFQ, (Nociceptin/Orphanin FQ).

3.4.2 Displacement Binding assays- F-compounds (#4, #5 and #6)

At the MOP receptor, #4, #5, #6 displaced the binding of [³H]-DPN in a concentration dependent and saturable manner. Binding affinities (pK_i) were: #4 (7.31), #5 (7.58) and #6 (7.91) (Figure 3.6; Table 3.2). The binding affinities of the test compounds #5 and #6 were not statistically different to that of the reference ligand, Fentanyl (8.13). Compound #4 was significantly different, displaying a lower binding affinity for MOP. At the DOP receptor, all ligands had nanomolar affinity: #4 (8.03), #5 (8.16) and #6 (8.17). Of the test compounds, only #4 was significantly different compared to Dmt-Tic-OH (8.95). Compounds (#4, #5, #6) displaced [³H]-DPN binding to CHO_{hKOP} membranes [NorBNI (10.16); #4 (7.29); #5 (7.02); #6 (7.13)]. [³H]UFP-101 was also displaced by the test compounds in CHO_{hNOP} membranes [N/OFQ (10.69) #4(7.28); #5(6.96); #6(7.48)].

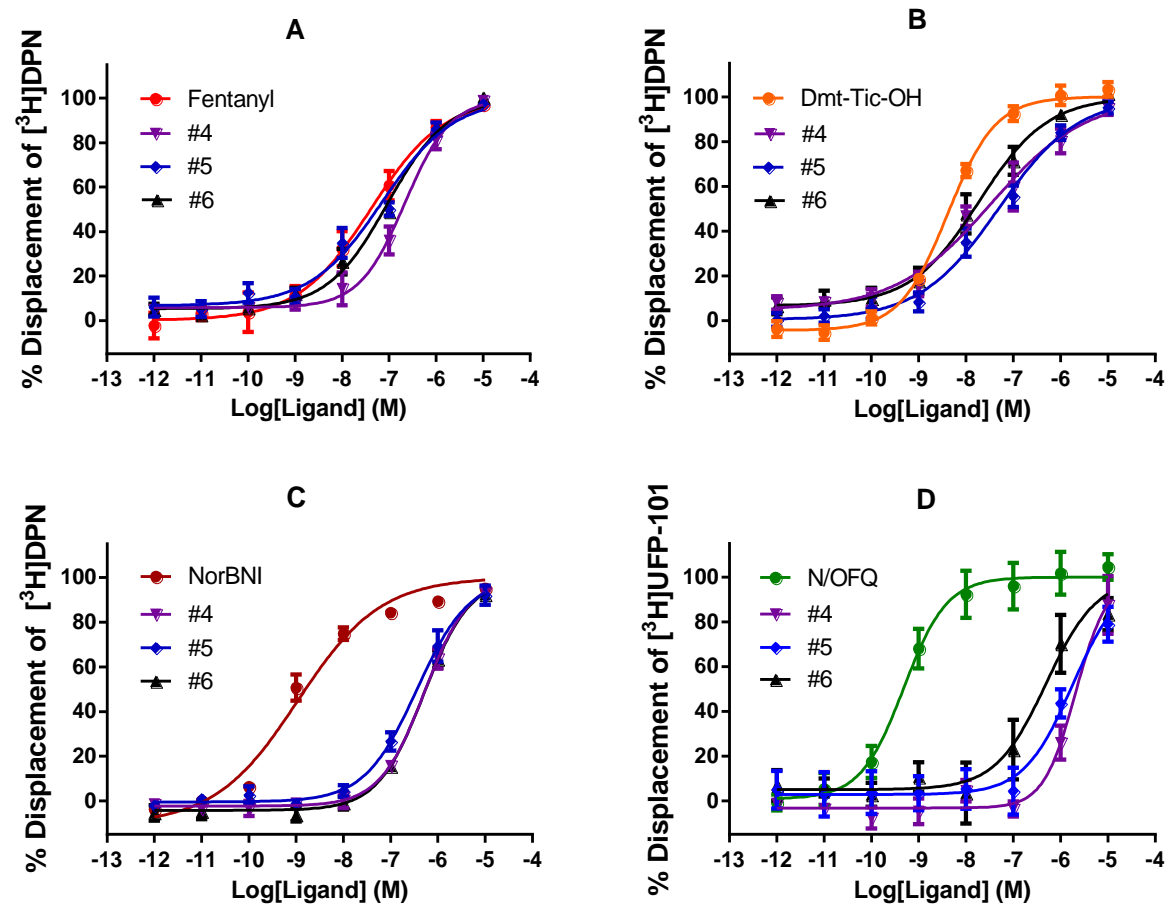


Figure 3.6: Displacement of tritiated diprenorphine ($[^3\text{H}]\text{-DPN}$) by Fentanyl, the conjugated F-compounds (#4, #5, #6) and reference ligands at (A) CHO_{hMOP} , (B) CHO_{hDOP} , (C) CHO_{hKOP} and the displacement of tritiated UFP-101 ($[^3\text{H}]\text{UFP-101}$) by the conjugated F-compounds and N/OFQ at (D) CHO_{hNOP} cell membranes. Data are means (\pm SEM) of eight experiments for all cell lines.

3.4.3 $GTP\gamma[^{35}S]$ functional assays-Compounds #4, #5 and #6

$GTP\gamma[^{35}S]$ assays were used as a functional activity screen. Compounds #4, #5 and #6 stimulated the binding of $GTP\gamma[^{35}S]$ in a concentration dependent and saturable manner at the MOP receptor (Figure 3.7). The pEC_{50} values of #5 (7.13) and #6 (7.52) showed no significant difference to that of Fentanyl (7.31) at MOP. The pEC_{50} for #4 (6.74) was significantly different to that of Fentanyl (7.32) at MOP. E_{max} values, compared to Fentanyl (3.88), for compounds #4: 1.18; #5: 2.19; #6: 1.98 were significantly different. Relative intrinsic activity ($\alpha-E_{max}$) and potency (pEC_{50}) values are summarised in Table 3.3.

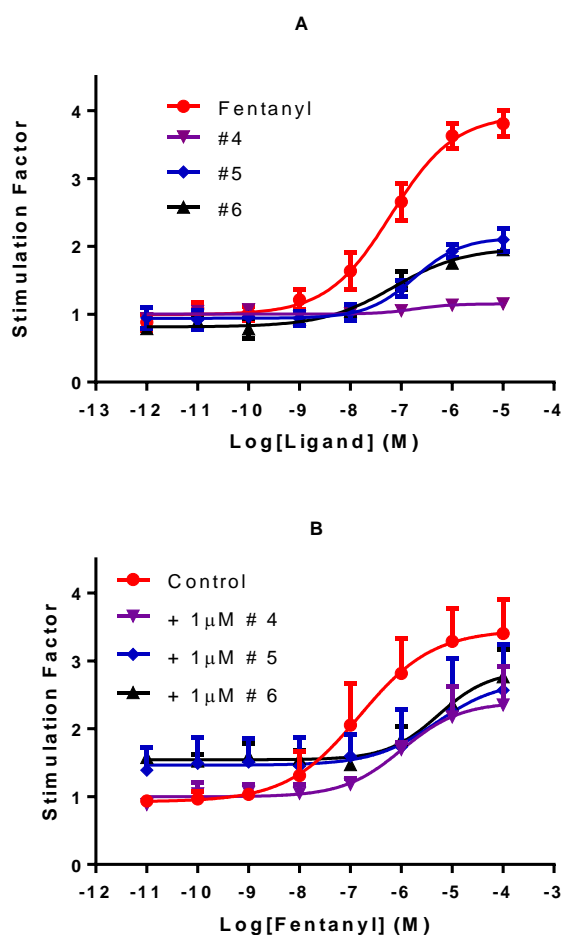


Figure 3.7: Ligand stimulated $GTP\gamma[^{35}S]$ binding by A) Fentanyl, and compounds #4, #5 and #6 are shown in CHO_{hMOP} cell membranes. (B) The compounds were co-incubated, at a concentration of $1\mu M$, with Fentanyl. Data are shown as mean (\pm SEM) for 5 experiments. The arrows within the graph demonstrate residual agonism.

Since compounds #4, #5 and #6 showed reduced efficacy at CHO_{hMOP} , these were screened in an antagonist assay (Figure 3.7). A fixed concentration ($1\mu M$) of the

bivalent compounds was added to varying concentrations of Fentanyl, in CHO_{hMOP} cells; there was a rightward shift in the Fentanyl concentration response curve. Both #5 and #6 displayed E_{max} values similar to Fentanyl (Table 3.3). E_{max} in the presence of #4 was significantly different to Fentanyl. The resulting pK_b values were: #4 (6.87), #5 (7.55) and #6 (7.81).

In the CHO_{hDOP} membranes, DPDPE (D-Pen², D-Pen⁵ Enkephalin) stimulated the binding of GTPγ [³⁵S] (pEC₅₀: 7.70; E_{max}: 2.76). Compounds #4, #5 and #6 did not stimulate the binding of GTPγ [³⁵S] (Figure 3.8). When compounds #4, #5 and #6 were co-incubated with the DOP agonist DPDPE, all compounds caused a rightward shift in the concentration response curves (Figure 3.8). Compounds, #5 and #6, produced pK_b values of 8.06 and 8.11 respectively. Compound #4 produced a pK_b of 6.85 (Table 3.3).

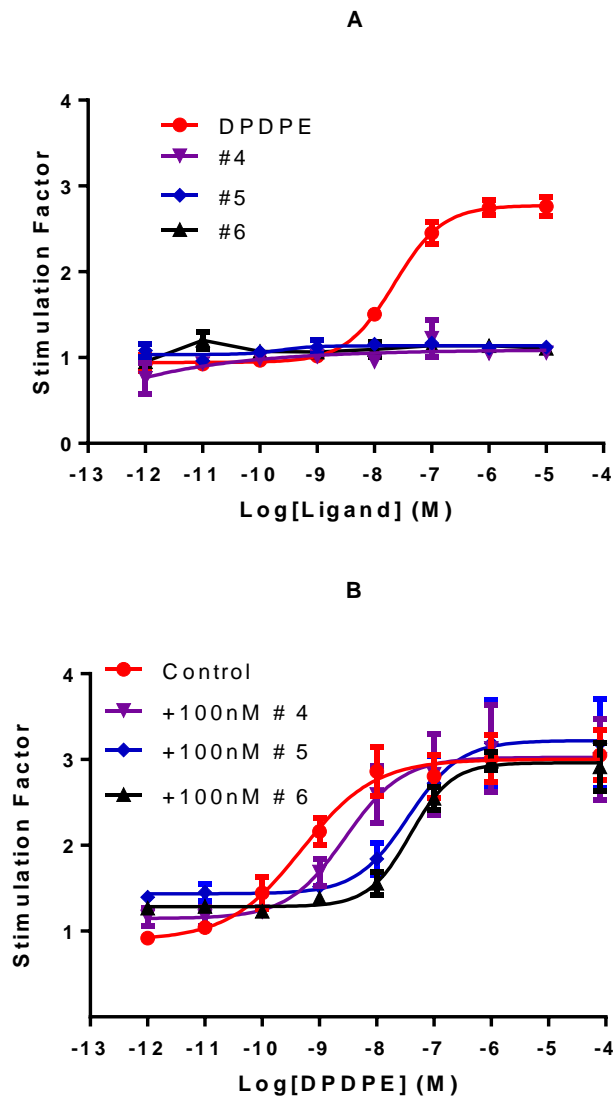


Figure 3.8: $\text{GTP}\gamma[^{35}\text{S}]$ functional response curves demonstrating (A) DPDPE stimulated $\text{GTP}\gamma[^{35}\text{S}]$ binding. The F-compounds (#4, #5, and #6) showed no activity in CHO_{hDOP} cell membranes. (B) DPDPE stimulated binding in the absence and presence of 100nM of test ligands. All data are the mean (\pm SEM) of five experiments. Reference ligand, DPDPE; [D-Pen², D-Pen⁵ Enkephalin].

Functional assays were performed in cell membranes expressing the KOP and NOP receptor; bivalents #4-#6 showed no agonist or antagonist activity at these receptors (Figure 3.9).

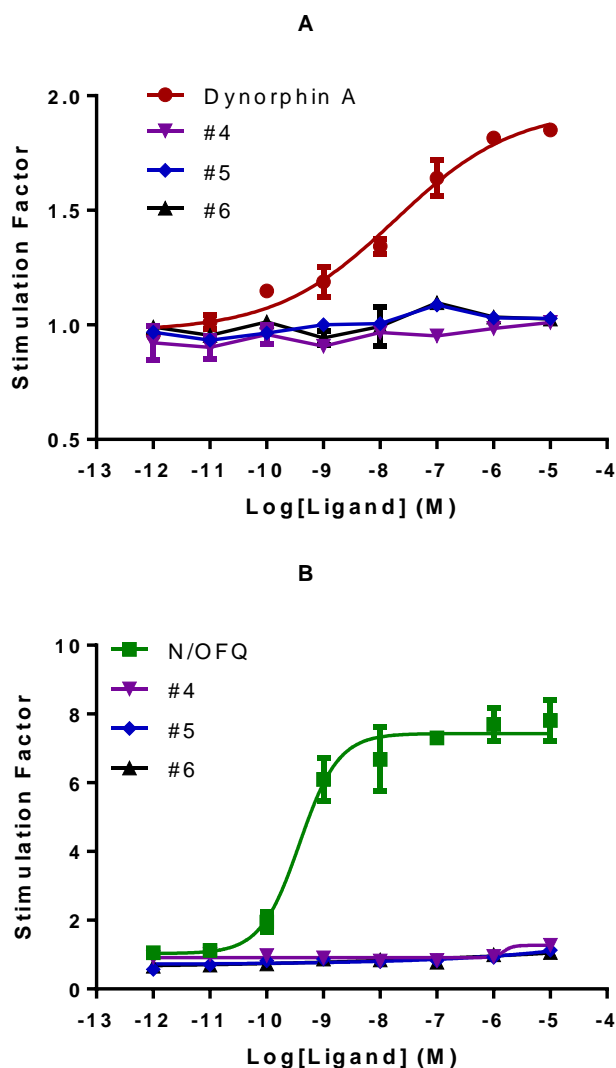


Figure 3.9: GTP γ [³⁵S] functional response curves demonstrating (A) Dynorphin-A stimulated GTP γ [³⁵S] binding. The F-compounds (#4, #5, and #6) showed no activity in CHO_{hKOP} cell membranes. (B) N/OFQ stimulated GTP γ [³⁵S] binding. The F-compounds (#4, #5, and #6) showed no activity in CHO_{hNOP} cell membranes. All data are mean (\pm SEM) of five experiments.

With respect to the reference compounds #1, #2, #3; compounds #4-#6 restore MOP binding. The substantial loss in MOP efficacy compared to Fentanyl indicated an alteration in the interaction between the Fentanyl pharmacophore and the MOP receptor. As previously noted in bivalent ligands, the distance between pharmacophores can affect both affinity and efficacy (Dietis et al., 2009). Moreover, the chemical nature of the linker may be important for bioactivity. With this in mind, with respect to compound #6, the linker length was simply increased by the addition of either one or two glycine molecules. Glycine was chosen as it is an extremely easy amino acid to

chemically alter. This makes it ideal for rapid synthesis and screening, to determine whether linker length is affecting the functional ability of the bivalent pharmacophores.

3.4.4 *Displacement Binding Assays- The Gly-extended (#7-extended by 2 carbon atoms and #8- extended by 4 carbon atoms) linker compounds*

Compounds #7 and #8 displaced [³H]-DPN at the MOP, DOP and KOP receptors in a concentration dependent and saturable manner, but failed to displace [³H]UFP-101 (Figure 3.10; Table 3.2). At the MOP receptor, #7 (pK_i: 7.94) and #8 (8.03) were not significantly different from Fentanyl (8.13). At the DOP receptor, the #7 (9.67) and #8 (9.71) both showed an increased affinity for the DOP receptor, when compared to both #6 (8.17) and the parent compound Dmt-Tic-OH (8.95). Differences in binding affinity between the two Gly-linker extended molecules were evident at the KOP receptor; #7 (8.14) showed nanomolar affinity for the KOP receptor. While there was no significant difference in the binding affinities of #6 (7.13) and #8 (7.35), #7 showed statistical differences from both of these compounds. The Gly extended compounds showed either weak (#8; 6.63), or no affinity (#7; inactive) for the NOP receptor (Table 3.2).

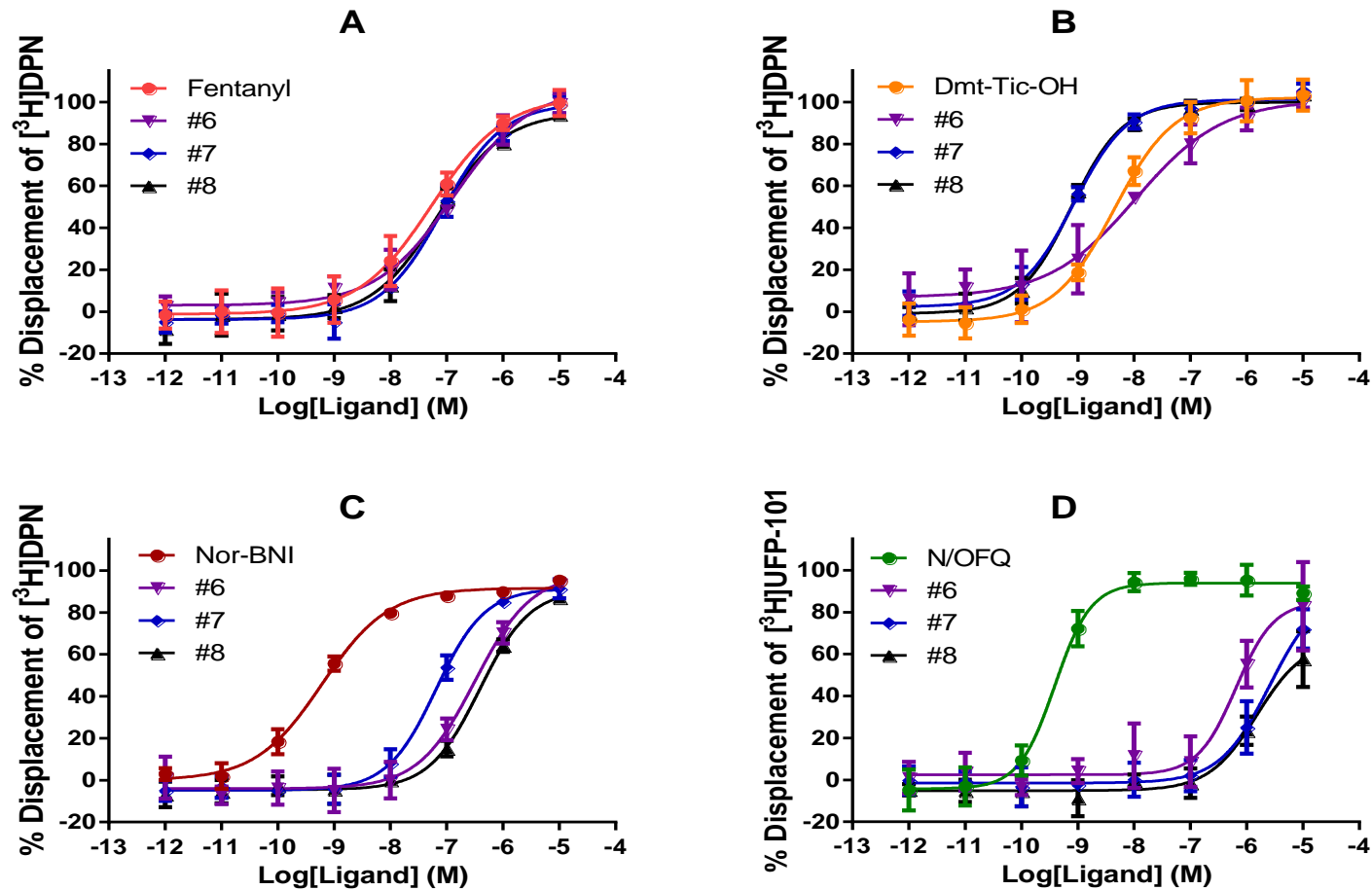


Figure 3.10: Displacement of tritiated Diprenorphine (³H)-DPN by the #6, the extended #6 compounds (#7 and #8) and reference ligands at (A) CHO_{hMOP}, (B) CHO_{hDOP}, (C) CHO_{hKOP} and the displacement of tritiated UFP-101 (³H)UFP-101 by #6, #7, #8 and N/OFQ at (D) CHO_{hNOP} cell membranes. Data are means (±SEM) of five experiments for all cell lines.

	pK_i (\pmSEM)			
	CHO_{hMOP}	CHO_{hDOP}	CHO_{hKOP}	CHO_{hNOP}
	Fentanyl	Dmt-Tic-OH	Nor-BNI	N/OFQ
Control	8.13 _(\pm0.04)	8.95 _(\pm0.04)	10.16 _(\pm0.02)	10.69 _(\pm0.10)
#1	N/A	N/A	N/A	N/A
#2	N/A	N/A	N/A	N/A
#3	N/A	N/A	N/A	N/A
#4	7.31 _(\pm0.06) *	8.03 _(\pm0.28) *	7.29 _(\pm0.04) ****	7.28 _(\pm0.07) ****
#5	7.58 _(\pm0.10)	8.16 _(\pm0.17)	7.02 _(\pm0.08) ****	6.96 _(\pm0.12) ****
#6	7.91 _(\pm0.23)	8.17 _(\pm0.22)	7.13 _(\pm0.04) ****	7.48 _(\pm0.05) ****
#7	7.94 _(\pm0.04)	9.67 _(\pm0.04) ***	8.14 _(\pm0.03) ****	N/A
#8	8.03 _(\pm0.04)	9.71 _(\pm0.01) ***	7.35 _(\pm0.04) ****	6.63 _(\pm0.26) ****
Analysis of Variance	significant	significant	significant	significant

Table 3.2: Radioligand binding data for the [Fentanyl]–[Dmt-Tic-OH] bivalent ligands. Tritiated Diprenorphine was used to determine binding affinity at CHO_{hMOP/DOP/KOP}, while [³H]UFP-101 was used to determine binding affinity at CHO_{hNOP}. Data are means (\pm SEM) of five experiments for the CHO_{hMOP} and CHO_{hDOP} cell lines and of three experiments for the remaining cell lines. If a significant difference (ANOVA) was detected, post-hoc testing using Bonferroni multiple comparisons was employed *p<0.05; ***p<0.0005; ****p<0.0001 compared to control.

3.4.5 GTP γ [³⁵S] functional assays- The gly-extended linker compounds activity

The Gly-extended compounds failed to stimulate the binding of GTP γ [35S], showing no efficacy at the MOP receptor (Figure 3.11). At 300nM compounds #7 and #8 produced pK_b values of 6.91 and 7.05 respectively (Table 3.3).

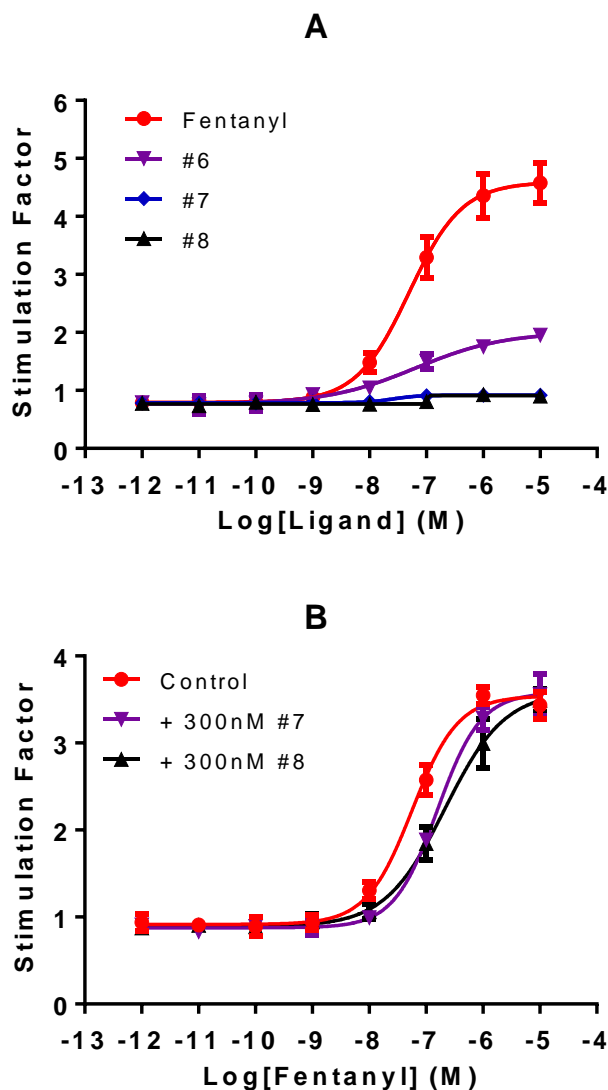


Figure 3.11: $GTP\gamma[^{35}S]$ functional response curves demonstrating (A) Ligand stimulated $GTP\gamma[^{35}S]$ binding by Fentanyl, the #6 and the Gly-extended compounds (#7, #8), is shown in CHO_{hMOP} cell membranes. (B) Fentanyl stimulated binding in the absence and presence of 300nM of the test ligands. Control ligand; Fentanyl. Data are shown as mean (\pm SEM) for 5 experiments.

Compounds #7 and #8 showed no activity at the DOP receptor (Figure 3.12, Table 3.3). However, when co-incubated with the DOP agonist DPDPE, both #7 (pKb: 9.42) and #8 (9.00) produced a rightward shift in the concentration response curve of DPDPE (Figure 3.12).

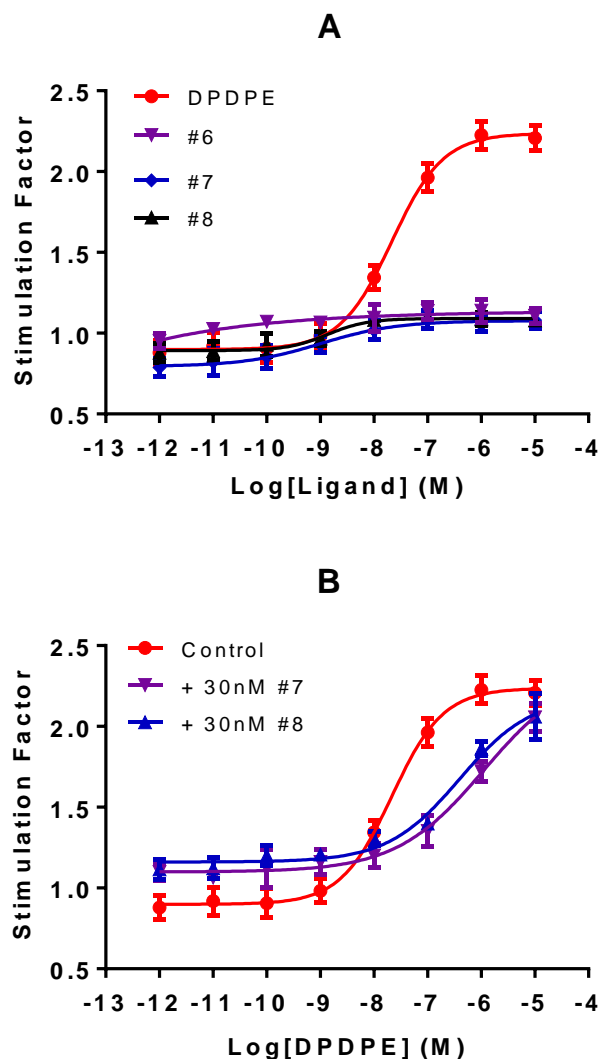


Figure 3.12: GTP γ [35 S] functional response curves demonstrating (A) Ligand-stimulated GTP γ [35 S] binding by DPDPE, #6 and the Gly-extended compounds (#7 and #8) in CHO_{hDOP} membranes. (B) DPDPE stimulated binding in the absence and presence of 30nM of the test ligands. Control ligand, DPDPE; [D-Pen²,D-Pen⁵ Enkephalin]. Data are shown as mean (\pm SEM) for 5 experiments.

Since #7 and #8 displayed binding affinity for KOP GTP γ [35 S] functional assays were performed. Both compounds were inactive *per se* (Figure 3.13). In antagonist experiments 300nM and 1 μ M for #7 and #8 respectively produced a weak, but measurable, rightward shift in the concentration response curve when co-incubated with Dynorphin-A. Compound #7 and #8 produced pK_b values of 6.96 (\pm 0.04) and 6.45 (\pm 0.07), respectively (Figure 3.13). In view of the low affinity at NOP for #7 and #8 functional assays were not performed.

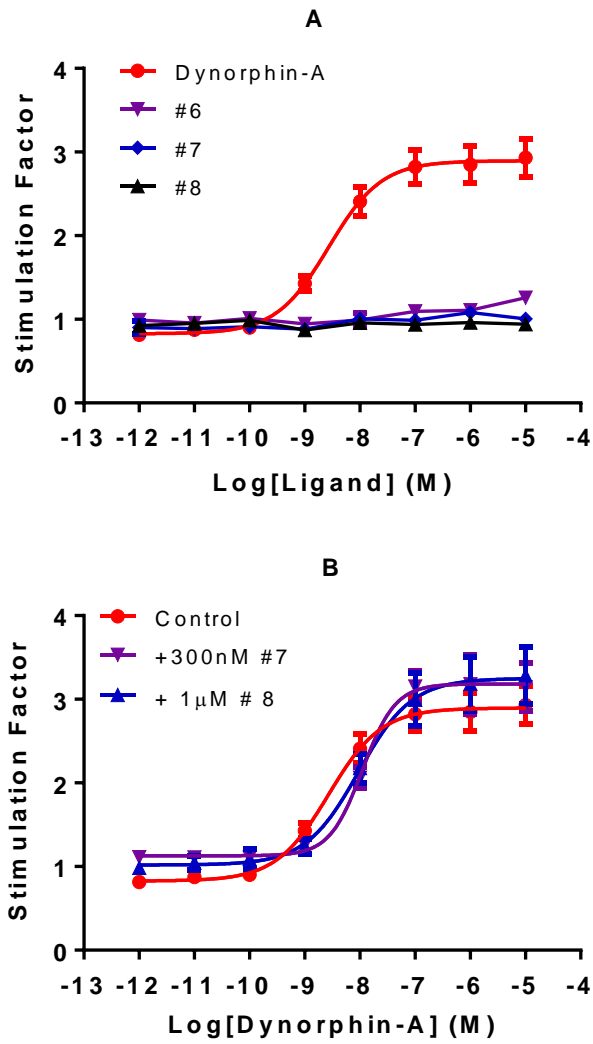


Figure 3.13: $GTP\gamma[^{35}S]$ functional response curves demonstrating (A) Ligand stimulated $GTP\gamma[^{35}S]$ in CHO_{hKOP} membranes. (B) Dynorphin-A stimulated binding in the absence and presence of #7 (300M) and #8 (1 μ M). Reference ligand; Dynorphin-A. Data are shown as mean (\pm SEM) for 5 experiments.

	Agonist Activity			Antagonist Activity
	pEC ₅₀	E _{max}	Relative Intrinsic activity	pK _b
CHO_{hMOP}				
Fentanyl	7.32(±0.12)	3.80(±0.12)	1	Inactive
#4	6.74(±1.02)*	1.18(±0.06)	0.06	6.87(±0.61)
#5	7.13(±0.29)	2.19(±0.46)	0.43	7.55(±0.28)
#6	7.52(±0.27)	1.98(±0.34)	0.35	7.81(±0.18)
#7	Inactive	-	Inactive	6.91(±0.08)
#8	Inactive	-	Inactive	7.05(±0.11)
Analysis of Variance	significant		N/A	N/A
CHO_{hDOP}				
Dmt-Tic	Inactive	-	Inactive	8.77(±0.11)
#4	Inactive	-	Inactive	6.85(±0.19)***
#5	Inactive	-	Inactive	8.06(±0.09)*
#6	Inactive	-	Inactive	8.11(±0.16)
#7	Inactive	-	Inactive	9.42(±0.14)**
#8	Inactive	-	Inactive	9.00(±0.15)
Analysis of Variance	N/A		N/A	significant

Table 3.3: Agonist and antagonist activity of the [Fentanyl]–[Dmt-Tic-OH] bivalent pharmacophores at CHO_{hMOP} and CHO_{hDOP}. Antagonist affinity was determined against Fentanyl (MOP) and DPDPE [D-Pen², D-Pen⁵ Enkephalin] (DOP). Relative intrinsic activity was determined by removal of basal activity and as a ratio to Fentanyl (full agonist) E_{max}. All experiments are represented as the mean (±SEM) for between three and five experiments. If a significant difference was detected (ANOVA), post-hoc testing using Bonferroni multiple comparisons was employed *p<0.05; **p<0.005; ***p<0.0001 compared to Fentanyl for MOP and Dmt-Tic for DOP. Abbreviation; N/A (Not applicable)

3.4.6 Beta-Arrestin Assays

β-arrestin recruitment in MOP cells was determined for Fentanyl and Morphine in CHO_{hMOP} cells (Figure 3.14). A range of concentrations of both Fentanyl and Morphine (1nM-10μM) were investigated to determine whether these ligands engaged β-arrestins (Figure 3.14). Maximum concentrations (10μM) of bivalent compounds were used to compare against Fentanyl and Morphine was used to measure β-arrestin activity (Figure 3.14).

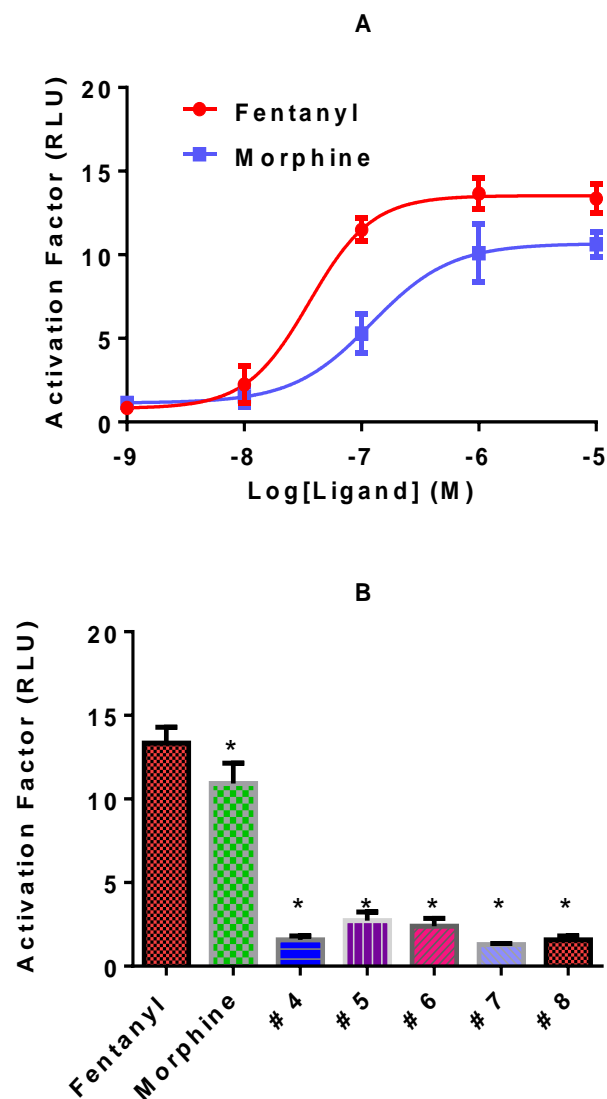


Figure 3.14: Beta-recruitment assays demonstrating (A) Fentanyl and Morphine concentration response curves for β -arrestin recruitment at MOP. (B) The recruitment of β -arrestin in the presence of 10 μ M of Fentanyl, Morphine and the various bivalent ligands. The activation factor is a ratio relative to basal β -arrestin activity. Data were significant (ANOVA) and * $p < 0.0001$ compared to Fentanyl post hoc Bonferroni test. Data are shown as mean (\pm SEM) for at least 5 experiments.

Fentanyl (E_{max} of 13.62 ± 0.45 ; pEC_{50} : 7.45 ± 0.07) produces a greater response with regards to β -arrestin recruitment when compared to Morphine (E_{max} : 10.80 ± 0.38 ; pEC_{50} : 6.88 ± 0.12). When compared to the maximum response of Fentanyl, the bivalent ligands showed poor ability to recruit β -arrestins. Response from the maximum concentration tested in rank order was: #5 (2.72 ± 0.21) < #6 (2.40 ± 0.19) < #4 (1.58 ± 0.09) < #8 (1.58 ± 0.09) < #7 (1.29 ± 0.03). The ability of these compounds to activate and recruit β -arrestins was significantly lower (analysis of variance; $p < 0.0001$)

than that of Fentanyl. When compared to Fentanyl, the intrinsic activity of these compounds to recruit β -arrestin is: #4: 0.12; #5: 0.20; #6: 0.18; #7: 0.09 and #8: 0.12.

In DOP cells, the ability of DPDPE to activate β -arrestin and the inhibition of this response by 10nM Dmt-Tic-OH (the parent pharmacophore) was measured (Figure 3.15). DPDPE produced a concentration dependent and saturable increase in β -arrestin recruitment with pEC_{50} and E_{max} of $7.56(\pm 0.09)$ and $14.58(\pm 0.61)$ respectively. Dmt-Tic-OH acts as a potent antagonist of DPDPE induced β -arrestin recruitment, with a pK_b of $9.20(\pm 0.11)$. All of the [Fentanyl]-[Dmt-Tic-OH] bivalent pharmacophores reduced the ability of DPDPE to activate and recruit β -arrestins. When compared to the activity of DPDPE at $1\mu M$ (13.46 ± 0.29), the presence of #4 (7.43 ± 0.29), #5 (9.51 ± 0.55) and #6 (9.56 ± 0.49) significantly reduced the ability of DPDPE to recruit β -arrestins ($p < 0.0001$; ANOVA, Bonferroni's multiple corrections). The presence of either 10nM #7 (6.44 ± 0.62) or 10nM #8 (5.56 ± 0.64) led to $\pm 50\%$ reduction in the ability of DPDPE to recruit β -arrestin (Figure 3.15).

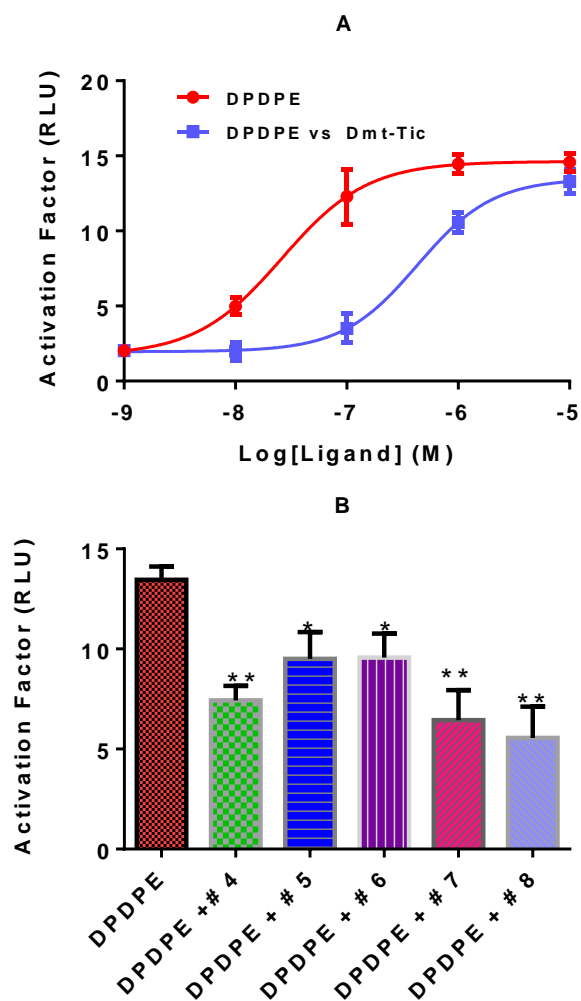


Figure 3.15: Beta-recruitment assays demonstrating (A) Concentration response curve in the absence, and presence, of 10nM Dmt-Tic-OH at DOP. (B) Shows the inhibition of 1 μ M DPDPE, produced by concentrations of 100nM for compounds #4, #5 and #6 or 10nM for compounds #7 and #8. Data were significant (ANOVA) and * $p < 0.0005$; ** $p < 0.0001$ compared to DPDPE post hoc Bonferroni test. Data are shown as mean (\pm SEM) for at least 5 experiments.

3.4.7 Characterisation and selection of potential Fentanyl pharmacophores for conjugation with Ro65-6570

Due to the failure of the initial Fentanyl compounds to produce a response at the MOP receptor, a number of Fentanyl derivatives (called the RR compounds), were developed. These compounds differ in the length of the amide bond in the northern region of Fentanyl's chemical structure (Table 3.4).

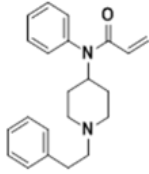
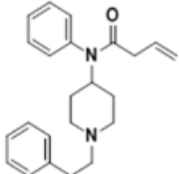
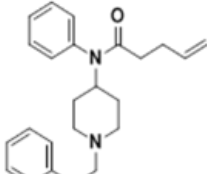
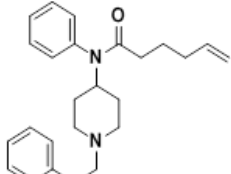
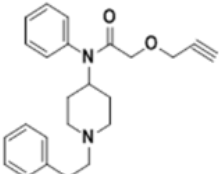
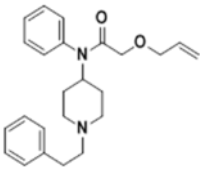
Chemical Structure	Name	Amide Bond Extension
	RR4	1 carbon bond
	RR5	2 carbon bonds
	RR6	3 carbon bonds
	RR7	4 carbon bonds
	RR8	Ether spacer and carbon bond
	RR9	Ether Spacer

Table 3.4: The chemical structure of the RR compounds. The adaptations to the amide linker length in the northern hemisphere of the Fentanyl structure are shown in the right hand column.

At the MOP receptor, all compounds displaced the binding of [³H]-DPN in a concentration dependent and saturable manner. Binding affinities (pK_i) at CHO_{hMOP} were: RR-4 (8.16), RR-5 (8.09), RR-6 (7.58), RR-7 (6.89), RR-8 (6.55) and RR9 (8.69). The binding affinities of RR-4, RR-5 and RR-6 were not significantly different from that of Fentanyl (8.13). RR-7 and RR-8 showed reduced binding, while RR-9 showed a significant increase in binding at the MOP receptor (Figure 3.16, Table 3.5). The rank order of binding was: RR-9>>RR-4>>RR-5>>RR-6>>RR-7>>RR-8

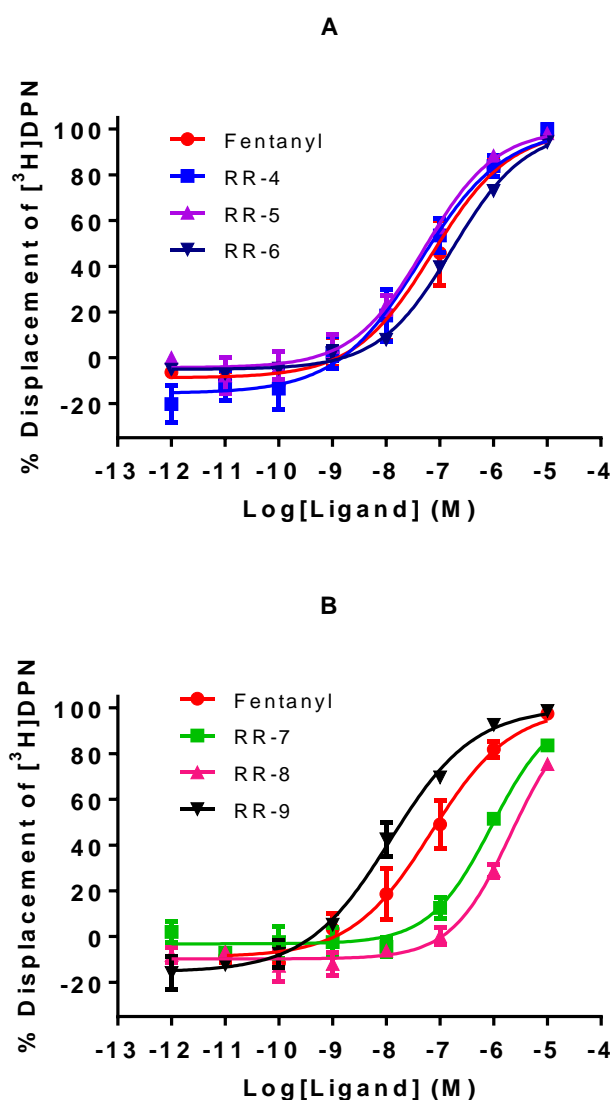


Figure 3.16: Displacement of tritiated Diprenorphine ([³H]-DPN) by Fentanyl and the RR compounds at CHO_{hMOP}. Data are shown as mean (±SEM) for 5 experiments.

Binding affinity was measured in cells expressing DOP, KOP and NOP. At DOP, RR4 (7.29) and RR-9 (7.00) showed moderate affinity, with the remainder of the compounds producing weak (<7) affinity. All compounds bound with weak, or no affinity at KOP and NOP (Table 3.5).

	Reference ligand ⁺	RR-4	RR-5	RR-6	RR-7	RR-8	RR-9	
MOP	8.13 (± 0.04)	8.16 (± 0.28)	8.09 (± 0.03)	7.58 (± 0.03)	6.89 (± 0.08) ^{**}	6.55 (± 0.08) ^{***}	8.69 (± 0.14) [*]	n=5
DOP	10.02 (± 0.26)	7.29 (± 0.27) ^{***}	6.77 (± 0.07) ^{***}	6.28 (± 0.31) ^{***}	5.91 (± 0.05) ^{***}	5.21 (± 0.15) ^{***}	7.00 (± 0.26) ^{***}	n=5
KOP	9.95 (± 0.02)	<5 ^{***}	5.97 (± 0.46) ^{***}	<5 ^{***}	<5 ^{***}	6.08 (± 0.31) ^{***}	6.74 (± 0.02) ^{***}	n=3
NOP	10.69 (± 0.10)	6.29 (± 0.04)	5.97 (± 0.08) ^{***}	6.16 (± 0.53) ^{***}	<5 ^{***}	<5 ^{***}	6.15 (± 0.16) ^{***}	n=3

⁺ = MOP: Fentanyl, DOP: Natrindole, KOP: norBNI, NOP: N/OFQ

Table 3.5: The pK_i values for the both the reference ligand and the RR- compound ligands of interest. The receptor binding affinities of the reference ligands and the RR compounds were calculated using the Cheng-Prusoff equation. Data are displayed as mean (\pm SEM) for either n=5 (MOP and DOP) or n=3 (KOP and NOP), dependent on the RR compounds binding affinity for the receptor. If a significant difference was detected (ANOVA), post-hoc testing using Bonferroni multiple comparisons was employed *p<0.05; **p<0.005; ***p<0.0001 compared to Fentanyl for MOP; Dmt-Tic for DOP; Nor-BNI for KOP and N/OFQ for NOP.

Following this initial screening, attempts were made to chemically conjugate the RR-compounds to Ro65-6570. Ro65-6570 is a potent, synthetic NOP agonist, which can be manipulated to accept a linker molecule. This will allow for the formation of a bivalent with dual synthetic components, decreasing the molecular weight of the compound. However, due to poor yields, only RR4, RR6 and RR7 were able to be conjugated to form [Fentanyl]-[Ro65-657] bivalent pharmacophores (Figure 3.4). This conjugation could only be achieved using maleimide, an unsaturated imide, using a Michael reaction. The Michael reaction involves the addition of an enolate (alkenes with a hydroxyl group) of a ketone or aldehyde to an α,β -unsaturated carbonyl compound at the β carbon. These chemical reactions lead to the synthesis of Ro-Mal-RR4 (termed MN1 from this point), Ro-Mal-RR6 (MN2) and Ro-Mal-RR7 (MN3).

3.4.8 $GTP\gamma[^{35}S]$ functional assays- The MN compounds

Compounds MN1, MN2 and MN3 stimulated the binding of $GTP\gamma[^{35}S]$ in a concentration dependent and saturable manner at the MOP receptor (Figure 3.17). The pEC_{50} values of MN1 (6.78), and MN3 (6.79) were not significantly different to Fentanyl (7.05). MN2 (6.39) was statistically significant when compared to Fentanyl. The pEC_{50} values for MN1 (6.78), MN2 (6.39) and MN3 (6.79) were statistically significant when compared to Ro65-6570 (6.17). The E_{max} values for Ro65-6570 (2.79), MN1 (1.95) MN2 (2.24) and MN3 (2.75) were significantly different when compared to Fentanyl (3.67) (Table 3.6).

In CHO_{hNOP} cell membranes, compounds MN1, MN2 and MN3 stimulated the binding of $GTP\gamma[^{35}S]$ in a concentration dependent and saturable manner (Figure 3.17). The pEC_{50} values of MN1 (8.01) and MN2 (7.36) were significantly different to Ro65-6570 (7.73), however MN3 (7.85) was not. The pEC_{50} values of MN1, MN2, MN3 and Ro-65-6570 were significantly different to N/OFQ (8.40). N/OFQ produced an E_{max} of 4.07. The E_{max} values of Ro65-6570 (E_{max} : 4.11), MN1 (3.95), MN2 (4.10) and MN3 (3.92) were not significantly different to that of N/OFQ at NOP (Table 3.6).

	MOP			NOP		
	pEC ₅₀	E _{max}	I.A	pEC ₅₀	E _{max}	I.A
Fentanyl/N/OFQ	7.05 \pm 0.04	3.67 \pm 0.39	1	8.40 \pm 0.08	4.07 \pm 0.23	1
Ro65-6570	6.17 \pm 0.04 ^a	2.79 \pm 0.26 ^d	0.62	7.73 \pm 0.05 ^e	4.11 \pm 0.21	1
MN1	6.78 \pm 0.12 ^c	1.95 \pm 0.30 ^d	0.25	8.01 \pm 0.04 ^{e,f}	3.95 \pm 0.23	0.94
MN2	6.39 \pm 0.04 ^{b,c}	2.24 \pm 0.29 ^d	0.33	7.36 \pm 0.12 ^{e, g}	4.10 \pm 0.15	1
MN3	6.79 \pm 0.09 ^c	2.75 \pm 0.31 ^d	0.56	7.85 \pm 0.02 ^e	3.92 \pm 0.10	0.96

Table 3.6: Agonist activity of the [Fentanyl]–[Ro65-6570] bivalent pharmacophores at CHO_{hMOP} and CHO_{hNOP}. Relative intrinsic activity (I.A) was determined by removal of basal activity and as a ratio of Fentanyl (full agonist) E_{max} in CHO_{hMOP} membranes or Ro65-6570 in CHO_{hNOP} membranes. Fentanyl was inactive at NOP (n=5). All experiments are represented as the mean (\pm SEM) with n=5 for MOP and n=7 for NOP. If a significant difference was detected by ANOVA Bonferroni multiple comparisons were employed. ^a p<0.005 less potent compared to Fentanyl, ^b p<0.05 less potent compared to Fentanyl; ^c p<0.05 more potent when compared to Ro65-6570, ^d p<0.05 reduced E_{max} when compared to Fentanyl; ^e p<0.0005 less potent compared to N/OFQ; ^f p<0.005 more potent when compared to Ro65-6570; ^g p<0.05 less potent when compared to Ro65-6570.

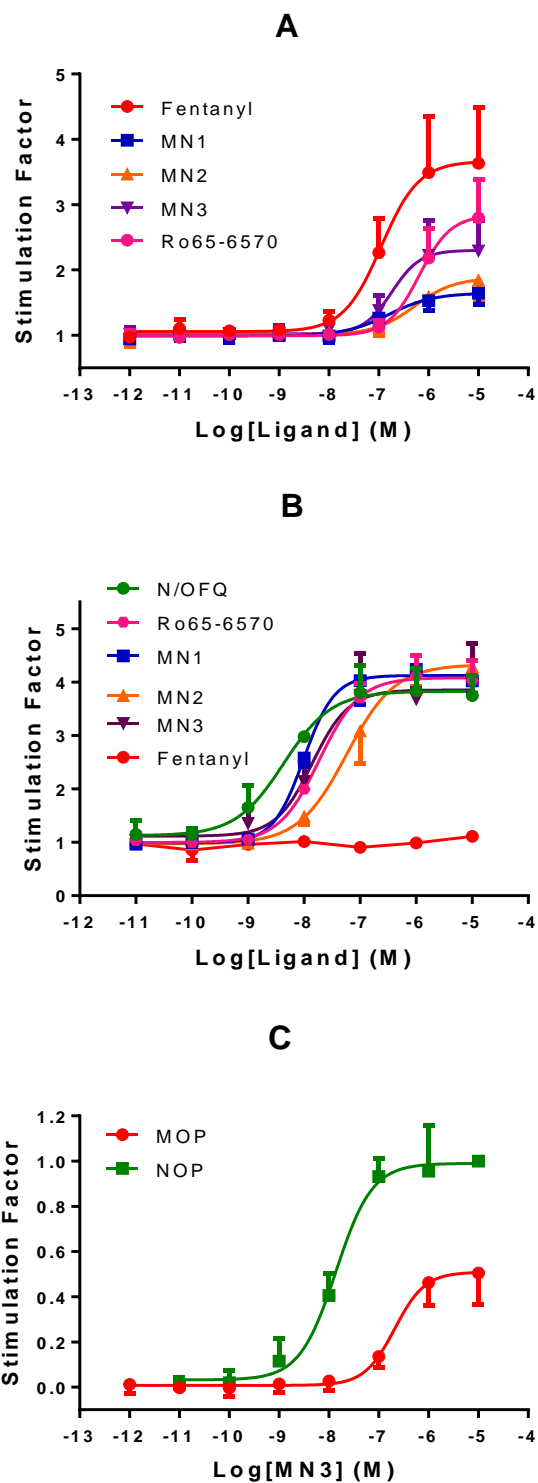


Figure 3.17: : $\text{GTP}\gamma^{[35\text{S}]}$ functional response curves demonstrating A) Ligand stimulated $\text{GTP}\gamma^{[35\text{S}]}$ binding by Fentanyl; MN1, MN2 and MN3 are shown in CHO_{hMOP} cell membranes. B) Ligand stimulated $\text{GTP}\gamma^{[35\text{S}]}$ binding by N/OFQ, Ro65-6570; MN1, MN2 and MN3 are shown in CHO_{hNOP} cell membranes. C) Normalised curves for MN3 in CHO_{hMOP} and CHO_{hNOP} membranes. Data are mean (\pm SEM) for five experiments.

3.5 Discussion

When in an unconjugated state, the various F-compounds show varying degrees of affinity for the opioid receptors (Figure 3.5; Table 3.2, Figure 3.16, Table 3.5). Once conjugated with the DOP antagonist Dmt-Tic-OH, all of the tested compounds show affinity for the MOP receptor, using displacement binding assays previously defined by this laboratory (Dietis et al., 2012). In the case of compounds #5 and #6, this affinity was comparable to that of the parent compound Fentanyl. Compound #4 showed a loss of affinity at the MOP receptor, when compared to both the other F-compounds and Fentanyl (Table 3.2, Figure 3.6). When the linker molecules were extended to produce #7 and #8, no discernible change in binding affinity was seen when compared to Fentanyl (Figure 3.10, Table 3.2). The rank order of binding affinity was Fentanyl>#8>#7>#6>#5>#4>1=2=3.

At the DOP receptor, again compounds #1, #2 and #3 showed no affinity. The bivalent pharmacophores #5 and #6 showed affinity for DOP similar to that of the parent compound Dmt-Tic-OH (Figure 3.6, Table 3.2). Compound #4 showed a reduction in binding affinity compared to Dmt-Tic-OH, while the extended linker molecules, #7 and #8, showed a significant increase in binding affinity for DOP. In this case the rank order of binding affinity is: #8>#7>Dmt-Tic-OH>#6>#5>#4.

At the KOP receptor, #4, #5, #7 and #8 (Figure 3.6 and Figure 3.10), with the exception of #4, displayed moderate binding affinities for this receptor. At the NOP receptor, all compounds demonstrated weak or no affinity for this receptor (Table 3.2).

In GTP γ [35S] functional assays, the #4, #5 and #6 produced a concentration dependent response at MOP, however discrepancies in both potency and efficacy were noted. Compounds #5 and #6 displayed similar potency to that of Fentanyl, whereas #4 demonstrated a loss of potency (Figure 3.7). The maximal response produced by #4, #5 and #6 was significantly lower than that of Fentanyl, and their relative intrinsic activity indicates a weak partial agonist profile (Table 3.3). Compounds #7 (linker extended by 2 carbon atoms) and #8 (linker extended by 4 carbon atoms), demonstrated no measurable activity at the MOP receptor (Figure 3.11), demonstrating a complete loss

of functional ability after extension of the linker molecule (Table 3.3). Since all compounds showed affinity for the MOP receptor, and partial agonists can act as antagonists in the presence of full agonists, antagonist assays were undertaken using compounds #4-#8 (Figure 3.7 and Figure 3.11). All compounds demonstrated an ability to antagonise the effects of Fentanyl at MOP (Table 3.3). The rank order of antagonist affinity is: #6>#5>#8>#7>#4.

At DOP, all compounds demonstrated no stimulation of the receptor in GTP γ [³⁵S] functional assays. In antagonist studies all compounds demonstrated antagonist ability in the presence of DPDPE (Figure 3.8 and Figure 3.12). While compounds #5 and #6 acted in a similar manner to the parent compound Dmt-Tic-OH, compounds #4, #7 and #8 all showed significant differences in function. Compound #4 showed a considerable loss of antagonist ability when compared to Dmt-Tic-OH. In contrast, the glycine-extended compounds, #7 and #8, both showed an increase in antagonist affinity when compared to Dmt-Tic-OH (Table 3.3).

As previously mentioned, compounds #7 and #8 demonstrated an increase in affinity for the KOP receptor. In functional assays, the compounds failed to stimulate the KOP receptor, but did show weak antagonist affinity in the presence of the KOP agonist Dynorphin -A (Figure 3.13).

Subsequent screening of the abilities of Fentanyl, Morphine and compounds #4, #5, #6, #7 and #8 to recruit β -arrestins confirmed the loss of functional ability of the bivalent pharmacophores at MOP. Fentanyl displayed higher efficacy and potency than that of Morphine with regards to β -arrestin recruitment, displaying full agonist activity in this assay. The pEC₅₀ of Fentanyl in this assay was comparable to that found in the GTP γ [³⁵S] functional assays (Table 3.3). Since the F-compounds displayed weak functional ability at their highest concentrations, a maximal dose (10 μ M) was tested in the β -arrestin assay. All of the test compounds displayed a similar large loss of functional ability, when compared to Fentanyl. This indicates that synthetic alterations to these Fentanyl derivatives have led to a loss of functional ability.

At DOP, compounds #4, #5, #6, #7 and #8 all demonstrated antagonist affinity, inhibiting the functional activity of the DOP receptor full agonist, DPDPE. Compounds

#7 and #8 produced the greatest inhibition of 10 μ M DPDPE. These experiments, coupled with the results of the GTP γ [³⁵S] antagonist assays, indicates that coupling of Dmt-Tic-OH to the linker molecule and Fentanyl, has not hindered its ability to act as an antagonist.

The failure of the Fentanyl pharmacophore to maintain agonist ability after conjugation with a second pharmacophore, has led to further Fentanyl derivatives being synthesised. The affinity of the uncoupled Fentanyl derivatives for MOP were tested, with the test compounds RR-4, RR-5 displaying similar binding affinity to Fentanyl, while RR-9 displays increased affinity for the MOP receptor (Table 3.5).

While numerous studies have demonstrated the linking of a MOP agonist to a DOP antagonist, the linking of two synthetic agonists targeting MOP and NOP have been less well described. As mentioned in previous sections, the dual targeting of MOP and NOP could provide for longer lasting analgesics, that have a lower addiction profile, or as potential addiction treatment compounds. In order to assess the potential of such synthetic bivalent pharmacophores, the newly screened RR compounds were conjugated with the synthetic NOP agonist, Ro65-6570.

Conjugation of the newly synthesised Fentanyl derivatives (RR4-9) proved difficult, with only RR4, RR6 and RR7 being able to be conjugated with the NOP agonist, Ro65-6570 (Figure 3.4). Due to the limited amount of compounds available, the resulting compounds (MN1, MN2 and MN3) were screened in GTP γ [³⁵S] assays to assess functional activity at MOP and NOP (Figure 3.17). All compounds acted as full agonists in CHO_{hNOP} membranes. Interestingly MN1 demonstrated an increase in potency when compared to Ro65-6570, however MN1 is less potent than N/O/FQ (Table 3.6). Conversely, MN2 demonstrated a loss of potency when compared to Ro65-657, indicating conjugation had negatively impacted the Ro65-6570 pharmacophore. MN3 produced a similar potency to Ro65-6570. MN1 and MN3 demonstrated similar potency to Fentanyl at MOP. Compared to Ro65-6570, which acts as a partial agonist at MOP, MN1 and MN3 demonstrated a higher potency, while MN2 displayed a lower potency. This would indicate that MN1 and MN3 action at MOP is mediated by the Fentanyl pharmacophore. (Figure 3.17, Table 3.6). Of the three compounds, MN3 demonstrates a novel ligand with moderate partial agonist activity at MOP and full

agonist activity at NOP and has potential uses in the treatment of dependence. A full receptor screen is required to determine the selectivity of the compounds at the opioid receptors.

The results displayed in this chapter demonstrate the difficulties of developing synthetic bivalent pharmacophores. The proximity of the pharmacophores was initially thought to influence the loss of functional activity; however extending the distance of the pharmacophores in compound #6 showed a complete loss of functional activity. This indicates that chemical alteration of the Fentanyl structure in these compounds is responsible for the loss of activity. The loss of agonist ability at MOP, for compounds #4, #5, #6, #7 and #8, indicates that these compounds are not suitable for further studies as they do not meet the desired criteria. The Fentanyl derivatives used to form the MN compounds demonstrated an increased intrinsic activity at MOP, however this was still moderate partial agonist activity. At NOP, the compounds demonstrated full agonist ability, demonstrating the synthesis of a novel group of MOP partial agonist/NOP full agonist bivalent pharmacophores.

Chapter 4 Characterisation of Novel Tetra-Branched Peptides

4.1 Introduction

Drug development has historically been based on the development of small synthetic compounds as they offer numerous advantages over peptides, whose larger structure leads to poor bio-availability and metabolic instability (via enzymatic degradation) resulting in a reduced duration of action. Conversely, while small molecules show improved bio-availability and a longer duration of action, they typically lose selectivity for the receptor of interest and show an increase in harmful side-effects (Craik et al., 2013). There is clearly an advantage to improving the duration of action of peptide drugs.

Recently, a group of novel core molecules, developed from the alteration of a maleimide moiety, have been produced by peptide welding technology (PWT) (Figure 4.1). These maleimide cores allows for the attachment of four peptides. PWT-1 and PWT-3 are linear iterations of maleimide, while PWT2 is a cyclic structure. These novel tetra-branched peptides potentially provide a prolonged therapeutic window due to their reduced susceptibility to enzymatic degradation (Guerrini et al., 2014).

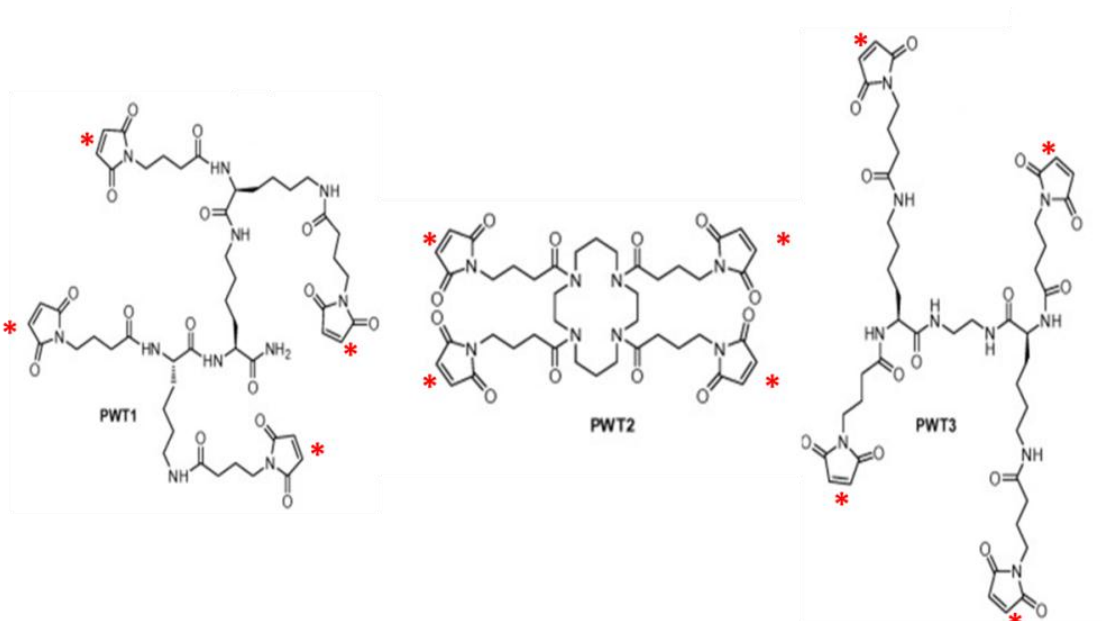


Figure 4.1: The PWT1, PWT2 and PWT3 core molecules. The sections indicated with (*) are the conjugation points for the peptide of interest (Guerrini et al., 2014).

All clinically available opioids are small molecules that target the MOP receptor and produce several side-effects. While the MOP receptor has proven to provide excellent analgesia, both the DOP and NOP receptors have also been shown to produce pain relief when activated. Currently, neither receptor is clinically targeted, although there is a mixed MOP/NOP ligand, cebranopadol on the horizon (Linz et al., 2014).

4.2 Hypothesis

We hypothesise that linking of four peptides to the PWT core will lead to compounds that retain affinity for the receptor of interest. Furthermore, these novel compounds may provide longer lasting duration of action when compared to linear peptides.

4.3 Aims

The aims of this chapter are to provide *in vitro* characterisation of both the PWT-N/OFQ compounds and PWT2-Leu-Enk using CHO cells expressing recombinant opioid receptors (CHO_{hMOP}, CHO_{hDOP}, CHO_{hKOP} and CHO_{hNOP}) to define their pharmacological properties (binding affinity and functional activity). pK_i values will be determined using [³H]-DPN and [³H]UFP-101 as radioligands. Functional activity will be measured by determining both the PWT-N/OFQ compounds and the ability of PWT2-Leu-Enk to stimulate binding of GTPγ[³⁵S]. In the case of PWT2-Leu-Enk, both calcium mobilisation assays and *ex vivo* tissue assays were also undertaken to further our understanding of their pharmacological profile. Calcium assays offer a high throughput screening system, while *ex vivo* bioassays allow for screening of the compound of interest in a low expression, but more intact system. The calcium mobilisation assays and bioassays were undertaken by myself in our collaborators' laboratories at the University of Ferrara.

4.4 **Results**

4.4.1 *PWT-N/OFQ derivatives*

The PWT-N/OFQ derivative binding profiles were determined using CHO cells expressing recombinant MOP, DOP, KOP and NOP receptors. The compounds showed little or no affinity for MOP, DOP and KOP. At NOP, PWT1-N/OFQ (pKi: 10.60), PWT2-N/OFQ (10.30) and PWT3-N/OFQ (10.10) showed similar binding affinity to that of N/OFQ (10.69) (Figure 4.2).

In GTP γ [35S] functional assays, PWT1-N/OFQ (pEC50: 9.99), PWT2-N/OFQ (10.04) and PWT3-N/OFQ (9.71) displayed a statistically significant increase in their pEC50 values when compared to N/OFQ (9.05) at the NOP receptor (Figure 4.2, Table 4.1). PWT1-N/OFQ (Emax: 4.00), PWT2-N/OFQ (4.06) and PWT3-N/OFQ (3.94) all demonstrated similar maximal responses to that of N/OFQ (3.75).

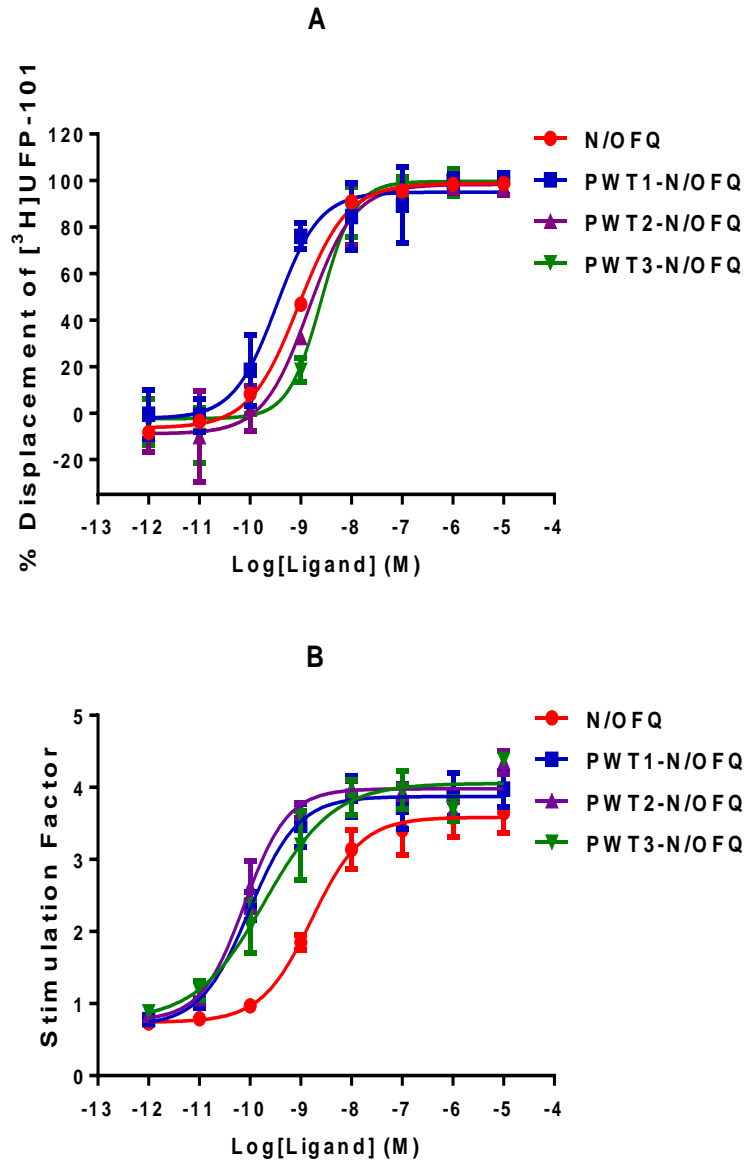


Figure 4.2: Assessment of the novel tetrabranchered PWT-N/OFQ compounds ability through A) Displacement of [³H]UFP-101 by N/OFQ and PWT derivatives in CHO_{hNOP} membranes. B) Functional assessment (GTPγ[³⁵S]) of the PWT-N/OFQ derivatives. Data are shown as mean (±SEM); for between four and six experiments.

	Binding Affinity		GTP γ [³⁵ S]	
	pK _i	pEC ₅₀	E _{max}	Relative intrinsic activity
N/OFQ	10.69 (\pm 0.10)	8.84 (\pm 0.08)	3.75(\pm 0.34)	1
PWT1-N/OFQ	10.60 (\pm 0.03)	9.99 (\pm 0.09) [*]	4.00 (\pm 0.31)	1
PWT2-N/OFQ	10.30 (\pm 0.04)	10.04 (\pm 0.14) [*]	4.06 (\pm 0.12)	1
PWT3-N/OFQ	10.10 (\pm 0.11)	9.71 (\pm 0.34) [*]	3.94 (\pm 0.14)	1

Table 4.1: Binding affinity (pK_i), potency (pEC₅₀) and intrinsic activity (E_{max} compared to N/OFQ) in GTP γ [³⁵S] functional assays in CHO_{hNOP} membranes. Data are mean (\pm SEM) of five and eight experiments. If a significant difference (ANOVA) was detected, post-hoc testing using Bonferroni multiple comparisons was employed * p<0.005; compared to N/OFQ.

4.4.2 PWT-Leu-Enk-Displacement binding studies

As previously mentioned in the section 4.1, the PWT2 moiety is a cyclic derivative of maleimide. This cyclic core structure proved to be the most stable of the PWT-structures and was chosen for further investigation with other peptides. In cells expressing the recombinant DOP receptor, DPDPE, Leu-Enkephalin and PWT2-Leu-Enk displaced [³H]-DPN in concentration dependent and saturable manner (Figure 4.3, Table 4.2). pK_i values for DPDPE (8.58) and PWT2-Leu-Enk (8.32) were significantly different than that of Leu-Enkephalin (8.77), however these differences were small. While Leu-Enkephalin (7.79) displaced [³H]-DPN in concentration dependent and saturable manner, PWT2-Leu-Enk failed to displace [³H]-DPN at MOP in a concentration dependent and saturable manner. At KOP and NOP, PWT2-Leu-Enk failed to displace [³H]-DPN or [³H]UFP-101 respectively.

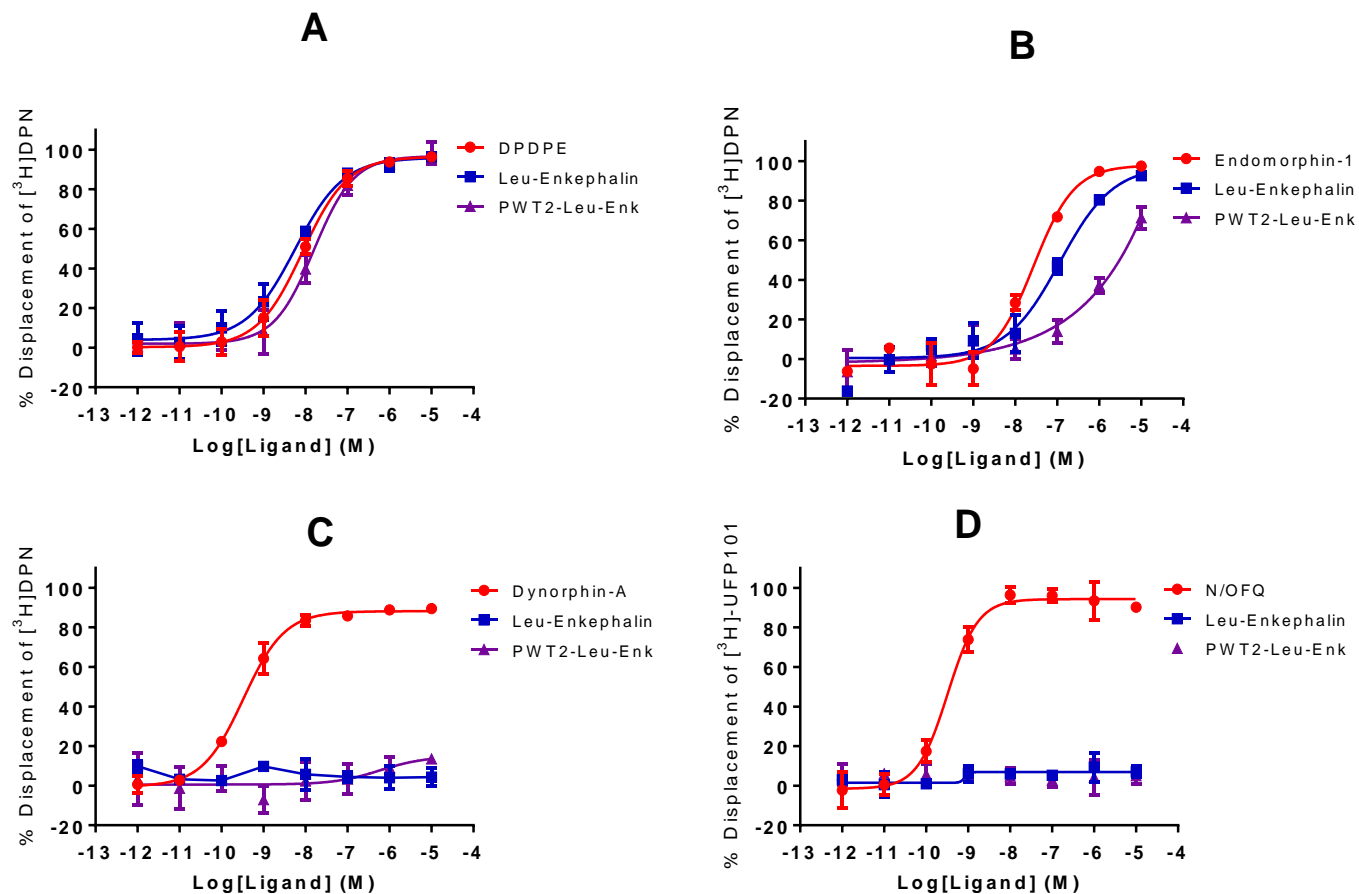


Figure 4.3: Displacement of [³H]-DPN by Leu-Enkephalin, PWT2-Leu-Enk and reference ligands at (A) CHO_{hDOP}, (B) CHO_{hMOP}, (C) CHO_{hKOP} and the displacement of [³H]-UFP-101 by Leu-Enkephalin, PWT2-Leu-Enk and Nociception/Orphanin FQ at (D) CHO_{hNOP} cell membranes. Data are means (\pm SEM) of between five and eight experiments for all cell lines. Reference ligands: Endomorphin-1; DPDPE [D-Pen²,D-Pen⁵ Enkephalin]; Dynorphin-A; N/OFQ, (Nociceptin/Orphanin FQ).

4.4.3 $GTP\gamma[{}^{35}S]$ functional assays

In $GTP\gamma[{}^{35}S]$ functional assays, Leu-Enkephalin, DPDPE and PWT2-Leu-Enk stimulated the binding of $GTP\gamma[{}^{35}S]$ in a concentration dependent and saturable manner in membranes from CHO_hDOP cells (Figure 4.4). pEC₅₀ values of DPDPE (8.31) and PWT2-Leu-Enk (8.40) showed no significant difference to that of Leu-Enkephalin at DOP. E_{max} values for DPDPE (1.65) and PWT2-Leu-Enk (1.74) were not significantly different from that of Leu-Enkephalin (1.77). Relative intrinsic activity (α -E_{max}) and potency (pEC₅₀) values are summarised in Table 4.2.

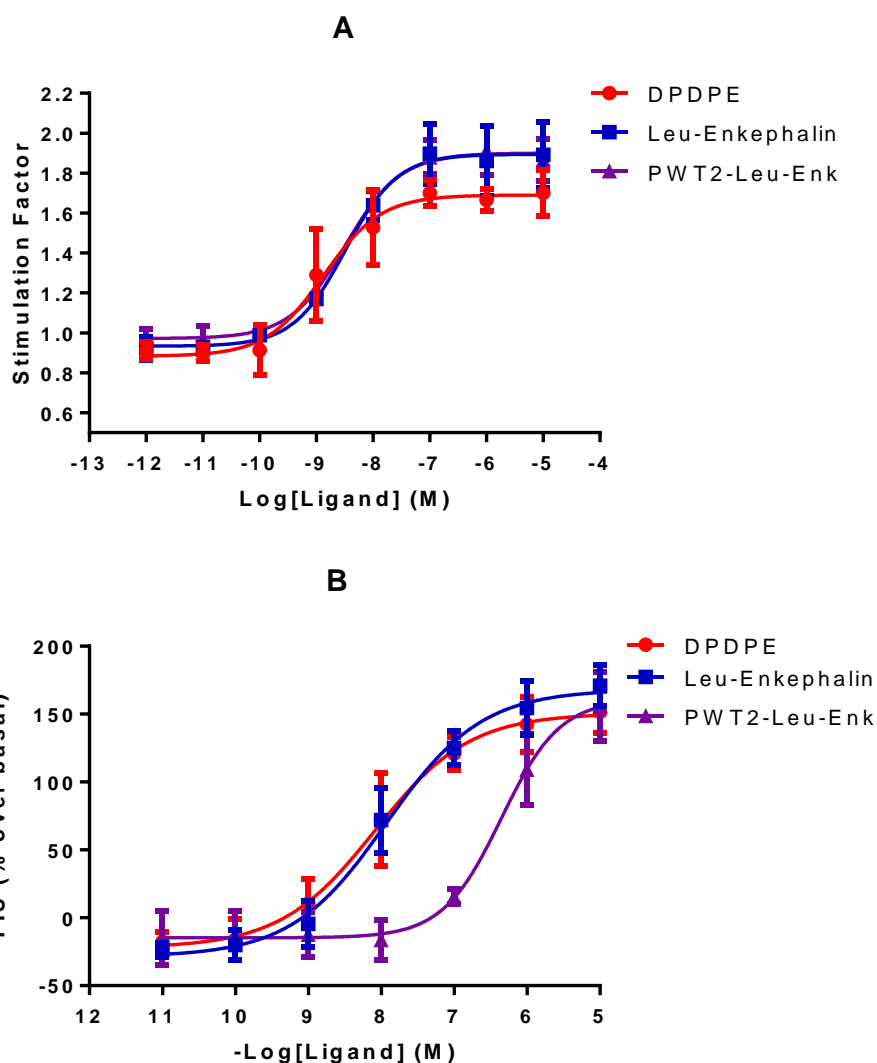


Figure 4.4: GTP γ [³⁵S] functional response assays demonstrating A) Ligand stimulated GTP γ [³⁵S] binding by DPDPE, Leu-Enkephalin and PWT2-Leu-Enk is shown in CHO_{hDOP} cell membranes. B) Concentration response curves to DPDPE, Leu-Enkephalin and PWT2-Leu-Enk in calcium mobilization experiments performed in CHO_{hDOP} cells stably expressing the G $\alpha_{qG66Di5}$ protein. All data are the mean (\pm SEM) for between 3 and 5 experiments.

4.4.4 Calcium mobilisation assays

In CHO_{hDOP} cells stably expressing G $\alpha_{qG66Di5}$ chimeric protein, both DPDPE (pEC₅₀ 8.09; maximal effect: 151% over the basal values) and Leu-Enkephalin (pEC₅₀ 7.95; maximal effect: 169% over the basal values) elicited a concentration dependent response displaying high potency (Figure 4.4). In concurrent experiments, PWT2-Leu-Enk displayed similar maximal effects (160% over the basal values) but reduced

potency (pEC_{50} ; 6.35) at the DOP receptor. Relative intrinsic activity ($\alpha-E_{max}$) and potency (pEC_{50}) values are summarised in Table 4.2.

	Binding Affinity	GTP γ [³⁵ S]			Calcium mobilisation			Twitch Assay (MVD)		
	pK _i	pEC ₅₀	E _{max}	Relative intrinsic activity	pEC ₅₀	E _{max}	Relative intrinsic activity	pEC ₅₀	E _{max}	Relative intrinsic activity
DPDPE	8.58 _(±0.02)	8.58 _(±0.14)	1.65 _(±0.05)	1	8.17 _(±0.23)	151 _(±9)	1	8.37 _(±0.06) *	85 ± 10	1
Leu-Enkephalin	8.77 _(±0.03)	8.40 _(±0.08)	1.77 _(±0.09)	1	7.95 _(±0.08)	169 _(±11)	1	7.58 _(±0.11)	81 ± 6	1
PWT2-Leu-Enk	8.32 _(±0.01)	8.40 _(±0.08)	1.74 _(±0.10)	1	6.35 _(±0.02) *	160 _(±11)	1	7.40 _(±0.06)	89 ± 3	1

Table 4.2: Binding affinity (pK_i), potency (pEC₅₀) and relative intrinsic activity (E_{max} compared to DPDPE) in GTP γ [³⁵S] functional assays; potency and relative intrinsic activity (E_{max} compared as a ratio to Leu-Enkephalin) in calcium mobilisation assays; potency and relative intrinsic activity (E_{max} compared as a ratio to Leu-Enkephalin) in twitch bioassays. Data are mean (±SEM) of between three and five experiments. If a significant difference (ANOVA) was detected, post-hoc testing using Bonferroni multiple comparisons was employed * p<0.0005; compared to Leu-Enkephalin.

4.4.5 Bioassays

In mouse *vas deferens* (mVD) preparations, DPDPE induced a full inhibition of the twitch response with a high potency (pEC_{50} : 8.37; E_{max} : 85% inhibition of twitch response). Both Leu-Enkephalin (pEC_{50} : 7.58; E_{max} : 81% inhibition of twitch response) and PWT2-Leu-Enk (pEC_{50} : 7.40; E_{max} : 89% inhibition of twitch response) fully inhibited the control twitch, in a concentration dependent manner (Figure 4.5). After washing and a period of 1 hour, mVD tissue was re-tested, in order to determine the repeatability of the assay. Both Leu-Enkephalin (pEC_{50} : 7.27; E_{max} : 88 % inhibition of twitch response) and PWT2-Leu-Enk (pEC_{50} : 7.42; E_{max} : 86% inhibition of twitch response) acted in a similar manner to the previous experiment.

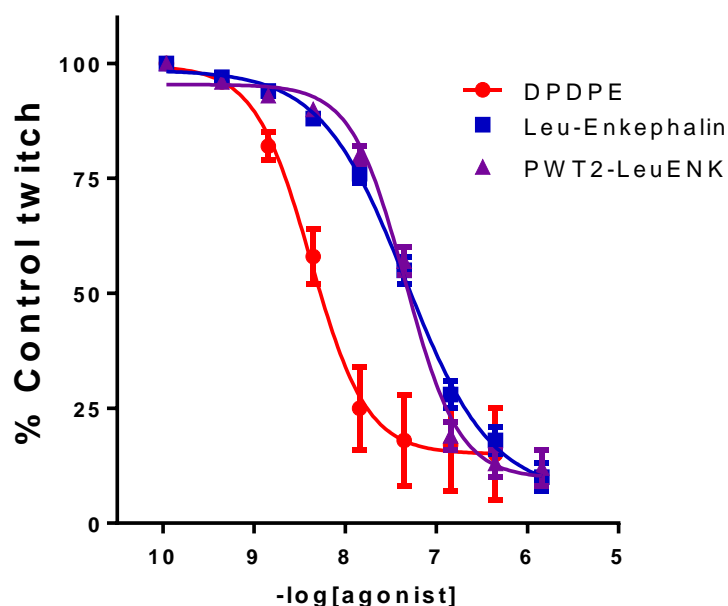


Figure 4.5. Concentration dependent inhibition response curves, in mouse *Vas Deferens*, for DPDPE, Leu-Enkephalin and PWT2-Leu-Enk. Data are the mean \pm SEM n=4 experiments.

4.5 Discussion

The above data demonstrate the successful coupling of four peptides to a core molecule. The PWT-N/OFQ derivatives all retained binding affinity for NOP, comparable with that of N/OFQ (Figure 4.2, Table 4.1). In $GTP\gamma[35S]$ functional assays, The PWT-N/OFQ derivatives all demonstrated full agonist activity.

Furthermore, they showed a significant increase in potency when compared to N/OFQ (Figure 4.2, Table 4.1). This demonstrates that the chemical alterations required to form the tetrabranched molecule have not negatively impacted the functional ability of the N/OFQ pharmacophore(s) or its selectivity for the NOP receptor. Furthermore, in experiments undertaken by our collaborators, it has been demonstrated that the *in vivo* potency of PWT2-N/OFQ is comparable with that seen in mouse models. In these studies, the effect of N/OFQ and PWT2-N/OFQ was studied in mouse locomotor experiments, with PWT2-N/OFQ displaying a longer duration of action than N/OFQ (Figure 4.6). This indicated a slower metabolism *in vivo* (Guerrini et al., 2014).

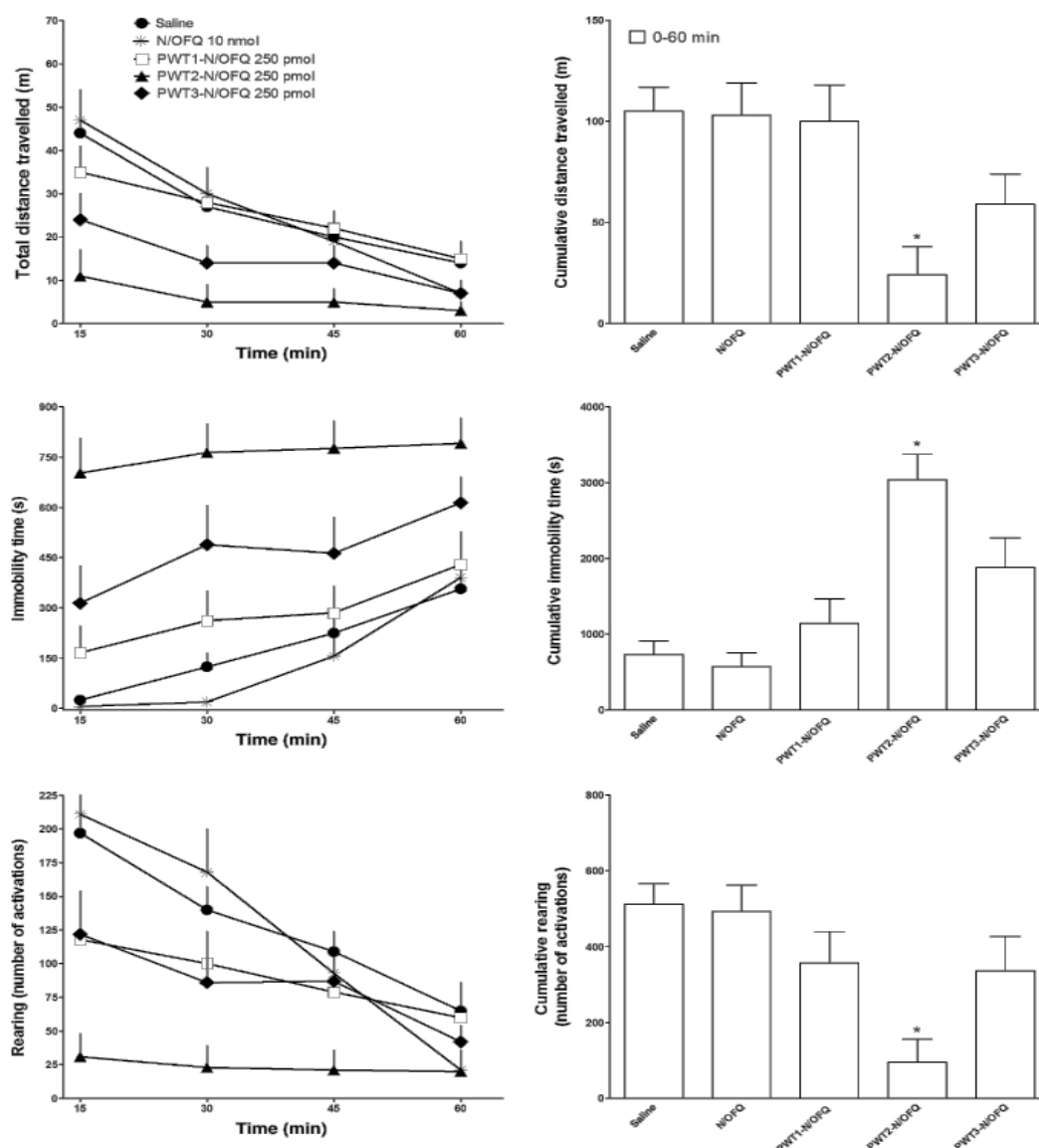


Figure 4.6: Mouse locomotor activity was monitored for 24 hours following injection of either 10nmol N/OFQ or 250pmol of its PWT derivatives. Results are shown as time course in the left panels and as cumulative effects in the right panels. This data demonstrates the prolonged activity of the PWT derivatives when compared N/OFQ in this study (Rizzi et al., 2014).

PWT2-Leu-Enk demonstrated an increase in selectivity for the DOP receptor, failing to displace [3H]-DPN at KOP, or displaying limited ability to displace [3H]-DPN at the highest concentrations used at MOP (Figure 4.3). In GTP γ [35S] functional assays, PWT2-Leu-Enk demonstrated full agonist ability at the DOP receptor (Figure 4.4), producing similar Emax values and pEC50 values to that of Leu-Enkephalin. This indicates that, unlike PWT2-N/OFQ, the formation of a tetrabranched Leu-Enkephalin molecule has no beneficial effects when compared to the single pharmacophore (i.e. increased potency). In calcium mobilisation assays, while PWT2-Leu-Enk acted as a full agonist at DOP, a significant loss in potency was detected when compared to Leu-Enkephalin (Figure 4.4). The disparity between GTP γ [35S] and calcium potency could be due to a state known as hemi-equilibrium. This occurs when equilibrium between receptor and agonist is not achieved due to the short time lapse between its administration and reaching the calcium peak level (Paton and Rang, 1965, Charlton and Vauquelin, 2010).

During time spent with collaborators at the University of Ferrara, the activity of these compounds was also studied in bioassays, specifically the mouse *vas deferens*. Agonist activity can be affected by receptor density, and this bioassay allows assessment of the functional ability of our compounds and to determine whether partial agonist activity is masked in recombinant systems, which usually have much higher expression than native tissues (McDonald et al., 2003a). Partial agonism is dependent on coupling efficiency with the receptor of interest, as well as receptor density. In these assays, PWT2-Leu-Enk acts as a full agonist, however both Leu-Enkephalin and PWT2-Leu-Enk show a decrease in potency when compared to DPDPE (Figure 4.5). This is contradictory to earlier findings in both the calcium mobilisation assay and GTP γ [³⁵S] assays, where Leu-Enkephalin matched DPDPE pEC₅₀ values. The most likely explanation is that Leu-Enkephalin and PWT2-leu-Enk are susceptible to enzymatic degradation.

The work in this chapter illustrates the successful synthesis of a tertabranched N/OFQ compound, which both improves the original peptide's potency and increases its duration of action. Conversely, the formation of a tetrabranched Leu-Enkephalin

compound, demonstrates no improvement in potency or resistance to enzymatic degradation shown by the PWT-N/OFQ derivatives.

Chapter 5 The Characterisation of Novel Peptidic Bivalent Pharmacophores Targeting MOP and NOP

5.1 Introduction

Compounds that simultaneously engage both MOP and NOP receptors provide analgesia, with a decreased dependence profile (Spagnolo et al., 2008, Khroyan et al., 2009a, Toll, 2013). In order to further understand the interactions of MOP and NOP, bivalent pharmacophores based on the MOP peptide agonist, Dermorphin, and the NOP peptide agonist, N/OFQ have been developed. Furthermore, in order to establish whether activation of the NOP receptor negatively impacts MOP signalling, a bivalent pharmacophore based on Dermorphin, and the NOP antagonist, UFP-101, has also been synthesised. Dermorphin and N/OFQ, or UFP-101, are joined at their C-termini by a thiol-maleimide linker molecule. The [Dermorphin]-[N/OFQ] (Figure 5.1) compound has been termed DeNO, while [Dermorphin]-[UFP-101] (Figure 5.2), will be referred to as DeUFP.

5.2 Hypothesis

We hypothesise that linking of Dermorphin with N/OFQ or UFP-101 will provide a compound that has affinity for both MOP and NOP. We also believe that, unlike the F-compounds, these peptidic bivalent pharmacophores will not lose their desired functional activity at the receptors of interest.

5.3 Aims

In this chapter, we aim to provide a detailed analysis of the signalling properties of DeNO and DeUFP. As with previous chapters, we will use CHO cells expressing recombinant opioid receptors (CHO_{hMOP} , CHO_{hDOP} , CHO_{hKOP} and CHO_{hNOP}) to define their pharmacological properties (binding affinity and functional activity). pK_i values for DeNO and DeUFP will be determined using [3H]-DPN and [3H]-UFP-101 as radioligands. Functional activity will be measured by determining both DeNO and DeUFP's ability to stimulate binding of $GTP\gamma[^{35}S]$. We will also assess the ability of DeNO and DeUFP to inhibit the formation of cAMP. Furthermore, the ability of DeNO

and DeUFP to activate the MAPK pathway will be investigated using standard western blotting techniques.

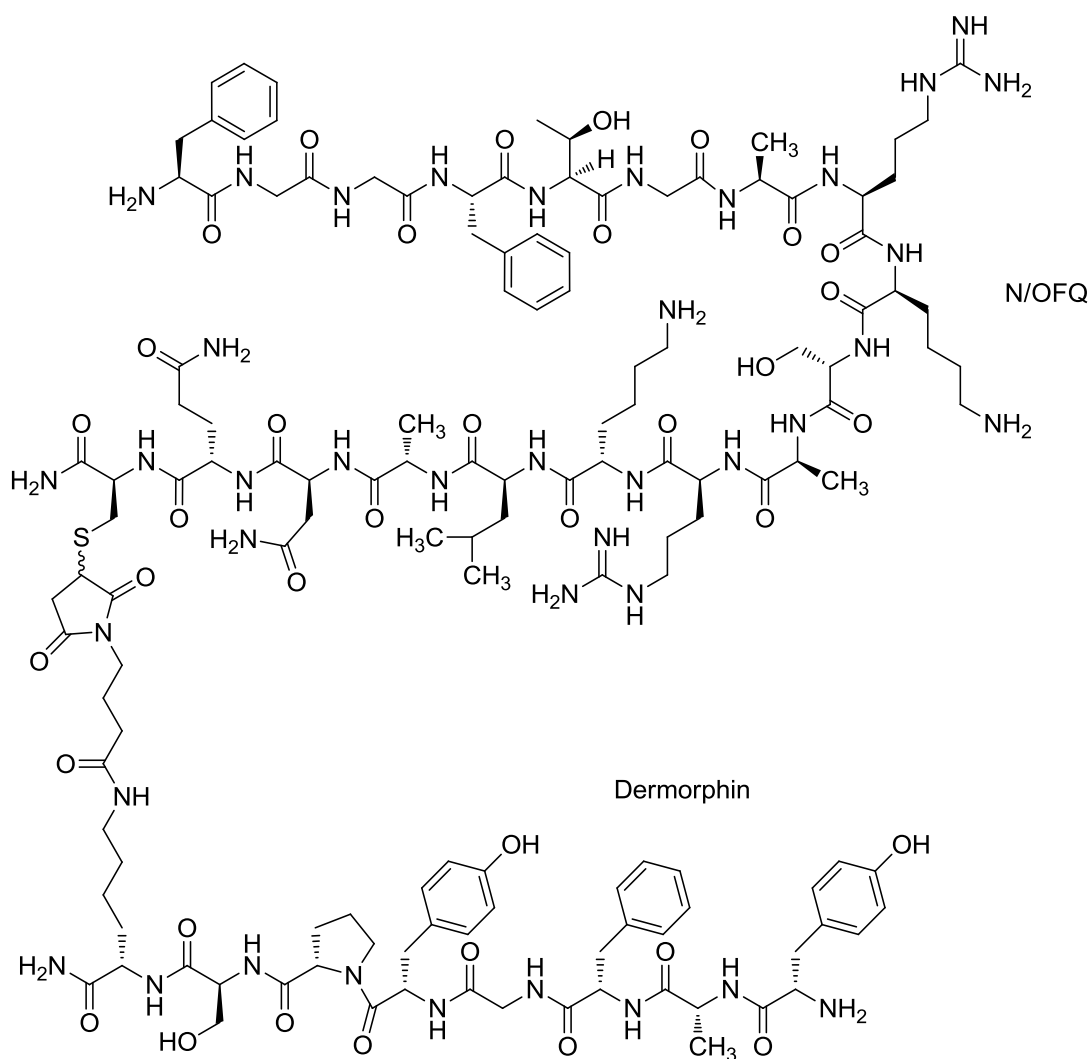


Figure 5.1: The chemical structure of the bivalent pharmacophore, DeNO.

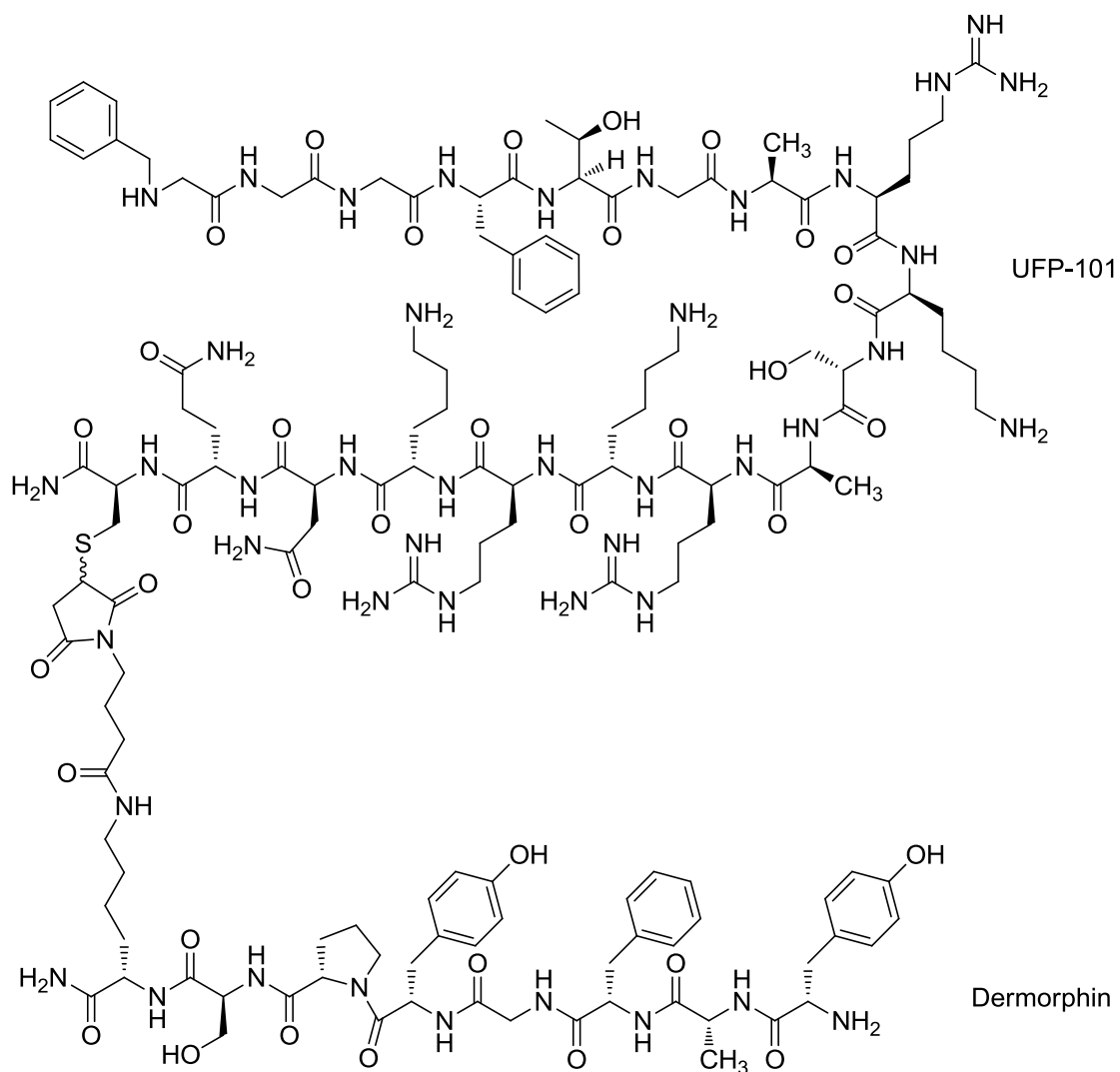


Figure 5.2 The chemical structure of the bivalent pharmacophore, DeUFP.

5.4 Results

5.4.1 Displacement Binding assays

In displacement binding studies at CHO_{hMOP} , Dermorphin, DeNO and DeUFP displaced the binding of $[^3\text{H}]\text{-DPN}$ in a concentration dependent and saturable manner (Figure 5.3). Both DeNO (pK_i : 9.55) and DeUFP (9.64) demonstrated a significant increase in affinity at MOP, when compared to the parent compound Dermorphin (8.69) (Table 5.1). At CHO_{hNOP} , DeNO and DeUFP displaced $[^3\text{H}]\text{UFP-101}$ in a concentration dependent and saturable manner (Figure 5.3). DeNO (10.22) and DeUFP (10.08) displayed similar pK_i values, for NOP, to their parent compounds N/OFQ (10.69) and UFP-101 (10.08) respectively.

At CHO_{hDOP}, both DeNO (8.12) and DeUFP (7.95) demonstrated an increase in affinity compared to their parent compounds. Dermorphin displayed an affinity of 7.17, while both N/OFQ and UFP-101 failed to displace [³H]-DPN at the DOP receptor. Furthermore, both DeNO (7.34) and DeUFP (7.61) showed affinity for the KOP receptor, whereas the parent compounds (Dermorphin, N/OFQ and UFP-101) failed to displace [³H]-DPN at this receptor (Figure 5.3).

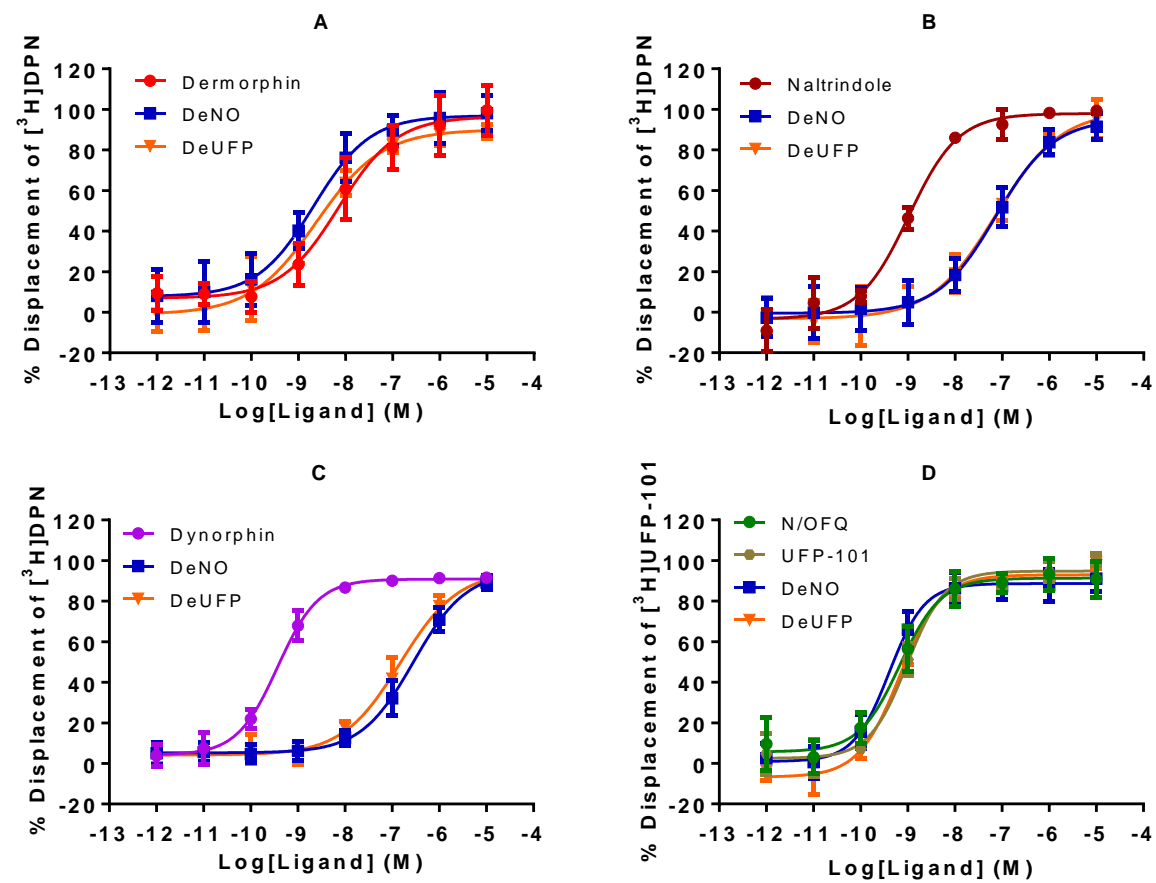


Figure 5.3: Displacement of [³H]-DPN by Dermorphin, DeNO, DeUFP and reference ligands at (A) CHO_{hMOP}, (B) CHO_{hDOP}, (C) CHO_{hKOP} and the displacement of [³H]UFP-101 by DeNO, DeUFP and N/OFQ at (D) CHO_{hNOP} cell membranes. Data are means (SEM) of between 5 and eight experiments for all cell lines. Reference ligands: Dermorphin; Naltrindole; Dynorphin-A; N/OFQ, (Nocicepton/Orphanin FQ).

	CHO _{hMOP}	CHO _{hNOP}	CHO _{hDOP}	CHO _{hKOP}
Reference ligand	-	-	10.02 (± 0.26)	10.16 (± 0.02)
Dermorphin	8.69 (± 0.10)	<5	7.17 (± 0.11)	<5
N/OFQ	<5	10.69 (± 0.10)	<5	<5
UFP-101	<5	9.87 (± 0.10)	<5	<5
DeNO	9.55 (± 0.10) [*]	10.22 (± 0.09)	8.12 (± 0.11) [*]	7.34 (± 0.13) [*]
DeUFP	9.64 (± 0.13) [*]	10.08 (± 0.08)	7.95 (± 0.13) [*]	7.61 (± 0.06) [*]

Table 5.1: The pK_i values for both the reference ligands, Dermorphin, N/OFQ, UFP-101, DeNO and DeUFP. Data are displayed as mean (\pm SEM) of between five and eight experiments. Statistical significance (*) demonstrates p<0.05, using one-way ANOVA with Bonferonni corrections, when compared to the reference ligands: Dermorphin (MOP), N/OFQ (NOP), Naltrindole (DOP) and Dynorphin-A (KOP).

5.4.2 GTP γ [³⁵S] functional Assays

Dermorphin, DeNO and DeUFP stimulated the binding of GTP γ [³⁵S] in a concentration dependent and saturable manner at the MOP receptor (Figure 5.4). DeNO (E_{max}: 2.68) and DeUFP (2.71) demonstrated similar maximal responses to that of Dermorphin (2.63). The pEC₅₀ values for DeNO (7.77) and DeUFP (8.02) showed no significant difference to that of the parent compound, Dermorphin (7.83) (Table 5.2).

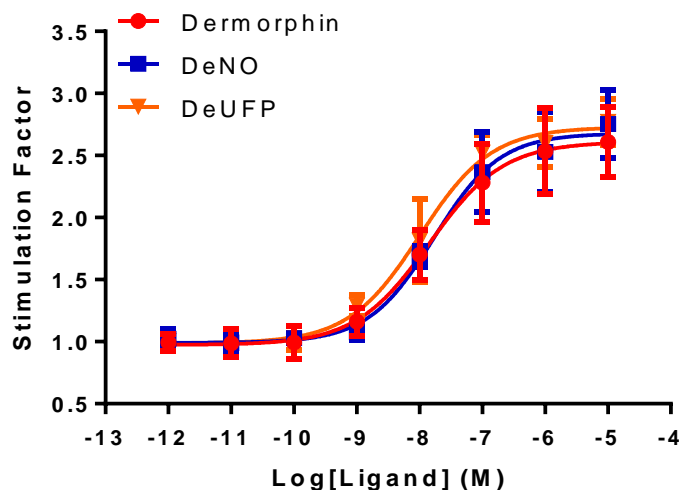


Figure 5.4: Ligand stimulated $\text{GTP}\gamma[^{35}\text{S}]$ binding by Dermorphin, DeNO and DeUFP are shown in CHO_{hMOP} cell membranes. Data are mean (\pm SEM) for five experiments.

At CHO_{hNOP} , N/OFQ, UFP-101, DeNO and DeUFP stimulated the binding of $\text{GTP}\gamma[^{35}\text{S}]$ in a concentration dependent and saturable manner (Figure 5.5). DeNO produced a maximal response (E_{max} : 2.49) similar to that of its parent compound, N/OFQ (2.57). DeUFP (1.31) demonstrated an E_{max} similar to that of UFP-101 (1.42). The pEC_{50} value of 9.35 achieved by DeNO was similar to that of N/OFQ (8.84). Furthermore, DeUFP (8.11) demonstrated a similar pEC_{50} to that of its parent compound, UFP-101 (8.23) (Table 5.2).

In order to determine whether DeUFP has antagonist affinity at NOP, 100nM of the compound was incubated in a range of concentrations of N/OFQ (1pM-10 μ M). The presence of DeUFP leads to a rightward shift in the concentration response curve of N/OFQ (Figure 5.5). DeUFP produces a pK_b of 8.67 (Table 5.2).

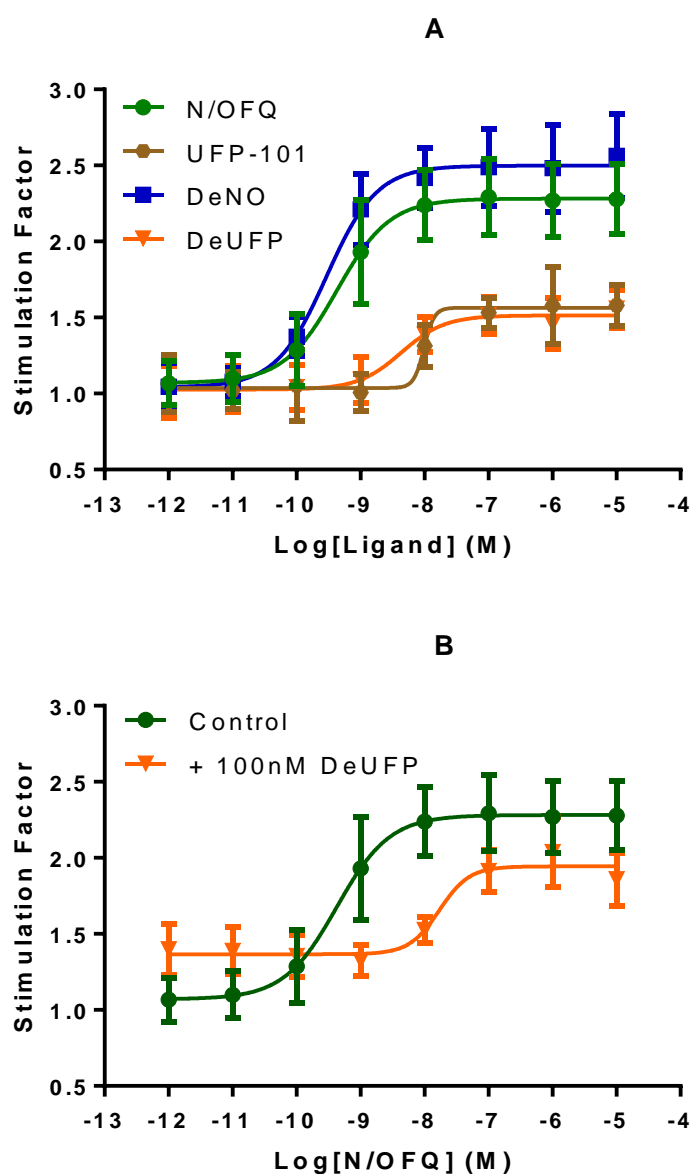


Figure 5.5: : $\text{GTP}\gamma[^{35}\text{S}]$ functional response curves demonstrating A) Ligand stimulated $\text{GTP}\gamma[^{35}\text{S}]$ binding by N/OFQ, UFP-101, DeNO and DeUFP are shown in CHO_{hNOP} cell membranes B) DeUFP was co-incubated, at a concentration of 100nM, with N/OFQ. Data are shown as mean (\pm SEM) between five and eight experiments.

Leu-Enkephalin, DeNO and DeUFP stimulated the binding of $\text{GTP}\gamma[^{35}\text{S}]$ in a concentration dependent and saturable manner in membranes expressing DOP receptors (Figure 5.6). DeNO (E_{max} : 1.84) and DeUFP (1.90) both produced maximal responses similar to that of the endogenous DOP peptide, Leu-Enkephalin (1.90). However, the pEC_{50} values for DeNO (6.78) and DeUFP (7.08) were significantly lower than that of Leu-Enkephalin (8.77) (Table 5.2).

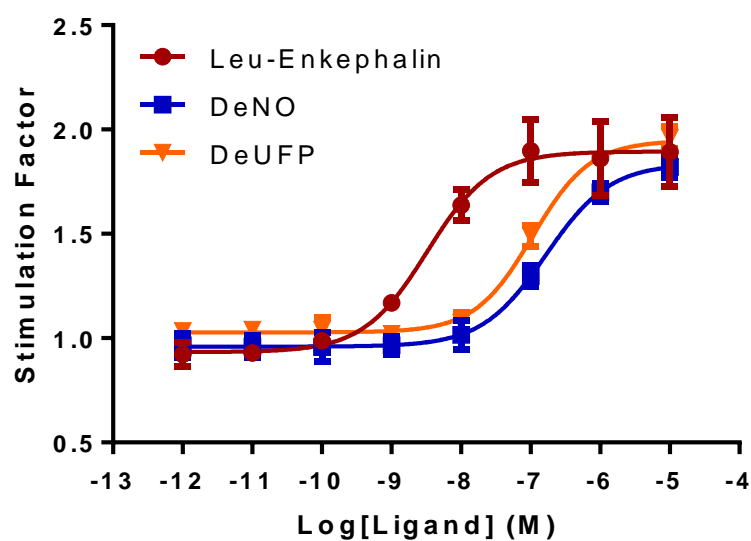


Figure 5.6: Ligand stimulated $\text{GTP}\gamma[^{35}\text{S}]$ binding by Leu-Enkephalin, UFP-101, DeNO and DeUFP are shown in CHO_{hDOP} cell membranes. Data are shown as mean (\pm SEM) for eight experiments.

At CHO_{hKOP} , Dynorphin-A, DeNO and DeUFP stimulated the binding of $\text{GTP}\gamma[^{35}\text{S}]$ in a concentration dependent and saturable manner (Figure 5.7). Both DeNO (E_{max} : 2.23) and DeUFP (2.16) produced a maximal response similar to that of Dynorphin-A (2.30). The pEC_{50} values, however, of DeNO (5.92) and DeUFP (6.64) were significantly lower than that of Dynorphin-A (9.34) (Table 5.2).

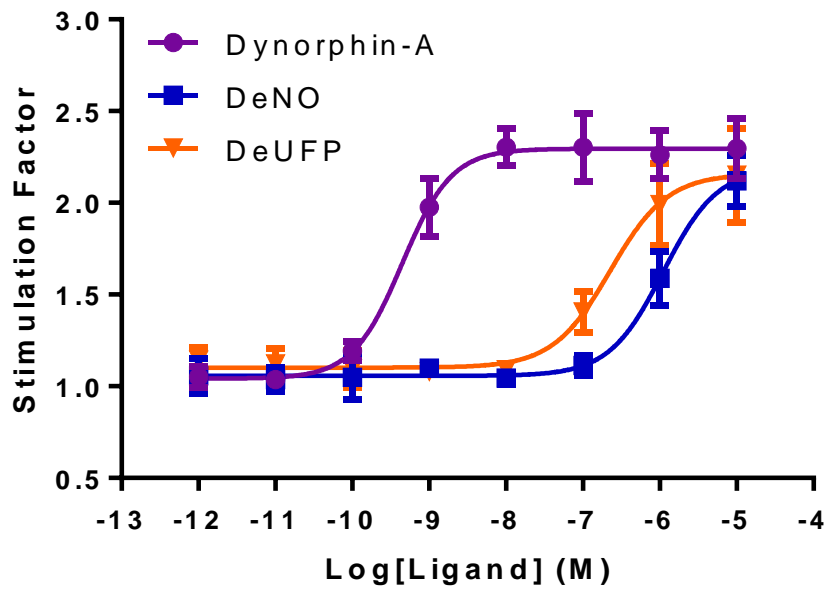


Figure 5.7: Ligand stimulated $GTP\gamma[^{35}S]$ binding by Dynorphin-A, UFP-101, DeNO and DeUFP are shown in CHO_{hKOP} cell membranes. Data are shown as mean (\pm SEM) for five experiments.

	CHO _{hMOP}			CHO _{hNOP}				CHO _{hDOP}			CHO _{hKOP}		
	pEC ₅₀	E _{max}	Relative intrinsic activity	pEC ₅₀	E _{max}	Relative intrinsic activity	pK _b	pEC ₅₀	E _{max}	Relative intrinsic activity	pEC ₅₀	E _{max}	Relative intrinsic activity
Reference Ligand	7.83 (±0.14)	2.61 (±0.14)	1	8.84 (±0.08)	2.57 (±0.17)	1	-	8.77 (±0.03)	1.90 (±0.10)	1	9.34 (±0.08)	2.30 (±0.09)	1
DeNO	7.77 (±0.08)	2.68 (±0.12)	1	9.35 (±0.09)	2.49 (±0.25)	1	-	6.78* (±0.04)	1.84 (±0.03)	1	5.92** (±0.07)	2.23 (±0.14)	1
DeUFP	8.02 (±0.13)	2.71 (±0.08)	1	8.23 (±0.21)	1.42* (±0.09)	0.27	8.67 (±0.10)	7.08* (±0.11)	1.90 (±0.05)	1	6.64** (±0.07)	2.16 (±0.15)	1
UFP-101	-	-	-	8.11 (±0.27)	1.31* (±0.12)	0.2	8.85 ⁺	-	-	-	-	-	-

Table 5.2: Agonist and antagonist activity of DeNO and DeUFP at CHO_{hMOP}, CHO_{hNOP}, CHO_{hDOP} and CHO_{hKOP}. Antagonist affinity was determined against N/OFQ (NOP). Relative intrinsic activity was determined by removal of basal activity and as a ratio of reference ligand (full agonist). E_{max}. All experiments are represented as the mean (±SEM) of between five and eight experiments. If a significant difference from the reference ligand was detected (ANOVA), post-hoc testing using Bonferroni multiple comparisons was employed with *=p<0.05, **=p<0.005. (†) indicates previous data shown by McDonald *et al*, demonstrating the pA₂ value for UFP-101 in the presence of N/OFQ (McDonald *et al.*, 2003b). Reference ligands=Dermorphin (MOP), N/OFQ (NOP), Leu-Enkephalin (DOP) and Dynorphin-A (KOP).

5.4.3 *Cyclic AMP functional assays*

To further assess functional activity of DeNO and DeUFP, inhibition of cyclic AMP (cAMP) formation was assessed. Since DeNO and DeUFP demonstrated higher affinity and potency at MOP and NOP, assays were undertaken in CHO_{hMOP} and CHO_{hNOP} cells.

Addition of forskolin in CHO_{hMOP} cells leads to a 24.3 (± 1.79) fold increase in cAMP production, when compared to basal activity (Figure 5.8). Co-incubation of 1 μ M Dermorphin, 1 μ M DeNO or 1 μ M DeUFP reverses the effects of forskolin, returning cAMP levels to basal. In CHO_{hNOP} cells, forskolin stimulation leads to a 21.23 (± 3.86) fold increase in cAMP production, when compared to basal activity (Figure 5.8). The addition of 1 μ M N/OFQ reverses forskolin stimulated cAMP production. The addition of 1 μ M DeNO has a similar effect, returning cAMP levels to basal when administered. DeUFP did not inhibit cAMP production since the difference between the means was not statistically significant (Figure 5.8).

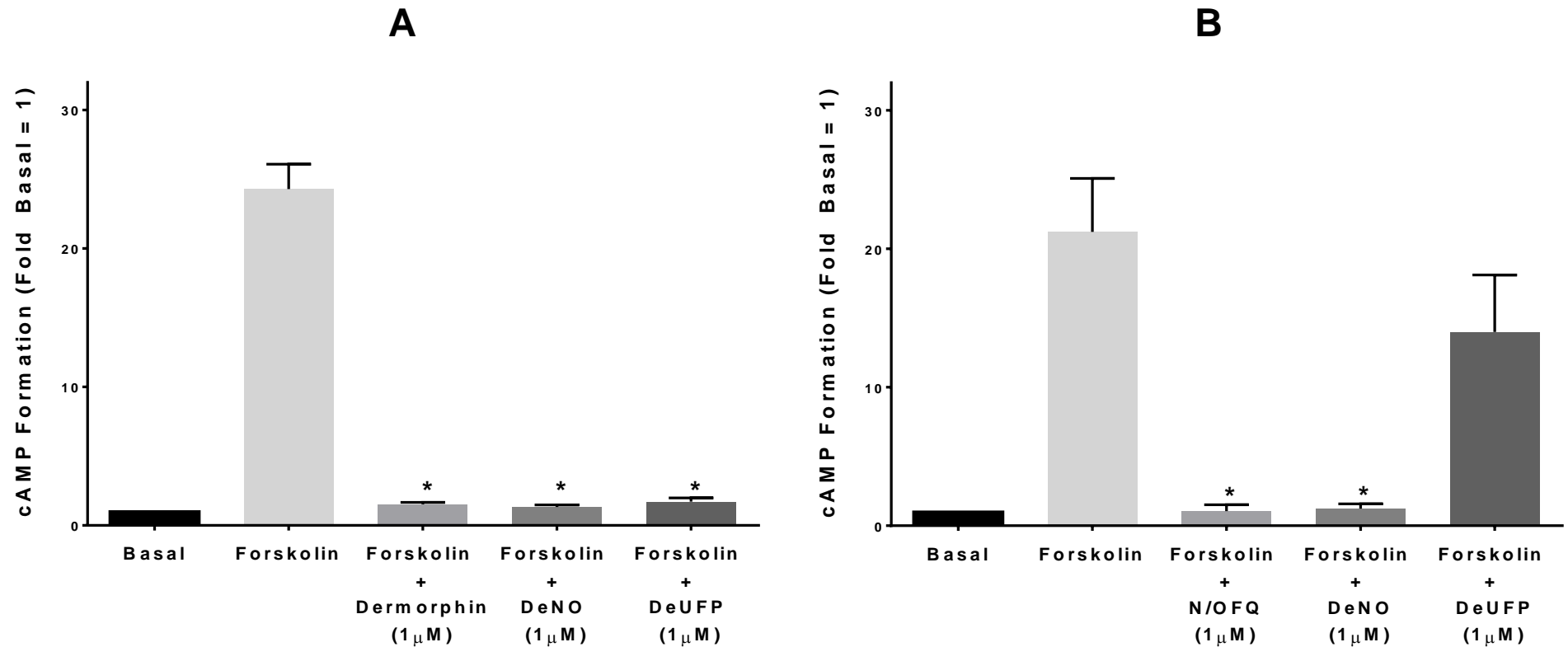


Figure 5.8: Cyclic AMP assays demonstrating A) Fold change in cyclic AMP formation relative to basal measured under varying conditions in CHO_{hMOP} cells ; basal, forskolin stimulated, forskolin and Dermorphin (1 μ M); forskolin and DeNO (1 μ M); forskolin and DeUFP(1 μ M). B) Fold change in cyclic AMP formation relative to basal measured under varying conditions in CHO_{hNOP} cells ; basal, forskolin stimulated, forskolin and N/OFQ (1 μ M); forskolin and DeNO (1 μ M); forskolin and DeUFP(1 μ M). Data are mean (\pm SEM) for five experiments. *=p< 0.0001; according to ANOVA followed by the Bonferroni test for multiple comparisons.

5.4.4 *Detection of MAPK activity through Western blot Densitometry*

As previously mentioned (section 1.2.4), the MAPK pathway is intricately involved in opioid signalling. To further assess how peptide conjugations affect signalling, western blotting has been undertaken to investigate the ERK1/2 and p38 MAPK pathways.

In CHO_{hMOP} cells, stimulation by 10µM Dermorphin, led to a 2.74 (\pm 0.29) fold increase in the phosphorylation of p38, when compared to basal. This demonstrated a statistically significant increase over basal activity (Figure 5.9). Administration of DeNO (3.15 ± 0.41) or DeUFP (2.93 ± 0.45) led to a similar increase in p-p38 activity. In phosphorylated ERK1/2 (p-ERK1/2) studies, the addition of 10 µM Dermorphin (13.69 ± 2.48), DeNO (13.46 ± 2.07) or DeUFP (12.56 ± 2.02) led to statistically significant increase over basal activity.

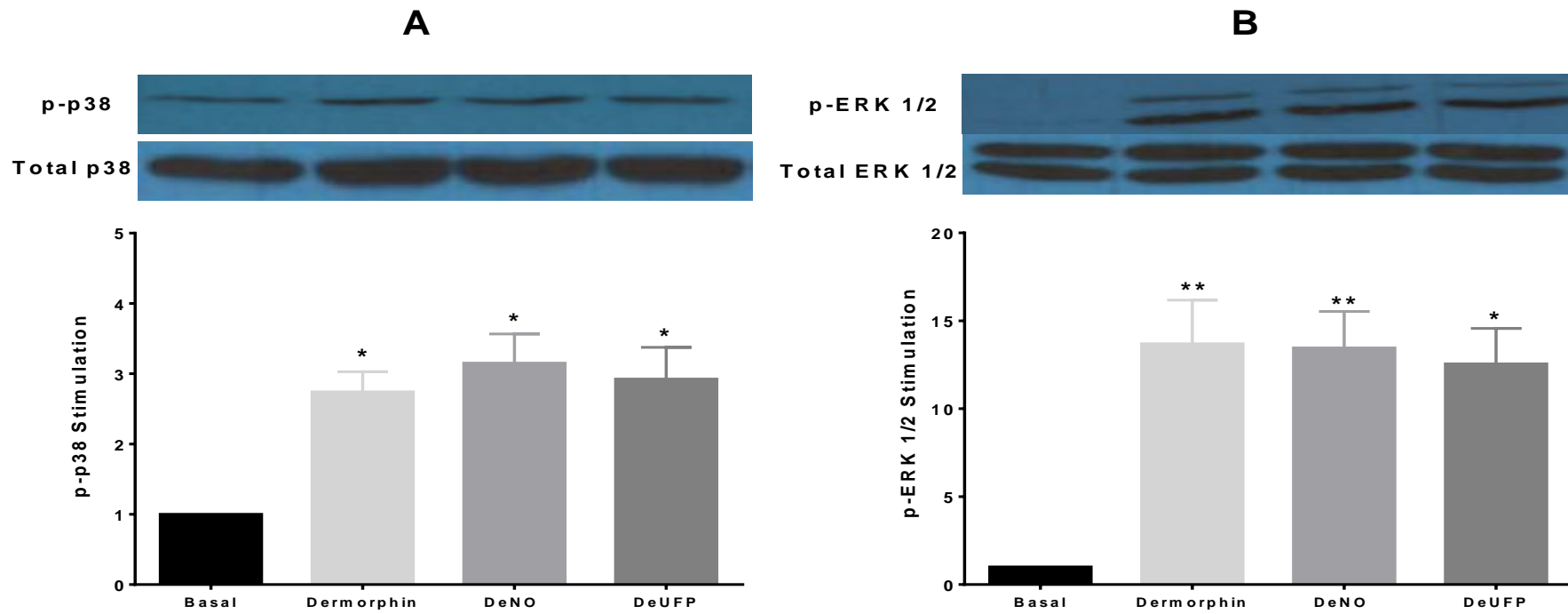


Figure 5.9: Western blot analysis demonstrating A) Representative blot of p38 phosphorylation (p-p38) and the fold increase in phosphorylation, compared to basal activity, at CHO_{hMOP} caused by Dermorphin (10 μ M), DeNO (10 μ M) and DeUFP (10 μ M). B) Representative blot of ERK1/2 phosphorylation (p-ERK1/2) and the % phosphorylation at CHO_{hMOP} caused by Dermorphin (10 μ M), DeNO (10 μ M) and DeUFP. Data are mean (\pm SEM) for n=5. *=p< 0.05, **=p<0.005; according to ANOVA followed by the Bonferroni's test for multiple comparisons, indicating a significant difference from basal activity.

In CHO_{hNOP} cells, no agonist induced stimulation of p38 was detected. In studies assessing the activation of p-ERK1/2, the addition of 10 μ M N/OFQ led to a fold increase of 16.28 ± 2.62), while DeNO (15.23 ± 1.55), UFP-101 (13.65 ± 1.06) and DeUFP (8.13 ± 0.71) led to statistically significant increases over basal activity (Figure 5.10).

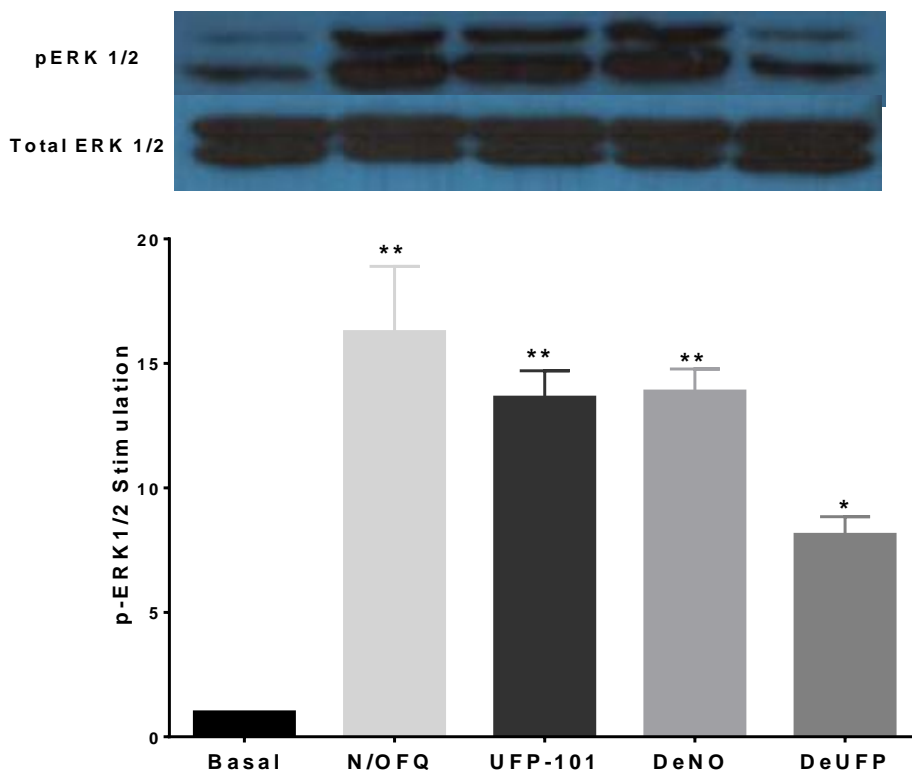


Figure 5.10: Representative blot of ERK1/2 phosphorylation (p-ERK1/2) and the fold increase over basal at CHO_{hNOP} caused by N/OFQ (10 μ M), DeNO (10 μ M) and DeUFP. Data are mean (\pm SEM) for n=5. *= p < 0.05, **= p <0.005; according to ANOVA followed by the Bonferroni test for multiple comparisons, indicating a significant difference from basal activity.

5.5 Discussion

Both DeNO and DeUFP showed a significant increase in binding affinity for the MOP receptor, when compared to the parent compound Dermorphin (Figure 5.3; Table 5.1). At NOP, DeNO demonstrated a similar affinity for NOP as its parent compound N/OFQ. DeUFP also displayed similar pK_i values to that of UFP-101. Interestingly,

both DeNO and DeUFP showed an increase in affinity for DOP and KOP, when compared with Dermorphin, N/OFQ and UFP-101 (Figure 5.3; Table 5.1). The rank order of binding affinity for both DeNO and DeUFP was: NOP>MOP>KOP>DOP.

In GTP γ [³⁵S] functional assays, DeNO and DeUFP demonstrated full agonist activity at MOP (Figure 5.4). These compounds showed similar potency to that of the parent compound, Dermorphin (Table 5.2). In CHO_{hNOP} cells, DeNO acted as a full agonist, displaying similar potency to N/OFQ (Figure 5.5). Both DeUFP and UFP-101 displayed weak partial agonist activity at NOP (Table 5.2). DeUFP also produced a similar potency to that of UFP-101. UFP-101 has been shown to act as an antagonist in low expression systems, however, in high expression systems, UFP-101 can behave as a partial agonist (Calo et al., 2005, Mahmoud et al., 2010). Recombinant systems often have higher expression of the receptor of interest. The higher expression of NOP receptors in our CHO cell lines has unmasked the partial agonist activity of UFP-101 and DeUFP. This is indicated by the presence of relative intrinsic activity of UFP-101 and DeUFP in the GTP γ [³⁵S] assays, as well as the significant increase in phosphorylation of ERK1/2 caused by 10 μ M DeUFP. While not statistically significant, there is also an increased inhibition of cAMP production produced by DeUFP. As mentioned in Chapter 3, one of the hallmarks of a partial agonist is the ability to act as an antagonist in the presence of a full agonist. Antagonist assays were undertaken with DeUFP and the compound demonstrated antagonist activity in the presence of N/OFQ, but display a raised basal activity over the control curve. This is indicative of DeUFP activity at 100nM (Figure 5.5).

The increase in affinity for DOP, in both DeNO and DeUFP, is mirrored by an increase in functional activity (Figure 5.6; Table 5.2). Both DeNO and DeUFP act as full agonists in CHO_{hDOP} and CHO_{hKOP} cells, however they display a lower potency at these receptors when compared to NOP and MOP (Figure 5.11). While functional assay results in CHO_{hMOP} and CHO_{hNOP} indicate that functional activity has not been hindered by conjugation to form a bivalent pharmacophore, the compounds display a loss of selectivity through the demonstration of full agonist ability in CHO_{hDOP} and CHO_{hKOP} cells.

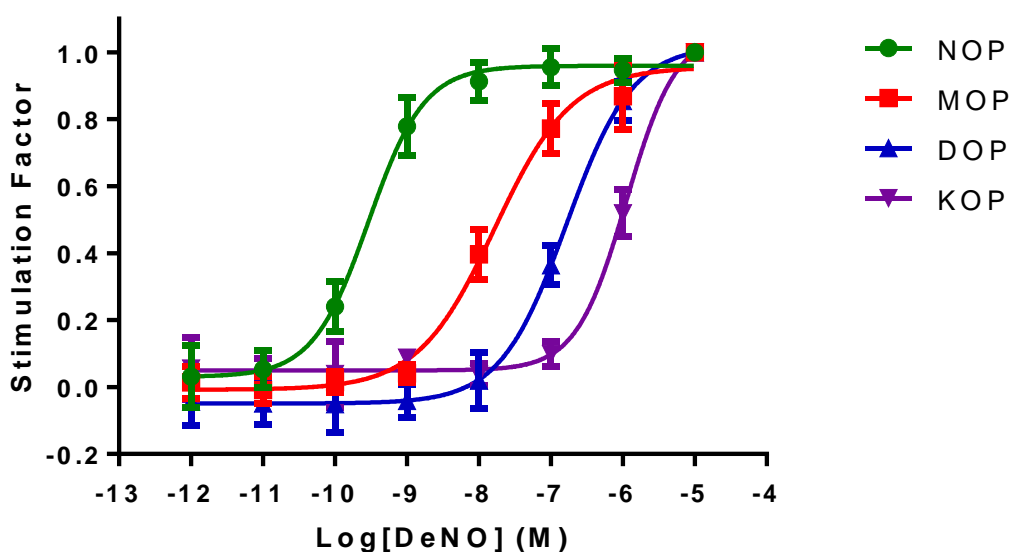


Figure 5.11: Normalised GTP γ [35 S] response curves for DeNO in CHO_{hNOP}, CHO_{hMOP}, CHO_{hDOP} and CHO_{hKOP} membranes.

Since DeNO and DeUFP demonstrated much higher potency values at MOP and NOP, when compared to activity at DOP and KOP, further downstream signalling was investigated in CHO_{hMOP} and CHO_{hNOP} cells. The activation of an opioid receptor leads to an inhibition of cAMP production (section 1.2.3; Figure 1.5). In assays measuring the levels of cAMP production via forskolin stimulation, our compounds demonstrated the ability to inhibit this action at maximal doses in CHO_{hMOP} cells (Figure 5.8). Furthermore, they produced similar results to Dermorphin, indicating no loss in downstream functional ability at MOP. At NOP, DeNO acted in a similar manner to N/OFQ, inhibiting forskolin stimulation (Figure 5.8). DeUFP did not inhibit cAMP production since the difference between the means was not statistically significant.

Opioid signalling has been shown to regulate the phosphorylation of the MAPK pathway, specifically the p38 and ERK1/2 pathways. In CHO_{hMOP} cells, Dermorphin, DeNO and DeUFP all demonstrated an ability to activate the p38 and ERK1/2 pathways (Figure 5.9). All three compounds produced a similar increase in phosphorylation over basal activity for both p-p38 and p-ERK1/2. In CHO_{hNOP} cells, p-p38 activity was not detected in either basal or stimulated samples. This is consistent with previous findings from other groups (Ross and Armstead, 2005). Stimulation with

N/OFQ, DeNO, UFP-101, but not DeUFP, led to a significant increase in ERK1/2 stimulation (Figure 5.10).

The results from this chapter indicate that conjugation of Dermorphin and N/OFQ or UFP-101 leads to the formation of a bivalent pharmacophore that retains functional activity at MOP and NOP. These compounds will allow for the assessment of MOP-NOP interactions in co-expression systems.

Chapter 6 Development of a MOP/NOP Co-Expression System

6.1 Introduction

In previous studies, we have demonstrated that DeNO acts as a full agonist at MOP and NOP, while DeUFP acts a full MOP agonist and partial agonist at NOP (Chapter 5). These studies were undertaken in recombinant systems expressing a single opioid receptor (MOP or NOP). While these studies allow us to better understand the pharmacological profile of DeNO and DeUFP at the receptor of interest, it does not allow for the possibility that these drugs will act different should both receptors be present. For this reason, it is important to determine the binding affinity and functional activity of these bivalent pharmacophores in a cellular system expressing MOP and NOP.

6.2 Hypothesis

We will make a continuous cell lines (CHO or HEK) that co-expresses MOP and NOP and hypothesise that presence of both receptors leads to changes in functional activity.

6.3 Aims

The aims of this chapter are to develop a cell line stably expressing recombinant MOP and NOP receptors (either CHO_{hMOP/NOP} or HEK_{hMOP/NOP}). This cell line will be used to evaluate dual ligands with sites of action at MOP and NOP. This process will involve the transfection of hNOP into available CHO_{hMOP} cell lines using transfection protocols detailed by previous work in this laboratory (Dietis, 2012). Selection pressure will be provided by 800µg.ml⁻¹ of geneticin and 800µg.ml⁻¹ hygromycin B. Following this, successful transfection of the receptor of interest will be measured through RT-qPCR to detect the presence of receptor RNA and receptor expression by saturation binding assays. Previous work in this laboratory has demonstrated the difficulty of developing a co-expression with near equal receptor density in CHO cell lines (Dietis, 2012). Should this issue arise, it will be addressed by the development of HEK cell lines expressing MOP, NOP and MOP and NOP. The receptor density of these novel HEK cell lines will be determined. Since HEK_{hOPIOID} cell lines are new to the lab, assessment of the optimal conditions for use in GTPγ[³⁵S] functional assay will be undertaken.

6.4 Results-CHO cell lines

6.4.1 Selection of an appropriate monoclonal CHO_{hMOP/NOP} cell batch

The mRNA levels of monoclonal CHO_{hMOP/NOP} cells, after surviving selection pressure, were measured by RT-qPCR with data expressed as ΔC_t for the gene of interest relative to a housekeeper gene, GAPDH (Table 6.1). Figure 6.1 presents a representative amplification plot produced by analysis of RT-qPCR data from our clones.

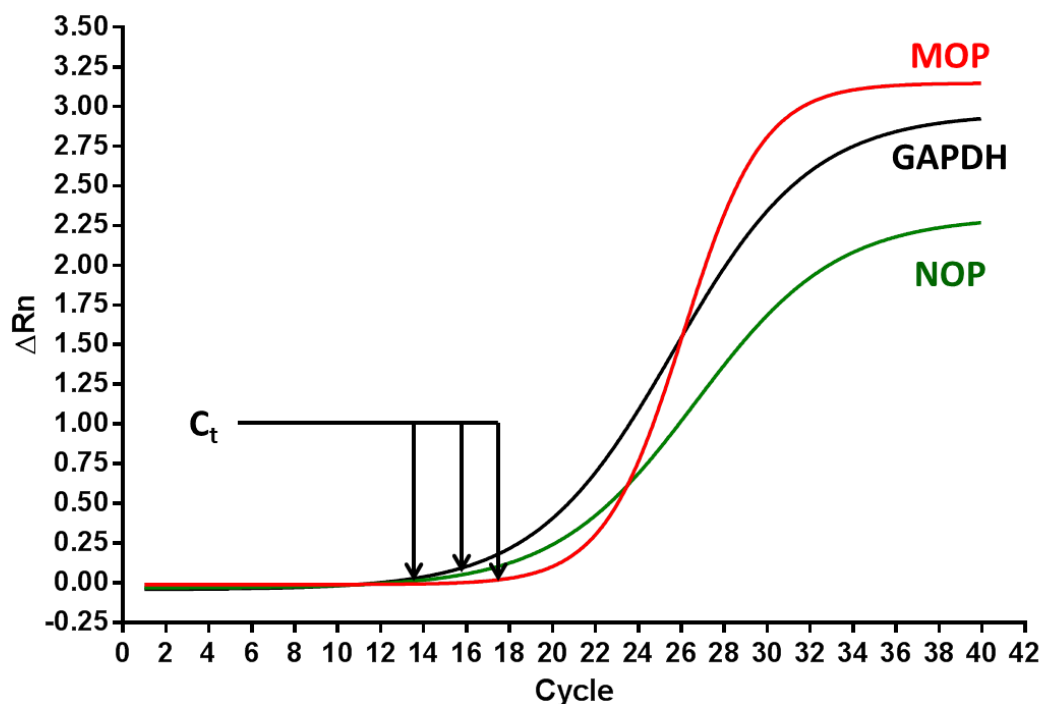
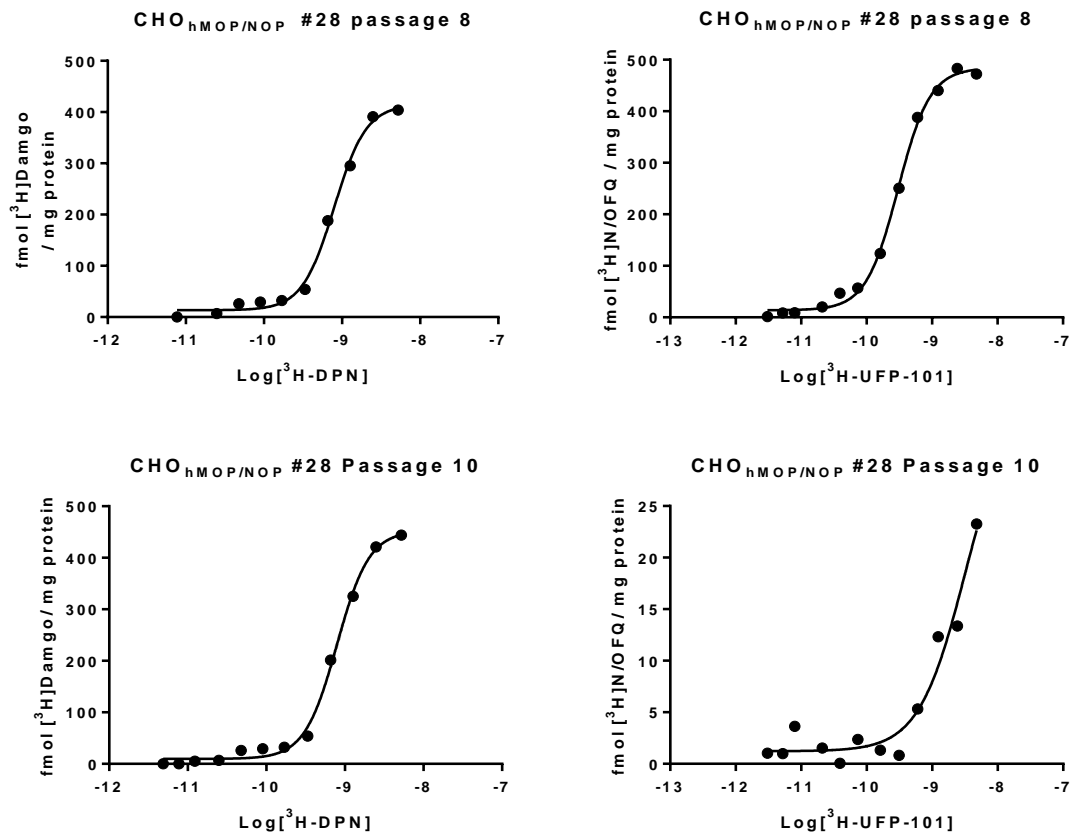


Figure 6.1: A representative amplification plot (in this case for CHO_{hMOP/NOP} cell batch 37, Table 6.2) from RT-qPCR. ΔRn corresponds to an increase of fluorescent signal at each time point. The StepOne[™] software automatically adjusts the ΔRn threshold for each sample (level of fluorescence chosen on the basis of baseline variability). The threshold value (C_t) is defined as the cycle number where signal increases above threshold levels for each sample. The lower the ΔC_t value, the higher the level of RNA expression.

Clone	GAPDH C _t	MOP C _t	Δ C _t Mean	GAPDH C _t	NOP C _t	Δ C _t Mean
CHO _{hMOP/NOP} #1	15.22	22.07	6.85	16.15	20.34	4.18
CHO _{hMOP/NOP} #2	21.73	26.56	4.82	23.54	26.97	3.43
CHO _{hMOP/NOP} #3	14.84	20.86	6.01	15.49	20.42	4.93
CHO _{hMOP/NOP} #6	27.90	33.80	5.90	29.51	31.86	2.36
CHO _{hMOP/NOP} #7	19.90	28.82	8.91	20.25	27.49	7.25
CHO _{hMOP/NOP} #8	21.90	30.91	9.01	22.24	26.79	4.55
CHO _{hMOP/NOP} #9	29.61	34.49	4.88	29.27	30.49	1.22
CHO _{hMOP/NOP} #11	27.32	31.93	4.61	26.67	28.18	1.52
CHO _{hMOP/NOP} #12	15.22	20.99	5.77	15.82	34.71	18.89
CHO _{hMOP/NOP} #13	15.52	23.30	7.78	16.23	34.25	18.02
CHO _{hMOP/NOP} #14	16.04	20.84	4.80	14.58	31.64	17.05
CHO _{hMOP/NOP} #15	34.59	36.51	1.92	29.8	35.45	5.65
CHO _{hMOP/NOP} #17	17.86	26.09	8.23	18.49	20.88	2.40
CHO _{hMOP/NOP} #18	14.46	22.41	7.96	13.64	19.91	6.27
CHO _{hMOP/NOP} #19	15.14	22.56	7.42	14.14	18.42	4.28
CHO _{hMOP/NOP} #20	14.84	20.52	5.67	13.77	17.23	3.46
CHO _{hMOP/NOP} #21	13.82	22.94	9.13	14.2	26.27	12.06
CHO _{hMOP/NOP} #22	14.95	20.82	5.87	14.63	23.54	8.91
CHO _{hMOP/NOP} #24	14.79	20.95	6.16	16.59	16.68	0.09
CHO _{hMOP/NOP} #26	15.90	22.08	6.18	15.11	21.58	6.47
CHO _{hMOP/NOP} #28	17.86	19.32	1.46	13.77	15.63	1.86
CHO _{hMOP/NOP} #29	14.46	18.30	3.84	14.20	38.32	24.12
CHO _{hMOP/NOP} #30	15.14	17.20	2.06	14.63	31.33	16.70

Table 6.1: C_t values for CHO_{hMOP/NOP} clones. The Δ C_t is determined by removing the C_t of the house keeper gene from the C_t of the gene of interest. The higher Δ C_t, the lower the amount of RNA for the gene of interest is present in the sample. Clones chosen for further analysis are shaded grey. Samples were screened from single cell RNA extractions.

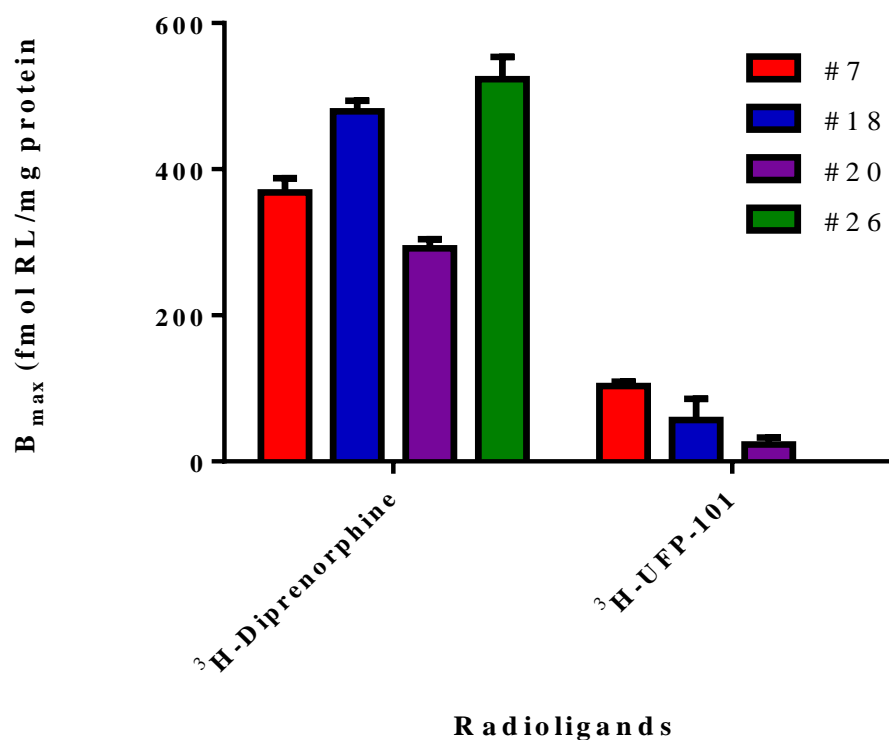
Initially, only clone #28 was assessed further for radioligand saturation binding assays (section 2.7), due to the close proximity of its MOP/NOP Δ C_t values. In these assays, the clone was incubated with a range of concentrations of either [³H]-DPN or [³H]-UFP-101 to determine the B_{max} (receptor expression). At passage 8, clone #28 expressed B_{max} values of 432 for MOP and 409 for NOP. However, by passage 10 there was a disparity in expression of MOP (487) and NOP (22.8) (Figure 6.2).



Radioligand	B_{max} of Clone #28	
	Passage 8	Passage 10
[³ H]-DPN	432±11.9	409±18.5
[³ H]UFP-101	487±28.7	22.8±18.9

Figure 6.2: Saturation analysis of the expression of $hMOP$ and $hNOP$ in Clone #28 cells over time. Data in lower part are represented as mean (\pm SEM) for three experiments at each passage.

Following the inability of clone #28 to stably express NOP, the remaining clones (Table 6.2) were studied in saturation binding assays, using [³H]-DPN and [³H]UFP-101. The results demonstrated no NOP expression in these cell lines, after 12 passages (Figure 6.3).



Radioligand	B _{max} of CHO _{hMOP/NOP} clones			
	#7	#18	#20	#26
[³ H]-DPN	368.3±11.3	479.3±8.3	291.7±7.4	523.3±17.6
[³ H]UFP-101	103±3.6	56.7±16.9	23±5.5	0

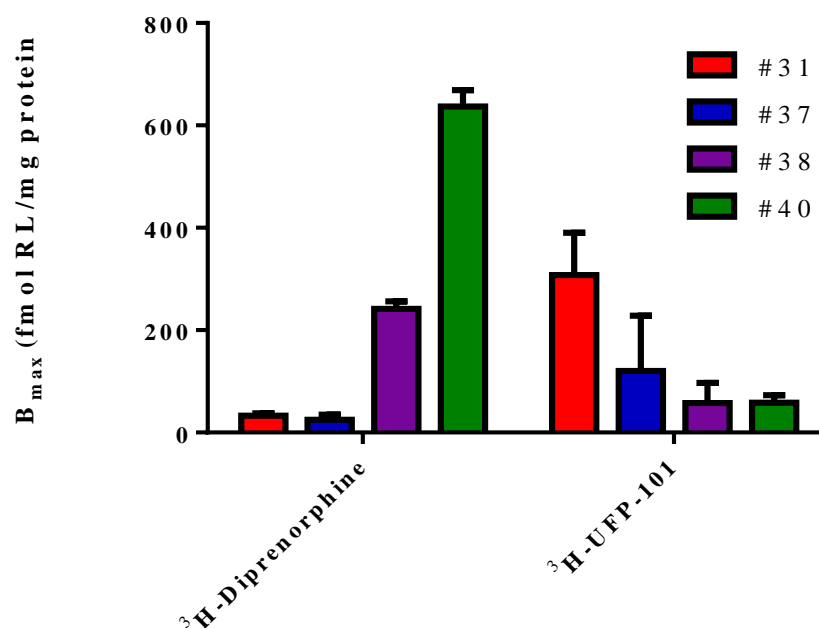
Figure 6.3: Determination of receptor density (B_{max}) for MOP and NOP receptors in four different batches of the monoclonal CHO_{hMOP/NOP} cell line by saturation binding assays. Data are represented as mean (\pm SEM) for three experiments.

Due to the failure of the initial batch of monoclonal CHO_{hMOP/NOP} cells to stably express the NOP receptor, the transfection and selection protocols were repeated, and a new batch of monoclonal CHO_{hMOP/NOP} cells was obtained. These cells were again screened, using RT-qPCR, for MOP and NOP RNA levels (Table 6.2). A number of cells indicated a similarity in ΔC_t values for MOP and NOP. The receptor expression of Clones #31, #37, #38 and #40 were all measured for MOP and NOP at passage 9, using [³H]-DPN and [³H]UFP-101 respectively (Figure 6.4). From these results, CHO_{hMOP/NOP} #31 showed B_{max} values of 33.1 for MOP and 307.6 NOP respectively. CHO_{hMOP/NOP} #37 (B_{max} ; MOP: 25.2, NOP: 120.4), CHO_{hMOP/NOP} #38 (MOP: 25.2, NOP: 120.4), CHO_{hMOP/NOP} #40 (MOP: 242, NOP: 57.5), CHO_{hMOP/NOP} #40 (MOP: 636.7, NOP:

58.5). These results again indicate a disparity between the ΔC_t values and the levels of expressed receptors in the CHO cells.

Clone	GAPDH C_t	MOP C_t	ΔC_t Mean	NOP C_t	ΔC_t Mean
CHO_{hMOP/NOP} #31	19.05	21.21	2.16	17.44	-1.6
CHO_{hMOP/NOP} #32	15.57	20.94	5.37	21.09	5.53
CHO_{hMOP/NOP} #33	16.44	21.47	5.034	35.69	19.25
CHO_{hMOP/NOP} #34	16.42	22.69	6.27	36.9	20.48
CHO_{hMOP/NOP} #35	16.34	22.99	6.65	38.2	21.86
CHO_{hMOP/NOP} #36	16.61	23.2	6.58	34.72	18.1
CHO_{hMOP/NOP} #37	19.81	18.56	-1.24	20.69	0.88
CHO_{hMOP/NOP} #38	20.74	20.59	-0.15	20.85	0.11
CHO_{hMOP/NOP} #39	20.03	20.29	0.26	34.54	14.51
CHO_{hMOP/NOP} #40	30.86	30.68	-0.18	30.38	-0.49
CHO_{hMOP/NOP} #41	21.02	21.52	0.5	25.46	4.43
CHO_{hMOP/NOP} #42	20.99	23.47	2.48	36.91	15.92

Table 6.2: C_t values for CHO_{hMOP/NOP} clones in the second wave of transfections. Highlighted clones were further assayed to determine expression of functional MOP and NOP receptors. Samples were screened from single cell RNA extractions.



Radioligand	B _{max} of CHO _{hMOP/DOP} clones			
	#31	#37	#38	#40
[³ H]-Diprenorphine	33.1±2.8	25.2±5.5	242±8.3	636.7±18.5
[³ H]UFP-101	307.6±47.7	120.4±62.4	57.5±22.9	58.5±8.3

Figure 6.4: Further determination of receptor density (B_{max}) for MOP and NOP receptors in four different batches of the monoclonal CHO_{hMOP/NOP} cell line by saturation binding assays. Data in lower part are represented as mean (\pm SEM) for three experiments.

6.5 Results- Development of HEK cell lines

Due to the failure of CHO cell lines to stably co-express similar levels of MOP and NOP receptors, work moved on to HEK cell lines. HEK cell lines have previously been shown to be capable of expressing modified MOP and NOP receptors (Wang et al., 2005). Initially, HEK cells will be transfected with either hMOP or hNOP, to generate HEK_{hMOP} and HEK_{hNOP} cell lines. Following successful identification of stable HEK_{hMOP} and HEK_{hNOP} monoclonal cell line, it will be transfected with the other gene of interest. Reverse transcription-qPCR and saturation binding studies will be used to determine stable receptor expression. Furthermore, as HEK_{hOPIOID} cell lines have not been used for functional GTP γ [³⁵S] studies in our laboratory, it is necessary to optimise buffer constituents, the optimal incubation period and the optimal GDP concentration.

6.5.1 *Cell death curve*

In order to determine the concentration of the necessary selection agent needed to maintain stock selection (MOP: Geneticin; NOP: Hygromycin B), wild type HEK cells were treated with a range of concentrations of geneticin (Table 6.3, Figure 6.5) or hygromycin B (Table 6.4, Figure 6.5). The addition of $800\mu\text{g.ml}^{-1}$ geneticin or hygromycin B led to 100% cell death after 4 days and was chosen as the concentration to use to provide selection pressure. Concentrations of $200\mu\text{g.ml}^{-1}$ geneticin or $200\mu\text{g.ml}^{-1}$ hygromycin B were required to produce cell death after 14 days, respectively. These concentrations will be used to provide stock pressure, once monoclonal cell lines are established.

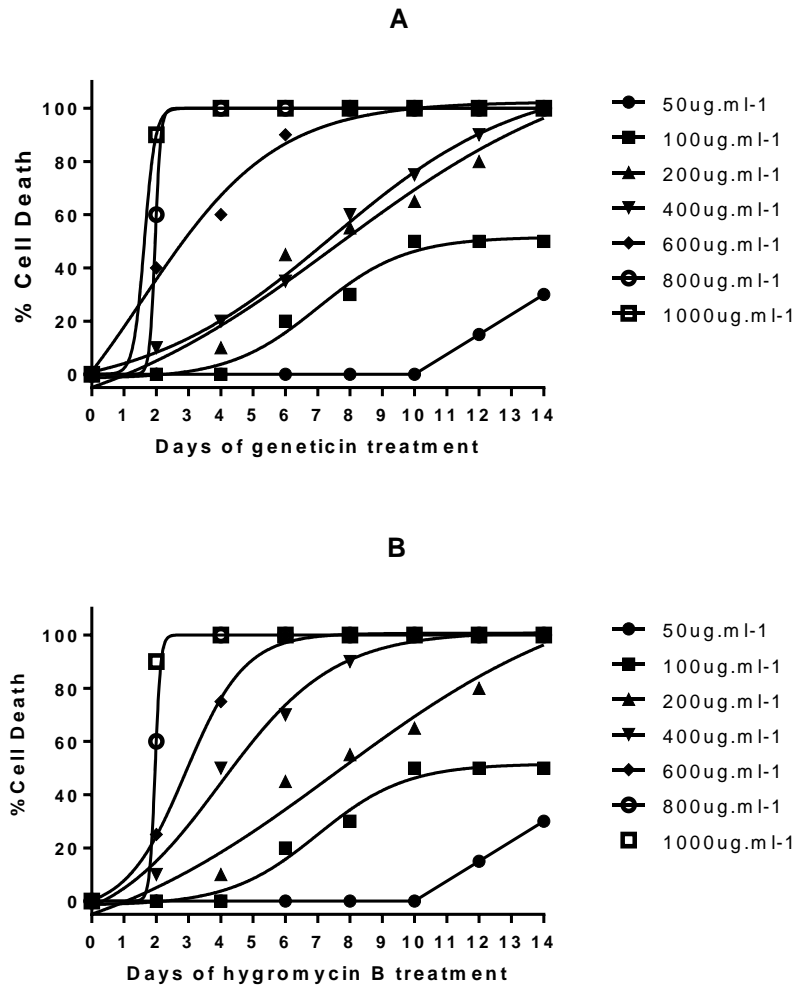


Figure 6.5: Assessment of geneticin and hygromycin treatment. A) Death curves of HEK cells in the presence of different concentrations of geneticin. B) Death curves of HEK cells in the presence of different concentrations of hygromycin B. Data are presented as a percentage of cell death. Cells were screened over a period of 14 days.

Geneticin ($\mu\text{g}\cdot\text{ml}^{-1}$)	Alive HEK _{WT} Cells (%)						
	Day 2	Day 4	Day 6	Day 8	Day 10	Day 12	Day 14
50	100	100	100	100	100	85	70
100	100	100	80	70	50	50	50
200	100	90	55	45	35	20	0
400	90	80	65	40	25	10	0
600	60	40	10	0	0	0	0
800	40	0	0	0	0	0	0
1000	10	0	0	0	0	0	0

Table 6.3: Representative table of live HEK cells, over a period of 14 days exposure to various concentrations of geneticin. A concentration of $800\mu\text{g}\cdot\text{ml}^{-1}$ geneticin produced 100% cell death after 4 days, and was chosen as the selection pressure. The concentration of geneticin which caused 100% cell death after 14 days, was $200\mu\text{g}\cdot\text{ml}^{-1}$, and was used as stock pressure.

Hygromycin B ($\mu\text{g}\cdot\text{ml}^{-1}$)	Alive HEK _{WT} Cells (%)						
	Day 2	Day 4	Day 6	Day 8	Day 10	Day 12	Day 14
50	100	100	100	100	100	100	85
100	100	100	100	80	70	50	50
200	100	100	90	55	45	35	20
400	100	90	50	30	10	0	0
600	100	75	25	0	0	0	0
800	50	0	0	0	0	0	0
1000	0	0	0	0	0	0	0

Table 6.4: Representative table of live HEK cells, over a period of 14 days exposure to various concentrations of hygromycin B. A concentration of $800\mu\text{g}\cdot\text{ml}^{-1}$ hygromycin B produced 100% cell death after 4 days, and was chosen as the selection pressure. The concentration of hygromycin B which caused 100% cell death after 14 days, was $200\mu\text{g}\cdot\text{ml}^{-1}$, and was used as stock pressure.

6.5.2 Selection of appropriate HEK_{hMOP} and HEK_{hNOP} monoclonal cell lines

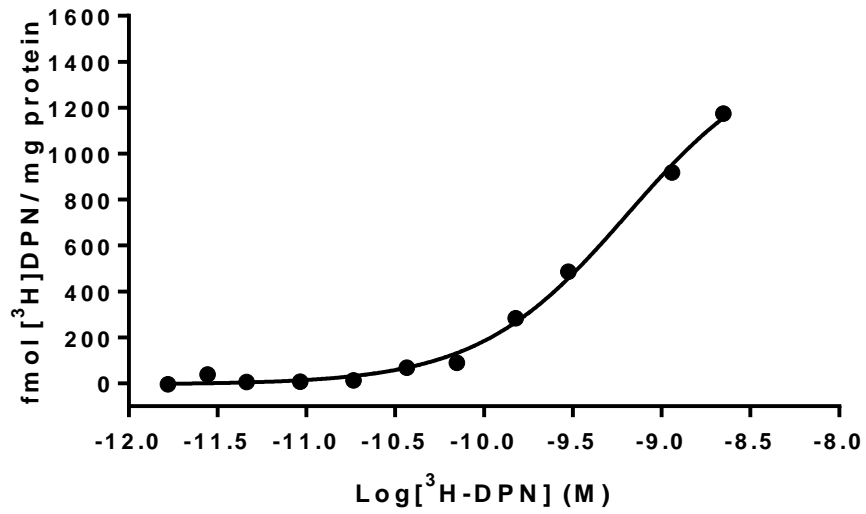
For MOP cells, any monoclonal HEK_{hMOP} cell that survived geneticin selection pressure, were screened for MOP gene expression, using RT-qPCR with data expressed as ΔC_t (Table 6.5). From a total of 10 isolated clones, 7 showed low ΔC_t values for the MOP gene. Due to growth performance, HEK_{hMOP} #1 was screened first at passage 3 using [^3H]-DPN, demonstrating a B_{max} of 1542 and a pK_d of 9.23 (Table 6.6, Figure

6.6). These results indicate a high expression of the MOP receptor, and as such the receptor expression was also measured at passage 10 to determine stability. The B_{\max} was 1603 and the pK_d of 9.26, indicated stable transfection in HEK_{hMOP} #1. Due to other clones displaying unstable receptor expression, poor cell growth, or having died after several passages, HEK_{hMOP} #1 was chosen for further study (Table 6.6).

Clone	GAPDH C_t	MOP C_t	ΔC_t Mean
HEK _{hMOP} #1	20.21	19.58	-0.62
HEK _{hMOP} #2	20.49	20.57	0.08
HEK _{hMOP} #3	19.89	24.68	4.79
HEK _{hMOP} #4	19.56	20.01	0.45
HEK _{hMOP} #5	18.85	18.31	-0.55
HEK _{hMOP} #6	19.62	36.43	16.81
HEK _{hMOP} #7	20.73	19.78	-0.95
HEK _{hMOP} #8	19.83	20.08	0.25
HEK _{hMOP} #9	21.75	20.76	-0.98
HEK _{hMOP} #10	19.45	28.53	9.07

Table 6.5: C_t values for HEK_{hMOP} clones. Clones shaded in grey showed low ΔC_t values and were screened using radioligand saturation binding. Samples were screened from single cell RNA extractions.

HEK_{hMOP} #1 Passage 3



HEK_{hMOP} #1 Passage 10

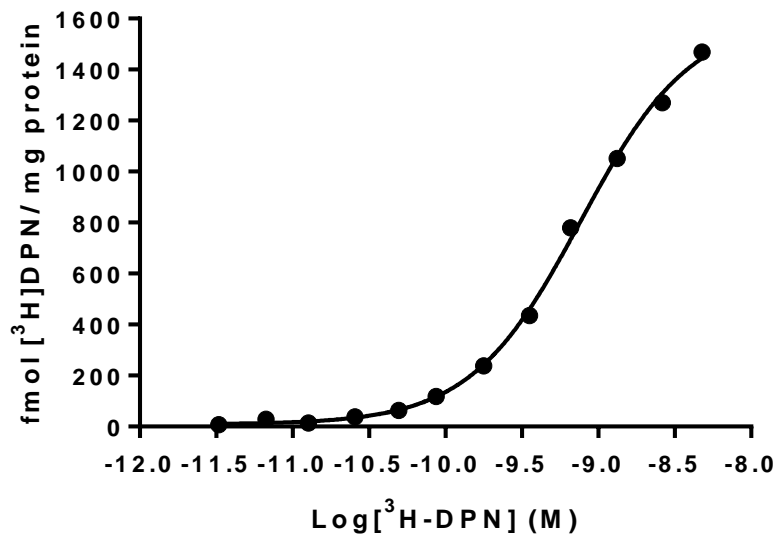


Figure 6.6: Representative saturation binding curves depicting receptor expression in HEK_{hMOP} #1 clones over a window of 7 passages. The B_{max} and pK_d values are shown in Table 6.6.

	Passage 3		Passage 10		Cell Growth
	pK _d	B _{max}	K _d	B _{max}	
HEK _{hMOP} #1	9.23	1542	9.26	1603	moderate
HEK _{hMOP} #2	9.26	1325	9.23	850	moderate
HEK _{hMOP} #4	9.28	1125			dead
HEK _{hMOP} #5	9.19	863			dead
HEK _{hMOP} #7	9.22	534	9.32	263	ultra slow
HEK _{hMOP} #8	9.25	1432			dead
HEK _{hMOP} #9	9.23	723	9.28	605	ultra slow

Table 6.6: The B_{max} and pK_d values obtained from saturation binding assays with HEK_{hMOP} monoclonal cell lines, over several passages. Areas shaded in dark, indicate that the cell died between passages. The rate of cell growth was also monitored, and aided the cell line choice for future experiments.

In the case of HEK_{hNOP} cell lines, any monoclonal cell line that survived hygromycin B selection pressure, was screened for NOP gene expression, using RT-qPCR with data expressed as ΔC_t (Table 6.7). From the 8 cells in which NOP gene expression was shown, only four survived selection pressure to reach passage 3 (Table 6.8). From those, HEK_{hNOP} #8 (B_{max}: 529) and #16 (B_{max}: 432) showed the highest expression of functional NOP receptor at passage 3 when screened using [³H]-UFP-101 in saturation binding assays. Receptor expression was monitored after 7 passages to determine stable expression. HEK_{hNOP} #8 (B_{max}: 887) showed an increase in NOP receptor expression after 10 passages (Figure 6.7). HEK_{hNOP} #16 showed stable expression of NOP receptor however displayed poor cell growth. HEK_{hNOP} #8 showed an average a pK_d of 9.01 (± 0.08) for [³H]UFP-101. Due to these results, and the increased expression of NOP receptors, HEK_{hNOP} #8 was chosen for use in further experiments.

Clone	GAPDH C_t	NOP C_t	ΔC_t Mean
HEK _{hNOP} #2	21.87	31.23	9.35
HEK _{hNOP} #3	21.53	30.77	9.24
HEK _{hNOP} #4	21.81	31.23	9.43
HEK _{hNOP} #8	21.38	20.22	-1.16
HEK _{hNOP} #9	22.74	21.29	-1.46
HEK _{hNOP} #13	21.16	19.93	-1.23
HEK _{hNOP} #16	22.47	20.75	-1.72
HEK _{hNOP} #17	21.20	19.88	-1.32
HEK _{hNOP} #19	22.37	21.37	-1.00
HEK _{hNOP} #23	21.40	20.12	-1.28
HEK _{hNOP} #25	31.84	29.73	-2.11

Table 6.7: C_t values for HEK_{hNOP} clones. Clones shaded in grey showed low ΔC_t values and were screened using radioligand saturation binding. Samples were screened from single cell RNA extractions.

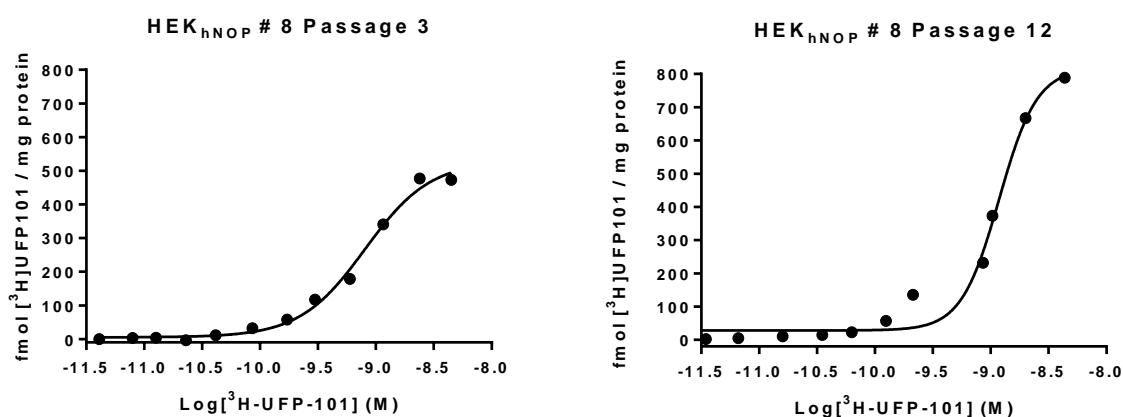


Figure 6.7: Representative saturation binding graphs depicting receptor expression in HEK_{hNOP} #1 clones over a window of 9 passages. The B_{max} and pK_d are shown in Table 6.8.

	Passage 3		Passage 10		Cell Growth
	pK _d	B _{max}	pK _d	B _{max}	
HEK_{hNOP} #8	9.09	529.4	8.93	887.0	good
HEK_{hNOP} #9					dead
HEK_{hNOP} #13					dead
HEK_{hNOP} #16	9	432.5	9.01	482.3	Ultra slow
HEK_{hNOP} #17	8.99	270.3			dead
HEK_{hNOP} #19					dead
HEK_{hNOP} #23					dead
HEK_{hNOP} #25	9.10	352.3			dead

Table 6.8: The B_{max} and pK_d values obtained from saturation binding assays with HEK_{hNOP} monoclonal cell lines, over several passages. Areas shaded in dark, indicate that the cell died between passages. The rate of cell growth was also monitored, and aided in choosing the cell line to use for future experiments.

6.5.3 Optimising GTPγ[³⁵S] assay in HEK cells

Following the determination of appropriate HEK_{hMOP} and HEK_{hNOP}, these cells were tested to establish functional activity. Initial experiments using previous protocols failed to demonstrate functional activity in HEK_{hMOP} cells using the known full agonist Dermorphin (Figure 6.8).

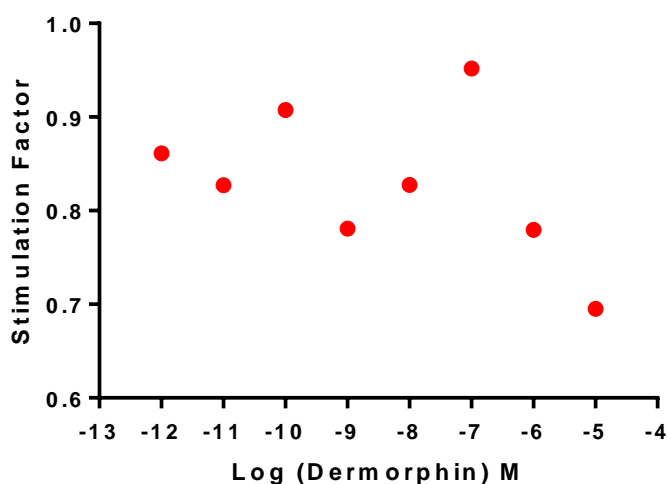


Figure 6.8: GTP γ [35 S] assays in HEK_{hMOP} cells using protocols demonstrated in previous chapters. Despite showing high expression of MOP receptor, addition of varying concentrations of Dermorphin failed to illicit a concentration dependent response.

From these initial functional studies, it can be seen that receptor expression and functional activity do not match. Further research indicated that the concentration of magnesium can play an important role in GTP γ [35 S] functional assays (Harrison and Traynor, 2003). Furthermore, previous works from other laboratories indicated that different constituents may be required for a HEK GTP γ [35 S] buffer (Brillet et al., 2003). With this in mind, HEK_{hMOP} and HEK_{hNOP} cells were incubated in four different buffers (Table 6.9). The results for HEK_{hMOP} displayed no functional activity while, in HEK_{hNOP} cell membranes, buffer 4 demonstrated a concentration response curve (Figure 6.9).

Component	Buffer		
	1	2	3
Tris-HCL	50mM	50mM	50mM
EGTA	0.2mM	0.2mM	0.2mM
NaCl	100mM	100mM	100mM
MgCl₂	1mM	5mM	10mM

	Component				
	HEPES	MgCl₂	NaCl	EDTA	DTT
Buffer 4	50mM	5mM	100mM	1mM	1mM

Table 6.10: Buffer compositions of HEK GTP γ [³⁵S] buffers. All buffers had pH 7.4 (NaOH).

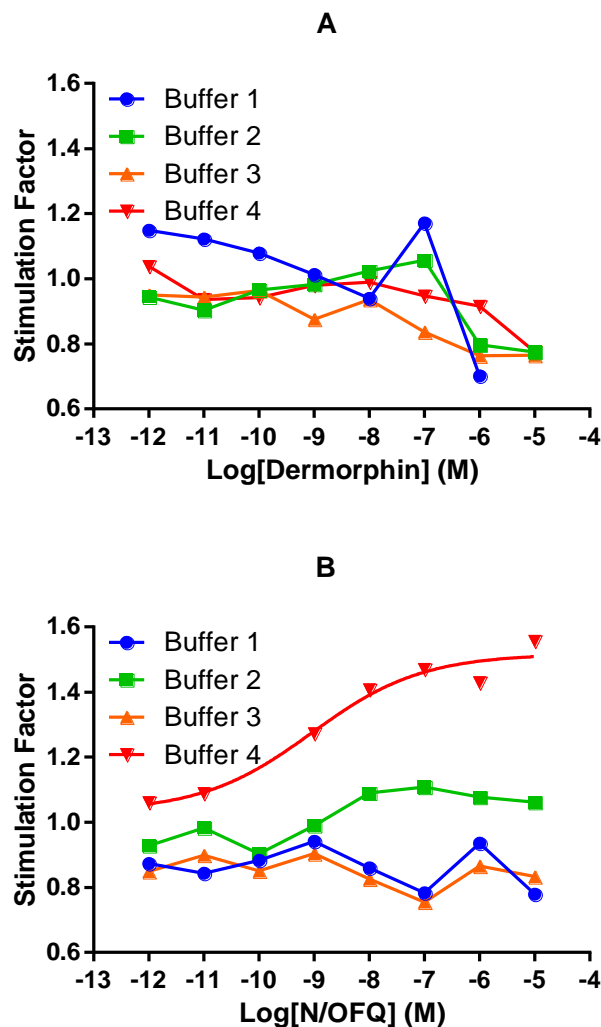


Figure 6.10: Assessment of optimal buffer conditions in HEK opioid cell lines A) Buffer validation for HEK_{hMOP} cells in a GTP γ [³⁵S] assay, using the agonist Dermorphin. B) Buffer validation for HEK_{hNOP} cells in a GTP γ [³⁵S] assay, using the agonist N/OFQ.

While HEK_{hNOP} had shown a functional response, HEK_{hMOP} failed to produce a response to Dermorphin. N/OFQ produced an E_{max} of 1.52 and a pEC_{50} of 9.04. Work by Brillet *et al* (2003), had demonstrated that 30 minutes was the optimal incubation period in HEK cells. In order to determine the ideal time period, both buffer 1 and buffer 4 were used in a time course assay. HEK_{hMOP} cells were incubated for 15, 30, 45 or 60 minutes, using a range of concentrations of Dermorphin (Figure 6.11). From these results it can be seen that using buffer 4 for a time period of 30 minutes produced a concentration response curve with an E_{max} value of 1.56 and a pEC_{50} value of 7.21. Buffer 4 is used in all HEK GTP γ [³⁵S] assays.

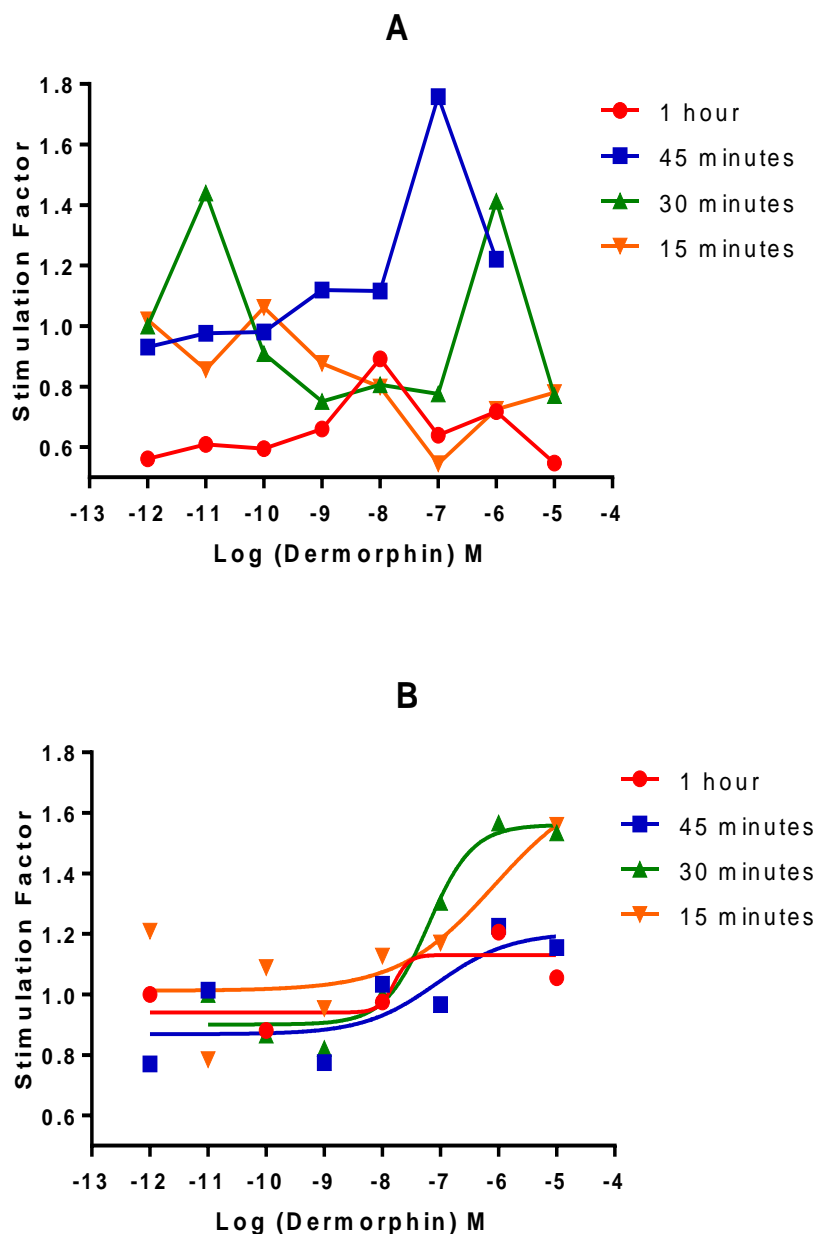


Figure 6.11: Assessment of the optimal GTP γ [35 S] incubation period. A) GTP γ [35 S] time course using buffer 1 in HEK_{hMOP} cells, using Dermorphin. B) GTP γ [35 S] time course using buffer 4 in HEK_{hMOP} cells, using Dermorphin.

Following validation of buffer type and the correct incubation period, assessment of GDP concentration was determined. GDP levels can affect both stimulation factor and pEC₅₀ values (Harrison and Traynor, 2003, Strange, 2010). In this assay a range of concentrations of GDP (10nM-10mM) were incubated with ~150pM GTP γ [35 S] and either 1 μ M Dermorphin for HEK_{hMOP} or 1 μ M N/OFQ for HEK_{hNOP}. In HEK_{hMOP} cell

membranes, a concentration of $3\mu\text{M}$ GDP was required to show the greatest difference in counts bound between basal levels and $1\mu\text{M}$ Dermorphin (Figure 6.12). In HEK_{hNOP} cell membranes, $33\mu\text{M}$ GDP produced the greatest difference between N/OFQ stimulated and basal counts (Figure 6.13). These concentrations will be used for all $\text{GTP}\gamma[^{35}\text{S}]$ functional assays in HEK_{hMOP} or HEK_{hNOP} cell lines.

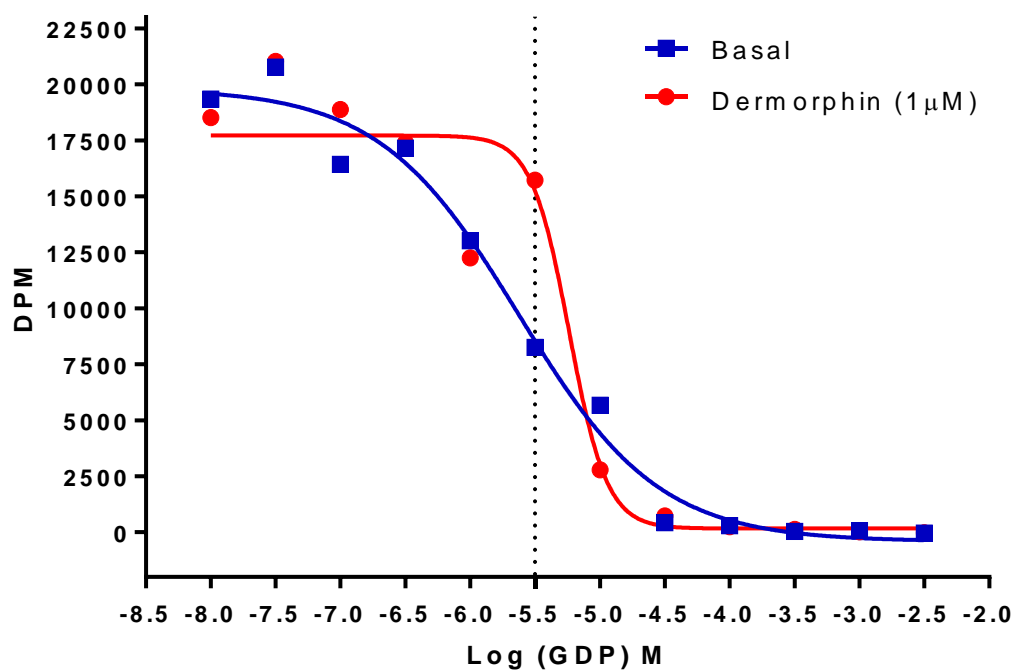


Figure 6.12: Representative curve of the determination of optimal GDP concentration in HEK_{hMOP} cell membranes. The dotted line indicates the concentration at which basal levels are most divergent from values obtained in the presence of $1\mu\text{M}$ Dermorphin. Above is a representative curve from three independent experiments.

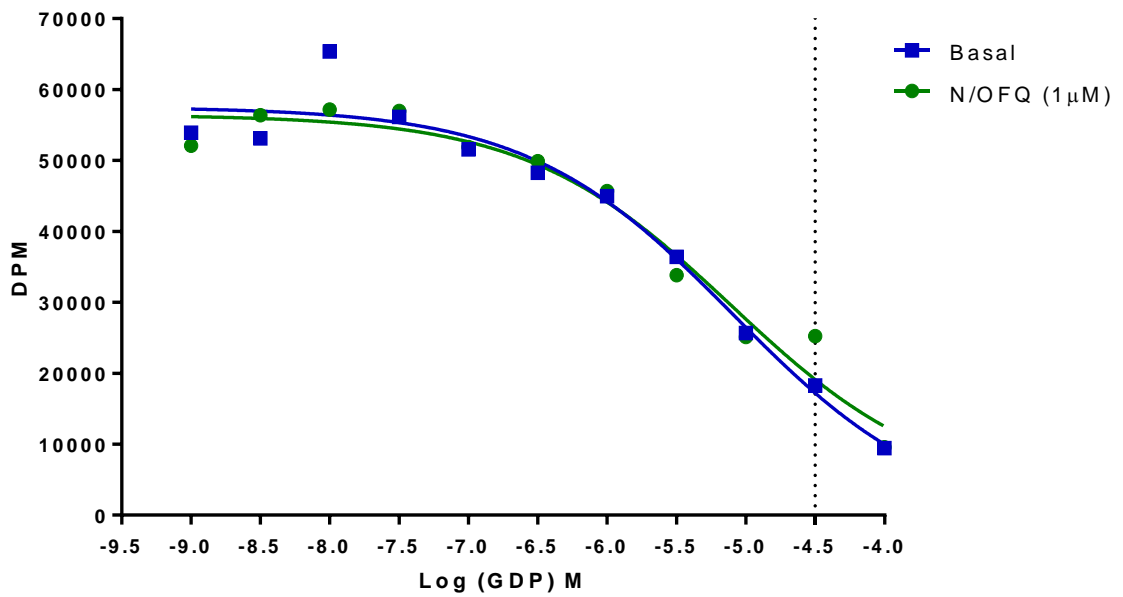


Figure 6.13: Representative curve of the determination of optimal GDP concentration in HEK_{hNOP} cell membranes. The dotted line indicates the concentration at which basal levels are most divergent from values obtained in the presence of 1 μM N/OFQ. Above is a representative curve from three independent experiments.

In order to assess whether both GDP concentrations and buffer 4, for a 30 minute incubation period, provided consistent and repeatable GTPγ[³⁵S] functional response curves, the experiment was repeated five times in the presence of 3 μM GDP for HEK_{hMOP} and 33 μM GDP for HEK_{hNOP} (Figure 6.14). The results demonstrated that in HEK_{hMOP} cell membranes, Dermorphin produced an E_{max} of 1.43 (±0.03) and pEC₅₀ of 8.13 (±0.06). In HEK_{hNOP} membranes, N/OFQ produced an E_{max} of 1.47 (±0.04) and pEC₅₀ 8.69 (±0.13).

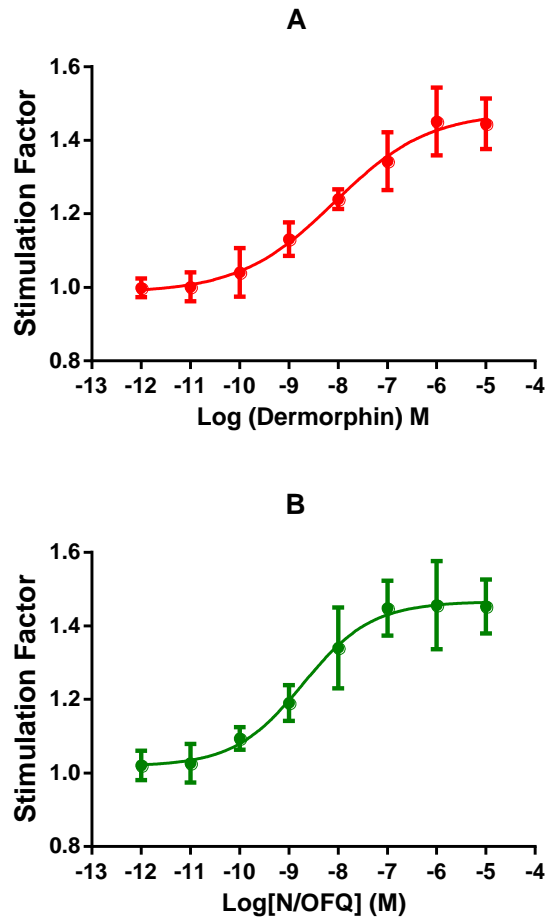


Figure 6.14: Ligand stimulated GTPγ[³⁵S] binding. A) Dermorphin stimulated GTPγ[³⁵S] binding is shown in HEK_{hMOP} cell membranes. B) N/OFQ stimulated GTPγ[³⁵S] binding is shown in HEK_{hNOP} cell membranes. Data are mean (±SEM) for five experiments.

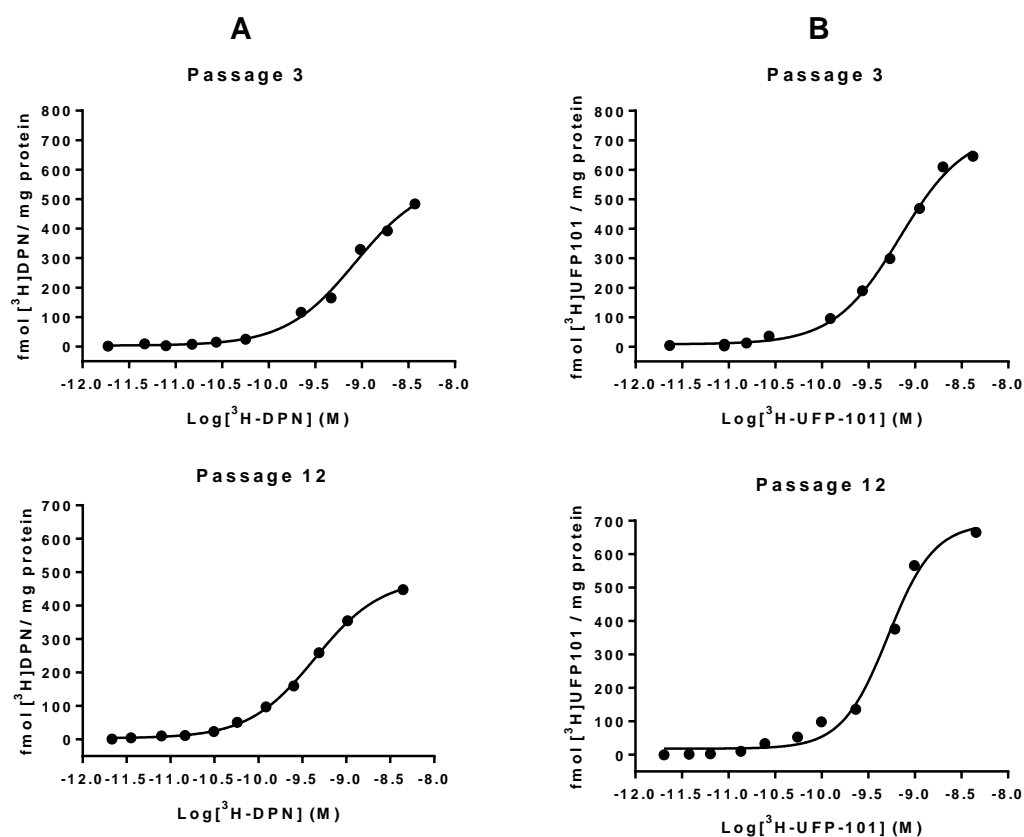
6.5.4 Development and selection of an appropriate monoclonal HEK_{hMOP/NOP} co-expression system

Following successful identification of stable HEK_{hMOP} and HEK_{hNOP} monoclonal cell lines, HEK_{hMOP} #1 was transfected with the hNOP plasmid, and the selection process was carried out as for HEK_{hNOP} monoclonal cells. From this process, 7 monoclonal cell lines were identified, however 2 died before RT-qPCR screening was completed. The remaining cell lines ΔC_t values for hMOP and hNOP were determined (Table 6.11). All 5 remaining cell lines displayed ΔC_t values for hMOP and hNOP, however only HEK_{hMOP/NOP} #1 was tested in saturation binding assays. The remaining clones all grew at ultra-slow rates, whereas HEK_{hMOP/NOP} #1 grew at a similar rate to that of HEK_{hMOP} #1 and HEK_{hNOP} #8.

Clone	GAPDH C _t	MOP C _t	Δ C _t Mean	GAPDH C _t	NOP C _t	Δ C _t Mean
HEK_{hMOP/NOP} #1	19.34	23.74	4.4	19.31	18.27	-1.04
HEK_{hMOP/NOP} #2	24.27	26.71	2.44	25.05	21.98	-3.07
HEK_{hMOP/NOP} #3	26.44	28.77	2.33	26.88	23.83	-3.05
HEK_{hMOP/NOP} #5	27.61	30.09	2.48	28.06	34.95	6.9
HEK_{hMOP/NOP} #7	20.42	22.87	2.47	20.31	19.19	-1.12

Table 6.11: C_t values for HEK_{hMOP/NOP}. Clone #1, shaded in grey, showed low Δ C_t values and were screened using radioligand saturation binding. Samples were screened from single cell RNA extractions.

In saturation binding assays, HEK_{hMOP/NOP} #1 was tested at passage 3 and 12, using [³H]-DPN at MOP and [³H]UFP-101 for NOP (Figure 6.15). At passage 3, the B_{max} for MOP was 502.8, and had a pK_d of 8.98 for [³H]-DPN. At passage 12, the B_{max} was 481, while the pK_d was 9.36. In saturation studies using [³H]UFP-101, the B_{max} for NOP was 807.7, while the pK_d was 9.07, at passage 3. At passage 12, the B_{max} was 787.7 and the pK_d was 9.29.



	Passage 3		Passage 12	
	pK_d	B_{max}	pK_d	B_{max}
$[^3H]$ -DPN	$8.98_{(\pm 0.12)}$	$502.8(\pm 56.57)$	$9.36_{(\pm 0.02)}$	$481_{(\pm 16.32)}$
$[^3H]$ UFP-101	$9.07_{(\pm 0.07)}$	$807.7(\pm 59.44)$	$9.29_{(\pm 0.05)}$	$787.6_{(\pm 35.48)}$

Figure 6.15: Determination of the presence of MOP and NOP receptors in HEK_{hMOP/NOP} #1. A) Representative saturation binding graphs depicting receptor expression in HEK_{hMOP/NOP} #1 clones over a window of 9 passages. B) Representative saturation binding curves depicting receptor expression in HEK_{hMOP/NOP} #1 clones over a window of 9 passages.

6.5.5 Determination of HEK_{hMOP/hNOP} functional ability-GTP γ [³⁵S]

In order to determine the optimal conditions for GTP γ [³⁵S] assays using HEK_{hMOP/NOP} #1 membranes, GDP concentration curves were undertaken (Figure 6.16). Concentrations of 1 μ M Dermorphin and 1 μ M N/OFQ were used for reference. In these assays, both Dermorphin and N/OFQ stimulation was greatest in the presence of 33 μ M GDP.

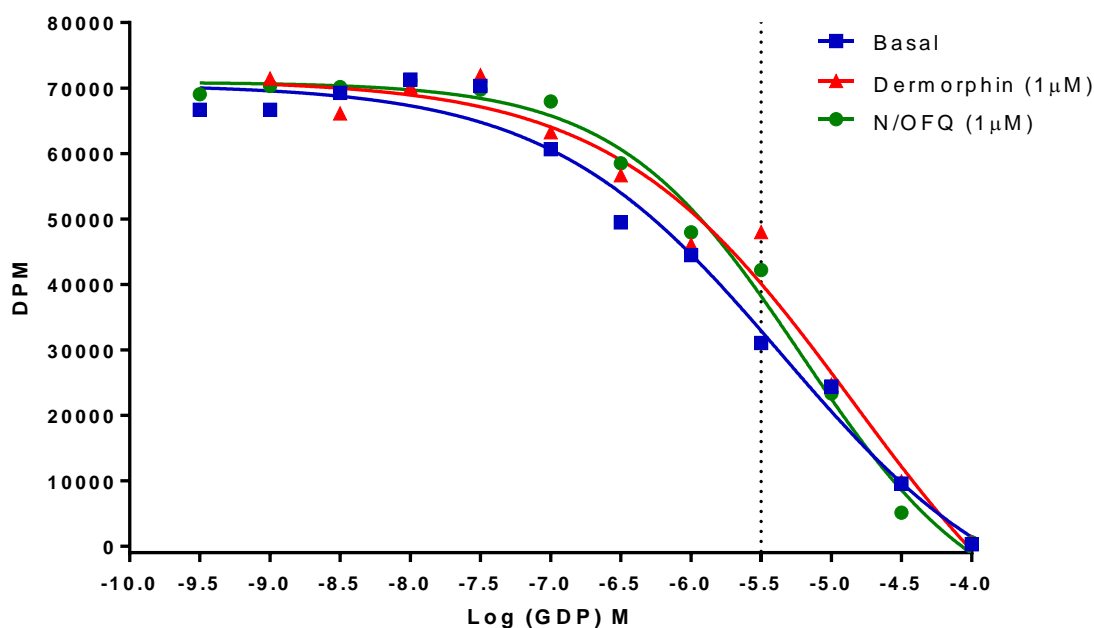


Figure 6.16: Determination of GDP concentration in HEK_{hMOP/NOP} cell membranes. The dotted line indicates the concentration at which basal levels are most divergent from values obtained in the presence of 1 μM Dermorphin or 1 μM N/OFQ. Above is a representative curve from three independent experiments.

Following identification of the correct GDP concentrations, GTPγ[³⁵S] assays were undertaken to determine the presence of functional MOP and NOP receptors in HEK_{hMOP/NOP} cell membranes (Figure 6.17). From these experiments it was determined that Dermorphin and N/OFQ displayed similar E_{max} values of 1.31 (± 0.04) and 1.25 (± 0.05), respectively (Student's t-test). Dermorphin produced a pEC_{50} value of 7.60 (± 0.05), while N/OFQ produced a significantly higher pEC_{50} of 9.27 (± 0.02) ($p < 0.0001$, Student's t-test).

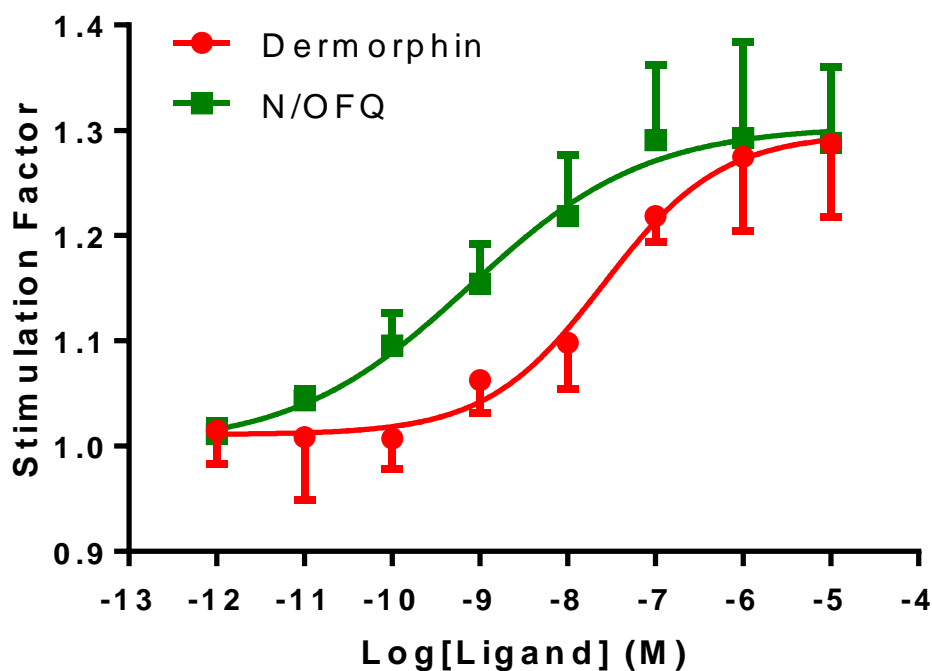


Figure 6.17: Ligand stimulated $GTP\gamma[^{35}S]$ binding of Dermorphin and N/OFQ is shown in $HEK_{hMOP/NOP}$ cell membranes. Data are mean (\pm SEM) of five experiments.

6.6 Discussion

Over two rounds of transfection and antibiotic selection produced 42 $CHO_{hMOP/NOP}$ monoclonal cell lines. All surviving cell lines were screened using RT-qPCR, as the amount of RNA transcribed correlates with the amount of protein translated. This, however, is not an absolute indicator of receptor expression, but does allow for a fast screening method to select the best clones for further analysis. It is interesting to note, that while all of the selected clones indicated high levels of transcribed hMOP and hNOP, saturation studies showed a disparity between receptor expression or only expression of one receptor (Figure 6.2, Figure 6.3 and Figure 6.4). Initially, $CHO_{hMOP/NOP}$ #28 was chosen for further study, due to the similar ΔCt values of MOP (1.46) and NOP (1.86). These values were matched in saturation binding assays, with $CHO_{hMOP/NOP}$ #28 displaying B_{max} values of 432 for MOP and 487 for NOP. However, after several passages, while MOP receptor expression remained constant, negligible NOP receptor expression was shown. This indicated NOP was not stably expressed

(Figure 6.2). Further CHO_{hMOP/NOP} clones were all tested for MOP and NOP expression, however all demonstrated a loss of expression of MOP or NOP (Figure 6.3 and Figure 6.4). This indicated that the CHO cell may be a poor host for co-expression studies involving MOP and NOP.

HEK cells have been previously shown to be capable of producing MOP and NOP double expression systems (Pan et al., 2002, Wang et al., 2005). Previous work in this laboratory had involved the use of CHO cells expressing single recombinant opioid receptors. Therefore, attempting to develop a HEK_{hMOP/NOP} co-expression system required the development of HEK_{hMOP} and HEK_{hNOP} cell lines. Plasmids for hMOP, containing antibiotic resistance for geneticin, and hNOP, containing antibiotic resistance to hygromycin B, were obtained for transfection into HEK cells. Following transfection and selection, via demonstration of antibiotic resistance (Figure 6.5, Table 6.3 and Table 6.4), HEK cells were measured for levels of RNA expression of the receptor of interest. Combined with cell growth rates, HEK_{hMOP} #1 (ΔC_t : -0.62) was chosen for further screening in saturation assays. Using [³H]-DPN, this cell line showed stable, high expression of MOP (B_{max} : 1542, pK_d : 9.23) and has been used in all work since. Of the HEK_{hNOP} monoclonal cell lines created, saturation assays using [³H]UFP-101 demonstrated that HEK_{hNOP} #8 (ΔC_t : -1.16; B_{max} : 743; pK_d : 9.01) displayed stable expression over several passages using RT-qPCR and saturation binding assays ([³H]UFP-101). HEK_{hNOP} #8 has been used in all work since.

Since HEK cells have not been previously used for GTP γ [³⁵S] functional assays, optimisation of the protocols was undertaken. Using current protocols, optimised for CHO cells, failed to illicit a concentration dependent response to Dermorphin in HEK_{hMOP} #1 cell membranes (Figure 6.8). The lack of response is contradictory to the levels of receptor expression shown in the HEK_{hMOP} #1 cell lines. This indicated that previous protocols would need to be adapted for HEK_{hOPIOID} GTP γ [³⁵S] assays. Initially a number of buffers were trialled, with increasing concentrations of magnesium. Magnesium has been shown to have an effect on the binding of GTP γ S to the G α subunit (Harrison and Traynor, 2003). Furthermore, work by Brillet *et al* (2003), indicated that different buffers may be required (Massotte et al., 2002, Brillet et al., 2003). All of the buffers failed to demonstrate any change in functional response to Dermorphin at HEK_{hMOP} (Figure 6.10). However, the addition of a range of

concentrations of N/OFQ did produce a concentration response curve when using buffer 4 (Figure 6.10). Further work involved characterising the time period needed to illicit a response in HEK cells. Again, work by Brillet *et al* (2003), indicated that a shortened time period of 30 minutes was required for GTP γ [³⁵S] assays in HEK cells. With this in mind, 4 time points were chosen to assess functional activity at HEK_{hMOP}, using buffer 1 and buffer 4. A range of concentrations of Dermorphin were used for 1 hour, 45 minutes, 30 minutes and 15 minutes. Of the time points studied, the 30 minute period in buffer 4 produced a concentration response curve with pEC₅₀ of 8.13 and E_{max} of 1.56.

To ensure that all aspects of the GTP γ [³⁵S] assay in HEK cells were optimal, GDP response curves were undertaken at HEK_{hMOP} and HEK_{hNOP}. From these curves it was demonstrated that the optimal concentration of GDP in HEK_{hMOP} cells was 3 μ M, unlike 33 μ M concentrations used in CHO_{hMOP} cells. Furthermore, HEK_{hNOP} cells required 33 μ M GDP, unlike 100 μ M required for CHO_{hNOP}. The experiment was repeated again to confirm the buffer, incubation period and GDP concentrations were correct (Figure 6.14). From the resulting curves, Dermorphin demonstrated an E_{max} of 1.43 and pEC₅₀ of 8.13 in HEK_{hMOP} cell membranes. In HEK_{hNOP} cell membranes, N/OFQ produced an E_{max} of 1.47 and a pEC₅₀ value of 8.69. The pEC₅₀ values obtained for Dermorphin or N/OFQ in experiments for HEK_{hMOP} or HEK_{hNOP} were not significantly different from those obtained in CHO_{hMOP} or CHO_{hNOP} cell membranes (Table 6.12).

	Potency (pEC ₅₀)			
	CHO _{hMOP}	HEK _{hMOP}	CHO _{hNOP}	HEK _{hNOP}
Dermorphin	7.83(\pm 0.14)	8.13(\pm 0.06)	/	/
N/OFQ	/	/	8.82 (\pm 0.08)	8.69 (\pm 0.13)

Table 6.12: Comparison between the potency (pEC₅₀) of Dermorphin and N/OFQ in CHO and HEK cell lines expressing MOP or NOP. Data are the mean (\pm SEM) for between five and eight experiments.

Following successful identification of HEK_{hMOP} and HEK_{hNOP} cell lines, HEK_{hMOP} #1 was transfected with the hNOP plasmid. HEK_{hMOP} #1 was chosen due to its high receptor expression and cell growth. Following selection pressure, 5 monoclonal HEK_{hMOP/NOP} monoclonal cell lines were tested using RT-qPCR for the presence of

MOP and NOP RNA. Due to growth performance, HEK_{hMOP/NOP} #1 (ΔC_t MOP: 4.4; NOP: -1.04) was tested for MOP and NOP receptor expression in saturation binding assays. In experiments using [³H]-DPN (for MOP), HEK_{hMOP/NOP} #1 demonstrated a B_{max} of 492. In experiments using [³H]UFP-101 (for NOP), HEK_{hMOP/NOP} #1 demonstrated a B_{max} of 750 (Figure 6.7). Moreover, this expression was shown to be stable, as the B_{max} values for MOP and NOP were tested over 9 passages.

GDP concentration response curves were undertaken in HEK_{hMOP/NOP} using Dermorphin and N/OFQ. Both Dermorphin and N/OFQ produced their greatest increase over basal activity in the presence of 33 μ M GDP. In a concentration response curve, using buffer 4 in a 30 minute incubation period, Dermorphin produced an E_{max} of 1.31 and a pEC_{50} value of 7.60. N/OFQ produced an E_{max} of 1.25 and a pEC_{50} value of 9.27. The pEC_{50} value for Dermorphin was significantly lower than that shown in HEK_{hMOP} cells. This result is expected, as previous studies in MOP/NOP co-expression systems have demonstrated a loss of potency for known MOP agonists (Wang et al., 2005).

The results from this chapter demonstrate the development of a MOP/NOP co-expression system in HEK cells. This monoclonal cell line will be used to study MOP/NOP bivalent pharmacophores identified in previous chapters. The cell line will allow for the identification of potential changes to binding affinity of these novel compounds, as well as changes to their signalling properties when compared to a single receptor expression system.

Chapter 7 **Study of Receptor Interactions in a Dual Expression System**

7.1 Introduction

A number of studies have demonstrated the ability of MOP and NOP to form heterodimers (Pan et al., 2002, Evans et al., 2010). These studies have used either human MOP/rat NOP receptor systems in CHO cells (Pan et al., 2002) or rat MOP/rat NOP co-expression systems (Wang et al., 2005) in HEK cells to determine the effects on binding or downstream signalling (cAMP or ERK1/2 phosphorylation). As far as we are aware, the cell line developed in Chapter 6 is the first human MOP and human NOP receptor system developed. This system will allow us to monitor for any changes in signalling brought about by the presence of both receptors in the same cell line.

7.2 Hypothesis

The interactions between MOP and NOP will lead to changes in affinity and functional activity of the full agonists Dermorphin and N/OFQ in the co-expression system. Furthermore, the bivalent peptides will demonstrate altered signalling due to engaging both receptors.

7.3 Aims

In this chapter, a detailed analysis of the signalling properties of DeNO and DeUFP will be provided in a dual MOP/NOP expression system. HEK cells expressing recombinant opioid receptors (HEK_{hMOP}, HEK_{hNOP} and HEK_{hMOP/NOP}) will be used to define the pharmacological properties (binding affinity and functional activity) of DeNO and DeUFP. pK_i values for DeNO and DeUFP will be determined using [³H]-DPN and [³H]UFP-101. Functional activity will be measured by determining both DeNO and DeUFP's ability to stimulate binding of GTPγ[³⁵S]. Furthermore, the ability of DeNO and DeUFP to activate the MAPK pathway will be investigated using standard western blotting techniques in the single expression and co-expression systems (Figure 7.1).

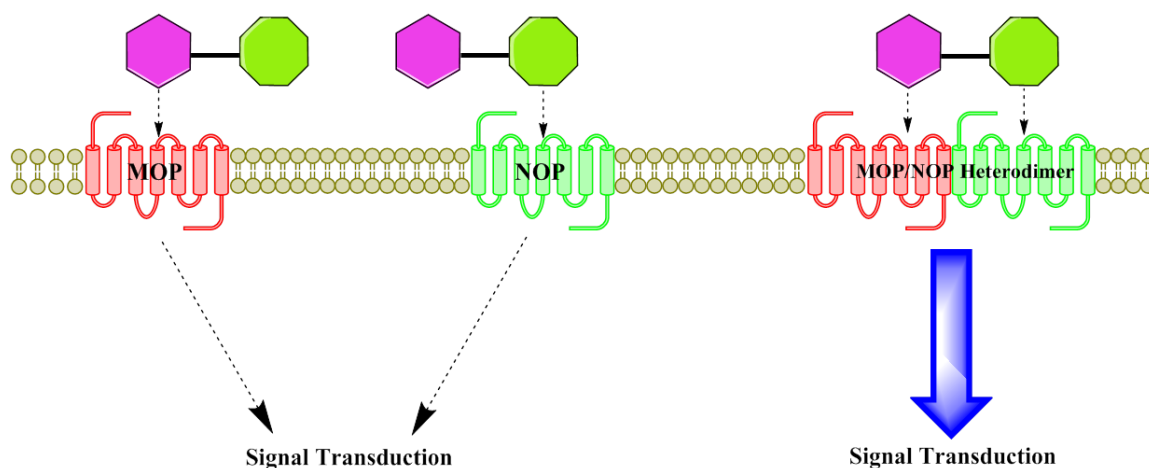


Figure 7.1: The interactions of our bivalent peptides will be assessed to determine whether activity in a dual expression system is altered. If MOP and NOP do not form a dimer, signalling pathways should act in a similar manner to the single expression systems (as shown by the left hand side of the figure). However, based on evidence of alterations in heterodimer signalling, if MOP and NOP were to form a single structural unit, the interaction of Dermorphin or N/OFQ with this heterodimer would lead to visible changes in the signalling pathway.

7.4 Results

7.4.1 *Displacement Binding studies of the Dermorphin derivatives*

In displacement binding studies at HEK_{hMOP}, Dermorphin, DeNO and DeUFP displaced the binding of [³H]-DPN in a concentration dependent and saturable manner (Figure 7.2, Table 7.1). Dermorphin produced a pK_i value of 8.32, while DeNO (9.00) and DeUFP (9.28) displayed a significant increase in affinity, when compared to Dermorphin. In HEK_{hNOP} cell membranes, N/OFQ, DeNO, DeUFP and UFP-101 displaced [³H]UFP-101 in a concentration dependent and saturable manner (Figure 7.2, Table 7.1). DeNO (pK_i: 9.69) and DeUFP (8.68) displayed similar binding affinity to that of their parent compounds, N/OFQ (9.39) and UFP-101 (8.61), respectively.

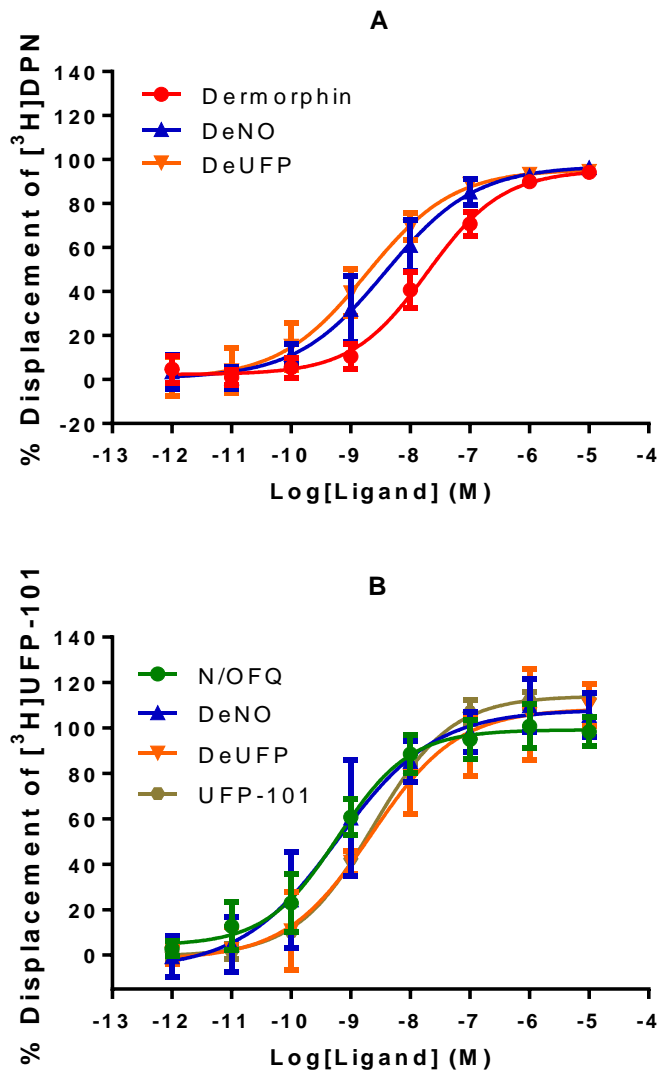


Figure 7.2: Displacement of [³H]-DPN by Dermorphin, DeNO, DeUFP and reference ligands at (A) HEK_{hMOP} and the displacement of [³H]UFP-101 by DeNO, DeUFP, N/OFQ and UFP-101 at (B) HEK_{hNOP} cell membranes. Data are means (SEM) of between five and eight experiments for all cell lines.

In HEK_{hMOP/NOP} cell membranes, Dermorphin, DeNO and DeUFP produced a concentration dependent and saturable displacement of [³H]-DPN (Figure 7.3, Table 7.1). Dermorphin and DeNO produced binding affinities of 7.86 and 7.94, respectively, which were not significantly different from each other. DeUFP (8.63) demonstrated a higher affinity for the MOP receptor in this cell line, when compared to Dermorphin and DeNO. Conversely, the pK_i values for Dermorphin and DeNO were significantly different from their binding affinities in HEK_{hMOP} cell membranes. DeUFP showed a

statistically significant decrease in binding at MOP, while conversely demonstrated an increase in affinity for the NOP receptor (Table 7.1). The ability of the bivalent peptides to produce increased displacement of [³H]-DPN was also seen. DeNO (average percentage displacement using 10 μ M DeNO: 131.9 \pm 3.92 %) and DeUFP (117.3 \pm 6.12) both demonstrated a statistically significant increase in displacement, when compared to Dermorphin (93.17 \pm 4.17) (ANOVA, Bonferroni multiple corrections; p<0.05).

N/OFQ, UFP-101, DeNO and DeUFP all demonstrated a concentration dependent and saturable displacement of [³H]UFP-101 in the HEK_{hMOP/NOP} cell line (Figure 7.3). The pK_i values of N/OFQ and UFP-101 were 8.96 and 8.71 respectively. DeNO (9.58) and DeUFP (9.22) displayed an increase in affinity when compared to their parent compounds. DeNO and UFP-101 displayed similar pK_i values to those in HEK_{hNOP} cell membranes (Table 7.1). DeUFP showed an increase in affinity for the NOP receptor in HEK_{hMOP/NOP} when compared to its pK_i value in HEK_{hNOP} cell membranes. N/OFQ demonstrated a loss of affinity for the NOP receptor in HEK_{hMOP/NOP} cell membranes.

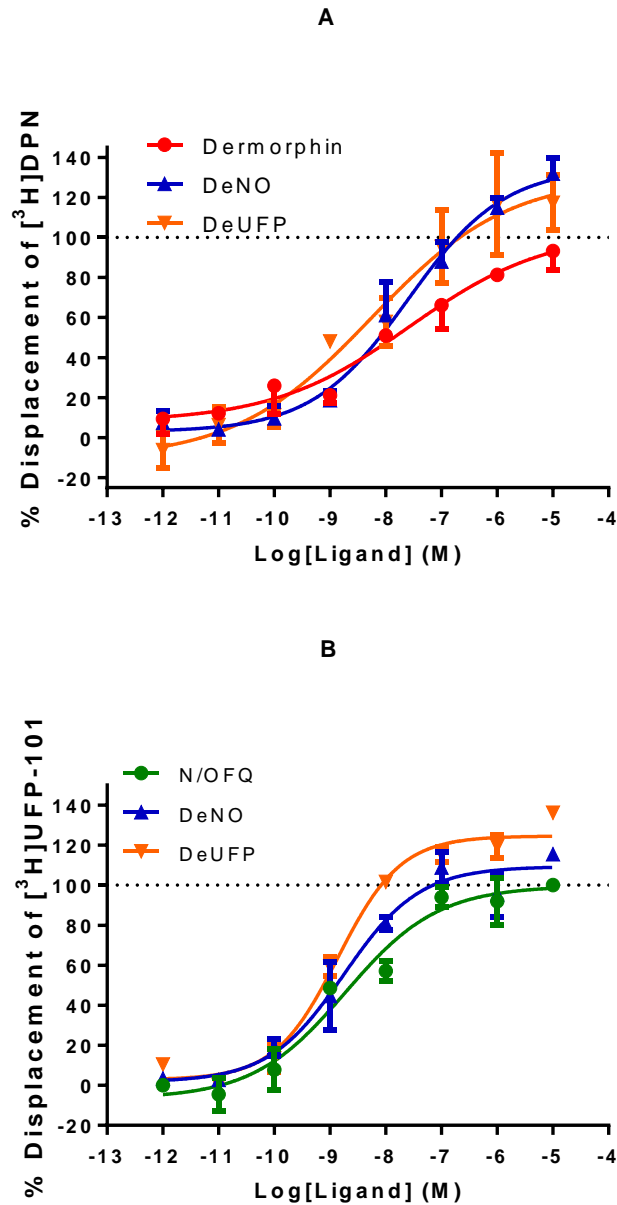


Figure 7.3: Determination of the affinity of various ligands in the HEK_{hMOP/NOP} cell line A) Displacement of [³H]-DPN in HEK_{hMOP/NOP} cell membranes by Dermorphin, DeNO and DeUFP. B) Displacement of [³H]UFP-101 in HEK_{hMOP/NOP} cell membranes by N/OFQ, UFP-101, DeNO and DeUFP. Data are the mean (\pm SEM) of between five and eight experiments.

To further investigate the interactions between MOP and NOP, Dermorphin was co-incubated with either N/OFQ or UFP-101. When Dermorphin was used as a displacer against [³H]-DPN, it produced a saturable displacement. However, when co-incubated with 1 μ M N/OFQ or 1 μ M UFP-101, Dermorphin demonstrated an ability to displace 181% or 135%, respectively, of [³H]-DPN (Figure 7.4). Moreover, in these experiments, compared to the displacement caused by Dermorphin alone at the lowest

concentration of 1 pM, when co-incubated with either N/OFQ or UFP-101, demonstrated 80% displacement of [³H]-DPN. When investigating [³H]UFP-101, N/OFQ leads to approximately 60% displacement of the radioligand, whereas the addition of 1 μM Dermorphin, or 0.1 μM naloxone, increases the ability of N/OFQ to displace [³H]UFP-101 up to 90%.

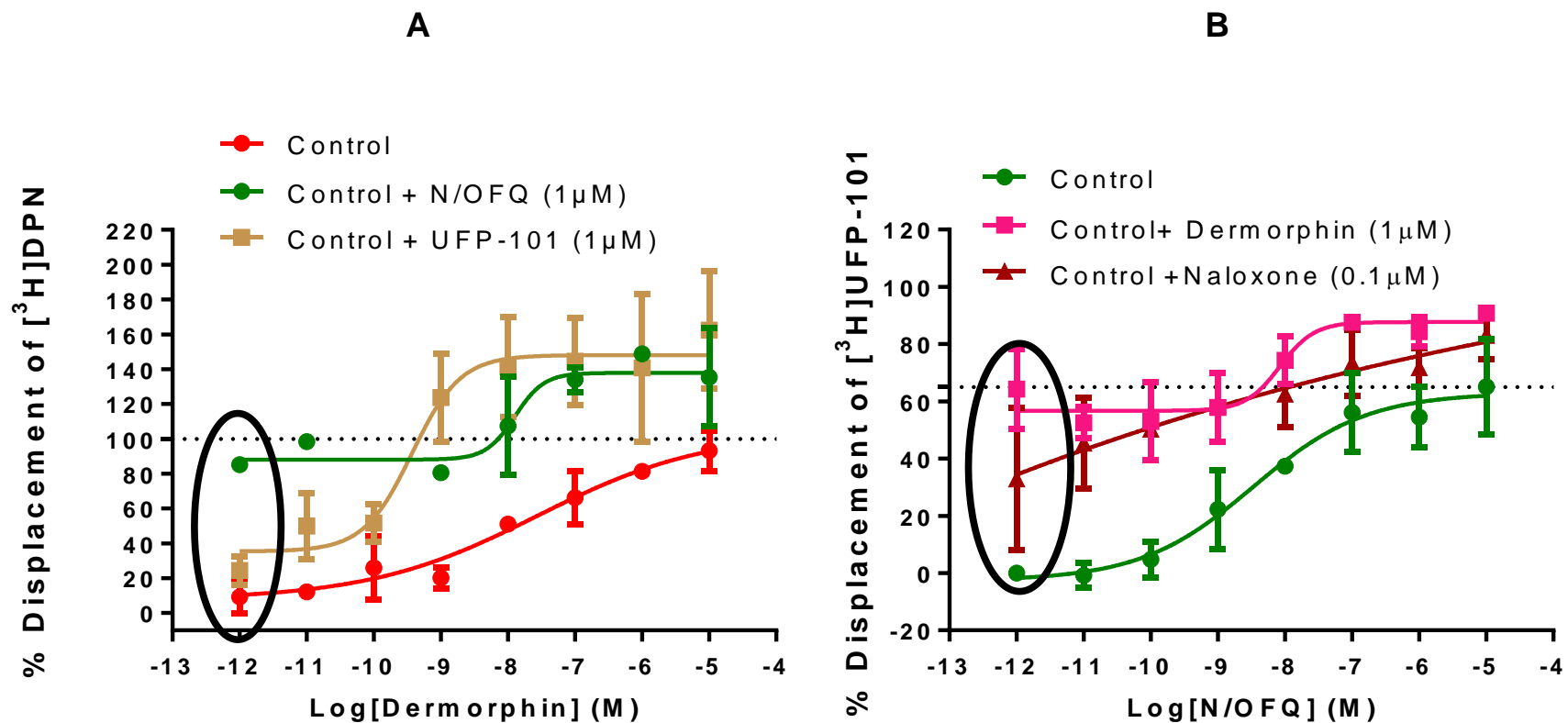


Figure 7.4: Determination of the affinity of various ligands in the HEK_{hMOP/NOP} cell line A) Displacement of [³H]-DPN in HEK_{hMOP/NOP} cell membranes by Dermorphin, in the absence, and presence, of 1 μM N/OFQ or UFP-101. B) Displacement of [³H]UFP-101 in HEK_{hMOP/NOP} cell membranes by N/OFQ, in the absence, and presence of 1 μM Dermorphin, or 0.1 μM naloxone. Circles indicate the ability of N/OFQ to displace [³H]-DPN in (A) and Naloxone and Dermorphin to displace [³H]UFP-101 in (B). Data are the mean (±SEM) for n=5 experiments.

	HEK _{hMOP}	HEK _{hNOP}	HEK _{hMOP/NOP} [³ H]-DPN	HEK _{hMOP/NOP} [³ H]UFP-101
Dermorphin	8.32 (±0.15) 4.79nM		7.86 (±0.14) 13.80nM	
N/OFQ		9.39 (±0.07) 0.41nM		8.96 (±0.13) ^B 1.09nM
UFP-101		8.61 (±0.12) 2.45nM		8.71 (±0.07) 1.95nM
DeNO	9.00 (±0.11) ^A 1nM	9.69 (±0.11) 0.20nM	7.94 (±0.16) ^C 11.48nM	9.58 (±0.17) ^A 2.63nM
DeUFP	9.28 (±0.11) ^A 0.52nM	8.68 (±0.08) 2.09nM	8.63 (±0.03) ^{A,C} 2.34nM	9.22 (±0.04) ^{A,C} 0.60nM

Table 7.1: The pK_i values for Dermorphin, N/OFQ, UFP-101, DeNO and DeUFP in HEK_{hMOP}, HEK_{hNOP} and HEK_{hMOP/NOP}. Data are displayed as mean (±SEM) of n=5 experiments. If a significant difference from the reference ligand was detected (ANOVA), post-hoc testing using Bonferroni multiple comparisons was employed; ^A = p<0.05. ^B=p<0.05 or ^C=p<0.005 if a difference was detected using two-tailed t-tests to compare the drug's binding affinities in each cell line.

7.4.2 GTPγ[³⁵S] functional studies

Dermorphin, DeNO and DeUFP stimulated the binding of GTPγ[³⁵S] in a concentration dependent and saturable manner in HEK_{hMOP} membranes (Figure 7.5). Dermorphin produced an E_{max} of 1.43 and pEC₅₀ of 8.13. DeNO (E_{max}: 1.53; pEC₅₀: 8.25) and DeUFP (1.44; 8.26) displayed similar efficacy and potency to that of Dermorphin at MOP (Table 7.2).

In HEK_{hNOP} membranes, N/OFQ and DeNO produced a concentration dependent and saturable stimulation of GTPγ[³⁵S] (Figure 7.5). N/OFQ and DeNO both produced an E_{max} of 1.47. N/OFQ produced a pEC₅₀ value of 8.69. DeNO produced a pEC₅₀ value of 9.24, which was statistically significant from that of N/OFQ (Table 7.2). DeUFP failed to produce a response in HEK_{hNOP} membranes.

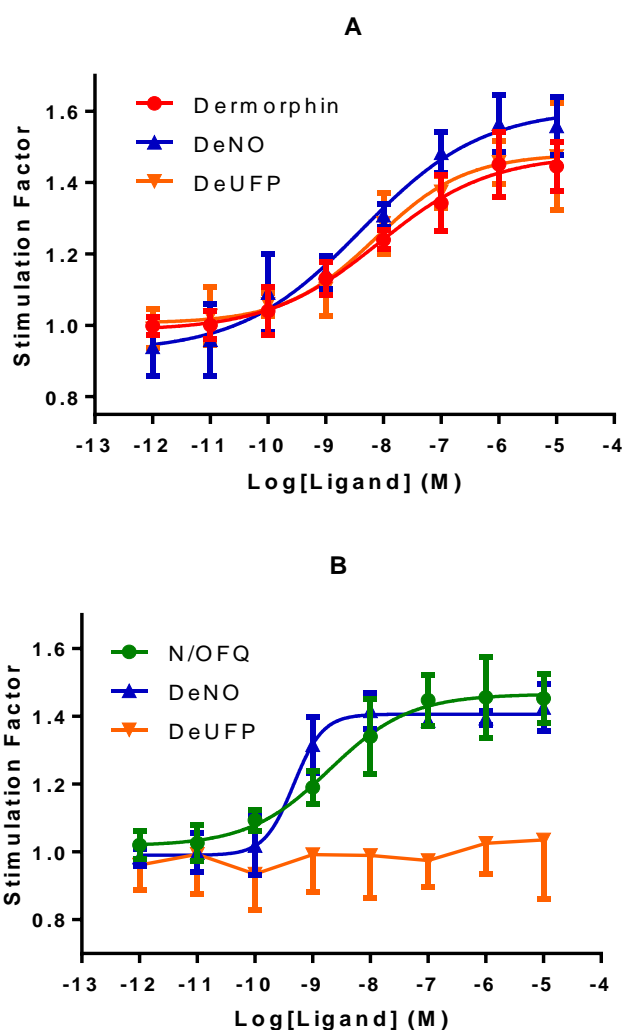


Figure 7.5: GTP γ [³⁵S] functional response assays demonstrating A) Ligand stimulated GTP γ [³⁵S] binding by Dermorphin, DeNO and DeUFP are shown in HEK_{hMOP} cell membranes. B) Ligand stimulated GTP γ [³⁵S] binding by N/OFQ, DeNO and DeUFP are shown in HEK_{hNOP} cell membranes. Data are mean (\pm SEM) for between five and eight experiments.

Dermorphin, N/OFQ, DeNO and DeUFP stimulated the binding of GTP γ [³⁵S] in a concentration dependent and saturable manner in HEK_{hMOP/NOP} membranes (Figure 7.6). Dermorphin and N/OFQ produced E_{max} values of 1.31 and 1.25, respectively. DeNO (1.25) and DeUFP (1.34) produced similar E_{max} values to that of Dermorphin and N/OFQ (Table 7.2). Dermorphin displayed a pEC_{50} value of 7.60, while N/OFQ produced a value of 9.23. DeNO produced a pEC_{50} value of 7.63, which was similar to Dermorphin, but statistically significant to that of N/OFQ. DeUFP produced a pEC_{50} value of 8.69, which was significantly higher than Dermorphin.

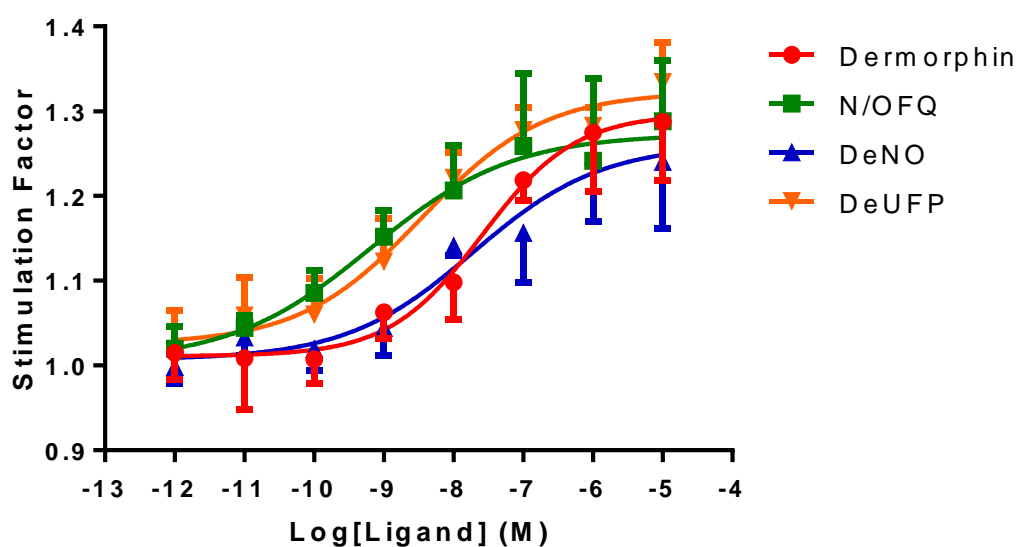


Figure 7.6: Ligand stimulated $\text{GTP}\gamma[^{35}\text{S}]$ binding by Dermorphin, N/OFQ, DeNO and DeUFP are shown in $\text{HEK}_{\text{hMOP/NOP}}$ cell membranes. Data are mean (\pm SEM) for $n=5$ experiments.

In order to ascertain whether conjugation of Dermorphin and either N/OFQ or UFP-101 had led to functional changes in the pharmacophores, unconjugated Dermorphin was co-incubated with either N/OFQ or UFP-101. When a range of concentrations of Dermorphin and N/OFQ ($10\mu\text{M}$ - 1pM) were co-incubated in $\text{HEK}_{\text{hMOP/NOP}}$ cell membranes, they stimulated $\text{GTP}\gamma[^{35}\text{S}]$ binding in a concentration dependent and saturable manner (Figure 7.7). The concentration response curve for these experiments was not significantly different from either Dermorphin or N/OFQ alone, producing an E_{max} of 1.31 (Table 7.2). The resulting curve produced a pEC_{50} value of 7.74. This was not significantly different from the pEC_{50} of Dermorphin (7.60) alone, but did show statistical significance when compared to pEC_{50} value of N/OFQ (9.28) (ANOVA, Bonferroni's multiple corrections, $p<0.0005$). When Dermorphin was co-incubated with $1\mu\text{M}$ of UFP-101, its E_{max} (1.33) remained unchanged, but its pEC_{50} value increased to 8.49, showing a statistical significant increase in potency (ANOVA, Bonferroni's multiple corrections, $p<0.005$).

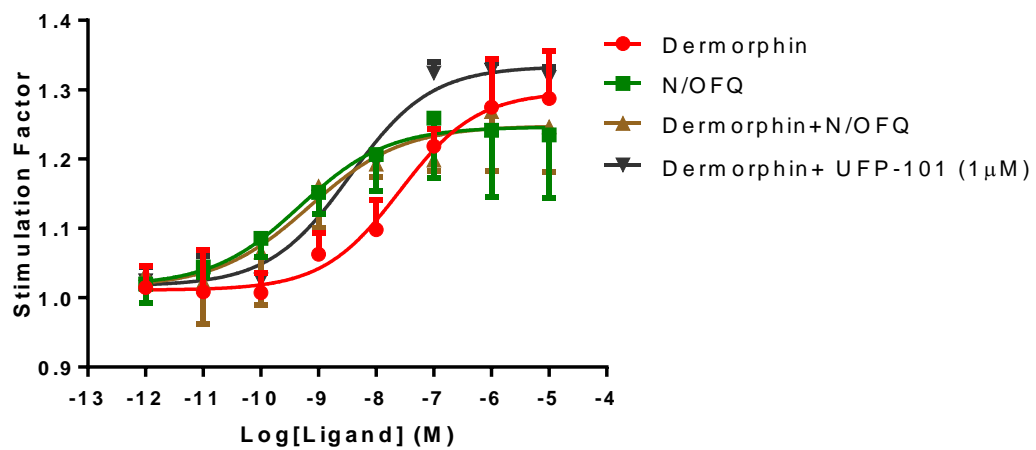


Figure 7.8: Ligand stimulated GTP γ [³⁵S] binding by Dermorphin, N/OFQ, Dermorphin and N/OFQ, and Dermorphin and 1 μ M UFP-101 are shown in HEK_{hMOP/NOP} cell membranes. Data are mean (\pm SEM) for n=5 experiments.

	HEK _{hMOP}			HEK _{hNOP}			HEK _{hMOP/NOP}		
	pEC ₅₀	E _{max}	Relative intrinsic activity	pEC ₅₀	E _{max}	Relative intrinsic activity	pEC ₅₀	E _{max}	Relative intrinsic activity
Dermorphin	8.13 _(±0.06) <i>7.40nM</i>	1.43 _(±0.03)	1				7.60 _(±0.07) ^{**} <i>25.12nM</i>	1.31 _(±0.04)	1
N/OFQ				8.69 _(±0.13) <i>2.04nM</i>	1.47 _(±0.04)	1	9.23 _(±0.16) [*] <i>0.59nM</i>	1.25 _(±0.05)	1
DeNO	8.25 _(±0.11) <i>5.62nM</i>	1.53 _(±0.03)	1	9.24 _(±0.19) <i>0.58nM</i>	1.47 _(±0.05)	1	7.63 _(±0.22) ^{a,b} <i>23.44nM</i>	1.26 _(±0.04)	1
DeUFP	8.26 _(±0.11) <i>5.50nM</i>	1.44 _(±0.03)	1				8.67 _(±0.15) <i>2.14nM</i>	1.34 _(±0.05)	1
Dermorphin + N/OFQ							7.74 _(±0.07) <i>18.20nM</i>	1.31 _(±0.04)	1
Dermorphin + 1uM UFP-101							8.49 _(±0.03) <i>3.24nM</i>	1.33 _(±0.01)	1

Table 7.2: Agonist activity of DeNO and DeUFP at HEK_{hMOP}, HEK_{hNOP} and HEK_{hMOP/NOP}. Relative intrinsic activity was determined by removal of basal activity and as a ratio of the reference ligand (MOP: Dermorphin; NOP: N/OFQ; MOP/NOP: Dermorphin) E_{max}. Data are the mean (±SEM) for between five and eight experiments. Where functional responses were measured in two cells lines only, a two-tailed t-test was used for statistical analysis. For functional responses in all three cell lines, ANOVA with post hoc Bonferroni multiple comparisons was utilised; *=p<0.05, **=p<0.0005, ^a=p<0.005 compared to MOP, ^b=p<0.0005 compared to NOP.

7.4.3 Determination of MAPK activity

Activation of p38 and ERK1/2 by the parent compounds Dermorphin and N/OFQ, as well as the bivalent peptides DeNO and DeUFP, was measured in the HEK cells expressing MOP, NOP and MOP/NOP. All compounds failed to stimulate p38 activity in HEK_{hMOP}, HEK_{hNOP} or HEK_{hMOP/NOP}. In HEK_{hMOP} cells, the addition of 10 μ M Dermorphin produced a 6.00 \pm 0.63 fold increase in phosphorylation of ERK1/2 when compared to basal activity (Figure 7.9). DeNO (10 μ M) produced a 7.33 \pm 0.27 fold increase over basal activity, while a 10 μ M concentration of DeUFP produced a 9.12 \pm 0.20 fold increase.

In HEK_{hNOP} cells, a 10 μ M concentration of N/OFQ produced a 38.57 \pm 3.04 fold increase phosphorylation of ERK1/2 over basal activity (Figure 7.9). DeNO (10 μ M) produced a 37.61 \pm 5.05 fold increase over basal activity, while DeUFP (10 μ M) produced a 1.62 \pm 0.35 fold increase.

In HEK_{hMOP/NOP} cells, 10 μ M concentrations of Dermorphin and N/OFQ produced 12.78 (\pm 0.47) and 8.86 (\pm 0.40) fold increases in ERK1/2 phosphorylation over basal activity, respectively (Figure 7.9). DeNO (10 μ M) produced a 22.56 (\pm 0.91) fold increase over basal activity, while DeUFP (10 μ M) produced an 8.98 (\pm 0.49) fold increase in phosphorylation.

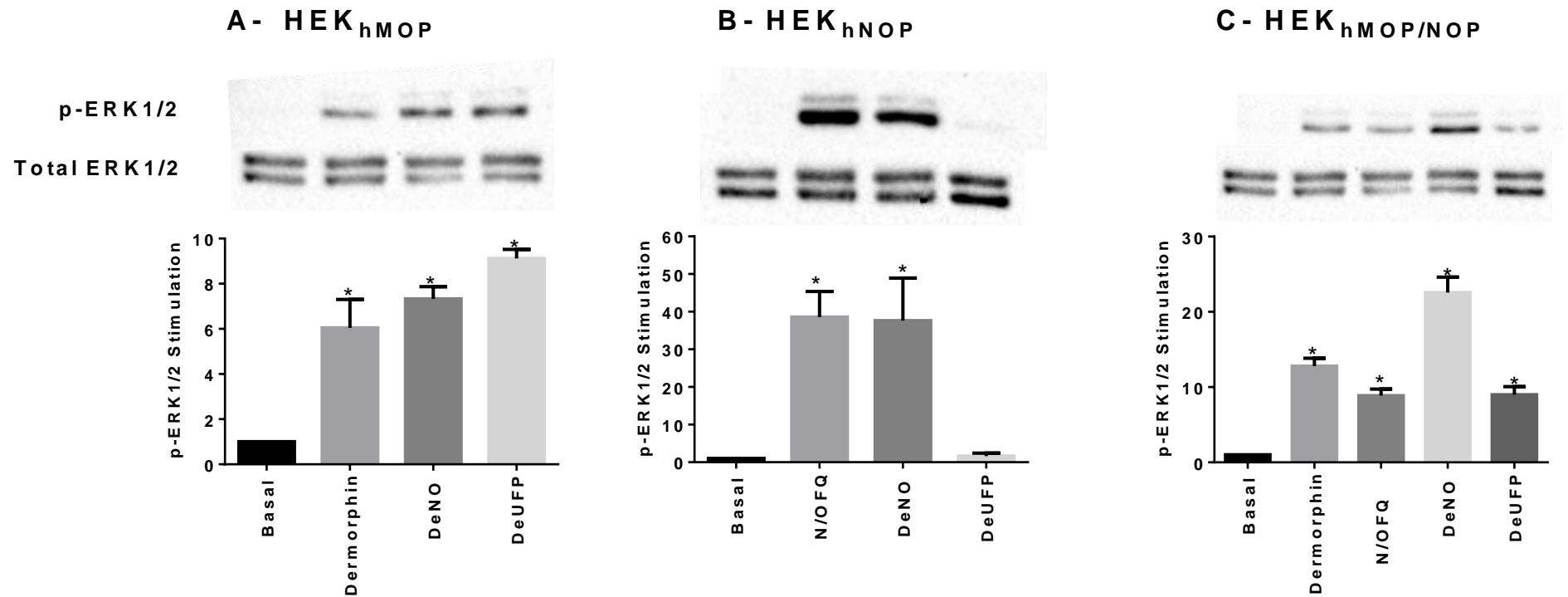


Figure 7.9: Western blot analysis demonstrating A) Representative blot of ERK1/2 phosphorylation (p-ERK1/2) and the fold increase in phosphorylation, compared to basal activity, caused by Dermorphin (10 μ M), DeNO (10 μ M) and DeUFP (10 μ M) in HEK_{hMOP} cells. B) Representative blot of ERK1/2 phosphorylation (p-ERK1/2) and the fold increase in phosphorylation, compared to basal activity, caused by N/OFQ (10 μ M), DeNO (10 μ M) and DeUFP (10 μ M) in HEK_{hNOP} cells. C) Representative blot of ERK1/2 phosphorylation (p-ERK1/2) and the fold increase in phosphorylation, compared to basal activity, caused by N/OFQ (10 μ M), DeNO (10 μ M) and DeUFP (10 μ M) in HEK_{hMOP/NOP} cells. Data are the mean (\pm SEM) for n=5 experiments. *= p <0.05, ANOVA with Bonferroni's multiple comparisons performed using the raw data.

7.5 Discussion

In displacement binding studies, Dermorphin, DeNO and DeUFP all produced full displacement of [³H]-DPN in HEK_{hMOP} cell membranes (Figure 7.2, Table 7.1), showing high affinity for the MOP receptor. As demonstrated in Chapter 5, DeNO and DeUFP display an increase in binding affinity for MOP when compared to Dermorphin. In HEK_{hNOP} cells, DeNO and DeUFP produced full displacement of [³H]UFP-101 and displayed a similar affinity to their parent compounds N/OFQ and UFP-101 (Figure 7.2, Table 7.1).

In HEK_{hMOP/NOP} cell membranes, significant changes to the affinities of Dermorphin, DeNO and DeUFP were noted, when [³H]-DPN was used as the radioligand (Figure 7.4, Table 7.1). Both Dermorphin and DeUFP displayed a loss of affinity for the MOP receptor. DeNO displayed the greatest loss of affinity, displaying a 10-fold loss in its pK_i value when compared to HEK_{hMOP} cell membranes. It is also noticeable that the binding affinity of DeNO is not significantly different to that of Dermorphin in HEK_{hMOP/NOP} cell membranes, which has not been demonstrated previously in the MOP single expression systems. Furthermore, while DeUFP demonstrated a loss of affinity when compared to its binding in HEK_{hMOP} cell membranes, it also demonstrated an increase in affinity compared to DeNO in HEK_{hMOP/NOP} cell membranes. This has previously not been seen in either the CHO_{hMOP} or HEK_{hMOP} cell lines (Chapter 5- Figure 5.3, Figure 7.2).

At low pM concentrations of Dermorphin there was no measureable displacement of [³H]-DPN. However, in the presence of either 1 μM N/OFQ or 1 μM UFP-101, the same pM concentrations of Dermorphin caused a significant displacement of [³H]-DPN of ~80%. From the results it can be seen that co-engaging the NOP receptor leads to changes in [³H]-DPN displacement. Both our bivalent peptides, and co-incubation of Dermorphin with either 1 μM N/OFQ or UFP-101, lead to a statistically significant increase in the displacement of [³H]-DPN (Figure 7.3, Figure 7.4).

In GTPγ[³⁵S] assays, Dermorphin, DeNO and DeUFP acted as full agonists in HEK_{hMOP} membranes (Figure 7.5). Both DeNO and DeUFP displayed similar

potency values to Dermorphin at the MOP receptor (Table 7.2). In HEK_{hNOP} cell membranes, N/OFQ and DeNO acted as full agonists, while DeUFP failed to stimulate a response in this cell line (Figure 7.5, Table 7.2). DeNO displayed an increase in potency at the NOP receptor, when compared to N/OFQ.

In HEK_{hMOP/NOP} cell membranes, Dermorphin, N/OFQ, DeNO and DeUFP displayed full agonist activity (Figure 7.6, Table 7.2). However, Dermorphin, N/OFQ and DeNO all demonstrated changes in their respective pEC₅₀ values when compared to those in the single expression systems. Dermorphin displayed a loss of potency in HEK_{hMOP/NOP} cell membranes, when compared to HEK_{hMOP}. DeNO also demonstrated a loss of potency in this system, when compared to both the HEK_{hMOP} and HEK_{hNOP} functional assays. Conversely, N/OFQ demonstrated an increase in potency in the MOP/NOP co-expression system. DeUFP potency in the MOP/NOP co-expression was comparable to its potency in the MOP single expression system. The changes in potency of DeNO and DeUFP in the HEK cell lines are demonstrated in Figure 7.10. From this data (normalised to each sample maximum response), it can be seen for DeNO that HEK_{hMOP} and HEK_{hMOP/NOP} response curves are very similar, whereas there is a leftward shift in the response curve found in HEK_{hNOP} cells. DeUFP displays similar response curves in HEK_{hNOP} and HEK_{hMOP/NOP} cells.

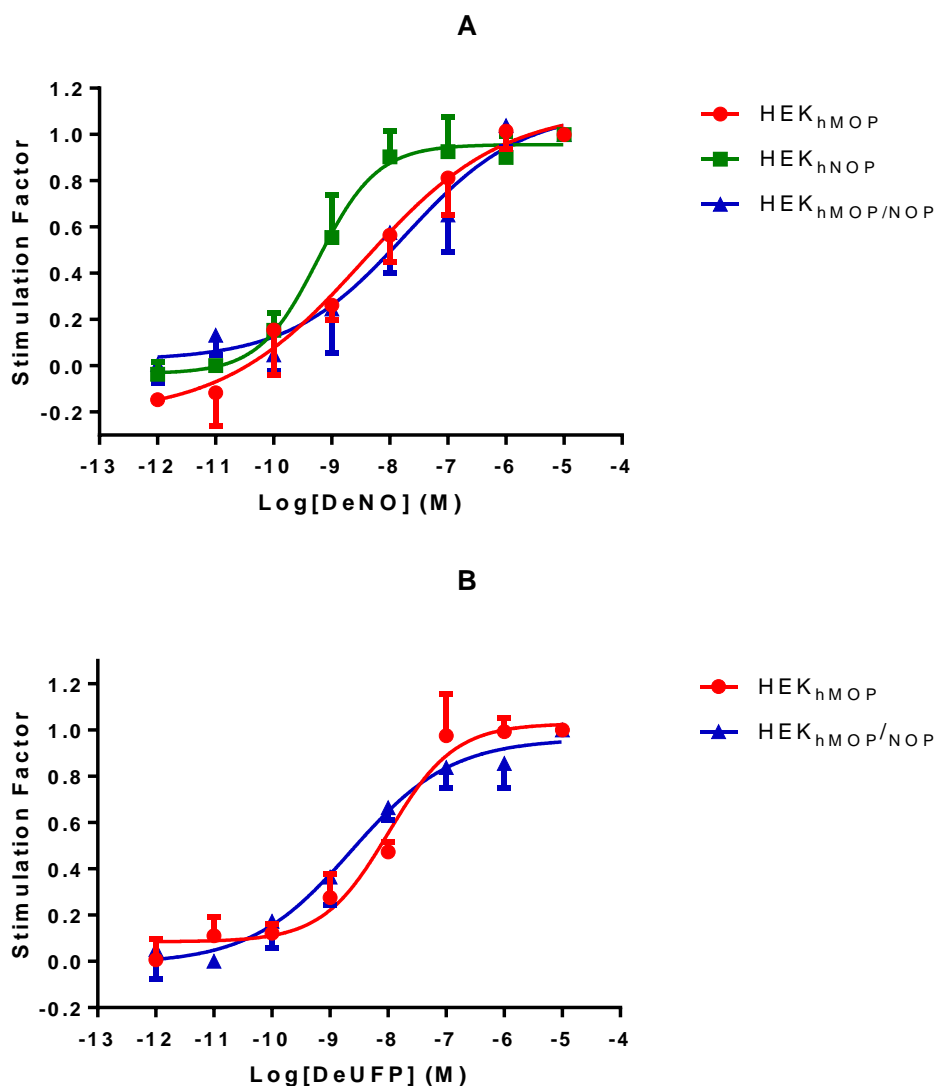


Figure 7.10: A) Normalised curves for DeNO in HEK_{hMOP}, HEK_{hNOP} and HEK_{hMOP/NOP} membranes. B) Normalised curves for DeUFP in HEK_{hNOP} and HEK_{hMOP/NOP} membranes. Data are mean (\pm SEM) for between five and eight experiments.

To further explore the interaction between MOP and NOP receptors, a range of concentrations of Dermorphin and N/OFQ (1pM-10 μ M), or Dermorphin and 1 μ M UFP-101, were co-incubated in a GTP γ [³⁵S] functional assay. The co-incubation of Dermorphin and N/OFQ produced a full agonist response; however, the potency detected was similar to that of Dermorphin, indicating a loss of potency by the N/OFQ component. Conversely, when Dermorphin was co-incubated with 1 μ M UFP-101, the potency measured was comparable with the potency of Dermorphin in a single expression system.

To further explore the effects bivalent pharmacophores have on downstream signalling in a dual expression system, ERK1/2 activity was measured (Figure 7.9). In HEK_{hMOP} cells, Dermorphin, DeNO and DeUFP all produced similar fold increases, over basal activity, in ERK1/2 phosphorylation. The ability of N/OFQ to activate ERK1/2 pathways in HEK_{hNOP} cells was matched by DeNO. DeUFP failed to produce a response in this cell line. In HEK_{hMOP/NOP} cell lines, Dermorphin, N/OFQ, DeNO and DeUFP all produced significant increases in ERK1/2 phosphorylation. While N/OFQ, Dermorphin and DeUFP all produced similar fold changes in phosphorylated ERK1/2, DeNO produced a significant increase in phosphorylation. This response could be seen as a cumulative response of Dermorphin and N/OFQ. It is interesting to note that such a response was not seen in GTP γ [³⁵S] assays, where DeNO produced an E_{max} similar to both Dermorphin and N/OFQ.

Collectively, these data strongly suggest that MOP and NOP interact on a cellular level, to produce changes in both MOP and NOP receptor signalling. The presence of the NOP receptor, leads to changes in the potency of the MOP agonist Dermorphin. By engaging both receptors, through the bivalent peptides or co-incubation of MOP and NOP ligands, significant changes in the signal transduction pathway can be seen.

Chapter 8 General Discussion

A significant aim of this thesis was the study of multi-pharmacophoric ligands that act at one or more opioid receptors. The basis of targeting two receptors simultaneously is founded on a large number of initial studies involving animal DOP receptor knockout studies (Figure 8.1). By removing the DOP, and following subsequent experiments the NOP receptor, or their corresponding endogenous peptide (either Leu-Enkephalin or N/OFQ), attenuation of tolerance to morphine was seen (Chung et al., 2006, Ueda et al., 2000, Ueda et al., 1997, Bohn et al., 1999, Zhu et al., 1999). Conversely, while blocking the activity of the NOP receptor may lead to an attenuation of tolerance, engaging the NOP receptor has been shown to alleviate dependence states (Rutten et al., 2011, Ciccocioppo et al., 2003). Furthermore, co-administration of N/OFQ with a MOP agonist can lead to synergistic increases in spinal analgesic action (Linz et al., 2014, Schröder et al., 2014).

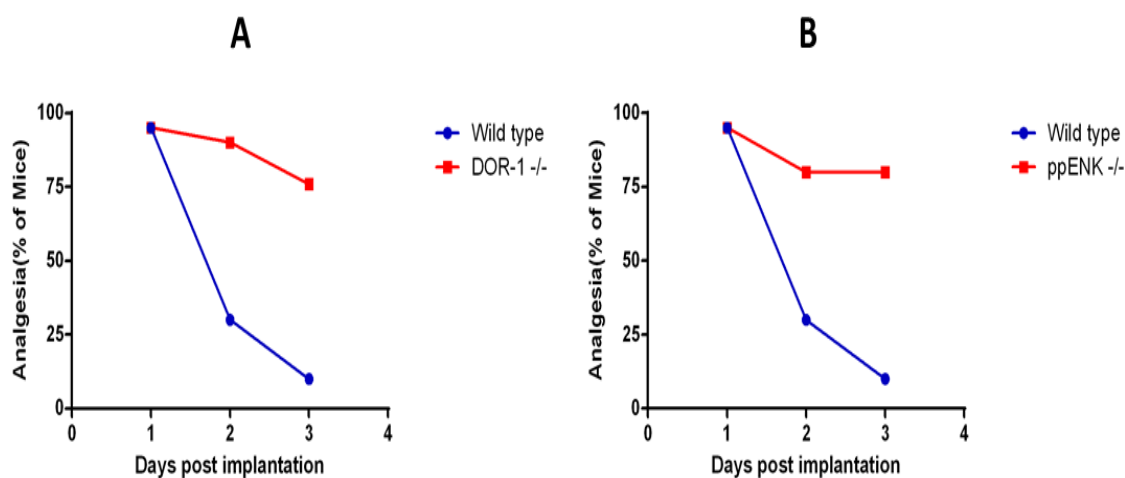


Figure 8.1: A) The development of morphine tolerance is abated in DOR-1 K/O mice. B) Similar results are seen in ppENK (which encodes Leu-Enkephalin) K/O mice, indicating that agonist activity at DOP is involved in the onset of tolerance (Nitsche et al., 2002).

The interactions of MOP and DOP and, to some extent, MOP and NOP are believed to occur through the formation of heterodimers (Evans et al., 2010, Gomes et al., 2004). The formation of this functional signalling unit provides multiple avenues with which to target the receptors (Figure 8.2).

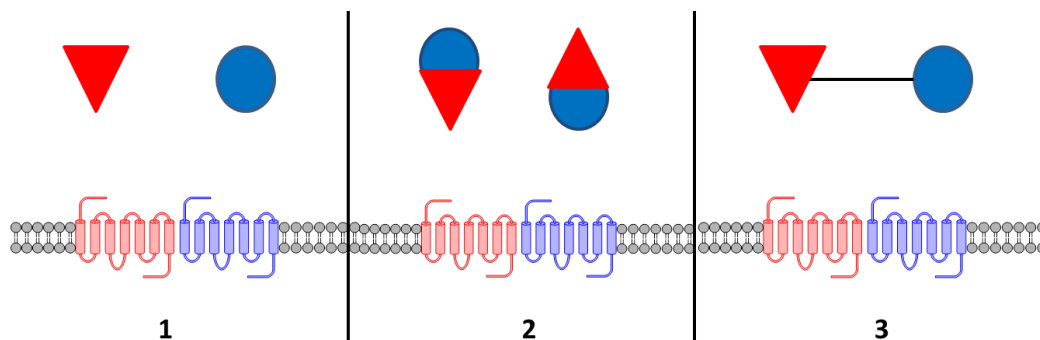


Figure 8.2: When targeting multiple receptors, it is possible to use a variety of methods. These methods include: 1) Polypharmacy: Two separate drugs can be used simultaneously to illicit the desired biological response. 2) A bifunctional non-selective ligand can be developed which has a structure which is promotes binding to both of the receptors. 3) Two separate drugs which can be joined by a linker to form a bivalent pharmacophore which can bind to both receptors (Dietis et al., 2009).

The pharmacokinetic and pharmacodynamic properties of bifunctional and bivalent ligands are more predictable than a cocktail of separate drugs, making them ideal candidates for studies involving opioid tolerance and addiction (Edwards and Aronson, 2000). Bivalent ligands are at a disadvantage to bifunctional ligands in that they often possess a larger molecular weight. This can lead to issues with bioavailability. However, the chemical synthesis of a bifunctional compound is much harder, making such compounds rarer.

In order to investigate the potential of bivalent pharmacophores targeted to MOP/DOP or MOP/NOP, synthetic bivalent pharmacophores based on Fentanyl conjugated with Dmt-Tic-OH or Ro65-6570 were developed. Additionally, peptide bivalent pharmacophores were developed to target both MOP and NOP. These compounds conjugated the MOP agonist Dermorphin to the NOP agonist N/OFQ or the NOP antagonist UFP-101. The synthetic bivalent pharmacophores have the advantage of having a relatively small molecular weight, reducing the risk of a decreased bioavailability. However, alteration of a synthetic ligand's chemical structure can lead to loss of functional activity or selectivity. Conversely, the structures of peptides are easily manipulated to accept linker molecule and, therefore, form bivalent pharmacophores. The molecular weight of these peptide pharmacophores, however, is often larger, reducing their ability to pass the blood brain barrier.

Since most of the adverse effects of opioids seen in the clinic are derived from the MOP receptor, it is reasonable to assume that engaging other opioid receptors capable of producing analgesia may provide a solution to reducing the risk of long-term opioid treatment. Peptides have high affinity for the opioid receptor(s) of interest and demonstrate fewer side effects. However, due to high susceptibility to enzymatic degradation, they have a short duration of action. The introduction of peptide welding technology (PWT) has allowed for four peptides to be joined by a maleimide core, producing a tetra-branched ligand (Guerrini et al., 2014). This tetra-branched ligand may provide ligands that maintain the activity of a single peptide, while increasing its duration of action.

When screening bivalent pharmacophores, it is necessary to understand whether any changes have occurred to the pharmacophores ability to engage the receptor(s) of interest. In order to determine how these compounds function at the receptor of interest, they have been screened in CHO or HEK cells expressing recombinant receptors. CHO cells provide stable expression of single receptors and experiments studying downstream functional assays have been well characterised. The HEK system offers the ability to stably express two receptors, however GTP γ [³⁵S] is less well characterised with regards to NOP signalling. Both systems will allow for the determination of the interactions of the drug and receptor(s) of interest and the subsequent activation of their signal transduction pathways.

The work from this thesis evaluated a number of multi-pharmacophoric ligands to determine the pharmacology in *in vitro* single expression and dual expression systems. The work has determined whether a conjugation of two or more pharmacophores has affected their functional ability. Those compounds which maintained functional ability were tested in the novel HEK_{hMOP/NOP} dual expression system.

8.1 Summary of the main findings

Figures 8.3-8.7 and Table 8.1 summarise the main findings of this thesis.

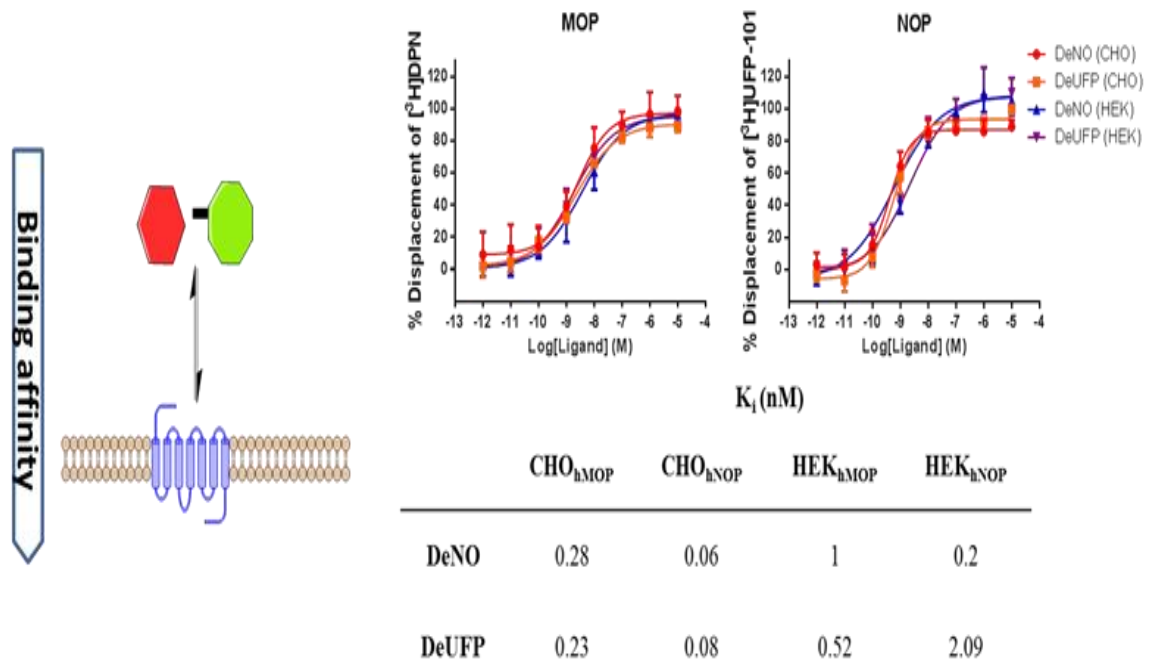


Figure 8.3 A summary of the binding results for DeNO and DeUFP in the various cell lines tested throughout this thesis, indicating the retention of binding affinity for both MOP and NOP.

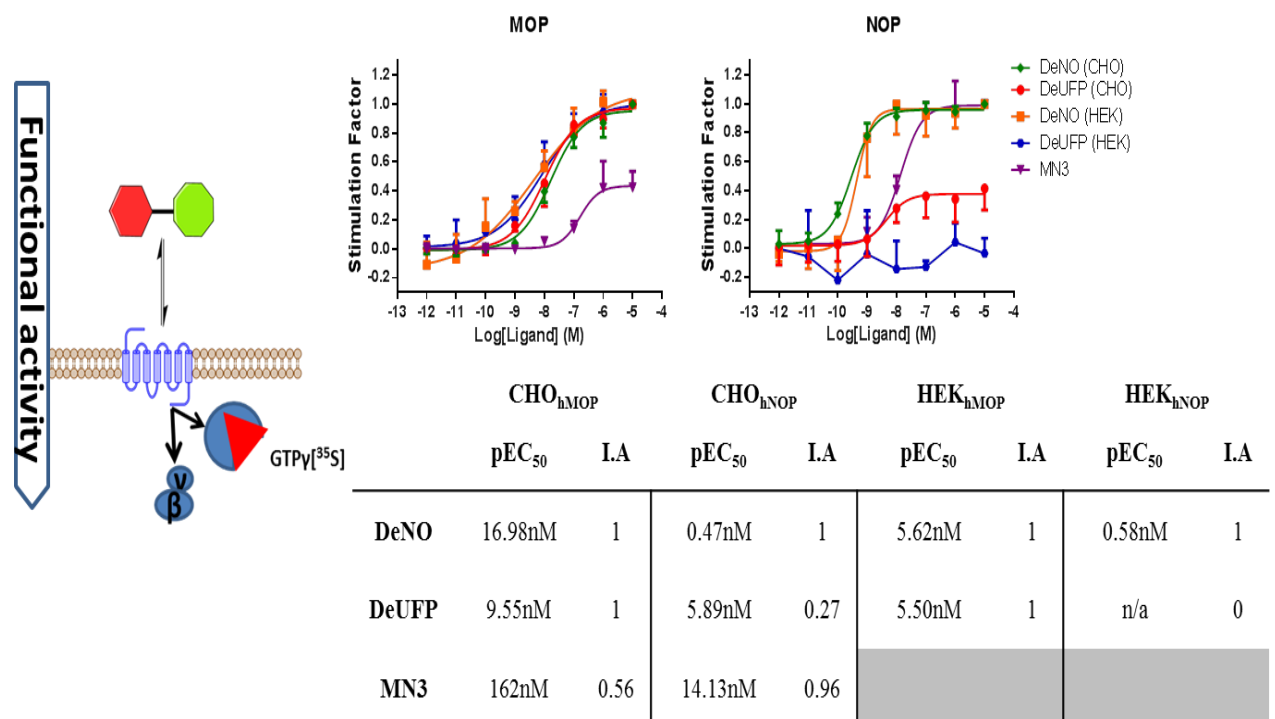


Figure 8.4: Summary of the GTP γ [³⁵S] results from the synthetic partial MOP agonist/full NOP agonist MN3, the peptidic full MOP/NOP agonist, DeNO and the full MOP agonist/NOP partial agonist DeUFP, from this thesis.

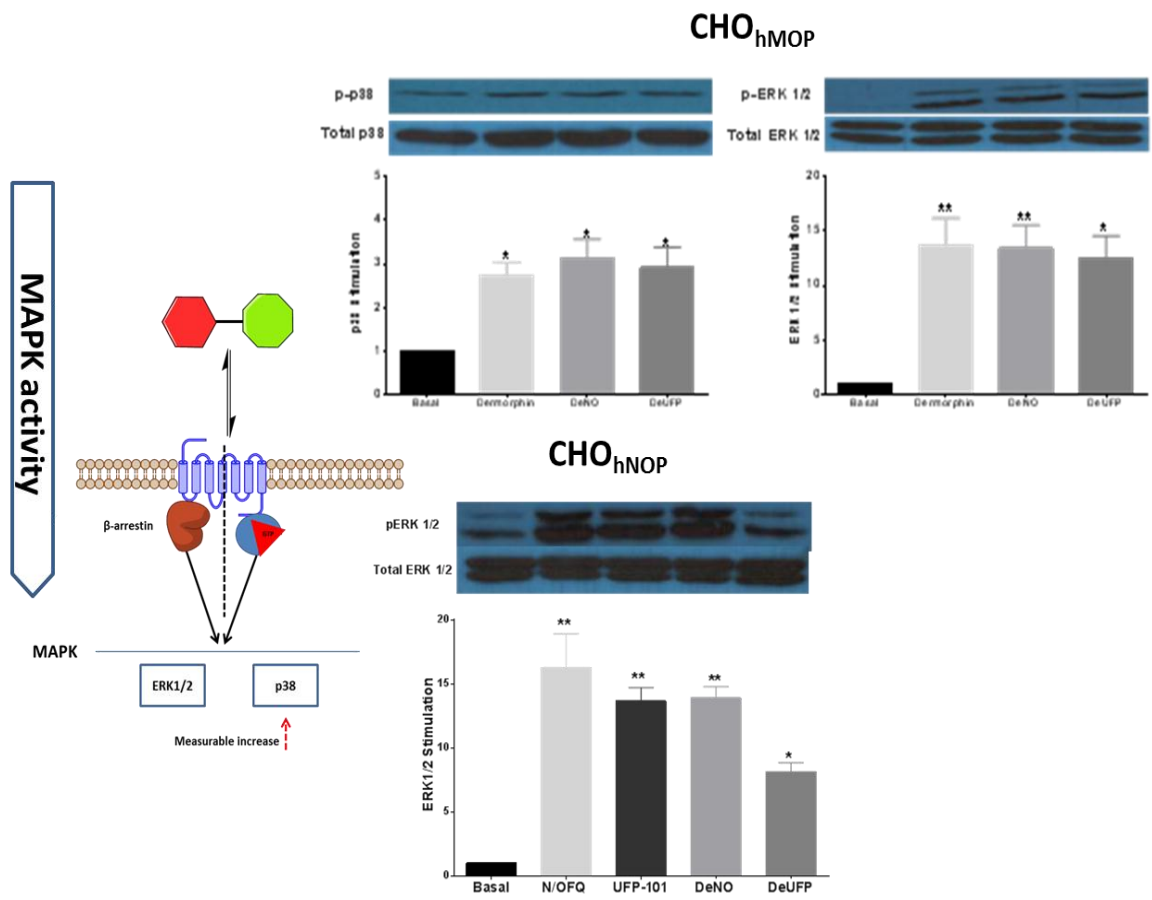


Figure 8.5: A summary of the Western blot analysis of DeNO and DeUFP.

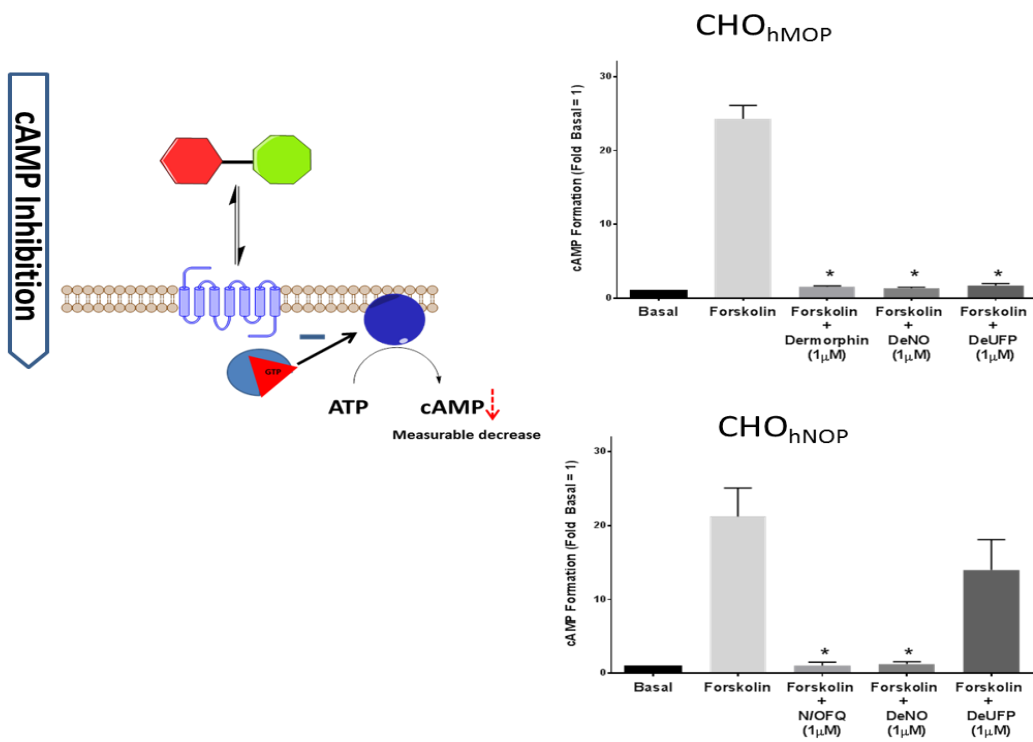


Figure 8.6: Summary of the cyclic AMP results for DeNO and DeUFP in CHO cell lines expressing MOP and NOP.

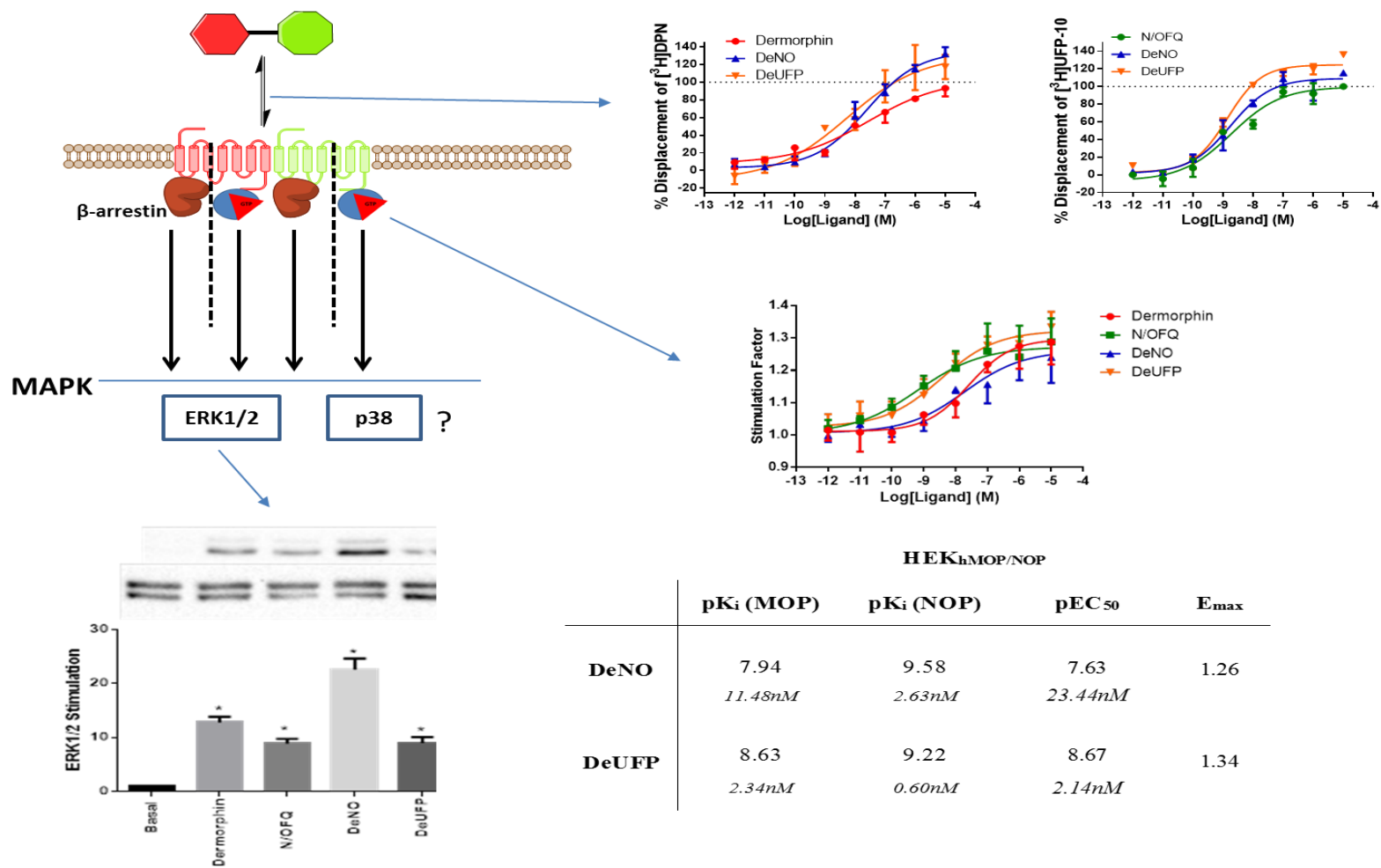


Figure 8.7: Summary of the key findings and the methods used in the co-expression system detailing the interactions of MOP and NOP when activated by DeNO and DeUFP.

In **Chapter 3**, the binding affinities of the Fentanyl bivalent pharmacophores were determined by displacement binding assays in CHO cells expressing recombinant human MOP, DOP, KOP or NOP receptors. Tritiated Diprenorphine was used to screen the bivalents at MOP, DOP or KOP, while [³H]UFP-101 was used to screen the bivalents at NOP. All of the compounds, with the exception of #4, displayed affinity at the MOP receptor similar to the reference ligand, Fentanyl. Compound #4 displayed a decrease in affinity for MOP. At DOP, compounds #4, #5 and #6 all displayed similar binding affinity to the reference compound, Dmt-Tic-OH. Compounds #7 and #8 displayed an increase in affinity for the DOP receptor. The bivalents all displayed high, nanoMolar affinity for KOP and NOP, indicating an increase in affinity over their parent compounds. The effect of binding was measured in functional assays. Compounds #4, #5 and #6 produced a weak stimulation of G-protein activation and limited recruitment of β-arrestins at MOP. Compounds #7 and #8 produced no G-protein response and weak β-arrestin recruitment. At DOP, the compounds failed to produce a functional response, but acted as potent antagonists, inhibiting the actions of the DOP agonist DPDPE to both stimulate G-proteins and recruit β-arrestins. The gain of binding affinity at KOP and NOP did not result in any functional activity for compounds #4-#8. Further Fentanyl derivatives were synthesised with longer carbon linker lengths, and conjugated with the NOP agonist Ro65-6570. MN1, MN2 and MN3 all produced stimulation of G-proteins, with MN2 and MN3 acting as partial agonists at MOP and full agonists at NOP.

In **Chapter 4**, the affinity and functional activity of the PWT-N/OFQ compounds were screened in CHO_{hNOP} to determine binding and functional activity. All of the compounds displayed similar binding affinity to that of their parent compound, N/OFQ. However, the PWT-N/OFQ compounds all displayed an increased potency with regards to G-protein stimulation. A further PWT-compound, PWT2-Leu-Enk, was screened for binding affinity at MOP, DOP, KOP and NOP using CHO cell membranes. PWT2-Leu-Enk showed similar affinity for the DOP receptor, as its parent compound Leu-Enkephalin. PWT2- showed a loss of affinity for the MOP and KOP receptors, when compared to Leu-Enkephalin. To screen functional activity, G-protein stimulation, calcium mobilisation and *ex vivo* twitch assays were undertaken. PWT2-Leu-Enk produced similar G-protein stimulation to its parent compound, Leu-Enkephalin, and to the DOP agonist DPDPE. Conversely, in calcium assays, PWT2-Leu-Enk displayed a

large decrease in potency when compared to DPDPE and Leu-Enkephalin. In the bioassays, PWT2-Leu-Enk produced a similar ability to inhibit the twitch response in the mouse *vas deferens*. Both PWT2-Leu-Enk and Leu-Enkephalin displayed a loss of potency in this assay, when compared to DPDPE, indicating they are susceptible to peptidase activity.

Chapter 5 focusses on the novel peptidic MOP/NOP bivalent pharmacophores, DeNO and DeUFP. Both compound affinities were measured in CHO cell membranes expressing MOP, NOP, DOP or KOP. Both DeNO and DeUFP displayed an increase in affinity for the MOP receptor, when compared to the parent compound Dermorphin. At NOP, DeNO and DeUFP displayed similar binding affinity to that of their respective parent compounds N/OFQ and UFP-101. Both DeNO and DeUFP displayed affinity for DOP and KOP, a trait not displayed by the parent compounds Dermorphin, N/OFQ or UFP-101. The functional activity of DeNO and DeUFP was measured at various points throughout the signal transduction cascade in CHO cells expressing MOP, NOP, DOP or KOP. Both DeNO and DeUFP produced G-protein stimulation at MOP, matching the potency and efficacy of the parent compound Dermorphin. At NOP, DeNO displayed full agonist activity, and produced similar potency to that of N/OFQ. Both DeUFP and UFP-101 acted as partial agonist in CHO_{hNOP} cell membranes. DeNO and DeUFP acted as weak agonists at DOP and KOP. In cAMP assays, DeNO and DeUFP inhibited the production of cAMP. At NOP, DeNO returned cAMP activity to basal levels. DeUFP produced a small decrease in cAMP production, consistent with its low partial agonist activity. Both DeNO and DeUFP displayed an ability to phosphorylate p38 and ERK1/2 in CHO_{hMOP} cells, acting in a similar manner to the parent compound Dermorphin. In CHO_{hNOP} cells, DeNO produced a similar increase in phosphorylation of ERK1/2 to that of N/OFQ. DeUFP and UFP-101 both produced smaller increases in ERK1/2 phosphorylation. At NOP, all compounds failed to produce phosphorylation of p38.

	CHO_{hMOP}				CHO_{hNOP}				CHO_{hDOP}			
	pK_i	pEC₅₀	pK_b	α-E_{max}	pK_i	pEC₅₀	pK_b	α-E_{max}	pK_i	pEC₅₀	pK_b	α-E_{max}
#6	7.91	7.52	n/a	0.35	7.48				8.17		7.81	0
MN3		6.83	I.A	0.42		7.85		1				
PWT2-N/OFQ					10.3	10.04		1				
PWT2-Leu-Enk									8.32	8.4		1
DeNO	9.55	7.77		1	10.22	9.35		1	8.12	6.78		1
DEUFP	9.64	8.02		1	10.08	8.23	8.67	0.27	7.95	7.08		1
Cebranopadol^A	9.15	8.92		1	9.05	7.89		0.89	7.74	6.99		1
SR-16435^B	8.57	7.53		0.3	8.12	7.54		0.45	>5			
[Dmt¹]-N/OFQ(1-13)-NH₂^C	10.52	8.19		1	10.52	8.92		1	9.4			

Table 8.1: Summary of the key results in this thesis, compared to known MOP/NOP compounds. The results from the known MOP/NOP compounds are taken from ^A: (Linz et al., 2014); ^B: (Khroyan et al., 2007); ^C: (Molinari et al., 2013). Shaded area indicates inactivity for the receptor.

The focus of **Chapter 6** was the development of a MOP/NOP dual expression system. In order to understand the pharmacological interactions between MOP and NOP, in the absence of DOP and/or KOP, the development of a MOP/NOP dual expression system was necessary. Initially CHO cells, previously transfected to express MOP, were transfected with the NOP receptor gene. Initial attempts to create a co-expression system in CHO cells lead to poor or unstable expression of MOP or NOP receptors. In line with our previous work, production of a CHO-based co-expression system proved challenging (Dietis, 2012). Further work led to the development of HEK cell lines expressing MOP, NOP and a stable MOP/NOP system. HEK_{hMOP/NOP} cells expressed similar numbers of MOP and NOP receptors and remained stable over a window of at least 9 passages. In order to determine whether the experimental conditions for GTP γ [³⁵S] assays in HEK cells were the same as CHO cells, a buffer validation process was undertaken. The experimental conditions for the HEK cells was determined to be different from that of CHO cells, requiring different concentrations of GDP (HEK_{hMOP}: 3 μ M; HEK_{hNOP}: 33 μ M; HEK_{hMOP/NOP}: 33 μ M) and a different buffer (**Buffer 4**: HEPES (50mM), MgCl₂ (5mM), NaCl (100mM), EDTA (1mM), DTT (1mM), pH 7.4 NaOH).

The focus of **Chapter 7** is to determine how the presence of both MOP and NOP affects the pharmacological profile of the known agonists, Dermorphin and N/OFQ, and our novel bivalent pharmacophores, DeNO and DeUFP. With regards to binding affinity, both the MOP agonist Dermorphin and the NOP agonist N/OFQ demonstrated a loss of binding affinity in the dual expression system. UFP-101, which demonstrated no functional activity in HEK_{hNOP} cells, did not show a change in affinity in HEK_{hMOP/NOP} membranes when compared to HEK_{hNOP}. With regards to binding at the MOP receptor in HEK_{hMOP/NOP} membranes, DeNO demonstrated a 10-fold loss of affinity. DeUFP demonstrated a ~5-fold loss of affinity for MOP, in the dual expression system. Conversely, DeNO demonstrated similar binding affinity for NOP in HEK_{hMOP/NOP} cell membranes as in HEK_{hNOP} cell membranes. DeUFP demonstrated an increase in binding affinity in the dual receptor system, with regards to NOP, when compared to the single receptor expression system. With regards to G-protein stimulation, Dermorphin and DeNO both showed a loss of potency in the dual expression system. N/OFQ demonstrated an increase in potency, while DeUFP retained the potency seen in the MOP single expression system. Furthermore, the co-incubation of N/OFQ and Dermorphin produced a similar potency to that shown by Dermorphin

alone or DeNO. Dermorphin co-incubated with a single concentration of UFP-101, demonstrated potency similar to that seen in the MOP single expression system. Finally, the ability of the compounds to phosphorylate ERK1/2 was studied in the dual expression system. Dermorphin, N/OFQ and DeUFP all produced similar increases in ERK1/2 phosphorylation. DeNO produced a much larger increase in ERK1/2 phosphorylation. HEK cell lines did not demonstrate the ability to engage p38 after 15 minute incubation periods with these compounds.

8.2 Comparing results to existing literature

8.2.1 The MOP/DOP bivalent pharmacophores

The initial study of bivalent pharmacophores focussed on the development of a MOP/DOP synthetic bivalent pharmacophore, based on Fentanyl. A true comparison is made difficult by the significant loss of agonist ability at MOP demonstrated by our compounds. Changes to the functional ability of one or both pharmacophores, in a bivalent ligand, have been demonstrated previously. The most notable study of the effects linker length plays in the development of a bivalent ligand is demonstrated in the MDAN series of compounds (Daniels et al., 2005). These compounds, based on Oxymorphone and Naltrindole, demonstrated an increase in potency as linker length was increased. Interestingly, the relationship between linker length and potency was inverted in the F-compounds. The relationship between potency and linker length of our compounds will be discussed in section 8.4.1. The most interesting comparison found for our compounds is that the Fentanyl derivative, compound #2 (unconjugated to a second pharmacophore in these studies), has been conjugated with an Enkephalin-like peptide (Podolsky et al., 2013). While there are no *in vitro* pharmacological data, this bivalent pharmacophore produced potent analgesic activity in a number of animal pain states. This could potentially be through the action of the Enkephalin pharmacophore, as Enkephalins have been previously shown to activate both MOP and DOP.

8.2.2 *The MOP/NOP bivalent pharmacophores*

The vast majority of compounds developed to target MOP and NOP simultaneously have been bifunctional compounds. One such example of bifunctional MOP/NOP ligands is the SR series of compounds developed by the Stanford Research Institute (Khroyan et al., 2007). The most well documented of these compounds, is SR16435, a synthetic MOP/NOP partial agonist with high binding affinity for MOP and NOP (Table 8.1). This compound most closely compares with MN3 (MOP partial agonist/NOP full agonist). In further studies, the *in vivo* properties of SR16435 were determined. While the compound did produce a delay in onset of tolerance, it produced CPP which is associated with opioid dependence. The authors argued this was due to the partial agonist activity at NOP being unable to attenuate the reward induced activity of the MOP partial agonist activity (Khroyan et al., 2007). Further work by the Zaveri group produced a MOP partial agonist/NOP full agonist, termed 5a (Blair Journigan et al., 2014). While this compound displayed a loss of the addictive properties associated with MOP receptor activity, a net loss in analgesic potency was noted, when compared to Morphine. In this regard, with MN3's full NOP agonist activity, it may act as a compound with antinociceptive activity, while producing an attenuation of MOP induced CPP, however *in vivo* work would be required to validate this theory.

With regards to DeNO, which displayed full agonist activity at MOP and NOP *in vitro*, the compounds with which it compares most favourably are Cebranopadol and [Dmt¹]N/OFQ(1-13)-NH₂. Cebranopadol is a synthetic non-selective opioid compound, developed by Grünenthal, which displays full MOP agonism and high partial agonism at the NOP receptor (Linz et al., 2014). [Dmt¹]N/OFQ(1-13)-NH₂ is a peptide non-selective opioid agonist, showing affinity for both the classical opioid receptors and the non-classical NOP receptor (Molinari et al., 2013). Cebranopadol displays higher affinity for the MOP receptor than DeNO, whereas the reverse is true for the NOP receptor where DeNO displays a higher affinity. DeNO displays an approximate 10-fold reduction in potency at MOP when compared to Cebranopadol, but has a 30-fold greater potency, and full agonist ability, at NOP (Table 8.1). When compared to [Dmt¹]N/OFQ(1-13)-NH₂, DeNO displayed lower affinity for all of the opioid receptors. DeNO, displayed higher potency for the NOP receptor, whereas the potency of [Dmt¹]N/OFQ(1-13)-NH₂ at MOP was greater than that of DeNO. DeUFP is at

present, the first recorded [MOP agonist] – [NOP partial agonist/antagonist⁺] with no presently published data with which to compare to.

8.2.3 *Peptides with prolonged duration of action*

The PWT compounds are designed to have an increased duration of action over single pharmacophoric opioid peptides. A direct comparison in the literature would prove impossible, however, numerous compounds have been developed to inhibit peptidases (enkephalinases), prolonging the action of endogenous peptides. One such compound is Spinorphin, an endogenous inhibitor of Enkephalin-degrading enzymes (Honda et al., 2001). The addition of Spinorphin enhanced and prolonged the antinociceptive effect of Leu-Enkephalin. The advantage provided by the PWT compounds (specifically PWT2-N/OFQ, due to its proven prolonged duration of action) over Spinorphin (and other protease inhibitor cocktails) is that a known and controlled concentration of the compound can be provided. While peptidase inhibitors prolong the action of endogenous peptides, the concentration of endogenous peptide in the circulation is not known or controlled, leading to potentially ineffective doses being available.

8.2.4 *Activity of agonists in a dual-expression system*

There are a limited number of publications demonstrating the signalling abilities of MOP and NOP in a cellular co-expression system (Pan et al., 2002, Wang et al., 2005). In the study by Pan *et al*, their work demonstrated the interaction of human MOP receptors in CHO cells previously transfected to express the murine NOP receptor, with regards to the binding of [³H]-N/OFQ. The co-addition of numerous MOP-selective agonists led to a displacement of [³H]-N/OFQ, previously not seen in single expression systems (Pan et al., 2002). The work undertaken in this thesis partially agrees with these findings (Figure 7.4). While the addition of MOP agonists did lead to changes in [³H]UFP-101 binding, the addition of the antagonist naloxone also led to increased displacement of the radioligand. The work from this thesis adds to the present data by

⁺ Cell-line dependent: Data from this thesis has demonstrated partial agonism in CHO cell lines, whereas no functional activity was detected in HEK cell lines.

demonstrating that the addition of NOP agonists and antagonists affects [³H]-DPN binding.

The functional consequence of MOP/NOP heterodimerisation was studied by Wang, *et al.* The findings from this work indicated that MOP agonists lost potency in cAMP assays in their co-expression system (HEK_{ratMOP/ratNOP}) (Wang et al., 2005). This would agree with the loss of potency, seen by Dermorphin, in our GTPγ[³⁵S] assays (Figure 7.6). With regards to activation of the NOP component of this heterodimer, Wang and colleagues did not detect any change in the inhibition of cAMP formation. This is inconsistent with our findings, which demonstrate an increase in potency for N/OFQ in the heterodimer, using GTPγ[³⁵S] (Table 7.2). The change in potency seen in our cell line may be due to the use of human MOP and NOP receptors in a human cell system (HEK cells) as opposed to rat receptors in a human cell system.

8.3 Mechanisms of action

8.3.1 Evidence of MOP/NOP heterodimerisation

The main aim of this thesis is the development of multi-pharmacophoric opioids that produce reduced adverse effects. In order to test such ligands, screening of the opioids affinity and functional activity in a signal transduction pathway are usually undertaken in a single expression system. In this thesis, both CHO and HEK cell lines have been transfected to express either human MOP or NOP receptors. While these cell lines provide valuable evidence of the activity of our bivalent compounds (such as DeNO) in the presence of a single receptor, it does not account for the activity of the compound in a co-expression system, where dimerisation can occur. Dimerisation is the physical association of two receptors, leading to changes in the association of the receptor with drugs and alterations in the receptors signal transduction cascades (Jordan and Devi, 1999).

The ability of NOP to heterodimerise with MOP has been demonstrated through proximity assays in *in vitro* studies (Evans et al., 2010). In addition to this, a large body of evidence indicates the co-expression and interaction of MOP and NOP *in vivo*. NOP receptors have been shown to co-express in the midbrain of the PAG and NRM neurons

(Houtani et al., 2000). Functional evidence of co-expression was provided via whole-cell patch-clamp recordings, which demonstrated that both N/OFQ and DAMGO hyperpolarise the same populations of PAG and NRM (Pan et al., 2000, Vaughan et al., 2001). The work by Pan *et al.*, demonstrated that NOP is expressed on OFF cells (inhibiting antinociceptive signalling) and is also co-expressed on ON cells in the rat RVM (Pan et al., 2000). This evidence suggests that not only do MOP and NOP co-localise throughout the pain signalling pathways, but demonstrate functional interactions. It is, therefore, necessary to identify the interactions of MOP/NOP bivalent ligands at the cellular level to better understand both the ligands potential ability *in vivo* and the functional consequences *in vitro*.

Due to the instability demonstrated by the previously available CHO_{hMOP} cell line, HEK cells expressing MOP or NOP were developed following which the MOP/NOP co-expression system was developed. The HEK_{hMOP/NOP} cell line was developed, expressing roughly 1.5 NOP receptors to every 1 MOP receptor (Figure 6.15). The advantage in using HEK cells over the CHO system was apparent due to stable expression of the receptors over a span of 9 passages. However, CHO cells express fewer G_{oi} proteins providing reduced background in GTPγ[³⁵S] assays (Burford et al., 2000). Furthermore, delayed onset of homologous phosphorylation of GPCRs, by GRK's, has been demonstrated in CHO cells when compared to HEK cells (Kim et al., 2004). These studies indicated that differential GRK isoforms found in human cell lines, such as HEK, lead to changes in activity when compared to animal cell lines (CHO). These differences in activity may account for changes in affinity when comparing CHO and HEK single expression systems. With this in mind, ligands were retested for binding and functional activity in HEK single expression systems first before comparisons were made with binding and functional data in the co-expression systems.

The first noticeable difference is the loss of binding affinity displayed by Dermorphin, DeNO and DeUFP for the MOP receptor in HEK_{hMOP/NOP} cells when compared to HEK_{hMOP} (Table 8.2). DeNO, displays the most noticeable loss in affinity for MOP, followed by DeUFP and Dermorphin. At NOP, the opposite is seen with DeUFP gaining affinity for the NOP receptor, and DeNO retaining its affinity for NOP, when compared to HEK_{hNOP} data. However, N/OFQ loses affinity for NOP in the dual

expression system. The net loss of binding affinity at MOP in the dual receptor system would imply that the presence of NOP is negatively affecting the binding ability of the NOP receptor. Since heterodimerisation is the structural linking of two receptors, the NOP receptor could be thought of as a negative allosteric modulator of MOP binding. It would also appear that simultaneously engaging both receptors does not positively affect an increase in MOP ligand binding. Conversely, it would appear that engaging the MOP receptor in the heterodimer, leads to a retention, or gain, in binding affinity for NOP ligands. This is evidenced by the loss of affinity of the single pharmacophore N/OFQ while the dual-pharmacophore, DeNO, retains its binding affinity for the NOP receptor. The increase in affinity of DeUFP at NOP provides further evidence of such an interaction. To further highlight the interactions of MOP and NOP, N/OFQ and UFP-101 were able to produce displacement of the classical opioid antagonist radioligand [³H]-DPN. Conversely, the addition of Dermorphin or Naloxone was able to displace [³H]-UFP-101 in conjunction with N/OFQ (Figure 7.4). As mentioned previously, the interaction of MOP and NOP at a structural level could affect the binding pocket of the NOP receptor. The crystal structure of MOP identified a binding pocket that is exposed to the extracellular surface, allowing for rapid dissociation of an opioid from the receptor. While the crystal structure of a heterodimer has not been determined as of yet, it is plausible that the linking of MOP and NOP leads to structural modifications affecting the binding pocket of MOP (Manglik et al., 2012). Due to its large binding pocket, the NOP receptor may be less affected by this physical interaction (Thompson et al., 2012).

The functional activity of these bivalents demonstrated that the loss of affinity seen at the MOP receptor, in the HEK_{hMOP/NOP} membranes, was seen in functional activity at MOP (Table 8.2). Dermorphin and DeNO both demonstrated a significant loss in potency when compared to results in the single expressing cell lines. Interestingly, it is the activity of DeNO and DeUFP that provides the most evidence for heterodimerisation of MOP and NOP in the co-expressing cell lines. DeNO produced a pEC₅₀ of 7.63 in HEK_{hMOP/NOP} membranes. This was similar to Dermorphin in the same cell line. However, it is significantly lower than the pEC₅₀ of N/OFQ (9.23). In HEK_{hNOP} cells, DeNO produced a significantly higher pEC₅₀ than N/OFQ (DeNO: 9.24; N/OFQ: 8.69). The HEK_{hMOP/NOP} dual expression expresses more NOP receptors than MOP, therefore if the receptors were acting independently, this would likely result

in a pEC_{50} closer to N/OFQ than Dermorphin, which is not the case. Furthermore, the co-incubation of a range of concentrations of N/OFQ and Dermorphin produces a similar response to that seen by DeNO and Dermorphin rather than N/OFQ. DeUFP, produces a similar potency to that seen in HEK_{hMOP} cell membranes. Since there is no functional activity for DeUFP in HEK_{hNOP} cell membranes, it is feasible to believe activity is provided solely by the Dermorphin pharmacophore. Furthermore, co-incubation of a set concentration of UFP-101 returned Dermorphin functional activity to the levels seen in the MOP single expression system. This indicates retention of function in the presence of a NOP antagonist.

There is the possibility that increased activity of GRKs or protein kinases, produced by activation of one of the receptors present in this system has led to rapid phosphorylation, or cross desensitisation, of the second receptor (Mandyam et al., 2002). While this argument does hold for the bivalent pharmacophore, DeNO, it does not explain the changes in potency seen by the single pharmacophores. For increased kinase activity to occur, a receptor would have to be activated through ligand occupancy. In this system, there are no endogenous opioids produced and, therefore, without the addition of a second ligand, up-regulation of kinases does not occur. Increased basal activity could account for the activity of the kinases; however DeUFP demonstrates an increase in potency in this system. DeUFP does not alter basal activity at the NOP receptor, as demonstrated by the functional studies in HEK_{hNOP} cell membranes. Therefore if the constitutive activity of NOP was responsible for kinase up-regulation and rapid desensitisation of MOP, a similar decrease in potency should be seen in DeUFP (Figure 8.8).

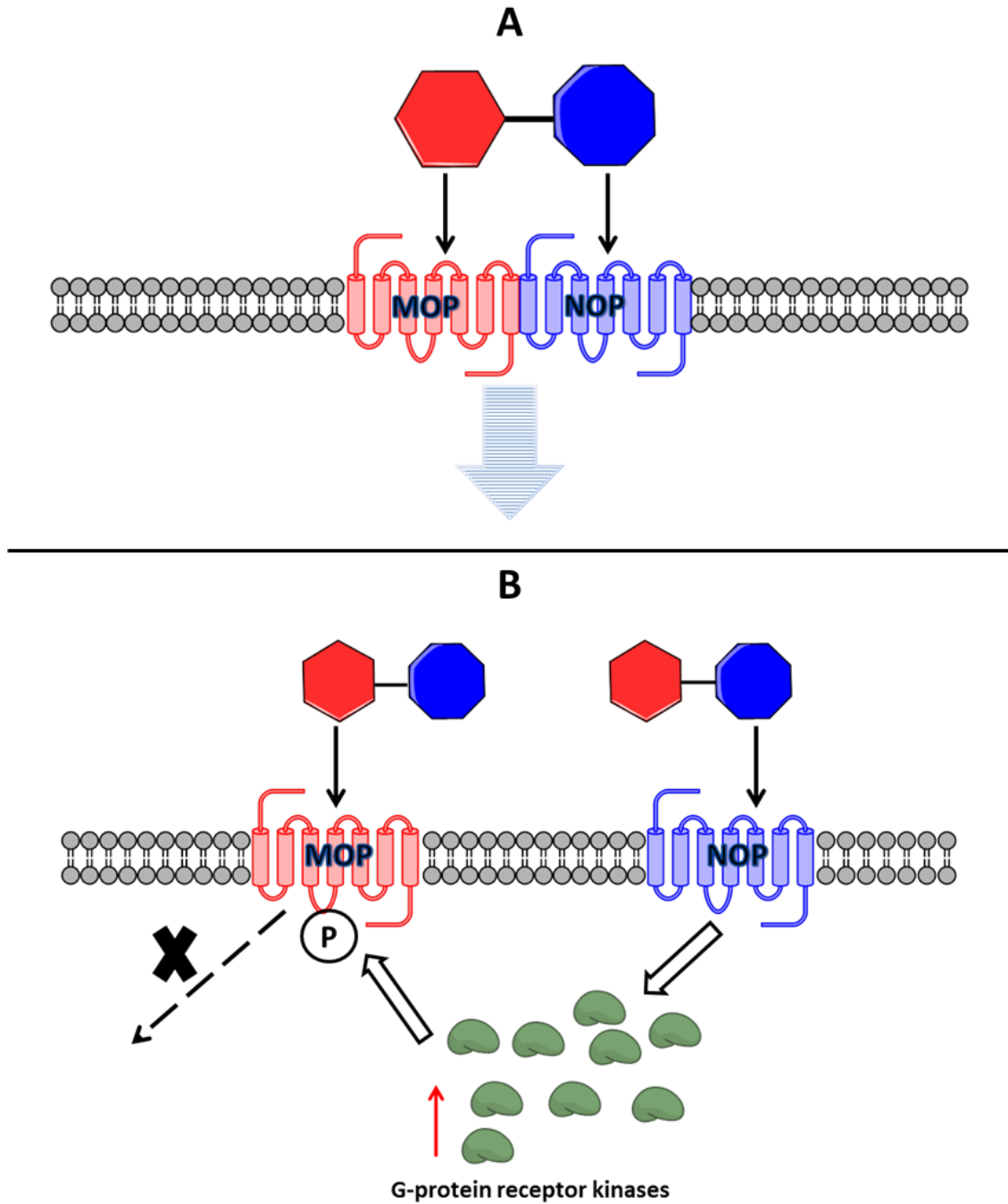


Figure 8.8: A) The signalling mechanisms demonstrated in the HEK_{hMOP/NOP} cell membranes indicate a structural association between MOP and NOP. The NOP receptor negatively impacts the signal transduction pathways associated with MOP receptor activation. B) Activation of NOP leads to increased G-protein receptor kinase activity, causing rapid desensitisation of the MOP receptor.

	CHO_{hMOP}		CHO_{hNOP}		HEK_{hMOP}		HEK_{hNOP}		HEK_{hMOP/NOP}		
	K_i	EC₅₀	K_i	EC₅₀	K_i	EC₅₀	K_i	EC₅₀	K_i (MOP)	K_i (NOP)	EC₅₀
Dermorphin	2.04nM	14.79nM			4.79nM	7.40nM			13.80nM		25.12nM
N/OFQ			0.02nM	1.45nM			0.41nM	2.04nM		1.09nM	0.59nM
DeNO	0.28nM	16.98nM	0.06nM	0.45nM	1nM	5.62nM	0.20nM	0.58nM	11.48nM	2.63nM	23.44nM
DeUFP	0.23nM	9.55nM	0.08nM	5.89nM	0.52nM	5.50nM	2.09nM		2.34nM	0.60nM	2.14nM

Table 8.2: A summary of the binding affinity and potency of Dermorphin, N/OFQ, DeNO and DeUFP in the various cell lines studied.

8.4 Unexpected and contentious issues arising from this thesis

8.4.1 *Alteration of the chemical structure of known ligands*

The process of chemically altering existing compounds can lead to the successful development of multifunctional pharmacophores such as PWT2-N/OFQ, DeNO and DeUFP. However, synthetic ligands can prove more difficult to modify. In the case of the F-compounds, the addition of a linker molecule and second pharmacophore led to a loss of functional activity when compared to Fentanyl. As can be seen from Figure 8.9, an increase in linker length positively affected the compounds affinity at MOP and DOP, but led to a loss of functional activity (Figure 8.9). For DOP, the reverse was true, with an increase in linker length positively affecting both the affinity and antagonist ability of the Dmt-Tic-OH pharmacophore. These findings are inconsistent to those previously described by Daniels *et al* (Daniels *et al.*, 2005). The optimal proximity between pharmacophores in these studies is a linker molecule of approximately 3 carbon atoms, whereas other studies have demonstrated increased efficacy with linker molecules ranging in size from 16 to 21 carbon atoms in length. The close proximity between Fentanyl and Dmt-Tic-OH could be producing a “forced-fit” in the MOP binding pocket, leading to the weak partial agonism displayed by these drugs. The loss of agonist ability demonstrated in the compounds separated by larger linkers could be demonstrative of the chemically altered Fentanyl pharmacophores loss of functional activity.

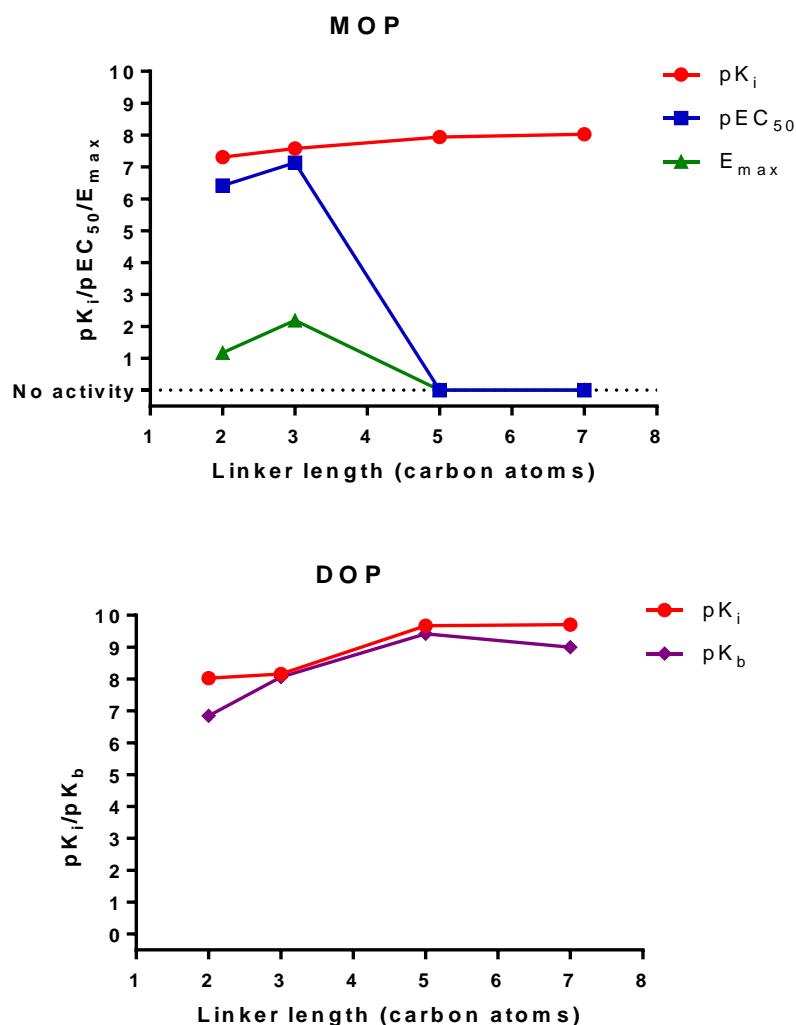


Figure 8.9: The effect of increasing linker length has on F-compound affinity (pK_i), potency (pEC_{50}), efficacy (E_{max}) and antagonist affinity (pK_b). As linker length increases, both potency and efficacy decrease at MOP. Conversely, an increase of linker length leads to increased antagonist affinity at DOP.

The synthesis of a series of Fentanyl pharmacophores has demonstrated differences in binding (Figure 8.10). The initial compounds #1 (linker with two carbon atoms added to the northern hemisphere of the compound), #2 (linker molecule of 3 carbon atoms) and #3 (2 carbon atoms and an oxygen atom in the linker molecule) demonstrated a complete loss of binding affinity at MOP. Further chemical synthesis produced Fentanyl pharmacophores containing increasing carbon atom linker length (i.e. RR4 contains a linker of 4 carbon atoms, RR5 has a linker of 5 carbon atoms, etc). These compounds all showed varying degrees of affinity for MOP. The sudden gain in affinity

with the addition of a fourth carbon atom is difficult to explain, but may be as a result of the electrostatic charges formed in the linker molecules themselves.

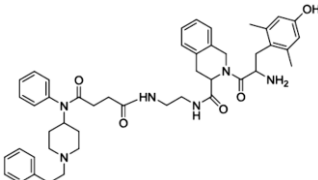
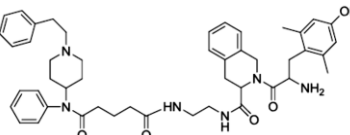
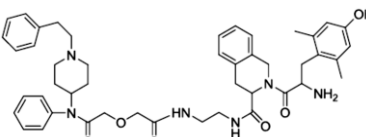
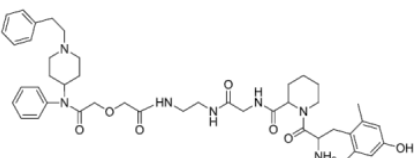
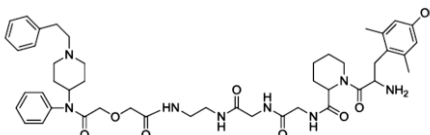
Structure	Compound #
	#4
	#5
	#6
	#7
	#8

Figure 8.10: The chemical structure of the Fentanyl-derivatives

8.4.2 *Clinical outcomes with MOP/DOP multipharmacophoric research*

The first reference to DOP antagonism attenuating morphine tolerance occurred in 1991 (Abdelhamid et al., 1991). Following on from this finding, numerous bivalent and bifunctional ligands have been developed, which have dual action as MOP agonist and DOP antagonists. The evidence from *in vitro* and *in vivo* (mouse and rat models) studies strongly supports the synergistic function of these ligands in attenuating tolerance. However, there has not been any development with regards to a clinically available opioid of this type. While mouse and rat studies dominate the literature involving these bivalent/bifunctional molecules, little evidence exists in primates to support the MOP agonist/DOP antagonist theory. Primates, such as the rhesus monkey, usually provide a more predictive assessment of the clinical outcomes of developmental opioids (Aceto et al., 2012). Work undertaken with MDAN-21 demonstrated a potential different mode of action for MOP-DOP neural substrates that underlie thermal nociception (Aceto et al., 2012). Little or no literature exists demonstrating an attenuation of tolerance through administration of these bifunctional/bivalent compounds. Conversely, a number of studies have demonstrated the effects of MOP/NOP agonists as potent analgesics with prolonged action (Molinari et al., 2013, Cremeans et al., 2012). It is possible that the results demonstrated in the rat and mouse models do not translate to the more complex systems of higher primates; ultimately man.

8.4.3 *UFP-101: Cell line specific functional activity?*

UFP-101 is classified in the literature as a NOP antagonist (Calo et al., 2005). However, in Chapter 5, UFP-101 produces a measurable increase over basal activity at NOP in the GTP γ [³⁵S] functional assays. This increase in functional activity is also seen in DeUFP in CHO_{hNOP} cell membranes. Furthermore, both UFP-101 and DeUFP produced an increase in ERK1/2 phosphorylation further demonstrating functional activity. This increase in functional activity led UFP-101 and DeUFP to be classified as low efficacy partial agonists in the CHO cells expressing the NOP receptor.

As was previously discussed in **Chapter 5**, receptor density can affect drug efficacy. In high expression systems, high numbers of receptors lead to a greater response.

Conversely, low expression systems produce smaller functional responses due to lower numbers of receptors expressed in that system. Partial agonists can behave as antagonists or full agonists depending on the receptor expression of the system studied (McDonald et al., 2003a). The CHO_{hNOP} cells used in these experiments have approximately 3-4 fold higher expression than that found in neuronal tissue. This increased activity may account for the discrepancy seen between the literature and our experiments.

However, work undertaken in Chapter 7 demonstrated no increase in functional activity for DeUFP. This loss of functional activity is unlikely to be explained by differences in receptor expression between CHO_{hNOP} (800fmol/mg of protein) and HEK_{hNOP} (816fmol/mg of protein). A direct comparison between these results is made difficult due to the different buffers used in these assays. Interestingly, N/OFQ shows little difference in its pEC₅₀ values between these two cell lines. It could be argued that the low stimulation factor demonstrated in the HEK_{hNOP} cell membranes may be masking the partial agonist activity of DeUFP in this cell line. However, DeUFP also fails to stimulate phosphorylation of ERK1/2. It is possible that ERK1/2 phosphorylation occurs at an earlier time point (drugs undergo a 15 minute incubation period before being lysed). A potential explanation for this loss of functional activity could be rapid phosphorylation of the receptor. Further characterisation of the ligand in downstream assays (including timepoint assays to monitor ERK1/2 activity) is required to accurately determine its pharmacological properties.

8.4.4 *Interactions with p38*

The ability of MOP to regulate p38 signalling is well documented. This activity has been shown to be both cell line and ligand dependent (Wang et al., 2009, Roux and Blenis, 2004, Cuadrado, 2010, Tan et al., 2009b, Pradhan et al., 2012). In CHO_{hMOP} Western blot experiments, both Dermorphin and the Dermorphin-derivatives engage p38 activity. Conversely, no p38 activity was seen in HEK_{hMOP} cell lines under the same experimental conditions.

This loss of activity could be as a result of differential phosphorylation of the MOP receptor in HEK cell lines. As has been previously mentioned, GPCR phosphorylation

occurs at a slower rate in CHO cells (Kim et al., 2004). The more rapid phosphorylation of the MOP receptor in HEK cells could lead to an earlier peak in p38 activity, which is missed at the 15 minute time point in our western blot analysis. Alternatively, differential phosphorylation of the receptor by GRK isoforms in CHO and HEK cells could lead to differential recruitment and attachment of β -arrestins in each cell line, resulting in changes to the phosphorylation of downstream MAPK activity.

8.4.5 *Discrepancies between RT-qPCR and radioligand binding*

RT-qPCR data is presented for a large number of CHO_{hMOP/NOP} clones (Table 6.1, Table 6.2). A large number of these clones demonstrated equal or greater ΔC_t values for NOP mRNA when compared to MOP mRNA. In initial screens, clone number #28 demonstrated equal ratios of MOP and NOP receptor mRNA. The clone was screened for functional receptors in radioligand binding assays, and showed similar expression of MOP and NOP (Figure 6.2). However, NOP receptor expression significantly decreased after 2 passages.

Further clones were studied in saturation binding assays. All of the clones demonstrated little or no NOP receptor expression in this initial batch of clones, despite providing positive RT-qPCR data. The discrepancy between functional expression and mRNA data is unexplained. It is possible that the stability of these co-expression systems is extremely limited, allowing for only a few passages of functional expression. It is also possible that while mRNA for both receptors is being produced, the CHO cell does not have the necessary translational machinery to convert human receptor mRNA into functional protein. Further investigation of mRNA translation in CHO cells is required to address this issue.

8.5 **Limitations**

8.5.1 *Comparisons between assays*

The numerous assays employed throughout this thesis are well validated through a number of years of research. However, the buffers used within each assay are different, and do not necessarily reflect a physiological environment. A prime example would be

the GTP γ [³⁵S] experiments between HEK and CHO, where levels of magnesium and sodium (both of which affect G-protein binding) are substantially different (Harrison and Traynor, 2003).

Direct comparison between assays is complicated by the cell state in each assay. Both radioligand binding and GTP γ [³⁵S] assays are undertaken in homogenised cell membranes, while the cAMP assays and MAPK western blots are undertaken in whole cells. Differences in levels of G-proteins, GRK's, arrestins and other intracellular mediators may produce changes in affinity, potency and efficacy. These experiments, however, provide us with the ability to detail the mechanisms of action for drugs in single receptor and co-expression systems, which would not be possible *in vivo* or *ex vivo*.

8.5.2 Evidence of physical interaction between MOP and NOP

While the evidence provided by the changes of signalling seen in **Chapter 7** strongly supports the heterodimerisation of MOP and NOP, a direct physical interaction is not demonstrated. Proximity assays would provide substantial evidence to support the heterodimerisation theory in this cell line.

Tagging receptors with fluorescent molecules may lead to changes in receptor expression (Scherrer et al., 2009). To account for such changes in cell-surface expression and to demonstrate in heterodimerisation in the cell line tested in this thesis, it is possible that fluorescent ligands (such as naloxone) could be used to demonstrate the proximity of the receptors in this cell line (Madsen et al., 2000). This process was not within the scope of the PhD.

8.6 Importance of the findings

As detailed previously, opioids provide strong analgesic action in the treatment of nociceptive pain. However, their use in the treatment of chronic pain is severely blighted by the development of adverse effects, such as tolerance and dependence. The implication that opioid receptors interact on a physical level, and signal as a single functioning unit, has had important ramifications in the development of opioid ligands.

The aim of this thesis was to identify multi-pharmacophoric ligands that act at one or more opioid receptor, which may hold future potential of providing analgesia with a reduction in adverse effects. These compounds have included chemical alteration of known synthetic opioids (Fentanyl), peptides with an increased duration of action, and peptides conjugated to form novel bivalent peptides. All of the compounds mentioned have been extensively screened *in vitro* to assess how such conjugation affects the pharmacophores involved.

The first of such bivalent pharmacophores were the F-compounds. Initially the focus of this thesis was on the conjugation of the MOP agonist, Fentanyl, and the DOP antagonist, Dmt-Tic-OH. The chemical alteration of Fentanyl led to large or complete losses in functional activity. While the F-compounds themselves will not provide functional use as clinical compounds, their conjugation has provided a number of significant details about this process. Of most interest, is that increases in linker length can have a marked impact on the functional activity of the compound of interest. Interestingly, the changes in linker length also demonstrated an ability to increase the antagonist affinity of the DOP pharmacophore. The studies may help influence what type and length of linker molecule is used in future studies of bivalent ligands.

The development of a MOP/NOP synthetic bivalent agonist was also studied using Fentanyl derivatives. From these studies, we have demonstrated the production of a MOP partial agonist/ NOP full agonist. This compound may have future clinical impact in studying opioid dependence *in vitro* and potentially *in vivo*. The impact of partial agonist Buprenorphine in the treatment of dependence is well studied and it is widely accepted that its effect in treating opioid and cocaine addiction is mediated through the NOP receptor (Bloms-Funke et al., 2000, Raisch et al., 2002, Schottenfeld et al., 1997, Jasinski et al., 1978). Further testing of MN3 *in vivo* in dependence states would be required to validate this theory. The development of synthetic bivalent pharmacophores has highlighted the difficulty in altering the structure of current, clinically-used, opioids.

Further work in the thesis has demonstrated the construction of novel, tetra-branched peptides that may have substantial impact in a clinical setting. While PWT2-Leu-Enk did not show a marked increase in potency when compared to Leu-Enkephalin or

DPDPE at DOP, PWT2-N/OFQ demonstrates a significant increase in potency over the N/OFQ peptide at NOP. PWT2-N/OFQ has demonstrated prolonged activity *in vivo* (Rizzi et al., 2014). This work indicates that, certainly for PWT2-N/OFQ, a peptide with prolonged action, and potentially reduced adverse effects, could have a place in the clinical setting.

The final group of compounds studied in this thesis were MOP/NOP bivalent peptides. The interaction between MOP and NOP, with regards to analgesia, is complex. Furthermore, work with N/OFQ and mixed ligands, such as cebranopadol, have demonstrated the potential for a drug with a reduced dependence profile and synergistic increases in analgesia (Ko and Naughton, 2009, Linz et al., 2014). The conjugation of Dermorphin and N/OFQ or UFP-101 produced a novel peptidic bivalent MOP-NOP agonist and MOP agonist-NOP partial agonists (in CHO cell lines). These compounds are the first reported bivalent ligands of their type. DeNO is a full agonist at both MOP and NOP, and as such acts as a novel research tool to investigate the interactions of MOP and NOP at a cellular level.

The development of these compounds allowed for the investigation of bivalent pharmacophores in a system that co-expresses MOP and NOP, without the presence of KOP or DOP. The development of the HEK_{hMOP/NOP} cell line demonstrates the first study of recombinant co-expressed human MOP and NOP receptors. From this work, it is evident to see that the presence of the NOP receptor has a negative impact on both the binding and signalling ability of the MOP receptor. Furthermore, the ability of DeUFP to retain signalling levels consistent with single expressing cell lines demonstrates the functional interactions of MOP and NOP. Taken together, the work from this thesis adds significant evidence to the theory of MOP/NOP heterodimerisation. Furthermore, it may help to explain the antinociceptive effects seen by N/OFQ supraspinally. As well as its overarching impact on dopaminergic neurons, the NOP receptor may attenuate dependence by negatively impacting the potency of MOP receptor agonists.

8.7 Future Work

Future areas of study to build on this thesis include:

1. **Physical evidence of MOP/NOP Heterodimerisation:** While the impact on signalling is apparent, demonstration of the proximity of the receptors would further add weight to this argument. By using fluorescent ligands, the current cell lines could be used to determine the proximity of the receptors.
2. **p38 activity: Is p38 activity cell line specific:** Is differential GRK or protein kinase activity required to engage this MAPK pathway? Is the activity being missed? Studies using ligand-stimulated timecourses, the addition of pertussis toxin and/or GRK knockout/inhibitor studies may help in determining p38 involvement in opioid signalling.
3. ***In vivo* studies of DeNO, DeUFP and MN3:** The ability of these compounds to attenuate dependence or demonstrate changes in analgesic action would be further enhanced by studies in well-defined animal paradigms.

8.8 Publications arising from this thesis

Full Papers:

Rizzi, A., Malfacini D., Cerlesi M. C, Ruzza C., Marzola E., **M. F. Bird**, Rowbotham D. J., Severo S., Guerrini R., Lambert D. G. and G. Calo (2014). *In vitro* and *in vivo* pharmacological characterization of nociceptin/orphanin FQ tetrabranched derivatives. *British journal of Pharmacology*, 2014 Sep; 171(17):4138-53. doi: 10.1111/bph.12799.

Bird M.F, Vardanyan R, Hraby V.J, Calò G, Guerrini R, Salvadori S, Trapella C, McDonald J, Rowbotham DJ & Lambert D. G. The development and characterisation of novel fentanyl-based bivalent pharmacophores. *British Journal of Anaesthesia* (in press).

Brown M, **Bird M.F**, Rowbotham D. J., Severo S., Guerrini R., Calo G., Lambert D. G. *In vitro* and *in vivo* pharmacological characterization of peptidic bivalent pharmacophores targeting MOP and NOP. (In preparation)

Bath M.F, **Bird M.F**, Thomas R.C., McDonald J., Thompson J. and Lambert D. G. Detection and characterisation of NOP receptor signalling in EOL-1 cells. (In preparation)

Reviews and editorials:

Lambert D.G., **Bird M.F.**, Rowbotham D.R. – Cebranopadol: A First In-Class Example of a NOP and opioid receptor agonist. *British Journal of Anaesthesia*. 2014 Sep; doi:10.1093/bja/aeu332.

Bird M.F. & Lambert D.G. Probing receptor function using radioligand binding. *For British journal of Anaesthesia* (In preparation).

Bird M.F. & Lambert D.G. Targeting multiple opioid receptor types simultaneously in pain management - the rationale and the evidence. *For Pain: Cancer section for the June 2015 issue of Current Opinion in Supportive & Palliative Care* (In preparation).

Abstracts

Anaesthetic Research Society meeting, hosted by the Royal College of Anaesthetists, London, December 2012:

Bird MF, Vardanyan RS, Guerrini R, Trapella C, Caló G, Rowbotham DJ and Lambert DG (2012). Characterization of novel fentanyl-based bivalent opioids. *Br J Anaesth* **110** (5): 860P-885P.

Anaesthetic Research Society meeting, hosted by Merton College, Oxford, April 2013:

Bird MF, Vardanyan RS, Guerrini R, Trapella C, Caló G, Rowbotham DJ and Lambert DG (2013). Further characterization of novel fentanyl-based bivalent opioids. *Br J Anaesth* **111** (2): 309P-320P.

Presentations:

Postgraduate Careers Symposium for the College of Medicine Biological Sciences and Psychology January 9 2014:

Bird MF. BioTechnology YES

Festival of Postgraduate Research, University of Leicester, 2014:

Bird MF. Developing Painkillers with Reduced Side Effects: A Multi-Target Approach.

Cell Signalling Group-meeting, Department of Cardiovascular Sciences, University of Leicester, 2013:

Bird MF. Characterisation of Novel Fentanyl-Based Bivalent Opioids.

BioTechnology Yes, Oxford, 2014:

Bird MF, Milano C, Gavrille A, Tu S. Sunniva- A Tan in a Pill

References

- ABDELHAMID, E. E., SULTANA, M., PORTOGHESE, P. S. & TAKEMORI, A. E. 1991. Selective blockage of delta opioid receptors prevents the development of morphine tolerance and dependence in mice. *Journal of Pharmacology and Experimental Therapeutics*, 258, 299-303.
- ABDULLA, F. A. & SMITH, P. A. 1998. Axotomy reduces the effect of analgesic opioids yet increases the effect of nociceptin on dorsal root ganglion neurons. *J Neurosci*, 18, 9685-94.
- ACETO, M. D., HARRIS, L. S., NEGUS, S. S., BANKS, M. L., HUGHES, L. D., AKGÜN, E. & PORTOGHESE, P. S. 2012. MDAN-21: A Bivalent Opioid Ligand Containing mu-Agonist and Delta-Antagonist Pharmacophores and Its Effects in Rhesus Monkeys. *International Journal of Medicinal Chemistry*, 2012, 6.
- ALMELA, P., GARCIA-NOGALES, P., ROMERO, A., MILANES, M. V., LAORDEN, M. L. & PUIG, M. M. 2009. Effects of chronic inflammation and morphine tolerance on the expression of phospho-ERK 1/2 and phospho-P38 in the injured tissue. *Naunyn Schmiedebergs Arch Pharmacol*, 379, 315-23.
- ARTTAMANGKUL, S., QUILLINAN, N., LOW, M. J., VON ZASTROW, M., PINTAR, J. & WILLIAMS, J. T. 2008. Differential Activation and Trafficking of μ -Opioid Receptors in Brain Slices. *Molecular Pharmacology*, 74, 972-979.
- BAGLEY, E. E., CHIENG, B. C., CHRISTIE, M. J. & CONNOR, M. 2005a. Opioid tolerance in periaqueductal gray neurons isolated from mice chronically treated with morphine. *Br J Pharmacol*, 146, 68-76.
- BAGLEY, E. E., GERKE, M. B., VAUGHAN, C. W., HACK, S. P. & CHRISTIE, M. J. 2005b. GABA transporter currents activated by protein kinase A excite midbrain neurons during opioid withdrawal. *Neuron*, 45, 433-45.
- BALLANTYNE, J. C., SULLIVAN, M. D. & KOLODNY, A. 2012. Opioid dependence vs addiction: A distinction without a difference? *Archives of Internal Medicine*, 172, 1342-1343.
- BECKETT, A. H. & CASY, A. F. 1954. Synthetic analgesics: stereochemical considerations. *J Pharm Pharmacol*, 6, 986-1001.
- BEE, L. & DICKENSON, A. 2009. Descending Modulation of Pain - Synaptic Plasticity in Pain. Springer New York.
- BELCHEVA, M. M., VOGEL, Z., IGNATOVA, E., AVIDOR-REISS, T., ZIPPEL, R., LEVY, R., YOUNG, E. C., BARG, J. & COSCIA, C. J. 1998. Opioid Modulation of Extracellular Signal-Regulated Protein Kinase Activity Is Ras-Dependent and Involves G $\beta\gamma$ Subunits. *Journal of Neurochemistry*, 70, 635-645.
- BILECKI, W., ZAPART, G., LIGEŻA, A., WAWRZCZAK-BARGIELA, A., URBAŃSKI, M. J. & PRZEWŁOCKI, R. 2005. Regulation of the extracellular signal-regulated kinases following acute and chronic opioid treatment. *Cellular and Molecular Life Sciences CMLS*, 62, 2369-2375.
- BLAIR JOURNIGAN, V., POLGAR, W. E., KHROYAN, T. V. & ZAVERI, N. T. 2014. Designing bifunctional NOP receptor–mu opioid receptor ligands from NOP-receptor selective scaffolds. Part II. *Bioorganic & Medicinal Chemistry*, 22, 2508-2516.
- BLOMS-FUNKE, P., GILLEN, C., SCHUETTLER, A. J. & WNENDT, S. 2000. Agonistic effects of the opioid buprenorphine on the nociceptin/OFQ receptor. *Peptides*, 21, 1141-1146.
- BOHN, L. M., LEFKOWITZ, R. J., GAINETDINOV, R. R., PEPPEL, K., CARON, M. G. & LIN, F. T. 1999. Enhanced morphine analgesia in mice lacking beta-arrestin 2. *Science*, 286, 2495-8.
- BONCI, A. & WILLIAMS, J. T. 1997. Increased probability of GABA release during withdrawal from morphine. *J Neurosci*, 17, 796-803.
- BOTNEY, M. & FIELDS, H. L. 1983. Amitriptyline potentiates morphine analgesia by a direct action on the central nervous system. *Annals of Neurology*, 13, 160-164.

- BRILLET, K., KIEFFER, B. L. & MASSOTTE, D. 2003. Enhanced spontaneous activity of the mu opioid receptor by cysteine mutations: characterization of a tool for inverse agonist screening. *BMC Pharmacol*, 3, 14.
- BURFORD, N. T., WANG, D. & SADEE, W. 2000. G-protein coupling of mu-opioid receptors (OP3): elevated basal signalling activity. *Biochem J*, 348 Pt 3, 531-7.
- CAHILL, C. M., MORINVILLE, A., LEE, M. C., VINCENT, J. P., COLLIER, B. & BEAUDET, A. 2001. Prolonged morphine treatment targets delta opioid receptors to neuronal plasma membranes and enhances delta-mediated antinociception. *J Neurosci*, 21, 7598-607.
- CALO, G., GUERRINI, R., RIZZI, A., SALVADORI, S., BURMEISTER, M., KAPUSTA, D. R., LAMBERT, D. G. & REGOLI, D. 2005. UFP-101, a peptide antagonist selective for the nociceptin/orphanin FQ receptor. *CNS Drug Rev*, 11, 97-112.
- CALVINO, B. & GRILO, R. M. 2006. Central pain control. *Joint Bone Spine*, 73, 10-16.
- CAO, J. L., HE, J. H., DING, H. L. & ZENG, Y. M. 2005. Activation of the spinal ERK signaling pathway contributes naloxone-precipitated withdrawal in morphine-dependent rats. *Pain*, 118, 336-49.
- CAO, J. L., LIU, H. L., WANG, J. K. & ZENG, Y. M. 2006. Cross talk between nitric oxide and ERK1/2 signaling pathway in the spinal cord mediates naloxone-precipitated withdrawal in morphine-dependent rats. *Neuropharmacology*, 51, 315-26.
- CARLEZON, W. A., JR., DUMAN, R. S. & NESTLER, E. J. 2005. The many faces of CREB. *Trends Neurosci*, 28, 436-45.
- CHEN, Y. & SOMMER, C. 2009. The Role of Mitogen-Activated Protein Kinase (MAPK) in Morphine Tolerance and Dependence. *Molecular Neurobiology*, 40, 101-107.
- CHENG, P. Y., LIU-CHEN, L.-Y. & PICKEL, V. M. 1997. Dual ultrastructural immunocytochemical labeling of μ and δ opioid receptors in the superficial layers of the rat cervical spinal cord. *Brain Research*, 778, 367-380.
- CHENG, Y. & PRUSOFF, W. H. 1973. Relationship between the inhibition constant (K₁) and the concentration of inhibitor which causes 50 per cent inhibition (I₅₀) of an enzymatic reaction. *Biochem Pharmacol*, 22, 3099-108.
- CHIENG, B. & CHRISTIE, M. D. 1996. Local opioid withdrawal in rat single periaqueductal gray neurons in vitro. *J Neurosci*, 16, 7128-36.
- CHIENG, B. & CHRISTIE, M. J. 2009. Chronic morphine treatment induces functional delta-opioid receptors in amygdala neurons that project to periaqueductal grey. *Neuropharmacology*, 57, 430-7.
- CHRISTIE, M. J. 2008. Cellular neuroadaptations to chronic opioids: tolerance, withdrawal and addiction. *Br J Pharmacol*, 154, 384-96.
- CHUNG, S., POHL, S., ZENG, J., CIVELLI, O. & REINSCHEID, R. K. 2006. Endogenous orphanin FQ/nociceptin is involved in the development of morphine tolerance. *J Pharmacol Exp Ther*, 318, 262-7.
- CICCARELLI, A., CALZA, A., SANTORU, F., GRASSO, F., CONCAS, A., SASSOÈ-POGNETTO, M. & GIUSTETTO, M. 2013. Morphine withdrawal produces ERK-dependent and ERK-independent epigenetic marks in neurons of the nucleus accumbens and lateral septum. *Neuropharmacology*, 70, 168-179.
- CICCOCIOPPO, R., ANGELETTI, S., SANNA, P. P., WEISS, F. & MASSI, M. 2000. Effect of nociceptin/orphanin FQ on the rewarding properties of morphine. *Eur J Pharmacol*, 404, 153-9.
- CICCOCIOPPO, R., ECONOMIDOU, D., FEDELI, A. & MASSI, M. 2003. The nociceptin/orphanin FQ/NOP receptor system as a target for treatment of alcohol abuse: a review of recent work in alcohol-preferring rats. *Physiol Behav*, 79, 121-8.
- CLAYTON, C. C., XU, M. & CHAVKIN, C. 2009. Tyrosine phosphorylation of Kir3 following kappa-opioid receptor activation of p38 MAPK causes heterologous desensitization. *J Biol Chem*, 284, 31872-81.
- CONKLIN, B. R., FARFEL, Z., LUSTIG, K. D., JULIUS, D. & BOURNE, H. R. 1993. Substitution of three amino acids switches receptor specificity of Gq alpha to that of Gi alpha. *Nature*, 363, 274-6.

- CORNISH, J. L., LONTOS, J. M., CLEMENS, K. J. & MCGREGOR, I. S. 2005. Cocaine and heroin ('speedball') self-administration: the involvement of nucleus accumbens dopamine and mu-opiate, but not delta-opiate receptors. *Psychopharmacology (Berl)*, 180, 21-32.
- CRAIK, D. J., FAIRLIE, D. P., LIRAS, S. & PRICE, D. 2013. The Future of Peptide-based Drugs. *Chemical Biology & Drug Design*, 81, 136-147.
- CREMEANS, C., GRULEY, E., KYLE, D. & KO, M.-C. 2012. Roles of Mu Opioid Receptors and Nociceptin/Orphanin FQ Peptide Receptors in Buprenorphine-Induced Physiological Responses in Primates. *Journal of Pharmacology and Experimental Therapeutics*.
- CUADRADO, A. N., ANGEL R 2010. Mechanisms and functions of p38 MAPK signalling. *Biochemical Journal*, 429, 403-417.
- CUI, Y., CHEN, Y., ZHI, J. L., GUO, R. X., FENG, J. Q. & CHEN, P. X. 2006. Activation of p38 mitogen-activated protein kinase in spinal microglia mediates morphine antinociceptive tolerance. *Brain Res*, 1069, 235-43.
- DANIELS, D. J., LENARD, N. R., ETIENNE, C. L., LAW, P.-Y., ROERIG, S. C. & PORTOGHESE, P. S. 2005. Opioid-induced tolerance and dependence in mice is modulated by the distance between pharmacophores in a bivalent ligand series. *Proceedings of the National Academy of Sciences of the United States of America*, 102, 19208-19213.
- DASCAL, N. 2001. Ion-channel regulation by G proteins. *Trends in Endocrinology & Metabolism*, 12, 391-398.
- DAVID, V., MATIFAS, A., GAVELLO-BAUDY, S., DECORTE, L., KIEFFER, B. L. & CAZALA, P. 2008. Brain regional Fos expression elicited by the activation of mu- but not delta-opioid receptors of the ventral tegmental area: evidence for an implication of the ventral thalamus in opiate reward. *Neuropsychopharmacology*, 33, 1746-59.
- DAVIS, K. L. 2002. *Neuropsychopharmacology: the fifth generation of progress: an official publication of the American College of Neuropsychopharmacology*, Lippincott Williams & Wilkins.
- DÉCAILLOT, F. M., ROZENFELD, R., GUPTA, A. & DEVI, L. A. 2008. Cell surface targeting of μ - δ opioid receptor heterodimers by RTP4. *Proceedings of the National Academy of Sciences*, 105, 16045-16050.
- DEL GIUDICE, M. R., BORIONI, A., BASTANZIO, G., SBRACCIA, M., MUSTAZZA, C. & SESTILI, I. 2011. Synthesis and pharmacological evaluation of bivalent antagonists of the nociceptin opioid receptor. *European Journal of Medicinal Chemistry*, 46, 1207-1221.
- DI GIANNUARIO, A. & PIERETTI, S. 2000. Nociceptin differentially affects morphine-induced dopamine release from the nucleus accumbens and nucleus caudate in rats. *Peptides*, 21, 1125-30.
- DIETIS, N. 2012. Strategies to Reduce Morphine Tolerance in Cancer: Evaluation of the Bifunctional Opioid UFP-505.
- DIETIS, N., GUERRINI, R., CALO, G., SALVADORI, S., ROWBOTHAM, D. J. & LAMBERT, D. G. 2009. Simultaneous targeting of multiple opioid receptors: a strategy to improve side-effect profile. *British Journal of Anaesthesia*, 103, 38-49.
- DIETIS, N., MCDONALD, J., MOLINARI, S., CALO, G., GUERRINI, R., ROWBOTHAM, D. J. & LAMBERT, D. G. 2012. Pharmacological characterization of the bifunctional opioid ligand H-Dmt-Tic-Gly-NH-Bzl (UFP-505). *British Journal of Anaesthesia*, 108, 262-270.
- DISCOVERX. 2013. *PathHunter® β -Arrestin GPCR Assay Platform* [Online]. Available: <http://www.discoverx.com/technologies-platforms/enzyme-fragment-complementation-technology/pathhunter-efc-cell-based-assay-platform/protein-protein-interactions/gpcrs-b-arrestin> [Accessed July 21, 2014 2014].
- EDWARDS, I. R. & ARONSON, J. K. 2000. Adverse drug reactions: definitions, diagnosis, and management. *The Lancet*, 356, 1255-1259.
- ELLIS, C. 2004. The state of GPCR research in 2004. *Nat Rev Drug Discov*, 3

- ENQUIST, J., KIM, J. A., BARTLETT, S., FERWERDA, M. & WHISTLER, J. L. 2011. A novel knock-in mouse reveals mechanistically distinct forms of morphine tolerance. *J Pharmacol Exp Ther*, 338, 633-40.
- ERBS, E., FAGET, L., SCHERRER, G., MATIFAS, A., FILLIOL, D., VONESCH, J.-L., KOCH, M., KESSLER, P., HENTSCH, D., BIRLING, M.-C., KOUTSOURAKIS, M., VASSEUR, L., VEINANTE, P., KIEFFER, B. & MASSOTTE, D. 2014. A mu-delta opioid receptor brain atlas reveals neuronal co-occurrence in subcortical networks. *Brain Structure and Function*, 1-26.
- EVANS, C. J. 2004. Secrets of the opium poppy revealed. *Neuropharmacology*, 47, Supplement 1, 293-299.
- EVANS, C. J., KEITH, D. E., JR., MORRISON, H., MAGENDZO, K. & EDWARDS, R. H. 1992. Cloning of a delta opioid receptor by functional expression. *Science*, 258, 1952-5.
- EVANS, R. M., YOU, H., HAMEED, S., ALTIER, C., MEZGHRANI, A., BOURINET, E. & ZAMPONI, G. W. 2010. Heterodimerization of ORL1 and opioid receptors and its consequences for N-type calcium channel regulation. *J Biol Chem*, 285, 1032-40.
- FAN, T., VARGHESE, G., NGUYEN, T., TSE, R., O'DOWD, B. F. & GEORGE, S. R. 2005. A role for the distal carboxyl tails in generating the novel pharmacology and G protein activation profile of mu and delta opioid receptor hetero-oligomers. *J Biol Chem*, 280, 38478-88.
- FAURE, M., VOYNO-YASENETSKAYA, T. A. & BOURNE, H. R. 1994. cAMP and beta gamma subunits of heterotrimeric G proteins stimulate the mitogen-activated protein kinase pathway in COS-7 cells. *Journal of Biological Chemistry*, 269, 7851-7854.
- FERRER-ALCON, M., GARCIA-FUSTER, M. J., LA HARPE, R. & GARCIA-SEVILLA, J. A. 2004. Long-term regulation of signalling components of adenylyl cyclase and mitogen-activated protein kinase in the pre-frontal cortex of human opiate addicts. *J Neurochem*, 90, 220-30.
- FIELDS, H. 2004. State-dependent opioid control of pain. *Nat Rev Neurosci*, 5, 565-575.
- FILIZOLA, M., OLMEA, O. & WEINSTEIN, H. 2002. Prediction of heterodimerization interfaces of G-protein coupled receptors with a new subtractive correlated mutation method. *Protein Eng*, 15, 881-5.
- FINN, A. K. & WHISTLER, J. L. 2001. Endocytosis of the Mu Opioid Receptor Reduces Tolerance and a Cellular Hallmark of Opiate Withdrawal. *Neuron*, 32, 829-839.
- FOORD, S. M., BONNER, T. I., NEUBIG, R. R., ROSSER, E. M., PIN, J.-P., DAVENPORT, A. P., SPEDDING, M. & HARMAR, A. J. 2005. International Union of Pharmacology. XLVI. G Protein-Coupled Receptor List. *Pharmacological Reviews*, 57, 279-288.
- FORD, C. P., MARK, G. P. & WILLIAMS, J. T. 2006. Properties and opioid inhibition of mesolimbic dopamine neurons vary according to target location. *J Neurosci*, 26, 2788-97.
- FUJITA, W., GOMES, I. & DEVI, L. A. 2014. Mu-Delta opioid receptor heteromers: New pharmacology and novel therapeutic possibilities. *British Journal of Pharmacology*, n/a-n/a.
- FUKUDA, K., KATO, S., MORIKAWA, H., SHODA, T. & MORI, K. 1996. Functional Coupling of the δ -, μ -, and κ -Opioid Receptors to Mitogen-Activated Protein Kinase and Arachidonate Release in Chinese Hamster Ovary Cells. *Journal of Neurochemistry*, 67, 1309-1316.
- GAVÉRIAUX-RUFF, C. & KIEFFER, B. L. 2002. Opioid receptor genes inactivated in mice: the highlights. *Neuropeptides*, 36, 62-71.
- GENDRON, L., LUCIDO, A. L., MENNICKEN, F., O'DONNELL, D., VINCENT, J. P., STROH, T. & BEAUDET, A. 2006. Morphine and pain-related stimuli enhance cell surface availability of somatic delta-opioid receptors in rat dorsal root ganglia. *J Neurosci*, 26, 953-62.
- GOMES, I., GUPTA, A., FILIPOVSKA, J., SZETO, H. H., PINTAR, J. E. & DEVI, L. A. 2004. A role for heterodimerization of μ and δ opiate receptors in enhancing morphine

- analgesia. *Proceedings of the National Academy of Sciences of the United States of America*, 101, 5135-5139.
- GOMES, I., JORDAN, B., GUPTA, A., TRAPAIDZE, N., NAGY, V. & DEVI, L. 2000. Heterodimerization of μ and δ opioid receptors: a role in opiate synergy. *The Journal of neuroscience: the official journal of the Society for Neuroscience*, 20, RC110.
- GRANIER, S., MANGLIK, A., KRUSE, A. C., KOBILKA, T. S., THIAN, F. S., WEIS, W. I. & KOBILKA, B. K. 2012. Structure of the δ -opioid receptor bound to naltrindole. *Nature*, 485, 400-404.
- GROER, C. E., SCHMID, C. L., JAEGER, A. M. & BOHN, L. M. 2011. Agonist-directed Interactions with Specific β -Arrestins Determine μ -Opioid Receptor Trafficking, Ubiquitination, and Dephosphorylation. *Journal of Biological Chemistry*, 286, 31731-31741.
- GROER, C. E., TIDGEWELL, K., MOYER, R. A., HARDING, W. W., ROTHMAN, R. B., PRISINZANO, T. E. & BOHN, L. M. 2007. An Opioid Agonist that Does Not Induce μ -Opioid Receptor—Arrestin Interactions or Receptor Internalization. *Molecular Pharmacology*, 71, 549-557.
- GUERRINI, R., CALÓ, G., LAMBERT, D. G., CARRÁ, G., ARDUIN, M., BARNES, T. A., MCDONALD, J., RIZZI, D., TRAPPELLA, C., MARZOLA, E., ROWBOTHAM, D. J., REGOLI, D. & SALVADORI, S. 2005. N- and C-Terminal Modifications of Nociceptin/Orphanin FQ Generate Highly Potent NOP Receptor Ligands. *Journal of Medicinal Chemistry*, 48, 1421-1427.
- GUERRINI, R., MARZOLA, E., TRAPPELLA, C., PELA, M., MOLINARI, S., CERLESI, M. C., MALFACINI, D., RIZZI, A., SALVADORI, S. & CALO, G. 2014. A novel and facile synthesis of tetra branched derivatives of nociceptin/orphanin FQ. *Bioorg Med Chem*, 22, 3703-12.
- GUPTA, A., MULDER, J., GOMES, I., ROZENFELD, R., BUSHLIN, I., ONG, E., LIM, M., MAILLET, E., JUNEK, M., CAHILL, C. M., HARKANY, T. & DEVI, L. A. 2010. Increased abundance of opioid receptor heteromers after chronic morphine administration. *Sci Signal*, 3, ra54.
- HABERSTOCK-DEBIC, H., KIM, K. A., YU, Y. J. & VON ZASTROW, M. 2005. Morphine promotes rapid, arrestin-dependent endocytosis of mu-opioid receptors in striatal neurons. *J Neurosci*, 25, 7847-57.
- HACKER, J., PEDERSEN, N. P., CHIENG, B. C., KEAY, K. A. & CHRISTIE, M. J. 2006. Enhanced Fos expression in glutamic acid decarboxylase immunoreactive neurons of the mouse periaqueductal grey during opioid withdrawal. *Neuroscience*, 137, 1389-96.
- HAN, M. H., BOLANOS, C. A., GREEN, T. A., OLSON, V. G., NEVE, R. L., LIU, R. J., AGHAJANIAN, G. K. & NESTLER, E. J. 2006. Role of cAMP response element-binding protein in the rat locus ceruleus: regulation of neuronal activity and opiate withdrawal behaviors. *J Neurosci*, 26, 4624-9.
- HARRISON, C. & TRAYNOR, J. R. 2003. The [35S]GTP γ S binding assay: approaches and applications in pharmacology. *Life Sciences*, 74, 489-508.
- HASBI, A., NGUYEN, T., FAN, T., CHENG, R., RASHID, A., ALIJANIARAM, M., RASENICK, M. M., O'DOWD, B. F. & GEORGE, S. R. 2007. Trafficking of preassembled opioid mu-delta heterooligomer-Gz signaling complexes to the plasma membrane: coregulation by agonists. *Biochemistry*, 46, 12997-3009.
- HE, L., FONG, J., VON ZASTROW, M. & WHISTLER, J. L. 2002. Regulation of Opioid Receptor Trafficking and Morphine Tolerance by Receptor Oligomerization. *Cell*, 108, 271-282.
- HE, S.-Q., ZHANG, Z.-N., GUAN, J.-S., LIU, H.-R., ZHAO, B., WANG, H.-B., LI, Q., YANG, H., LUO, J., LI, Z.-Y., WANG, Q., LU, Y.-J., BAO, L. & ZHANG, X. 2011. Facilitation of μ -Opioid Receptor Activity by Preventing δ -Opioid Receptor-Mediated Codegradation. *Neuron*, 69, 120-131.
- HENDRY, I. A., KELLEHER, K. L., BARTLETT, S. E., LECK, K. J., REYNOLDS, A. J., HEYDON, K., MELLICK, A., MEGIRIAN, D. & MATTHAEI, K. I. 2000. Hypertolerance to morphine in Gz α -deficient mice. *Brain Research*, 870, 10-19.

- HERLITZE, S., GARCIA, D. E., MACKIE, K., HILLE, B., SCHEUER, T. & CATTERALL, W. A. 1996. Modulation of Ca²⁺ channels [beta][gamma] G-protein py subunits. *Nature*, 380, 5.
- HONDA, M., OKUTSU, H., MATSUURA, T., MIYAGI, T., YAMAMOTO, Y., HAZATO, T. & ONO, H. 2001. Spinorphin, an endogenous inhibitor of enkephalin-degrading enzymes, potentiates leu-enkephalin-induced anti-allodynic and antinociceptive effects in mice. *Jpn J Pharmacol*, 87, 261-7.
- HOUTANI, T., NISHI, M., TAKESHIMA, H., SATO, K., SAKUMA, S., KAKIMOTO, S., UEYAMA, T., NODA, T. & SUGIMOTO, T. 2000. Distribution of nociceptin/orphanin FQ precursor protein and receptor in brain and spinal cord: a study using in situ hybridization and X-gal histochemistry in receptor-deficient mice. *J Comp Neurol*, 424, 489-508.
- HUGHES, J., SMITH, T. W., KOSTERLITZ, H. W., FOTHERGILL, L. A., MORGAN, B. A. & MORRIS, H. R. 1975. Identification of two related pentapeptides from the brain with potent opiate agonist activity. *Nature*, 258, 577-80.
- IBBA, M., KITAYAMA, M., MCDONALD, J., CALO, G., GUERRINI, R., FARKAS, J., TOTH, G. & LAMBERT, D. G. 2008. Binding of the novel radioligand [(3)H]UFP-101 to recombinant human and native rat nociceptin/orphanin FQ receptors. *Naunyn Schmiedebergs Arch Pharmacol*, 378, 553-61.
- INGRAM, S. L., VAUGHAN, C. W., BAGLEY, E. E., CONNOR, M. & CHRISTIE, M. J. 1998. Enhanced opioid efficacy in opioid dependence is caused by an altered signal transduction pathway. *J Neurosci*, 18, 10269-76.
- INGRAM, S. L. & WILLIAMS, J. T. 1994. Opioid inhibition of I_h via adenylyl cyclase. *Neuron*, 13, 179-86.
- ITO, H., TUNG, R. T., SUGIMOTO, T., KOBAYASHI, I., TAKAHASHI, K., KATADA, T., UI, M. & KURACHI, Y. 1992. On the mechanism of G protein beta gamma subunit activation of the muscarinic K⁺ channel in guinea pig atrial cell membrane. Comparison with the ATP-sensitive K⁺ channel. *The Journal of General Physiology*, 99, 961-983.
- JANECKA, A., PERLIKOWSKA, R., GACH, K., WYREBSKA, A. & FICHNA, J. 2010. Development of opioid peptide analogs for pain relief. *Curr Pharm Des*, 16, 1126-35.
- JASINSKI, D. R., PEVNICK, J. S. & GRIFFITH, J. D. 1978. Human pharmacology and abuse potential of the analgesic buprenorphine: A potential agent for treating narcotic addiction. *Archives of General Psychiatry*, 35, 501-516.
- JOLAS, T., NESTLER, E. J. & AGHAJANIAN, G. K. 1999. Chronic morphine increases GABA tone on serotonergic neurons of the dorsal raphe nucleus: association with an up-regulation of the cyclic AMP pathway. *Neuroscience*, 95, 433-443.
- JORDAN, B. A. & DEVI, L. A. 1999. G-protein-coupled receptor heterodimerization modulates receptor function. *Nature*, 399, 697-700.
- JUTKIEWICZ, E. M., BALADI, M. G., FOLK, J. E., RICE, K. C. & WOODS, J. H. 2006. The convulsive and electroencephalographic changes produced by nonpeptidic delta-opioid agonists in rats: comparison with pentylentetrazol. *J Pharmacol Exp Ther*, 317, 1337-48.
- KAHSAI, A. W., XIAO, K., RAJAGOPAL, S., AHN, S., SHUKLA, A. K., SUN, J., OAS, T. G. & LEFKOWITZ, R. J. 2011. Multiple ligand-specific conformations of the beta2-adrenergic receptor. *Nat Chem Biol*, 7, 692-700.
- KEITH, D. E., ANTON, B., MURRAY, S. R., ZAKI, P. A., CHU, P. C., LISSIN, D. V., MONTEILLET-AGIUS, G., STEWART, P. L., EVANS, C. J. & ZASTROW, M. V. 1998. μ -Opioid Receptor Internalization: Opiate Drugs Have Differential Effects on a Conserved Endocytic Mechanism In Vitro and in the Mammalian Brain. *Molecular Pharmacology*, 53, 377-384.
- KEITH, D. E., MURRAY, S. R., ZAKI, P. A., CHU, P. C., LISSIN, D. V., KANG, L., EVANS, C. J. & VON ZASTROW, M. 1996. Morphine Activates Opioid Receptors without Causing Their Rapid Internalization. *Journal of Biological Chemistry*, 271, 19021-19024.

- KENAKIN, T. 2011. Functional Selectivity and Biased Receptor Signaling. *Journal of Pharmacology and Experimental Therapeutics*, 336, 296-302.
- KERCHNER, G. A. & ZHUO, M. 2002. Presynaptic Suppression of Dorsal Horn Inhibitory Transmission by μ -Opioid Receptors. *Journal of Neurophysiology*, 88, 520-522.
- KEST, B., HOPKINS, E., PALMESE, C. A., CHEN, Z. P., MOGIL, J. S. & PINTAR, J. E. 2001. Morphine tolerance and dependence in nociceptin/orphanin fq transgenic knockout mice. *Neuroscience*, 104, 217-222.
- KEST, B., LEE, C. E., MCLEMORE, G. L. & INTURRISI, C. E. 1996. An antisense oligodeoxynucleotide to the delta opioid receptor (DOR-1) inhibits morphine tolerance and acute dependence in mice. *Brain Res Bull*, 39, 185-8.
- KHROYAN, T. V., POLGAR, W. E., JIANG, F., ZAVERI, N. T. & TOLL, L. 2009a. Nociceptin/orphanin FQ receptor activation attenuates antinociception induced by mixed nociceptin/orphanin FQ/ μ -opioid receptor agonists. *J Pharmacol Exp Ther*, 331, 946-53.
- KHROYAN, T. V., POLGAR, W. E., JIANG, F., ZAVERI, N. T. & TOLL, L. 2009b. NOP Receptor Activation Attenuates Antinociception Induced by Mixed NOP/ μ -Opioid Receptor Agonists. *Journal of Pharmacology and Experimental Therapeutics*.
- KHROYAN, T. V., ZAVERI, N. T., POLGAR, W. E., ORDUNA, J., OLSEN, C., JIANG, F. & TOLL, L. 2007. SR 16435 [1-(1-(bicyclo[3.3.1]nonan-9-yl)piperidin-4-yl)indolin-2-one], a novel mixed nociceptin/orphanin FQ/ μ -opioid receptor partial agonist: analgesic and rewarding properties in mice. *J Pharmacol Exp Ther*, 320, 934-43.
- KIEFFER, B. L. 1999. Opioids: first lessons from knockout mice. *Trends Pharmacol Sci*, 20, 19-26.
- KIEFFER, B. L., BEFORT, K., GAVERIAUX-RUFF, C. & HIRTH, C. G. 1992. The delta-opioid receptor: isolation of a cDNA by expression cloning and pharmacological characterization. *Proc Natl Acad Sci U S A*, 89, 12048-52.
- KIM, O.-J., GARDNER, B. R., WILLIAMS, D. B., MARINEC, P. S., CABRERA, D. M., PETERS, J. D., MAK, C. C., KIM, K.-M. & SIBLEY, D. R. 2004. The Role of Phosphorylation in D1 Dopamine Receptor Desensitization: EVIDENCE FOR A NOVEL MECHANISM OF ARRESTIN ASSOCIATION. *Journal of Biological Chemistry*, 279, 7999-8010.
- KING, M. A., ROSSI, G. C., CHANG, A. H., WILLIAMS, L. & PASTERNAK, G. W. 1997. Spinal analgesic activity of orphanin FQ/nociceptin and its fragments. *Neurosci Lett*, 223, 113-6.
- KO, M. C. & NAUGHTON, N. N. 2009. Antinociceptive effects of nociceptin/orphanin FQ administered intrathecally in monkeys. *J Pain*, 10, 509-16.
- KO, M. C., WOODS, J. H., FANTEGROSSI, W. E., GALUSKA, C. M., WICHMANN, J. & PRINSSSEN, E. P. 2009. Behavioral effects of a synthetic agonist selective for nociceptin/orphanin FQ peptide receptors in monkeys. *Neuropsychopharmacology*, 34, 2088-96.
- KO, M. C. H., WEI, H., WOODS, J. H. & KENNEDY, R. T. 2006. Effects of Intrathecally Administered Nociceptin/Orphanin FQ in Monkeys: Behavioral and Mass Spectrometric Studies. *Journal of Pharmacology and Experimental Therapeutics*, 318, 1257-1264.
- KOCH, W. J., HAWES, B. E., ALLEN, L. F. & LEFKOWITZ, R. J. 1994. Direct evidence that Gi-coupled receptor stimulation of mitogen-activated protein kinase is mediated by G beta gamma activation of p21ras. *Proceedings of the National Academy of Sciences*, 91, 12706-12710.
- KOFUJI, P., DAVIDSON, N. & LESTER, H. A. 1995. Evidence that neuronal G-protein-gated inwardly rectifying K⁺ channels are activated by G beta gamma subunits and function as heteromultimers. *Proceedings of the National Academy of Sciences*, 92, 6542-6546.
- KOHOUT, T. A. & LEFKOWITZ, R. J. 2003. Regulation of G Protein-Coupled Receptor Kinases and Arrestins During Receptor Desensitization. *Molecular Pharmacology*, 63, 9-18.

- KOOB, G. F. & VOLKOW, N. D. 2010. Neurocircuitry of addiction. *Neuropsychopharmacology*, 35, 217-38.
- KUTYAVIN, I. V., AFONINA, I. A., MILLS, A., GORN, V. V., LUKHTANOV, E. A., BELOUSOV, E. S., SINGER, M. J., WALBURGER, D. K., LOKHOV, S. G., GALL, A. A., DEMPCY, R., REED, M. W., MEYER, R. B. & HEDGPETH, J. 2000. 3'-minor groove binder-DNA probes increase sequence specificity at PCR extension temperatures. *Nucleic Acids Res*, 28, 655-61.
- LAMBERT, D. G. 2008. The nociceptin/orphanin FQ receptor: a target with broad therapeutic potential. *Nat Rev Drug Discov*, 7, 694-710.
- LAW, P. Y., WONG, Y. H. & LOH, H. H. 2000. Molecular mechanisms and regulation of opioid receptor signaling. *Annu Rev Pharmacol Toxicol*, 40, 389-430.
- LE MERRER, J., BECKER, J. A., BEFORT, K. & KIEFFER, B. L. 2009. Reward processing by the opioid system in the brain. *Physiol Rev*, 89, 1379-412.
- LECK, K. J., BARTLETT, S. E., SMITH, M. T., MEGIRIAN, D., HOLGATE, J., POWELL, K. L., MATTHAEI, K. I. & HENDRY, I. A. 2004. Deletion of guanine nucleotide binding protein alpha z subunit in mice induces a gene dose dependent tolerance to morphine. *Neuropharmacology*, 46, 836-46.
- LEINCO TECHNOLOGIES. 2014. *General Western Blot protocol* [Online]. Available: http://www.leinco.com/general_wb [Accessed 01/10/2014].
- LI, S. X., WANG, Z. R., LI, J., PENG, Z. G., ZHOU, W., ZHOU, M. & LU, L. 2008. Inhibition of Period1 gene attenuates the morphine-induced ERK-CREB activation in frontal cortex, hippocampus, and striatum in mice. *Am J Drug Alcohol Abuse*, 34, 673-82.
- LINZ, K., CHRISTOPH, T., TZSCHENTKE, T. M., KOCH, T., SCHIENE, K., GAUTROIS, M., SCHRODER, W., KOGEL, B. Y., BEIER, H., ENGLBERGER, W., SCHUNK, S., DE VRY, J., JAHNEL, U. & FROSCH, S. 2014. Cebranopadol: a novel potent analgesic nociceptin/orphanin FQ peptide and opioid receptor agonist. *J Pharmacol Exp Ther*, 349, 535-48.
- LIU, X., KAI, M., JIN, L. & WANG, R. 2009. Computational study of the heterodimerization between mu and delta receptors. *J Comput Aided Mol Des*, 23, 321-32.
- LIU, Y. Q., ZHANG, Y. Z. & GAO, P. J. 2004. Novel Concentration-Killing Curve Method for Estimation of Bactericidal Potency of Antibiotics in an In Vitro Dynamic Model. *Antimicrobial Agents and Chemotherapy*, 48, 3884-3891.
- LOHSE, M. J., MAIELLARO, I. & CALEBIRO, D. 2014. Kinetics and mechanism of G protein-coupled receptor activation. *Current Opinion in Cell Biology*, 27, 87-93.
- LORD, J. A., WATERFIELD, A. A., HUGHES, J. & KOSTERLITZ, H. W. 1977. Endogenous opioid peptides: multiple agonists and receptors. *Nature*, 267, 495-9.
- LOWRY, O. H., ROSEBROUGH, N. J., FARR, A. L. & RANDALL, R. J. 1951. Protein measurement with the Folin phenol reagent. *J Biol Chem*, 193, 265-75.
- MA, J. & PAN, Z. Z. 2006. Contribution of brainstem GABA(A) synaptic transmission to morphine analgesic tolerance. *Pain*, 122, 163-73.
- MA, W., ZHENG, W. H., POWELL, K., JHAMANDAS, K. & QUIRION, R. 2001. Chronic morphine exposure increases the phosphorylation of MAP kinases and the transcription factor CREB in dorsal root ganglion neurons: an in vitro and in vivo study. *Eur J Neurosci*, 14, 1091-104.
- MACEY, T. A., LOWE, J. D. & CHAVKIN, C. 2006. Mu Opioid Receptor Activation of ERK1/2 Is GRK3 and Arrestin Dependent in Striatal Neurons. *Journal of Biological Chemistry*, 281, 34515-34524.
- MADSEN, B. W., BEGLAN, C. L. & SPIVAK, C. E. 2000. Fluorescein-labeled naloxone binding to mu opioid receptors on live Chinese hamster ovary cells using confocal fluorescent microscopy. *J Neurosci Methods*, 97, 123-31.
- MAHMOOD, T. & YANG, P. C. 2012. Western blot: technique, theory, and trouble shooting. *N Am J Med Sci*, 4, 429-34.
- MAHMOUD, S., MARGAS, W., TRAPPELLA, C., CALO, G. & RUIZ-VELASCO, V. 2010. Modulation of silent and constitutively active nociceptin/orphanin FQ receptors by

- potent receptor antagonists and Na⁺ ions in rat sympathetic neurons. *Mol Pharmacol*, 77, 804-17.
- MANDYAM, C. D., THAKKER, D. R., CHRISTENSEN, J. L. & STANDIFER, K. M. 2002. Orphanin FQ/nociceptin-mediated desensitization of opioid receptor-like 1 receptor and mu opioid receptors involves protein kinase C: a molecular mechanism for heterologous cross-talk. *J Pharmacol Exp Ther*, 302, 502-9.
- MANDYAM, C. D., THAKKER, D. R. & STANDIFER, K. M. 2003. Mu-opioid-induced desensitization of opioid receptor-like 1 and mu-opioid receptors: differential intracellular signaling determines receptor sensitivity. *J Pharmacol Exp Ther*, 306, 965-72.
- MANGLIK, A., KRUSE, A. C., KOBILKA, T. S., THIAN, F. S., MATHIESEN, J. M., SUNAHARA, R. K., PARDO, L., WEIS, W. I., KOBILKA, B. K. & GRANIER, S. 2012. Crystal structure of the [micro]-opioid receptor bound to a morphinan antagonist. *Nature*, 485, 321-326.
- MARINELLI, S., VAUGHAN, C. W., SCHNELL, S. A., WESSENDORF, M. W. & CHRISTIE, M. J. 2002. Rostral Ventromedial Medulla Neurons That Project to the Spinal Cord Express Multiple Opioid Receptor Phenotypes. *The Journal of Neuroscience*, 22, 10847-10855.
- MARTINI, L. & WHISTLER, J. L. 2007. The role of mu opioid receptor desensitization and endocytosis in morphine tolerance and dependence. *Current Opinion in Neurobiology*, 17, 556-564.
- MASSOTTE, D., BRILLET, K., KIEFFER, B. & MILLIGAN, G. 2002. Agonists activate Gi1 α or Gi2 α fused to the human mu opioid receptor differently. *Journal of Neurochemistry*, 81, 1372-1382.
- MATTHES, H. W., MALDONADO, R., SIMONIN, F., VALVERDE, O., SLOWE, S., KITCHEN, I., BEFORT, K., DIERICH, A., LE MEUR, M., DOLLE, P., TZAVARA, E., HANOUNE, J., ROQUES, B. P. & KIEFFER, B. L. 1996. Loss of morphine-induced analgesia, reward effect and withdrawal symptoms in mice lacking the mu-opioid-receptor gene. *Nature*, 383, 819-23.
- MAZEI-ROBISON, M. S. & NESTLER, E. J. 2012. Opiate-Induced Molecular and Cellular Plasticity of Ventral Tegmental Area and Locus Coeruleus Catecholamine Neurons. *Cold Spring Harbor Perspectives in Medicine*, 2.
- MCBRIDE, W. J., MURPHY, J. M. & IKEMOTO, S. 1999. Localization of brain reinforcement mechanisms: intracranial self-administration and intracranial place-conditioning studies. *Behav Brain Res*, 101, 129-52.
- MCDONALD, J., BARNES, T. A., OKAWA, H., WILLIAMS, J., CALO, G., ROWBOTHAM, D. J. & LAMBERT, D. G. 2003a. Partial agonist behaviour depends upon the level of nociceptin/orphanin FQ receptor expression: studies using the ecdysone-inducible mammalian expression system. *British Journal of Pharmacology*, 140, 61-70.
- MCDONALD, J., CALO, G., GUERRINI, R. & LAMBERT, D. G. 2003b. UFP-101, a high affinity antagonist for the nociceptin/orphanin FQ receptor: radioligand and GTP γ 35S binding studies. *Naunyn-Schmiedeberg's Archives of Pharmacology*, 367, 183-187.
- MCDONALD, J. & LAMBERT, D. 2005. Opioid receptors. *Continuing Education in Anaesthesia, Critical Care & Pain*, 5, 22-25.
- MCNALLY, G. P. & AKIL, H. 2003. Selective down-regulation of hippocampal glucocorticoid receptors during opiate withdrawal. *Molecular Brain Research*, 118, 152-155.
- MELCHIORRI, P. & NEGRI, L. 1996. The dermorphin peptide family. *Gen Pharmacol*, 27, 1099-107.
- MELZACK, W. A. 1965. Pain Mechanism: A New Theory. *Science*, 150, 971-979.
- MEUNIER, J. C., MOLLEREAU, C., TOLL, L., SUAUDEAU, C., MOISAND, C., ALVINERIE, P., BUTOUR, J. L., GUILLEMOT, J. C., FERRARA, P., MONSARRAT, B. & ET AL. 1995. Isolation and structure of the endogenous agonist of opioid receptor-like ORL1 receptor. *Nature*, 377, 532-5.

- MIYATAKE, M., RUBINSTEIN, T. J., MCLENNAN, G. P., BELCHEVA, M. M. & COSCIA, C. J. 2009. Inhibition of EGF-induced ERK/MAP kinase-mediated astrocyte proliferation by μ opioids: integration of G protein and β -arrestin 2-dependent pathways. *Journal of Neurochemistry*, 110, 662-674.
- MOLINARI, S., CAMARDA, V., RIZZI, A., MARZOLA, G., SALVADORI, S., MARZOLA, E., MOLINARI, P., MCDONALD, J., KO, M. C., LAMBERT, D. G., CALO, G. & GUERRINI, R. 2013. [Dmt1]N/OFQ(1-13)-NH₂: a potent nociceptin/orphanin FQ and opioid receptor universal agonist. *Br J Pharmacol*, 168, 151-62.
- MONTEILLET-AGIUS, G., FEIN, J., ANTON, B. & EVANS, C. J. 1998. ORL-1 and mu opioid receptor antisera label different fibers in areas involved in pain processing. *J Comp Neurol*, 399, 373-83.
- MOULÉDOUS, L., DÍAZ, M. F. & GUTSTEIN, H. B. 2007. Extracellular signal-regulated kinase (ERK) inhibition does not prevent the development or expression of tolerance to and dependence on morphine in the mouse. *Pharmacology Biochemistry and Behavior*, 88, 39-46.
- MULLER, D. L. & UNTERWALD, E. M. 2004. In vivo regulation of extracellular signal-regulated protein kinase (ERK) and protein kinase B (Akt) phosphorylation by acute and chronic morphine. *J Pharmacol Exp Ther*, 310, 774-82.
- MURPHY, N. P. & MAIDMENT, N. T. 1999. Orphanin FQ/nociceptin modulation of mesolimbic dopamine transmission determined by microdialysis. *J Neurochem*, 73, 179-86.
- NEAL, C. R., JR., MANSOUR, A., REINSCHIED, R., NOTHACKER, H. P., CIVELLI, O., AKIL, H. & WATSON, S. J., JR. 1999a. Opioid receptor-like (ORL1) receptor distribution in the rat central nervous system: comparison of ORL1 receptor mRNA expression with (125)I-[(14)Tyr]-orphanin FQ binding. *J Comp Neurol*, 412, 563-605.
- NEAL, C. R., JR., MANSOUR, A., REINSCHIED, R., NOTHACKER, H. P., CIVELLI, O. & WATSON, S. J., JR. 1999b. Localization of orphanin FQ (nociceptin) peptide and messenger RNA in the central nervous system of the rat. *J Comp Neurol*, 406, 503-47.
- NELSON, L. & SCHWANER, R. 2009. Transdermal fentanyl: pharmacology and toxicology. *J Med Toxicol*, 5, 230-41.
- NERSESYAN, H. & SLAVIN, K. V. 2007. Current approach to cancer pain management: Availability and implications of different treatment options. *Ther Clin Risk Manag*, 3, 381-400.
- NESTLER, E. J. 2012. Transcriptional mechanisms of drug addiction. *Clin Psychopharmacol Neurosci*, 10, 136-43.
- NITSCHKE, J. F., SCHULLER, A. G. P., KING, M. A., ZENGH, M., PASTERNAK, G. W. & PINTAR, J. E. 2002. Genetic Dissociation of Opiate Tolerance and Physical Dependence in δ -Opioid Receptor-1 and Preproenkephalin Knock-Out Mice. *The Journal of Neuroscience*, 22, 10906-10913.
- NOBLES, K. N., XIAO, K., AHN, S., SHUKLA, A. K., LAM, C. M., RAJAGOPAL, S., STRACHAN, R. T., HUANG, T. Y., BRESSLER, E. A., HARA, M. R., SHENOY, S. K., GYGI, S. P. & LEFKOWITZ, R. J. 2011. Distinct phosphorylation sites on the beta(2)-adrenergic receptor establish a barcode that encodes differential functions of beta-arrestin. *Sci Signal*, 4, ra51.
- OLIANAS, M. C., DEDONI, S., BOI, M. & ONALI, P. 2008. Activation of nociceptin/orphanin FQ-NOP receptor system inhibits tyrosine hydroxylase phosphorylation, dopamine synthesis, and dopamine D1 receptor signaling in rat nucleus accumbens and dorsal striatum. *Journal of Neurochemistry*, 107, 544-556.
- ONG, E. & CAHILL, C. 2014. Molecular Perspectives for mu/delta Opioid Receptor Heteromers as Distinct, Functional Receptors. *Cells*, 3, 152-179.
- PAN, Y.-X., BOLAN, E. & PASTERNAK, G. W. 2002. Dimerization of morphine and orphanin FQ/nociceptin receptors: generation of a novel opioid receptor subtype. *Biochemical and Biophysical Research Communications*, 297, 659-663.

- PAN, Z. Z., HIRAKAWA, N. & FIELDS, H. L. 2000. A Cellular Mechanism for the Bidirectional Pain-Modulating Actions of Orphanin FQ/Nociceptin. *Neuron*, 26, 515-522.
- PIERCE, K. L. & LEFKOWITZ, R. J. 2001. Classical and new roles of beta-arrestins in the regulation of G-protein-coupled receptors. *Nat Rev Neurosci*, 2, 727-33.
- PITCHER, J. A., FREEDMAN, N. J. & LEFKOWITZ, R. J. 1998. G protein-coupled receptor kinases. *Annu Rev Biochem*, 67, 653-92.
- PODOLSKY, A. T., SANDWEISS, A., HU, J., BILSKY, E. J., CAIN, J. P., KUMIROV, V. K., LEE, Y. S., HRUBY, V. J., VARDANYAN, R. S. & VANDERAH, T. W. 2013. Novel fentanyl-based dual mu/delta-opioid agonists for the treatment of acute and chronic pain. *Life Sci*, 93, 1010-6.
- POLAKIEWICZ, R. D., SCHIEFERL, S. M., DORNER, L. F., KANSRA, V. & COMB, M. J. 1998a. A mitogen-activated protein kinase pathway is required for mu-opioid receptor desensitization. *J Biol Chem*, 273, 12402-6.
- POLAKIEWICZ, R. D., SCHIEFERL, S. M., GINGRAS, A. C., SONENBERG, N. & COMB, M. J. 1998b. mu-Opioid receptor activates signaling pathways implicated in cell survival and translational control. *J Biol Chem*, 273, 23534-41.
- PRADHAN, A. A., BEFORT, K., NOZAKI, C., GAVÉRIAUX-RUFF, C. & KIEFFER, B. L. 2011. The delta opioid receptor: an evolving target for the treatment of brain disorders. *Trends in Pharmacological Sciences*, 32, 581-590.
- PRADHAN, A. A., SMITH, M. L., KIEFFER, B. L. & EVANS, C. J. 2012. Ligand-directed signalling within the opioid receptor family. *British Journal of Pharmacology*, 167, 960-969.
- PREMONT, R. T. & GAINETDINOV, R. R. 2007. Physiological roles of G protein-coupled receptor kinases and arrestins. *Annu Rev Physiol*, 69, 511-34.
- PRINSTER, S. C., HAGUE, C. & HALL, R. A. 2005. Heterodimerization of g protein-coupled receptors: specificity and functional significance. *Pharmacol Rev*, 57, 289-98.
- PUNCH, L. J., SELF, D. W., NESTLER, E. J. & TAYLOR, J. R. 1997. Opposite modulation of opiate withdrawal behaviors on microinfusion of a protein kinase A inhibitor versus activator into the locus coeruleus or periaqueductal gray. *J Neurosci*, 17, 8520-7.
- RAEHAL, K. M., SCHMID, C. L., GROER, C. E. & BOHN, L. M. 2011. Functional Selectivity at the μ -Opioid Receptor: Implications for Understanding Opioid Analgesia and Tolerance. *Pharmacological Reviews*, 63, 1001-1019.
- RAEHAL, K. M., WALKER, J. K. L. & BOHN, L. M. 2005. Morphine Side Effects in β -Arrestin 2 Knockout Mice. *Journal of Pharmacology and Experimental Therapeutics*, 314, 1195-1201.
- RAISCH, D. W., FYE, C. L., BOARDMAN, K. D. & SATHER, M. R. 2002. Opioid Dependence Treatment, Including Buprenorphine/Naloxone. *Annals of Pharmacotherapy*, 36, 312-321.
- RANG, H., DALE, M., RITTER, J. & ROD FLOWER, S. 2007. *Rang & Dale's Pharmacology: With STUDENT CONSULT Online Access (Rang and Dale's Pharmacology)*, Churchill Livingstone.
- RAU, K. K., CAUDLE, R. M., COOPER, B. Y. & JOHNSON, R. D. 2005. Diverse immunocytochemical expression of opioid receptors in electrophysiologically defined cells of rat dorsal root ganglia. *Journal of Chemical Neuroanatomy*, 29, 255-264.
- RIVERO, G., LLORENTE, J., MCPHERSON, J., COOKE, A., MUNDELL, S. J., MCARDLE, C. A., ROSETHORNE, E. M., CHARLTON, S. J., KRASEL, C., BAILEY, C. P., HENDERSON, G. & KELLY, E. 2012. Endomorphin-2: a biased agonist at the mu-opioid receptor. *Mol Pharmacol*, 82, 178-88.
- RIZZI, A., MALFACINI, D., CERLESI, M. C., RUZZA, C., MARZOLA, E., BIRD, M. F., ROWBOTHAM, D. J., SEVERO, S., GUERRINI, R., LAMBERT, D. G. & CALO, G. 2014. In vitro and in vivo pharmacological characterization of nociceptin/orphanin FQ tetrabranch derivatives. *Br J Pharmacol*.

- ROMINGER, D. H., COWAN, C. L., GOWEN-MACDONALD, W. & VIOLIN, J. D. 2014. Biased ligands: pathway validation for novel GPCR therapeutics. *Current Opinion in Pharmacology*, 16, 108-115.
- ROSS, J. & ARMSTEAD, W. M. 2005. NOC/oFQ activates ERK and JNK but not p38 MAPK to impair prostaglandin cerebrovasodilation after brain injury. *Brain Research*, 1054, 95-102.
- ROUX, P. P. & BLENIS, J. 2004. ERK and p38 MAPK-Activated Protein Kinases: a Family of Protein Kinases with Diverse Biological Functions. *Microbiology and Molecular Biology Reviews*, 68, 320-344.
- ROZENFELD, R. & DEVI, L. A. 2007. Receptor heterodimerization leads to a switch in signaling: β -arrestin2-mediated ERK activation by μ - δ opioid receptor heterodimers. *The FASEB Journal*, 21, 2455-2465.
- RUTTEN, K., DE VRY, J., BRUCKMANN, W. & TZSCHENTKE, T. M. 2010. Effects of the NOP receptor agonist Ro65-6570 on the acquisition of opiate- and psychostimulant-induced conditioned place preference in rats. *Eur J Pharmacol*, 645, 119-26.
- RUTTEN, K., DE VRY, J., BRUCKMANN, W. & TZSCHENTKE, T. M. 2011. Pharmacological blockade or genetic knockout of the NOP receptor potentiates the rewarding effect of morphine in rats. *Drug and Alcohol Dependence*, 114, 253-256.
- SAAL, D., DONG, Y., BONCI, A. & MALENKA, R. C. 2003. Drugs of abuse and stress trigger a common synaptic adaptation in dopamine neurons. *Neuron*, 37, 577-82.
- SADÉE, W., WANG, D. & BILSKY, E. J. 2005. Basal opioid receptor activity, neutral antagonists, and therapeutic opportunities. *Life Sciences*, 76, 1427-1437.
- SAKOORI, K. & MURPHY, N. P. 2008. Endogenous nociceptin (orphanin FQ) suppresses basal hedonic state and acute reward responses to methamphetamine and ethanol, but facilitates chronic responses. *Neuropsychopharmacology*, 33, 877-91.
- SALVADORI, S., BALBONI, G., GUERRINI, R., TOMATIS, R., BIANCHI, C., BRYANT, S. D., COOPER, P. S. & LAZARUS, L. H. 1997. Evolution of the Dmt-Tic pharmacophore: N-terminal methylated derivatives with extraordinary delta opioid antagonist activity. *J Med Chem*, 40, 3100-8.
- SANCHEZ-BLAZQUEZ, P., GARCIA-ESPANA, A. & GARZON, J. 1997. Antisense oligodeoxynucleotides to opioid mu and delta receptors reduced morphine dependence in mice: role of delta-2 opioid receptors. *J Pharmacol Exp Ther*, 280, 1423-31.
- SCHALLMACH, E., STEINER, D. & VOGEL, Z. 2006. Adenylyl cyclase type II activity is regulated by two different mechanisms: Implications for acute and chronic opioid exposure. *Neuropharmacology*, 50, 998-1005.
- SCHERRER, G., IMAMACHI, N., CAO, Y.-Q., CONTET, C., MENNICKEN, F., O'DONNELL, D., KIEFFER, B. L. & BASBAUM, A. I. 2009. Dissociation of the Opioid Receptor Mechanisms that Control Mechanical and Heat Pain. *Cell*, 137, 1148-1159.
- SCHILLER, P. W., FUNDYTUS, M. E., MEROVITZ, L., WELTROWSKA, G., NGUYEN, T. M., LEMIEUX, C., CHUNG, N. N. & CODERRE, T. J. 1999. The opioid mu agonist/delta antagonist DIPP-NH(2)[Psi] produces a potent analgesic effect, no physical dependence, and less tolerance than morphine in rats. *J Med Chem*, 42, 3520-6.
- SCHOTTENFELD, R. S., PAKES, J. R., OLIVETO, A., ZIEDONIS, D. & KOSTEN, T. R. 1997. Buprenorphine vs methadone maintenance treatment for concurrent opioid dependence and cocaine abuse. *Archives of General Psychiatry*, 54, 713-720.
- SCHRÖDER, W., LAMBERT, D. G., KO, M. C. & KOCH, T. 2014. Functional plasticity of the N/OFQ-NOP receptor system determines analgesic properties of NOP receptor agonists. *British Journal of Pharmacology*, n/a-n/a.
- SCHULZ, S. & HOLLT, V. 1998. Opioid withdrawal activates MAP kinase in locus coeruleus neurons in morphine-dependent rats in vivo. *Eur J Neurosci*, 10, 1196-201.
- SCHULZ, S., SCHREFF, M., NUSS, D., GRAMSCH, C. & HOLLT, V. 1996. Nociceptin/orphanin FQ and opioid peptides show overlapping distribution but not co-localization in pain-modulatory brain regions. *Neuroreport*, 7, 3021-5.

- SEGER, R. & KREBS, E. G. 1995. The MAPK signaling cascade. *The FASEB Journal*, 9, 726-35.
- SESACK, S. R. & GRACE, A. A. 2010. Cortico-Basal Ganglia reward network: microcircuitry. *Neuropsychopharmacology*, 35, 27-47.
- SHARMA, S. K., KLEE, W. A. & NIRENBERG, M. 1975. Dual regulation of adenylate cyclase accounts for narcotic dependence and tolerance. *Proc Natl Acad Sci U S A*, 72, 3092-6.
- SHARMAN, J. L., BENSON, H. E., PAWSON, A. J., LUKITO, V., MPAMHANGA, C. P., BOMBAIL, V., DAVENPORT, A. P., PETERS, J. A., SPEDDING, M., HARMAR, A. J. & NC-IUPHAR 2013. IUPHAR-DB: updated database content and new features. *Nucleic Acids Research*, 41, D1083-D1088.
- SHENOY, S. K. & LEFKOWITZ, R. J. 2011. beta-Arrestin-mediated receptor trafficking and signal transduction. *Trends Pharmacol Sci*, 32, 521-33.
- SIMPSON, A. W. 2006. Fluorescent measurement of [Ca²⁺]_i: basic practical considerations. *Methods Mol Biol*, 312, 3-36.
- SONG, X., COFFA, S., FU, H. & GUREVICH, V. V. 2009. How does arrestin assemble MAPKs into a signaling complex? *J Biol Chem*, 284, 685-95.
- SPAGNOLO, B., CALO, G., POLGAR, W. E., JIANG, F., OLSEN, C. M., BERZETEGURSKE, I., KHROYAN, T. V., HUSBANDS, S. M., LEWIS, J. W., TOLL, L. & ZAVERI, N. T. 2008. Activities of mixed NOP and mu-opioid receptor ligands. *Br J Pharmacol*, 153, 609-19.
- STANLEY, T. H. 1992. The history and development of the fentanyl series. *J Pain Symptom Manage*, 7, S3-7.
- STRANGE, P. G. 2010. Use of the GTPgammaS ([35S]GTPgammaS and Eu-GTPgammaS) binding assay for analysis of ligand potency and efficacy at G protein-coupled receptors. *Br J Pharmacol*, 161, 1238-49.
- STRUNGS, E. G. & LUTTRELL, L. M. 2014. Arrestin-dependent activation of ERK and Src family kinases. *Handb Exp Pharmacol*, 219, 225-57.
- SUKHTANKAR, D. D., ZAVERI, N. T., HUSBANDS, S. M. & KO, M. C. 2013. Effects of spinally administered bifunctional nociceptin/orphanin FQ peptide receptor/mu-opioid receptor ligands in mouse models of neuropathic and inflammatory pain. *J Pharmacol Exp Ther*, 346, 11-22.
- TAN, M., WALWYN, W. M., EVANS, C. J. & XIE, C.-W. 2009a. p38 MAPK and β -Arrestin 2 Mediate Functional Interactions between Endogenous μ -Opioid and α 2A-Adrenergic Receptors in Neurons. *Journal of Biological Chemistry*, 284, 6270-6281.
- TAN, M., WALWYN, W. M., EVANS, C. J. & XIE, C. W. 2009b. p38 MAPK and beta-arrestin 2 mediate functional interactions between endogenous micro-opioid and alpha2A-adrenergic receptors in neurons. *J Biol Chem*, 284, 6270-81.
- THOMPSON, A. A., LIU, W., CHUN, E., KATRITCH, V., WU, H., VARDY, E., HUANG, X.-P., TRAPPELLA, C., GUERRINI, R., CALO, G., ROTH, B. L., CHEREZOV, V. & STEVENS, R. C. 2012. Structure of the nociceptin/orphanin FQ receptor in complex with a peptide mimetic. *Nature*, 485, 395-399.
- TIAN, J. H., ZHANG, W., FANG, Y., XU, W., GRANDY, D. K. & HAN, J. S. 1998. Endogenous orphanin FQ: evidence for a role in the modulation of electroacupuncture analgesia and the development of tolerance to analgesia produced by morphine and electroacupuncture. *Br J Pharmacol*, 124, 21-6.
- TOLL, L. 2013. The use of bifunctional NOP/mu and NOP receptor selective compounds for the treatment of pain, drug abuse, and psychiatric disorders. *Curr Pharm Des*, 19, 7451-60.
- TRAFTON, J. A. & BASBAUM, A. I. 2004. [d-Ala²,N-MePhe⁴,Gly-ol⁵]enkephalin-induced internalization of the μ opioid receptor in the spinal cord of morphine tolerant rats. *Neuroscience*, 125, 541-543.
- TSAO, P. I. & VON ZASTROW, M. 2000. Type-specific Sorting of G Protein-coupled Receptors after Endocytosis. *Journal of Biological Chemistry*, 275, 11130-11140.

- TSO, P. H. & WONG, Y. H. 2003. Molecular basis of opioid dependence: role of signal regulation by G-proteins. *Clinical and Experimental Pharmacology and Physiology*, 30, 307-316.
- UEDA, H., INOUE, M., TAKESHIMA, H. & IWASAWA, Y. 2000. Enhanced spinal nociceptin receptor expression develops morphine tolerance and dependence. *J Neurosci*, 20, 7640-7.
- UEDA, H., YAMAGUCHI, T., TOKUYAMA, S., INOUE, M., NISHI, M. & TAKESHIMA, H. 1997. Partial loss of tolerance liability to morphine analgesia in mice lacking the nociceptin receptor gene. *Neurosci Lett*, 237, 136-8.
- VAUGHAN, C. W., CONNOR, M., JENNINGS, E. A., MARINELLI, S., ALLEN, R. G. & CHRISTIE, M. J. 2001. Actions of nociceptin/orphanin FQ and other prepronociceptin products on rat rostral ventromedial medulla neurons in vitro. *J Physiol*, 534, 849-59.
- WALDHOER, M., BARTLETT, S. E. & WHISTLER, J. L. 2004. Opioid Receptors *Annual Review of Biochemistry*, 73, 953-990.
- WANG, H.-B., GUAN, J.-S., BAO, L. & ZHANG, X. 2008. Distinct Subcellular Distribution of δ -Opioid Receptor Fused with Various Tags in PC12 Cells. *Neurochemical Research*, 33, 2028-2034.
- WANG, H.-B., ZHAO, B., ZHONG, Y.-Q., LI, K.-C., LI, Z.-Y., WANG, Q., LU, Y.-J., ZHANG, Z.-N., HE, S.-Q., ZHENG, H.-C., WU, S.-X., HÖKFELT, T. G. M., BAO, L. & ZHANG, X. 2010. Coexpression of δ - and μ -opioid receptors in nociceptive sensory neurons. *Proceedings of the National Academy of Sciences*, 107, 13117-13122.
- WANG, H.-L., HSU, C.-Y., HUANG, P.-C., KUO, Y.-L., LI, A. H., YEH, T.-H., TSO, A.-S. & CHEN, Y.-L. 2005. Heterodimerization of opioid receptor-like 1 and μ -opioid receptors impairs the potency of μ receptor agonist. *Journal of Neurochemistry*, 92, 1285-1294.
- WANG, Z., MA, W., CHABOT, J. G. & QUIRION, R. 2009. Cell-type specific activation of p38 and ERK mediates calcitonin gene-related peptide involvement in tolerance to morphine-induced analgesia. *Faseb j*, 23, 2576-86.
- WATTS, V. J. & NEVE, K. A. 2005. Sensitization of adenylyl cyclase by Gai/o-coupled receptors. *Pharmacology & Therapeutics*, 106, 405-421.
- WEINHOLD, F. 2001. Chemistry. A new twist on molecular shape. *Nature*, 411, 539-41.
- WETTSCHURECK, N. & OFFERMANN, S. 2005. *Mammalian G Proteins and Their Cell Type Specific Functions*.
- WHALEN, E. J., RAJAGOPAL, S. & LEFKOWITZ, R. J. 2011. Therapeutic potential of β -arrestin- and G protein-biased agonists. *Trends in Molecular Medicine*, 17, 126-139.
- WHISTLER, J. L. & VON ZASTROW, M. 1998. Morphine-activated opioid receptors elude desensitization by β -arrestin. *Proceedings of the National Academy of Sciences*, 95, 9914-9919.
- WHO 2009. WHO Guidelines Approved by the Guidelines Review Committee. *Guidelines for the Psychosocially Assisted Pharmacological Treatment of Opioid Dependence*. Geneva: World Health Organization
- World Health Organization.
- WIKIPEDIA. 2014. *Taqman* [Online]. Available: <http://en.wikipedia.org/wiki/TaqMan> [Accessed 01/10/14].
- WILLIAMS, J. T., INGRAM, S. L., HENDERSON, G., CHAVKIN, C., VON ZASTROW, M., SCHULZ, S., KOCH, T., EVANS, C. J. & CHRISTIE, M. J. 2013. Regulation of μ -opioid receptors: desensitization, phosphorylation, internalization, and tolerance. *Pharmacol Rev*, 65, 223-54.
- WOLFE, J. T., WANG, H. G., HOWARD, J., GARRISON, J. C. & BARRETT, P. Q. 2003. T-type calcium channel regulation by specific G-protein beta gamma subunits. *Nature*, 424, 209-213.
- WU, H., WACKER, D., MILENI, M., KATRITCH, V., HAN, G. W., VARDY, E., LIU, W., THOMPSON, A. A., HUANG, X.-P., CARROLL, F. I., MASCARELLA, S. W., WESTKAEMPER, R. B., MOSIER, P. D., ROTH, B. L., CHEREZOV, V. &

- STEVENS, R. C. 2012. Structure of the human [kgr]-opioid receptor in complex with JDTic. *Nature*, 485, 327-332.
- ZAVERI, N. T. 2011. The nociceptin/orphanin FQ receptor (NOP) as a target for drug abuse medications. *Curr Top Med Chem*, 11, 1151-6.
- ZEILHOFER, H. U. & CALO, G. 2003. Nociceptin/Orphanin FQ and Its Receptor—Potential Targets for Pain Therapy? *Journal of Pharmacology and Experimental Therapeutics*, 306, 423-429.
- ZHANG, X., BAO, L. & GUAN, J.-S. 2006. Role of delivery and trafficking of δ -opioid peptide receptors in opioid analgesia and tolerance. *Trends in Pharmacological Sciences*, 27, 324-329.
- ZHANG, Z., XIN, S.-M., WU, G.-X., ZHANG, W.-B., MA, L. & PEI, G. 1999. Endogenous δ -Opioid and ORL1 Receptors Couple to Phosphorylation and Activation of p38 MAPK in NG108-15 Cells and This Is Regulated by Protein Kinase A and Protein Kinase C. *Journal of Neurochemistry*, 73, 1502-1509.
- ZHENG, H., LOH, H. H. & LAW, P. Y. 2008. Beta-arrestin-dependent mu-opioid receptor-activated extracellular signal-regulated kinases (ERKs) Translocate to Nucleus in Contrast to G protein-dependent ERK activation. *Mol Pharmacol*, 73, 178-90.
- ZHU, Y., KING, M. A., SCHULLER, A. G. P., NITSCHKE, J. F., REIDL, M., ELDE, R. P., UNTERWALD, E., PASTERNAK, G. W. & PINTAR, J. E. 1999. Retention of Supraspinal Delta-like Analgesia and Loss of Morphine Tolerance in δ Opioid Receptor Knockout Mice. *Neuron*, 24, 243-252.
- ZUO, Z. 2005. The Role of Opioid Receptor Internalization and β -Arrestins in the Development of Opioid Tolerance. *Anesthesia & Analgesia*, 101, 728-734.

